

Surface Charge Characterization and Flotation of an Ultramafic Ni-Ore

Salah Uddin



**Department of Mining and Materials Engineering
McGill University
Montreal, QC, Canada**

**A thesis submitted to McGill University
in partial fulfillment of the requirements of the degree of
Doctor of Philosophy**

© Salah Uddin, November, 2011

Table of contents

Abstract	1
Résumé	2
Acknowledgements	4
Contributions of author and co-authors in the published (and to be submitted) work presented in this thesis	7
Layout of the Thesis	9
References	11
List of figures	12
List of tables	20
1. Introduction	21
1.1. Background	21
1.1.1. <i>Nickel ores</i>	21
1.1.2. <i>Research objectives</i>	23
1.1.3. <i>Particle charging</i>	23
1.1.4. <i>Bubble charging</i>	27
1.2. References	29
2. Literature Review	32
2.1. Surface charge characterization: particles	32
2.1.1. <i>Electrophoresis</i>	33
2.1.2. <i>Streaming potential</i>	34
2.1.3. <i>Electro-osmosis</i>	35

2.1.4. <i>Sedimentation potential</i>	36
2.1.5. <i>Electro-acoustic method</i>	38
2.2. Flotation	40
2.3. Fibre disintegration	43
2.4. Surface charge characterization: bubble swarms	46
2.5. Surface charge characterization: bubbles in presence of particles	49
2.6. Nomenclature	52
2.7. References	53
3. A Surface Charge Characterization Device Using Sedimentation	60
Potential for Single and Mixed Particle Systems	
3.1. Abstract	60
3.2. Introduction	61
3.3. Theory	61
3.3.1. <i>Sedimentation and zeta potential</i>	61
3.3.2. <i>Particle volume fraction: Maxwell's conductivity model</i>	63
3.3.3. <i>Viscosity of suspension</i>	64
3.4. Apparatus	64
3.4.1. <i>Background</i>	64
3.4.2. <i>Cell and accessories</i>	64
3.5. Experimental	66
3.5.1. <i>Samples</i>	66
3.5.2. <i>Procedure: single-mineral systems</i>	68
3.5.3. <i>Procedure: mixed-mineral systems</i>	68

3.6. Results	70
3.6.1. <i>Single-mineral systems</i>	70
3.6.2. <i>Mixed-mineral systems</i>	73
3.7. Discussion	77
3.8. Conclusions	79
3.9. Acknowledgements	80
3.10. Nomenclature	80
3.11. References	81
4. An Apparatus to Measure Electrical Charge of Bubble Swarms	84
4.1. Abstract	84
4.2. Introduction	85
4.3. Background to apparatus	86
4.4. Theory	86
4.4.1. <i>Sedimentation potential</i>	86
4.4.2. <i>Gas holdup: Maxwell's conductivity model</i>	87
4.5. Experimental	88
4.5.1. <i>Cell and accessories</i>	88
4.5.2. <i>Procedure</i>	90
4.6. Results	92
4.6.1. <i>Example of basic readings</i>	92
4.6.2. <i>Validation: Determination of iep for de-ionized water</i>	95
4.6.3. <i>Effect of non-ionic surfactant (frother)</i>	98
4.6.4. <i>Ionic surfactants</i>	99

4.6.5. <i>Effect of Mg ions</i>	100
4.7. Discussion	102
4.8. Conclusions	106
4.8. Acknowledgements	106
4.9. Nomenclature	107
4.10. References	108
5. Effect of Particles on the Electrical Charge of Gas Bubbles in Flotation	111
5.1 Abstract	111
5.2. Introduction	112
5.3. Background	113
5.3.1. <i>Particle charging</i>	113
5.3.2. <i>Bubble-particle electrostatic interaction studies</i>	114
5.3.3 <i>Sedimentation potential</i>	114
5.4. Experimental	115
5.4.1. <i>Reagents and minerals</i>	115
5.4.2. <i>Apparatus</i>	117
<u>5.4.2.1 Bubble sedimentation potential</u>	117
<u>5.4.2.2. Visualization</u>	119
5.4.3. <i>Procedure</i>	120
<u>5.4.3.1 Bubble sedimentation potential</u>	120
<u>5.4.3.2 Visualization</u>	121
<u>5.4.3.3 Micro-electrophoresis</u>	121
5.5. Results	122

5.5.1. <i>Bubble sedimentation potential</i>	122
<u>5.5.1.1 Alumina and silica</u>	122
<u>5.5.1.2. Clinochrysotile</u>	125
5.5.2. <i>Visualization tests</i>	127
5.6. Discussion	130
5.7. Conclusions	132
5.8. Acknowledgements	133
5.9. References	133
6. Fibre Disintegration and Flotation of an Ultramafic Ore	136
6.1. Abstract	136
6.2. Introduction	137
6.3. Background	137
6.4. Experimental	137
6.4.1. <i>Ore mineralogy</i>	137
6.4.2. <i>Sedimentation potential</i>	138
6.4.3. <i>Grinding</i>	138
6.4.4. <i>Flotation</i>	139
6.4.5. <i>Illustration of fibre disintegration</i>	140
6.5. Results	141
6.5.1. <i>Sedimentation tests</i>	141
6.5.2. <i>Effect of acid treatment</i>	143
6.5.3. <i>Flotation</i>	144
6.5.4. <i>Illustrating fibre disintegration</i>	148

6.6. Discussion	151
6.7. Conclusions	153
6.8. Acknowledgements	153
6.9. References	154
7. Processing an Ultramafic Ore Using Fibre Disintegration by Acid Attack	156
7.1. Abstract	156
7.2. Introduction	156
7.3. Background	157
7.4. Experimental	157
7.4.1. <i>Ore mineralogy</i>	157
7.4.2. <i>Flotation without acid treatment</i>	157
7.4.3. <i>Flotation with acid treatment</i>	158
7.4.4. <i>Illustration of fibre disintegration</i>	159
7.4.5. <i>Analytical methods</i>	159
7.4.6. <i>Bubble size distribution</i>	160
7.5. Results	161
7.5.1. <i>Effect of acid treatment</i>	161
7.5.2. <i>Flotation</i>	162
7.5.3. <i>Illustrating fibre disintegration</i>	165
7.5.4. <i>Bubble size</i>	168
7.5.5. <i>Evidence of elemental sulphur</i>	169
7.6. Discussion	171
7.7. Conclusions	174

7.8. Acknowledgements	175
7.9. References	175
8. Conclusions and Perspectives	178
8.1. Conclusions and contributions to original knowledge	178
8.1.1. <i>Overview</i>	178
8.1.2. <i>Surface charge study: particles</i>	178
8.1.3. <i>Surface charge study: bubbles</i>	180
8.1.4. <i>Fibre disintegration</i>	183
8.2. Future directions	186
8.2.1. <i>Modification of the PSP apparatus</i>	186
8.2.2. <i>Ore flotation: test with higher feed concentration</i>	186
8.2.3. <i>Micro-flotation using ionic collectors</i>	187
8.3. References	187
Appendices	189
Appendix I – Sedimentation potential setup: particles	189
Appendix II – Additional characterizations from chapter 7	190
Appendix III – Gravity separation	193
<i>Experimental</i>	194
<i>Results</i>	195
<i>Discussion</i>	198
Appendix IV – Sedimentation potential setup: bubble swarms	199
Appendix V – Sample MatLab program to calculate zeta potential	200
References	205

Abstract

About 300 million tonnes of inferred Ni resource in ultramafic hosted rocks is present in ‘Thompson Nickel Belt’ in north central Manitoba. The processing challenges result from electrostatic interaction between pentlandite (the main Ni-mineral) and serpentine (the main gangue and one of the MgO minerals). As a contribution to meeting the challenge, the thesis examines the role of particle and bubble surface charge and the effect of fibre disintegration on flotation behavior of an ultramafic Ni ore sample. For surface charge characterization the sedimentation potential technique was used. A novel integrated device was developed to measure sedimentation potential, conductivity and pH simultaneously. Maxwell’s model was used to calculate volume fraction of dispersed phase from conductivity, and zeta potential, when appropriate, was calculated from the Smoluchowski equation. The technique was validated by showing good agreement with iso-electric point for alumina, silica and bubble suspensions with electrophoresis measurements. The technique was extended to characterize mixed minerals including ultramafic ore, and bubbles in the presence of particles. The results provided some evidence of metal ion adsorption on particles and the possibility of non-hydrophobic particle attachment to bubbles. The latter was reinforced by visualization studies of a pendant bubble exposed to particle suspensions.

A novel fibre disintegration strategy was devised combining both chemical (acid) and physical (grinding) treatment based on work to enhance carbon dioxide uptake by serpentine. Using HCl, subsequent conventional flotation (amyl xanthate, soda ash and MIBC) gave significantly improved results over the untreated ore. Using H₂SO₄, arguably the practical option led to flotation without collector due to elemental sulphur

formation on pentlandite, and without frother due to high ionic strength solutions. Improved Ni grade-recovery with higher MgO mineral rejection was achieved. Structural changes in the fibres were followed using various spectroscopic techniques and a mechanism of fibre disintegration suggested.

Résumé

Environ 300 millions de tonnes de ressources inférées de Ni ultramafiques hébergé est présent dans 'ceinture nickélique de Thompson dans le centre-nord du Manitoba. Le traitement des défis résultant de l'interaction électrostatique entre pentlandite (le principal Ni-minéraux) et la serpentine. En tant que contribution à relever le défi, la thèse examine le rôle des particules et la charge de surface des bulles et l'effet de la désintégration des fibres sur le comportement de flottaison d'un échantillon de minerai de nickel ultramafiques. Pour la caractérisation de charge de surface de la technique de sédimentation potentielle a été utilisée. Un nouveau dispositif intégré a été développé pour mesurer le potentiel de sédimentation, la conductivité et le pH simultanément. Le modèle de Maxwell a été utilisée pour calculer la fraction volumique de phase dispersée de la conductivité, et le potentiel zêta, le cas échéant, a été calculée à partir de l'équation de Smoluchowski. La technique a été validée en montrant un bon accord avec l'iso-électrique de point pour les suspensions d'alumine, de silice et de bulles avec des mesures d'électrophorèse. La technique a été étendue afin de caractériser les minéraux mélangés, y compris de minerai ultramafiques, et des bulles dans la présence de particules. Les résultats ont fourni des preuves de ion métallique adsorption sur les particules et la possibilité de l'attachement des particules non-hydrophobe à bulles. Ce

dernier a été renforcée par des études de la visualisation d'une bulle Pendentif exposés à des suspensions de particules.

Une stratégie nouvelle fibre de désintégration a été conçu combinant à la fois chimique (acide) et physiques (broyage) un traitement basé sur le travail pour améliorer l'absorption du dioxyde de carbone par la serpentine. En utilisant HCl, à la suite de flottation conventionnelle (amyl xanthate, la cendre de soude et de MIBC) a donné des résultats nettement améliorés au cours des minerais non traités. Utiliser H₂SO₄, sans doute l'option la pratique conduit à de flottaison sans collecteur due à la formation du soufre élémentaire sur la pentlandite, et sans buse due à des solutions à haute force ionique. Amélioration de qualité Ni-reprise avec le rejet supérieur de MgO de a été atteint. Les changements structurels dans les fibres ont été suivis en utilisant diverses techniques de spectroscopie et d'un mécanisme de désintégration de fibre suggéré.

Acknowledgements

First, I would like to acknowledge my supervisor Prof. James A. Finch, from whom I have learned mineral processing. This was an enormous privilege for me being accepted as one of his PhD students. To me the most important part was his encouragement, I felt more lively and energetic every time I have had a conversation with him on my projects. He, with enthusiasm, went through the detail of all my work and gave me directions, perspectives and motivations. His helping me with scientific writing that comprises precise, consistent, logical and comprehensible expression of complicated ideas and research procedures was invaluable. I think what makes him the best is his unfaltering faith and confidence in his graduate students. He stands for students even at the most adverse moment and assists with patience, intelligence and experience to the end to overcome setbacks. I can not expect anything better than what I have had from Prof. Finch as a supervisor in my PhD.

I am grateful to Dr. Rao who taught me the theoretical and practical aspects of handling batch flotation and chemical analysis. It was exceptionally fruitful to share ideas with him regarding the development of the new flotation strategy. I greatly appreciate the role of Dr. Mirnezami in my research. She was the first to bring to me the idea of using sedimentation potential to characterize minerals. Her showing me the electrophoresis measurement technique along with many constructive suggestions was particularly valuable for my work. I am greatly indebted to Dr. Cesar Gomez for his advice regarding the design and construction of various apparatus. His keen knowledge on the design aspects of engineering instruments was certainly very effectual.

Funding from Vale is gratefully acknowledged. It was an immense opportunity to learn and deal with solving practical problems being a part of 'Vale-Cytec-University Research Consortium' on processing ultramafic Ni-ore. Permission to publish the research works in conferences and peer reviewed journals by Vale is greatly appreciated. I would also like to thank Vale for organizing the progress review meetings on ultramafic ore research which provided a congenial atmosphere to share knowledge between researchers from McGill University, McMaster University, Columbia University, Cytec Industries Inc. and Vale Base Metals Technology Development.

Support for the fundamental research described in this thesis was received through Natural Sciences and Engineering Research Council of Canada (NSERC) Collaborative Research and Development program under the Chair in Mineral Processing. Co-sponsors are Vale, Teck Resources, Barrick Gold, Xstrata Process Support, Shell Canada, SGS Lakefield, COREM and Flottec. All the constructive advice and suggestions given at the annual Chair Sponsors' Meeting and on various other occasions enriched the research.

I would like to thank my M. Eng. Supervisor Prof. M. Hasan for his dedicated teaching of computational fluid dynamics based process modeling, simulation and use of open source codes. My learning to strive to solve complex problems helped me enormously in my PhD research. My four years' experience as a teaching assistant in undergraduate courses: Heat, Mass and Fluid Flow, Applied Fluid Dynamics and Advanced Process Engineering with Prof. F. A. Mucciardi were also very beneficial in understanding many fundamental ideas used in this work. For me to have the opportunity to use Raman and FT-IR spectroscopy, I gratefully thank Prof. R. Chromik and Prof. S. N. Nazhat. My boundless thanks go to my friend Mr. Wei Zhang for his constant

encouragement and demonstration of various aspects of bubble measurements, and to Dr. Mario Gomez for assistance with Raman Spectroscopy and XPS.

I am also indebted to the other research associates and non-academic staffs: Frank Rosenblum and Raymond Langlois for the sedimentation setup; Helen Campbell for SEM; Ranjan Roy and Andrew Golsztajn (Chemical Engineering Department) for ICP-OES; George Kopp (Chemistry Department) for help in design, fabrication and modification of the glass columns; and Charles Burtles (Electrical Engineering Department) for help in circuit design. I would like to thank all members of McGill Mineral Processing Group and my friends in this department.

Finally, I would like to express my deep gratitude to almighty God, my creator, who gave me the ability to acquire and apply knowledge. There are no words for me to pronounce my acknowledgement to my parents. It was there endless love, passionate sacrifice and perpetual motivation which made it possible for me to pursue the achievement of the highest level of education from one of the best universities while born and grew up in one of the least privileged populations in the world. I would also like to thank my beloved younger sister Dr. Jebun Nesa and my brother-in-law Dr. Khandker Arifeen for being always beside me with encouragement and solace.

Contributions of author and co-authors in the published (and to be submitted) work presented in this thesis

Uddin, S., Mirnezami, M., Finch, J. A., 2010. A surface charge characterization device using sedimentation potential for single and mixed particle systems. *Colloids and Surfaces A*, 371, 64–70.

Uddin, S., Rao, S. R., Mirnezami, M., Finch, J. A., 2011. Fibre disintegration and flotation of an ultramafic Ni-ore. *Miner. Eng.* To be submitted.

Uddin, S., Rao, S. R., Mirnezami, M., Finch, J. A., 2011. Processing an ultramafic ore using fiber disintegration by acid attack. *Int. J. Miner. Process.* In press, doi: [10.1016/j.minpro.2011.09.015](https://doi.org/10.1016/j.minpro.2011.09.015).

Uddin, S., Jin, L., Mirnezami, M., Finch, J. A., 2011. An apparatus to measure electrical charge of bubble swarms. *Chem. Eng. Sci.* To be submitted.

Uddin, S., Li, Y., Mirnezami, M., Finch, J. A., 2011. Effect of particles on the electrical charge of gas bubbles in flotation. *Miner. Eng.* To be submitted.

In all these works, the author has designed the surface charge characterization apparatus for particles and bubble swarms. Software for instrument control, data acquisition and post-processing was developed by the author. All test works regarding particle charge characterization was done by the author. Assistance was taken from

summer co-op students, L. Jin and Y. Li to perform the test works stated in the last two papers (regarding bubble charge characterization). Initial proposal to use sedimentation technique to characterize minerals and bubbles was made by Dr. M. Mirnezami. She also advised the use of the visualization technique with a pendant bubble exposed to agitated suspensions. Much advice and direction was given by Prof. J. A. Finch, especially on designing test works to characterize mixed particle systems and to interpret and validate results in bubble-particle systems.

In the fibre disintegration/flotation paper, the author devised the treatment procedure for ultramafic ore to increase Ni recovery and gangue rejection. All tests from sample preparation to analysis were done by the author. Assistance was provided by Prof. J. A. Finch to produce the correct mass balance. At different stages countless positive suggestions were provided by Dr. S. R. Rao and Dr. M. Mirnezami.

Precise and comprehensible expression of many complex, interrelated ideas was required in the papers: Generous assistance was provided by Prof. J. A. Finch in this regard.

In the defence of this statement a document that has all the signatures in one place will be presented.

JAF

MM

and SRR

LJ

YL

Layout of the Thesis

This thesis has been prepared on the basis of manuscripts. Five original research papers have been slightly modified to fit the purposes of this thesis. The material in chapter 3 was published first in two peer reviewed conference papers (Uddin et al., 2009; Uddin et al. 2010a) and later published to an international peer reviewed journal (Uddin et al., 2010b). Some of the contents of chapter 6 were published as a conference paper (Uddin et al., 2010c) and in process of publication in a journal (Uddin et al., 2011a). The content in chapter 7 has been accepted for publication in a journal (Uddin et al., 2011b). The material in chapter 4 is in process of submission in a journal (Uddin et al., 2011c). Draft version of the contents of chapter 5 has been submitted in a conference (Uddin et al., 2011d). Final version is in process of submission (Uddin et al., 2011e). In this section the layout of the thesis is provided with the connections and relations between the chapters.

The **first chapter** of the thesis gives a brief background on the Thompson ultramafic Ni-ore and the problems which are investigated in this study.

The **second chapter** of the thesis consists of a detailed literature review. It consists of background information on various surface charge characterization techniques used for particles and gas bubbles. It was to provide the reader with the relevant background information and concept of the works that have been previously conducted and how it relates to the improvement done in the current research. In the flotation part, it discusses the major factors that could adversely affect flotation of the ore. The background of the fibre disintegration technique was provided which was used to counter

entanglement discussing the structural features of the dominant mineral. It, also, gives a brief summary on the prior works done on collectorless flotation of sulphide ores.

In the **third chapter**, design and application of the particle surface charge characterization apparatus is discussed.

Chapter four shows the design and application of the surface charge characterization device for bubble swarms. It has been developed to study the electrostatic interaction between negatively charged gas bubbles and positively charged clinochrysotile, the dominant ore fraction.

The technique has been extended in **chapter five** where it describes the effect of particles on surface electrical charge of gas bubbles. Sedimentation tests were performed along with visualization and zeta potential measurements to understand the interaction between the bubbles and clinochrysotile in various surfactant solutions.

Sixth chapter describes the use of both charge characterization and flotation technique to identify the reason behind poor flotation response commonly observed in case of ultramafic ore. In this chapter, the newly devised fibre disintegration technique is introduced using hydrochloric acid (HCl) and flotation results between the treated and the untreated ore were compared.

Modification of the technique from more practical perspective is discussed in **chapter seven**, where sulphuric acid (H_2SO_4) is used for fibre disintegration followed by collectorless flotation of the low pH slurry.

Finally, in **chapter eight**, overall conclusions of the studies conducted in the current research is stated, in addition to what new knowledge this work has provided for

the relevant academic and industrial research areas along with potential future directions of work in this area.

References

- Uddin, S., Mirnezami, M., Finch, J. A., 2009. An approach to measure zeta potential using sedimentation potential method, In: *Advances in Mineral Processing Science and Technology*, Gomez, C. O., Nasset, J. E., Rao, S. R. (editors), CIM, Sudbury, ON, pp. 409 – 420.
- Uddin, S., Mirnezami, M., Finch, J. A., 2010a. Charge characterization of single and mixed mineral systems, In: *EPD Congress: Extraction and Processing Division*, Vidal, E. E. (editor), TMS, Seattle, WA, pp. 359 – 367.
- Uddin, S., Mirnezami, M., Finch, J. A., 2010b. A surface charge characterization device using sedimentation potential for single and mixed particle systems. *Colloid Surface A*, 371, 64–70.
- Uddin, S., Mirnezami, M., Rao, S. R., Finch, J. A., 2010c. Effect of fibre disintegration on flotation of an ultramafic Ni-Ore, in: Pawlik, M. (Ed.), *Proc. Rheology in Minerals Processing*, CIM, Vancouver, BC, pp. 307 – 317.
- Uddin, S., Rao, S. R., Mirnezami, M., Finch, J. A., 2011a. Surface charge characterization and flotation of an ultramafic Ni-ore. *Miner. Eng.* To be submitted.
- Uddin, S., Rao, S. R., Mirnezami, M., Finch, J. A., 2011b. Processing an ultramafic ore using fiber disintegration by acid attack. *Int. J. Miner. Process.* In press, doi: [10.1016/j.minpro.2011.09.015](https://doi.org/10.1016/j.minpro.2011.09.015).
- Uddin, S., Jin, L., Mirnezami, M., Finch, J. A., 2011c. An apparatus to measure electrical charge of bubble swarms. *Chem. Eng. Sci.* To be submitted.
- Uddin, S., Li, Y., Mirnezami, M., Finch, J. A., 2011d. Role of electrical charge on gas bubbles in flotation, *Flotation' 11*, MEI, Cape Town, SA, Nov 14-17 (Submitted).
- Uddin, S., Li, Y., Mirnezami, M., Finch, J. A., 2011e. Effect of particles on the electrical charge of gas bubbles in flotation. *Miner. Eng.* To be submitted.

List of figures

Chapter 1

- Fig. 1. Surface hydration of silica and metal sulphide (MS).....pp. 23
- Fig. 2. (A) Electrical double layer and (B) zeta potential.....pp. 25
- Fig. 3. (Left) Zeta potential of goethite as a function of pH and (Right) Flotation recovery of goethite as function of pH with sulfonate, $R-SO_3^-$ and amine, $R-NH_3^+$ collector typespp. 26
- Fig. 4. Zeta potential as a function of pH for serpentine and gas bubbles.....pp. 28

Chapter 2

- Fig. 1. Summary of various approaches to measure zeta potential.....pp. 32
- Fig. 2. Movement of charged particles (A and B) in an electric field.....pp. 32
- Fig. 3. Generation of streaming potential.....pp. 35
- Fig. 4. Generation of electro-osmotic flow by applied potential.....pp. 36
- Fig. 5. Schematic presentation of sedimentation potential generation.....pp. 37
- Fig. 6. Generation of dipole in an applied acoustic field (Dukhin et al., 2000).....pp. 38
- Fig. 7. ‘Conventional’ flotation procedure.....pp. 42
- Fig. 8. Chrysotile fibre structure (Bernstein and Hoskins, 2006).....pp. 44
- Fig. 9. Chrysotile fibre disintegration by acid attack (Bernstein and Hoskins, 2006)pp. 44

Chapter 3

- Fig. 1. Sedimentation apparatus and accessories.....pp. 66
- Fig. 2. Experimental cycles (first three are shown here).....pp. 69

Fig. 3. Potential difference as a function of time for alumina suspension at ca. pH 8
.....pp. 71

Fig. 4. Potential difference as a function of time for alumina suspension at ca. pH 9
.....pp. 71

Fig. 5. Resistance as a function of time for alumina suspension at pH \approx 9.....pp. 72

Fig. 6. Volume fraction as a function of time for alumina suspension at pH \approx 9.....pp. 72

Fig. 7. Zeta potential as a function of pH for alumina suspension: (\blacklozenge) zeta potential
measured by sedimentation method and (\square) zeta potential measured by electrophoresis
.....pp. 73

Fig. 8. Zeta potential as a function of pH for silica suspension: (\blacklozenge) zeta potential
measured by sedimentation method and (\square) zeta potential measured by electrophoresis
.....pp. 73

Fig. 9. Sedimentation potential (SP) as a function of time for set 1 (A) and set 2 (B) in
cycle 2 Note: the three groups of 10 readings are the three fractions collected.....pp. 74

Fig. 10. Silica Peak Height @ 2 Theta \sim 26 deg. as a function of fraction for set 1 (A) and
set 2 (B).....pp. 75

Fig. 11. Difference between Avg(SP1) and Avg(SP3) as a function of experimental
cycles for set 1 (A) and set 2 (B).....pp. 76

Fig. 12. SEM micrograph and EDAX Microanalysis on two selected particles for first
fraction of set 2.....pp. 77

Chapter 4

Fig. 1. Bubble column and accessories (dimensions in millimetre).....pp. 89

Fig. 2. Bubble size analyzer (dimensions in millimetre).....pp. 91

Fig. 3. Potential difference for background (E_B) and in presence of bubbles (E_O) as a function of readings (A) pH ca. 3 and (B) pH ca. 8.....pp. 92

Fig. 4. Gas holdup vs. flowrate in presence of (DF250, pH ca. 6.0).....pp. 93

Fig. 5. Sedimentation potential and gas holdup as a function of flowrate in presence of $5 \times 10^{-5} \text{M}$ SHS (pH ca. 6.0).....pp. 93

Fig. 6. Bubble size in presence of, from top left to bottom right: de-ionized water (only), 10^{-2}M KCl, HTAB and MIBC (dimensions in mm)pp. 94

Fig. 7. Bubble sedimentation potential (BSP) of bubbles as a function of pH in de-ionized water (\blacktriangle , 10^{-2}M KCl background, error bar represents standard deviation of 3 repeats) compared with zeta potential (ZP) data of Takahashi (2005) (\square)pp. 96

Fig. 8. Bubble sedimentation Potential (BSP) as function of pH in (A) MIBC and (B) DF250 at concentrations of (\blacktriangle) 0, (\blacksquare) 10, and (\blacklozenge) 100 ppm and natural pH (ca. 6)pp. 98

Fig. 9. Effect of ionic surfactant concentration on bubble sedimentation potential (BSP) in presence of SHS (anionic) and HTAB (cationic) (pH ca. 6).....pp. 100

Fig. 10. Bubble sedimentation potential (BSP) vs. pH in presence of 10^{-2}M MgCl_2 (\blacksquare)pp. 100

Fig. 11. Bubble sedimentation potential (BSP) as a function of MgCl_2 and fixed concentration of SHS ($5 \times 10^{-5} \text{M}$ (most probably $1 \times 10^{-4} \text{M}$)pp. 101

Fig. 12. Three possible arrangements in the SHS - Mg^{2+} system as a function of increasing relative concentration of Mg (A, B, C).....pp. 105

Chapter 5

Fig. 1. XRD of (A) sample derived from ore and (B) match for clinochrysotile.....pp. 115

Fig. 2. Apparatus to measure bubble sedimentation potential in presence of particles (dimensions in millimetre).....pp. 118

Fig. 3. Apparatus for visual investigation of bubble-particle attachment.....pp. 120

Fig. 4. Bubble sedimentation potential (BSP) as a function of particle concentration, (▲) alumina and (■) silica in presence of 20 ppm DF250.....pp. 123

Fig. 5. Bubble sedimentation potential (BSP) as a function of particle concentration, (▲) alumina + SHS and (■) silica + HTAB (Note: BSP in absence of particles is close to the value at 0.05 g/700 mL).....pp.123

Fig. 6. Zeta potential (ZP) as a function of alumina concentration, (▲) alumina only and (■) alumina + SHS.....pp. 124

Fig. 7. Zeta potential (ZP) as a function of silica concentration, (▲) silica only and (■) silica + HTAB.....pp. 124

Fig. 8. Bubble sedimentation potential (BSP) as a function of clinochrysotile concentration in (▲) $10^{-2}M$ KCl, (■) $10^{-3}M$ KCl + MIBC (20 ppm) and (●) $10^{-3}M$ KCl + DF250 (20 ppm).....pp. 126

Fig. 9. Bubble sedimentation potential (BSP) as a function of clinochrysotile concentration in SHS.....pp. 126

Fig . 10. Results of visualization tests: alumina (38-44 μm)-SHS system with increasing particle concentration (in 300mL).....pp. 127

Fig. 11. Results of visualization tests: alumina-DF250 at three particle sizes; and alumina-HTAB with 25-38 μm particles (all concentrations, 2g/300mL).....pp.128

Fig. 12. Results of visualization tests: silica (2g/300mL, 38-44 μm) in presence HTAB, DF250 and SHS.....pp. 129

Fig. 13. Results of visualization tests: clinochrysotile (2g/300mL, -25 μm) with background electrolyte, SHS, MIBC, and HTAB.....pp.129

Chapter 6

Fig. 1. The X-ray powder diffraction pattern of the ore together with the match for clinochrysotile from a search of the Powder Diffraction File # 00-052-1562 (PDF), (vertical lines, major peaks are indicated with arrows).....pp. 138

Fig. 2. Flow sheet for fibre disintegration / flotation tests.....pp. 139

Fig. 3. Settling slurry in different pH conditions; (A) Dispersed, (B) Partially agglomerated and (C) Agglomerated.....pp. 141

Fig. 4. Settling slurry at (A) pH 9, (B) pH 11 and (C) pH 11 with EDTA.....pp. 141

Fig. 5. Sedimentation potential as a function of pH at different MgCl_2 concentrationpp. 142

Fig. 6. Sedimentation potential as a function of pH: effect of EDTA.....pp. 142

Fig. 7. Distribution of wt% Mg in the solution as function of HCl concentration...pp. 144

Fig. 8. Froth appearance at (A) 0 wt% HCl, (B) 5 wt% HCl, (C) 10 wt% HCl and (D) 15 wt% HCl.....pp. 145

Fig. 9. Ni grade vs. recovery as a function of HCl concentration.....pp. 146

Fig. 10. Ni recovery vs. MgO rejection as a function of HCl concentration.....pp. 146

Fig. 11. Insol content in concentrate 1 and tail as a function of acid concentration..pp. 147

Fig. 12. Ore sample (A) untreated; (B) ground with HCl, (C) short fibres in it and (D) corresponding microanalysis.....pp. 148

Fig. 13. XPS analysis for untreated and acid treated ore. Si2p and Mg1s peaks are indicated.....pp. 149

Fig. 14. XPS high-resolution spectra of O1s peak for untreated and acid treated orepp. 149

Chapter 7

Fig. 1. Flowsheet with acid treatment.....pp. 159

Fig. 2. Froth appearance after 1 min (A) untreated ore, (B) treated with 15 wt% H₂SO₄ (approach 1).....pp. 163

Fig. 3. Nickel grade vs. recovery: treated (approaches 1 and 2) vs. untreated ore (note error bars are the range for the three repeats).....pp. 164

Fig. 4. Nickel recovery vs. MgO rejection: treated (approaches 1 and 2) vs. untreated orepp. 164

Fig. 5. XRD of (A) concentrate 1 from approach 1 and match for (B) pyrrhotite (Po) and (C) pentlandite (Pn) (clinocrysotile (Ctl) – cf Fig. 1, chapter 4).....pp. 165

Fig. 6. FT-IR spectra 500 to 2000 cm⁻¹ (left) and 3000 to 4000 cm⁻¹ (right) of (A) ground, untreated ore; (B) ground ore, HCl; and (C) ground ore, H₂SO₄.....pp. 166

Fig. 7. XRD of (A) ground ore, ground with (B) HCl and (C) H₂SO₄.....pp. 167

Fig. 8. Ore sample (A) untreated; ground with (B) HCl, and (C), (D) H ₂ SO ₄	pp. 168
Fig. 9. Bubble size distribution in (A) tap water and (B) MgSO ₄ (pH 2.8) solution.....	pp. 169
Fig. 10. (A) Extracted crystalline substance from concentrate and (B) microanalysis on one of the crystals.....	pp. 170
Fig. 11. Raman spectra of the (A) extracted material and (B) standard sample of elemental sulphur.....	pp. 170
Fig. 12. A possible mechanism of fibre disintegration.....	pp. 173
Fig. 13. A conceptual circuit to process ultramafic ore (Pn – Pentlandite; Po – Pyrrhotite).....	pp. 174

Appendices

Fig. 1. Particle sedimentation apparatus with accessories.....	pp. 189
Fig. 2. Slurry pH in different again times.....	pp. 190
Fig. 3. Froth phase with aeration time.....	pp. 191
Fig. 4. XRD of the concentrate in (A) no-frother and (B) with frother.....	pp. 192
Fig. 5. XPS spectra of the (A) concentrate and (B) standard sample of elemental sulphur.....	pp. 193
Fig. 6. Mozley Table.....	pp. 194
Fig. 7. Three gravity separated fractions: heavy, middle and light.....	pp. 194
Fig. 8. Microanalysis of heavy fraction.....	pp. 196
Fig. 9. Microanalysis of light fraction.....	pp. 196
Fig. 10. XRD of (A) heavy fraction and match for (B) pyrrhotite and (C) magnetite.....	pp. 197
Fig. 11. XRD of (A) light fraction and match for (B) clinochrysotile.....	pp. 197

Fig. 12. XRD of (A) ore and (B) light fraction (note: peaks in A at ca. $2\theta=44^\circ$ and 65° may come from pyrrhotite and magnetite – cf Fig. 10).....pp. 198

Fig. 13. Sedimentation potential apparatus for bubble swarms.....pp. 199

List of tables

Chapter 3

Table 1 Size-related properties.....pp. 67

Table 2 Some chemical and physical properties.....pp. 67

Table 3 Sample setspp. 69

Chapter 4

Table 1 Description of reagents used.....pp. 91

Table 2 Iso-electric-point of bubbles from literature.....pp. 96

Chapter 5

Table 1 Description of reagents used (RG – Reagent grade).....pp. 116

Table 2 Description of particles used.....pp. 116

Table 3 Iso-electric-point of bubbles from the literature compared to sedimentation method (last row); taken from Uddin et al. (2011).....pp. 119

Chapter 6

Table 1 Metallurgical balance (average of the two tests): leach and flotation with 15wt% HCl.....pp. 144

Chapter 7

Table 1 Metallurgical balance (average of the three tests): leach and flotation, approach 1 (A) and approach 2 (B). (Note: composition of ‘mass loss’ is inferred from grams mass loss and solution assay.) A) Approach 1: 2-hr aging and frother (DF250) addition.

B) Approach 2: 5-min aeration, no frother for cons 1 and 2.....pp. 161

1. Introduction

1.1. Background

1.1.1. Nickel ores

There are two major sources of nickel: sulphide ores and laterites. Sulphide ores range from massive (90% sulphide, up to 10% Ni) to sulphide matrix (20-50% sulphide) to disseminated (0.5% Ni). Massive and sulphide matrix ores are characterized by high pyrrhotite content that often represents the principal separation challenge in flotation of the main Ni mineral, pentlandite. Flotation typically employs combinations of xanthate collector, MIBC frother, soda ash pH modifier (Eltham and Tilyard, 1973; Pietrobon et al., 1997; Fuerstenau and Somasundaran, 2003), carboxy-methyl-cellulose (CMC) dispersant (Sun, 1943; Edwards et al., 1980; Wellham et al., 1992; Hogendam et al., 1998; Bremmel et al., 2005) and sometimes diethylenetriamine (DETA) as pyrrhotite depressant (Xu et al., 1997). Canadian examples are the ores of the Sudbury district, Raglan in northern Quebec and Voisey's Bay, Labrador. Sulphide ores represent the bulk of current supply of nickel and also yield significant by-products such as platinum-group elements (PGE).

Laterites, result from extensive weathering of sulphide ore and the Ni is present in a variety of silicate minerals in a largely iron oxy-hydroxide matrix (Dalvi et al., 2004). The main current processing option is pressure acid leaching (PAL).

As a result of decreasing massive/sulphide matrix ore reserves and the technical challenge and cost of treating laterites, increasing attention is directed to disseminated ultramafic deposits. The name 'ultramafic' reflects the high content of magnesium-iron

silicate gangue minerals (referred to as MgO minerals) derived from weathering of primary minerals such as olivine.

There is several hundred million tonnes of inferred Ni resource in ultramafic hosted rocks in the 'Thompson Nickel Belt' located in north central Manitoba (Dai et al., 2009). This is the deposit of interest in this study. Similar deposits are in northern Quebec, Western Australia, north central China, Zimbabwe and Finland (Mani et al., 1997).

The principal processing problem in common with these potential ores is the presence of high content of MgO minerals of the serpentine family (Three polymorphs are common in the serpentine mineral group – antigorite, lizardite and chrysotile. Three forms of chrysotile are known – clinochrysotile (monoclinic), orthochrysotile (orthorhombic) and parachrysotile (orthorhombic) (Wicks and Whittaker, 1975)). Some of these minerals are fibrous in nature, for example chrysotile, the dominant serpentine mineral in the Thompson area. The fibres produce entanglement and viscous slurries which hamper grinding and the first (rougher) stage of flotation. In cleaner flotation stages, electrostatic interaction between positively charged MgO minerals and the negatively charged major Ni mineral pentlandite is considered to reduce selectivity in the processing of Thompson area ores (Dai et al., 2009). Recent discussions have raised the possibility of positively charge MgO minerals attaching electrostatically to negatively charged bubbles. High rejection of MgO minerals is required to avoid increasing slag melting temperature in Ni smelting.

1.1.2. Research objectives

Given the suspected impact of electrostatic interaction between MgO minerals and pentlandite part of the research focussed on characterizing surface charge of particles and bubbles. The progression is evident in a series of three chapters: Starting with single and mixed minerals, going to bubble swarms and then to bubbles with particles (chapters 3, 4 and 5). To address entanglement, two chapters considered ways to disintegrate the fibres followed by flotation experiments (chapters 6 and 7).

1.1.3. Particle charging

The surface of the solid particle in electrolyte solutions acquires charge by various mechanisms (Hunter, 1991). For most minerals of interest, the main mechanism results from a hydrated surface generated as per Fig. 1.

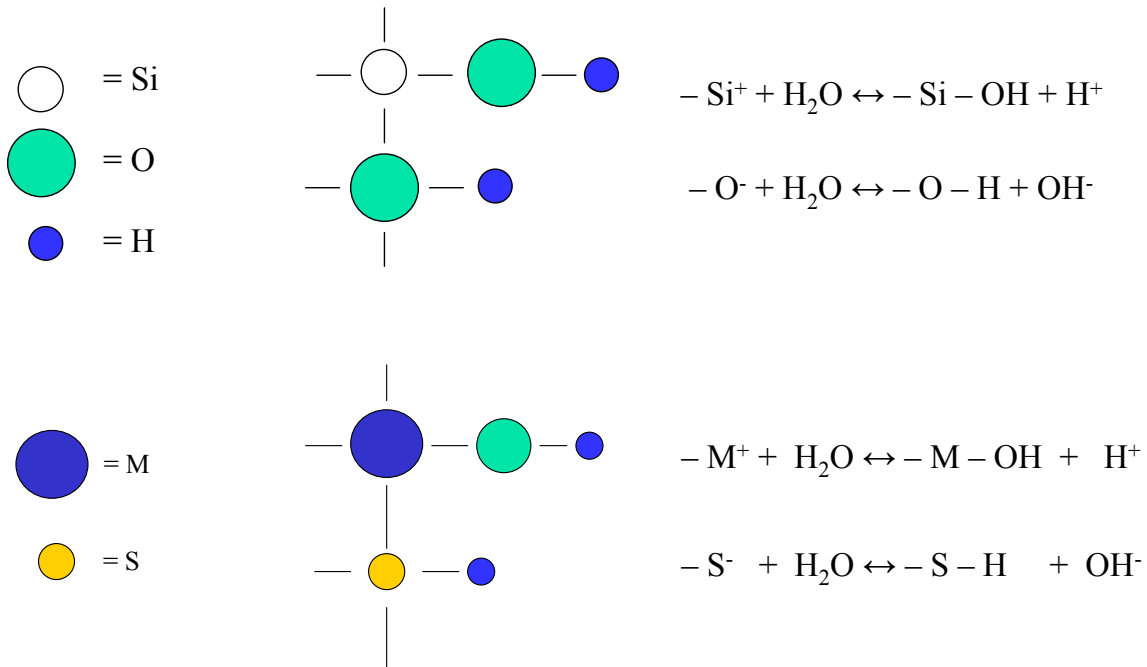
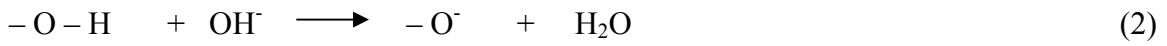


Fig. 1. Surface hydration of silica and metal sulphide (MS)

Generally, hydration products react with H^+ to form positive sites and OH^- to form negative sites. The reactions for silica and metal sulfide are shown below:



Thus the surface is composed of neutral MOH, positive and negative sites and the net charge depends on pH of the suspension. In general, at low pH the surface becomes positive and at high pH it becomes negative. Other surface charging mechanisms include: adsorption or dissociation of lattice ions, ionization or dissociation of surface groups, and isomorphous substitution (predominant in clay minerals).

To sustain electroneutrality of the system, counter ions are attracted to the particle surface. Thus there exists a concentration distribution of counter ions with distance from the surface. Fig. 2(A) illustrates this distribution for a net negative surface charge showing the accumulation of positive (counter) ions on the solution side of the interface which constitutes electrical double layer (EDL). Zeta potential is the potential at the surface of inner layer (sometimes called plane of shear) which approximately coincides with the slip plane when the particle moves relative to the aqueous phase. The pH at which the net electrical charge is zero is called the iso-electric point (iep).

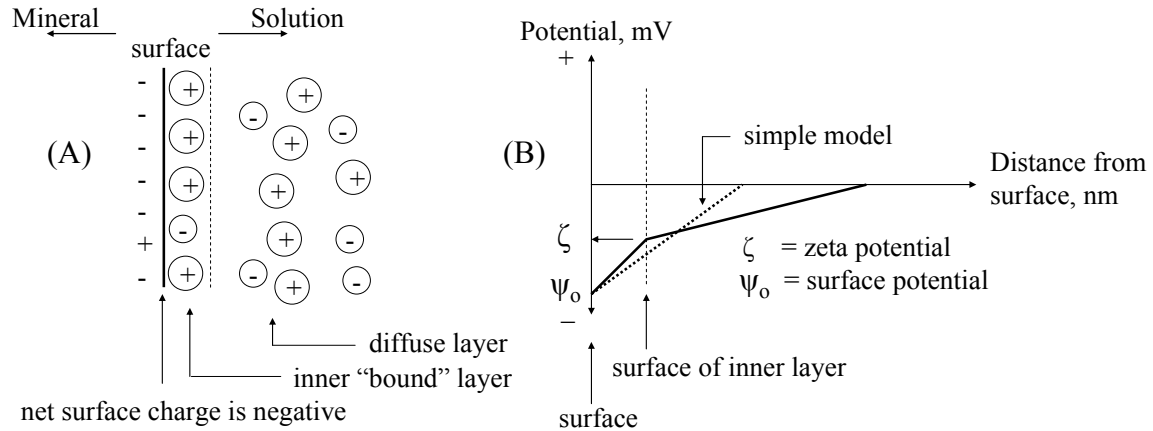


Fig. 2. (A) Electrical double layer and (B) zeta potential

Zeta potential plays an important role in many mineral flotation systems. One example (Fig. 3) is the interaction of goethite ($\text{FeO}\cdot\text{OH}$) with ionic collectors, one with a positive and the other with a negative reactive group. Surface charge of goethite is positive below the iep and the negatively charged sulfonates are electrostatically attracted and held, a physical adsorption process. Consequently, flotation is promoted. Above the iep, the negatively charged goethite surface attracts positively charged aminium-based collector ions and the subsequent physical adsorption promotes flotation in this pH range. Due to electrostatic repulsion the effect of sulfonate collector below the iep and the amine above iep is negligible (Iwasaki et al., 1960).

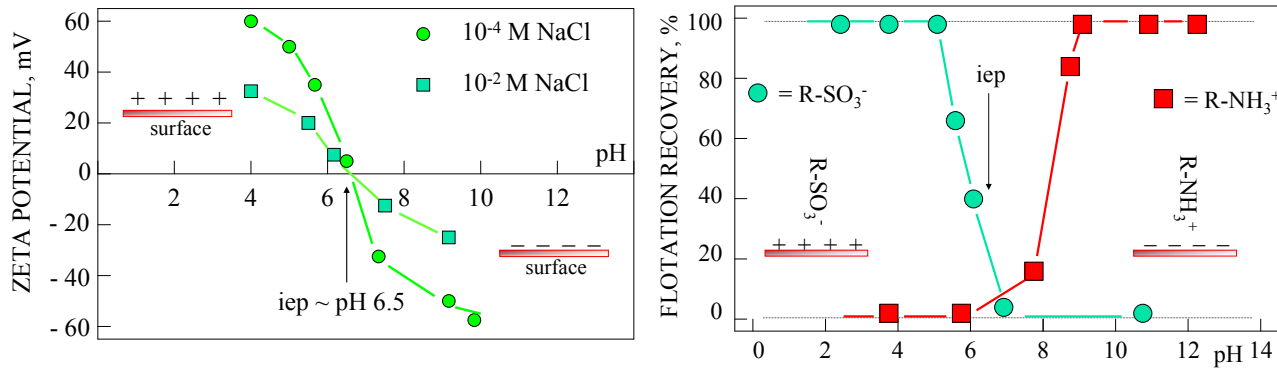


Fig. 3. (Left) Zeta potential of goethite as a function of pH and (Right) flotation recovery of goethite as function of pH with sulfonate, $R-SO_3^-$ and amine, $R-NH_3^+$ collector types

For surface charge characterization an integrated device has been developed to measure sedimentation potential, conductivity, pH and volume fraction of solid on-line. Instrument control, data acquisition and data processing were performed by a program developed in this study using Matlab R2008a. To validate, zeta potential was calculated for single mineral systems using Smoluchowski equation and compared with electrophoresis measurements. The device went through three evolutions.

The first extension of the technique (chapter 3) was into mixed but gravity separable alumina/silica systems. Sufficient column height along with size difference between the two minerals allowed gravity fractionation during settling. Sedimentation potential was measured over time and correctly identified the transition from one mineral to the next. Analytical techniques were used to interpret the measurements and a correlation between surface charge and sample composition was found.

The second extension was to try to characterize non-separable mixed system, the ultramafic ore (chapter 6). To probe the surfaces, use was made of EDTA (ethylenediaminetetraacetic acid). As a chelating agent, it can remove adsorbed positively

charged metal ions from the surface ‘cleaning’ the surface to expose more negative sites. As a weak acid, EDTA may reduce Mg/Si ratio at the interface by extracting Mg (Park et al., 2003).

1.1.4. Bubble charging

Electrical charge at the gas-liquid interface may play a role in flotation contributing to particle-bubble and bubble-bubble interactions. Over most of the pH range (> pH 3-4) the bubble surface is negatively charged. The commonly considered charging mechanisms are: preferential orientation of the water dipoles with hydrogen towards the water, which attracts anions to the interface (Alty, 1926); and adsorption of OH^- ions to satisfy hydration energy (Yoon and Yordan, 1986; Kim et al., 2000). The presence of many solute ions can influence bubble surface charge. Measurement of bubble charge has helped understand the bubble interaction with certain collectors and inorganic ions in flotation systems (Usui and Sasaki, 1978; Li and Somasundaran, 1991).

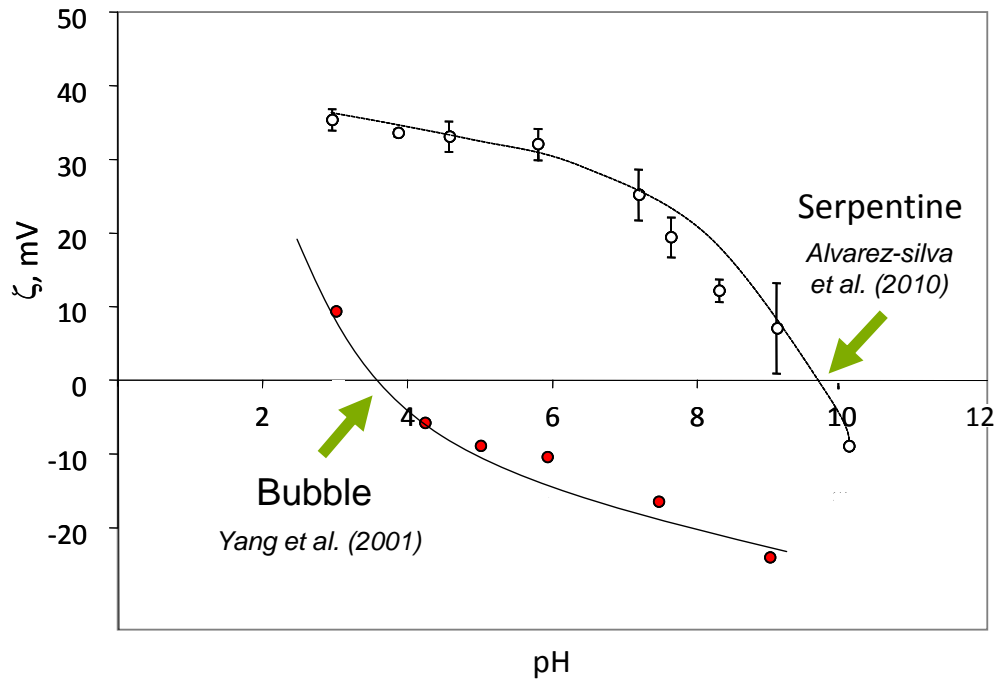


Fig. 4. Zeta potential as a function of pH for serpentine and gas bubbles

Consequently, the particle sedimentation potential (PSP) setup was modified to measure bubble sedimentation potential (BSP) in a system approaching flotation condition which requires:

- 1) Swarm of bubbles
- 2) Bubbles of size (diameter) ca. 0.5 – 2.5 mm
- 3) Presence of commercial surfactants, collectors and frothers
- 4) Presence of metal ions such as Mg

The modified apparatus allowed in-process measurement of the system variables associated with surface electrical charge, i.e. solution conductivity, gas holdup, pH and bubble size distribution.

Attachment of hydrophobic particles is the dominant recovery process in flotation but other interactions may be at play, for example electrostatic, which depends on the electrical charge on bubbles and particles (Mayers, 1991). The possibility of electrostatic interaction in recovery of chrysotile was stimulated by recent efforts to process Thompson area ultramafic Ni-ore (Xu et al., 2011) (Fig. 4). In this regard, further adaptation of the technique to measure BSP in presence of particles is discussed in chapter 5. The technique introduces a direct way to investigate bubble-particle interactions under flotation-like conditions to reveal non-hydrophobic attachment. To augment the BSP data visual inspection of a pendant bubble exposed to agitated suspensions is included.

1.2. References

- Alty, T., 1926. The origin of the electrical charge on small particles in water. Proceedings of the Royal Society of London, Series A, vol. 122 (760), pp. 235–251.
- Alvarez-Silva, M., Uribe-Salas, A., Mirnezami, M., Finch, J. A., 2010. The point of zero charge of phyllosilicate minerals using the Mular–Roberts titration technique. *Miner. Eng.*, 23, 383 – 389.
- Bremmel, K. E., Fornasiero, D., Ralston, J., 2005. Pentlandite-lizardite interactions and implications for their separation by flotation. *Colloid Surface A*, 252, 207 – 212.
- Dai, Z., Bos, J-A. Quinn, P., Lee, A., Xu, M., 2009. Flowsheet development for thompson ultramafic low-grade nickel ores, in: Gomez, C. O.; Nasset, J. E.; Rao, S. R. (Eds.), *Proc. Advances in Mineral Processing Science and Technology. Conference of Metallurgists, CIM, Sudbury, Ontario*, pp. 217 – 228.
- Dalvi, A. D., Bacon W.G., Osborne, R. C., 2004. The past and the future of nickel laterites. In: *Proceedings of PDAC International Convention, Toronto, 2004*.
- Edwards, G.R., Kipkie, W. B., Agar, G. E., 1980. The effect of slime coating of the serpentine minerals, chrysotile and lizardite on pentlandite flotation. *Int. J. Miner. Process.*, 7, 33 – 42.

- Eltham, J. A., Tilyard, P. A., 1973. An approach to the flotation of Western Australian nickel ores. In: Proceedings of the AusIMM Conference, WA, pp. 417 – 429.
- Fuerstenau, M. C., Somasundaran, P., 2003. Flotation, in: Fuerstenau, M. C., Han, K. N., (Eds.), Principles of Mineral Processing. SME, Colorado, pp. 245.
- Hogendam, C. W., de Keizer, A., Cohen, M. A., Bijsterbosch, B. H., 1998. Adsorption mechanisms of carboxymethyl cellulose on mineral surfaces. *Langmuir*, 14, 3825 – 3839.
- Hunter, R. J., 1991. Foundations of Colloid Science, Vol. 1, Claredon Press, Oxford, pp. 374.
- Iwasaki, I., Cooke, S.R.B. and Colombo, A.F., 1960. The flotation characteristics of goethite. U.S. Bureau of Mines R.I. 5593.
- Li, C., Somasundaran, P., 1991. Reversal of bubble charge in multivalent inorganic salt solutions – effect of magnesium. *J. Colloid Interf. Sci.* 146, 215–218.
- Mani, H, Xu, M., Quinn, P., Stratton-Crawley, R., 1997. The effect of ultramafic mineralogy on pentlandite flotation, in: Finch, J. A., Rao, S. R., Holubec, I. (Eds.), Proc. Processing of Complex Ores, Conference of Metallurgists, CIM, Sudbury, Ontario, 1997, pp. 63 – 76.
- Myers, D., 1991. Surfaces, Interfaces, and Colloids: Principles and Applications. VCH Publishers, Inc., New York, pp. 69–84.
- Park, A-H. A., Jadhav, R., Fan, L-S., 2003. CO₂ mineral sequestration: chemically enhanced aqueous carbonation of serpentine. *Can. J. Chem. Eng.*, 81, 885 – 890.
- Pietrobon, M. C., Grano, S. R., Sobieraj, S., Ralston, J., 1997. Recovery mechanisms for pentlandite and MgO bearing gangue minerals in nickel ores from Western Australia. *Miner. Eng.*, 10, 775 – 786.
- Schechter, R.S., Graciaa, A., and Lachaise, J., 1998. The electrical state of a gas/water interface. *J. Colloid Interf. Sci.* 204, 398–399.
- Senior, G. D., Thomas, S. A., 2005. Development and implementation of a new flowsheet for the flotation of a low grade nickel ore”, *Int. J. Miner. Process.*, 78, 49 – 61.
- Sun, S. C., 1943. The mechanism of slime coating. *Trans. AIME*, 153, 479 – 492.
- Trahar, W. J., 1981. A rational interpretation of the role of particle size in flotation. *Int. J. Miner. Process.*, 8, 289 – 327.

- Usui, S., Sasaki, H., 1978. Zeta potential measurements of bubbles in aqueous surfactant solutions. *J. Colloid Interf. Sci.* 65, 36–45.
- Wellham, E. J., Elber, L., Yan, D.S., 1992. The role of carboxy methyl cellulose in the flotation of a nickel sulphide transition ore. *Miner. Eng.*, 5, 381 – 395.
- Wicks, F. J., Whittaker, E. J. W., 1975. A reappraisal of the structures of the serpentine minerals. *Can. Mineral.*, 13 (3), 227–243.
- Xu, Z., Rao, S. R., Finch, J. A., Kelebek, S., Wells, P., 1997. “Role of Diethylenetriamine (DETA) in Pentlandite-pyrrhotite Separation: I. Complexation of Metals with DETA”, *Trans. IMM: Sect. C*, 106, C15–C20, 1997.
- Yang, C., Dabros, T., Li, D., Czarnecki, J., Masliyah, J.H., 2001. Measurement of the zeta potential of gas bubbles in aqueous solutions by microelectrophoresis method. *J. Colloid Interf. Sci.* 243, 128–135.
- Xu, M., Scholey, K., Marcuson, S., 2011. Vale-Cytec-University Research Consortium on Processing Low Grade Ultramafic Nickel Ore. Conference of Metallurgists (COM), 2011, Montreal, Canada.

2. Literature Review

2.1. Surface charge characterization: particles

Zeta potential measuring instruments have been designed to determine the variables to calculate zeta potential using appropriate theories. The various techniques have their advantages and disadvantages and their performance varies widely depending on the system of interest. The approaches can be summarized in Fig. 1.

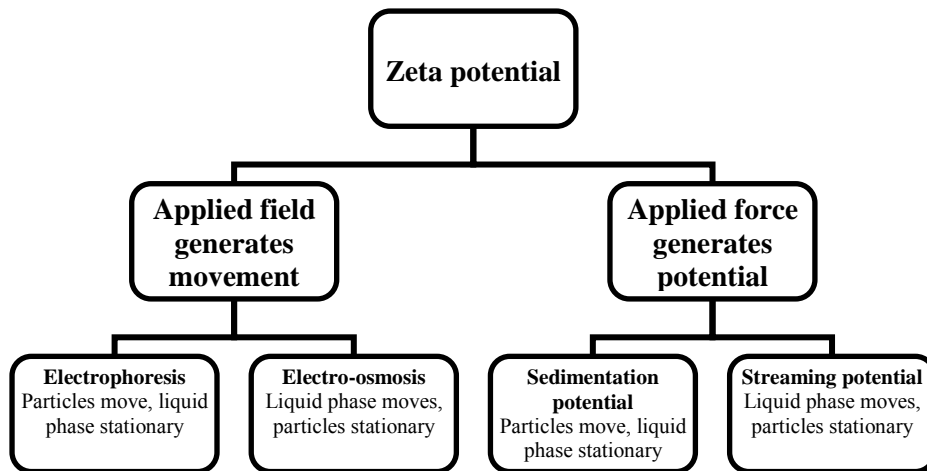


Fig. 1. Summary of approaches to measure zeta potential

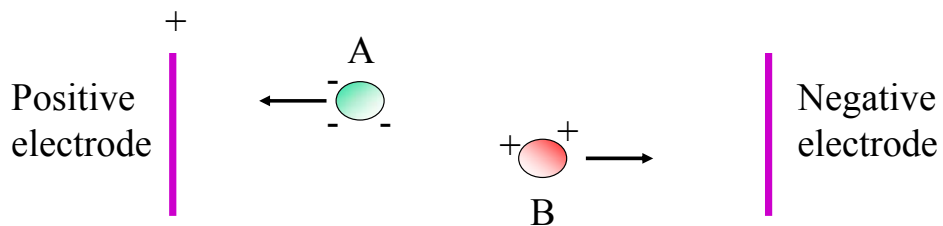


Fig. 2. Movement of charged particles (A and B) in an electric field

2.1.1. Electrophoresis

Movement of a charged particle relative to a medium due to an external field is known as electrophoresis. Direction of motion gives the sign of the surface charge and velocity gives its magnitude. This is illustrated in Fig. 2.

Based on the assumption of thick double layer, $\kappa a \ll 1$, Huckel (1925) proposed the following relationship between electrophoretic velocity and zeta potential (see nomenclature):

$$\vec{v}_e = \frac{2}{3} \frac{\epsilon_r \epsilon_0}{\eta} \zeta \vec{E}_{app} \quad (1)$$

This can, also, be expressed in terms of electrophoretic mobility, $\mu_e (= \frac{\vec{v}_e}{\vec{E}_{app}})$:

$$\mu_e = \frac{2}{3} \frac{\epsilon_r \epsilon_0}{\eta} \zeta \quad (2)$$

There are several techniques of determining zeta potential through measurement of electrophoretic mobility. Among the early methods, moving boundary (Tison, 1977) and mass transport electrophoresis methods (Homola and Robertson, 1975) paved the way for the current commercial techniques. The most widespread electrophoresis method is micro-electrophoresis which involves direct tracking of moving particles under a force field with an optical system.

However, due to its manual nature (i.e. visual tracking) the method can be biased (James, 1979). Automatic tracking of particles is also possible today using video camera and digital image processing. Regardless, due to electro-osmotic flow near the container (cylindrical or rectangular) wall, electrophoretic velocity formulation has to be corrected by knowing the flow profile (Oka and Furusawa, 1998). Moreover slurries should be

sufficiently diluted (0.1%v/v) and monodisperse for visual observation of moving individual particles i.e. the system is far moved from its condition to flotation systems.

2.1.2. Streaming potential

Flow of electrolytic solution over a stationary particle sample creates imbalance of charge distribution in the diffuse layer by piling up charge in the flow direction. Samples can be sandwiched between two flat plates or packed in a porous plug. The accumulation of ions causes a potential difference called the streaming potential (Fig. 3). The relationship between streaming potential and zeta potential is given below (Christoforou et al., 1985).

$$\frac{E_{str}}{\Delta P} = \frac{\varepsilon_r \varepsilon_0 A}{\eta L \lambda} \zeta \quad (3)$$

This technique is especially suitable for coarse material with high settling velocity. It has been shown that streaming potential can influence the velocity profile by an electro-viscous effect which was not taken into account in the formulation of equation 3 (Erickson and Li, 2001). One way of resolving the problem is by measuring streaming current rather than streaming potential. But the streaming current can be as low as 1 nA/kPa which is difficult to measure accurately using available instruments (Werner et al., 1998). The formulation also assumes fully developed and irrotational flow which has to persist during the measurement.

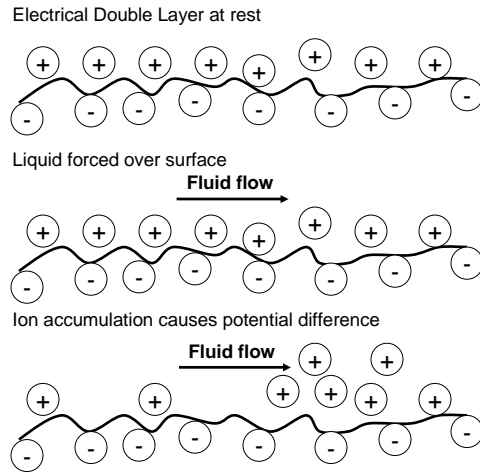


Fig. 3. Generation of streaming potential

2.1.3. Electro-osmosis

This is somewhat the reverse of the streaming potential technique. When an external electric field is applied between two points of an electrolyte solution in contact with a solid surface, the electric force imparts motion to the ions in the diffuse layer (Fig. 4). The moving ions drag liquid, which is known as electro-osmotic flow, and the phenomenon is called electro-osmosis (Dukhin and Derjaguin, 1974). The electro-osmotic velocity can be related to zeta potential, as follows (Hunter, 1981):

$$\vec{v}_{eo} = -\frac{\epsilon_r \epsilon_0}{\eta} \zeta \vec{E}_{app} \quad (4)$$

A major difficulty with this technique is to control and measure the electro-osmotic flow which could be as low as $\sim 10^{-2}$ cm³/s (Hsieh, 2006). The flow is very sensitive to the chemistry of the system which is easily affected by small changes in solution pH, ionic strength and dielectric constant. Moreover, this method is susceptible

to the same problems associated with streaming potential technique due to the similarities in principle.

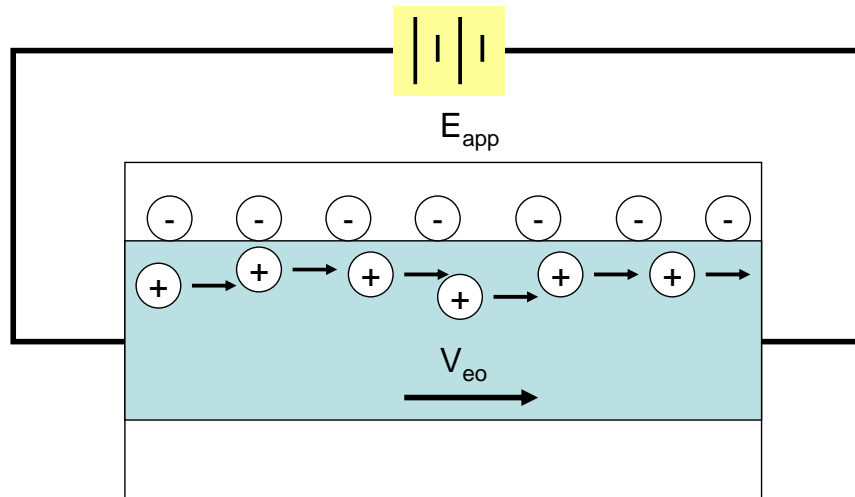


Fig. 4. Generation of electro-osmotic flow by applied potential

2.1.4. Sedimentation potential

Sedimentation potential is the potential difference that arises when charged particles settle in a force field (usually gravity). Charge destabilization created by the fluid drag surrounding each falling particle induces numerous dipoles in the suspension. These individual dipoles sum to produce the macroscopic potential difference between two points in a column. This phenomenon was first discovered by Dorn (1880) and is often called the “Dorn effect” (Booth, 1956; Saville, 1982). Fig. 5 describes the principle.

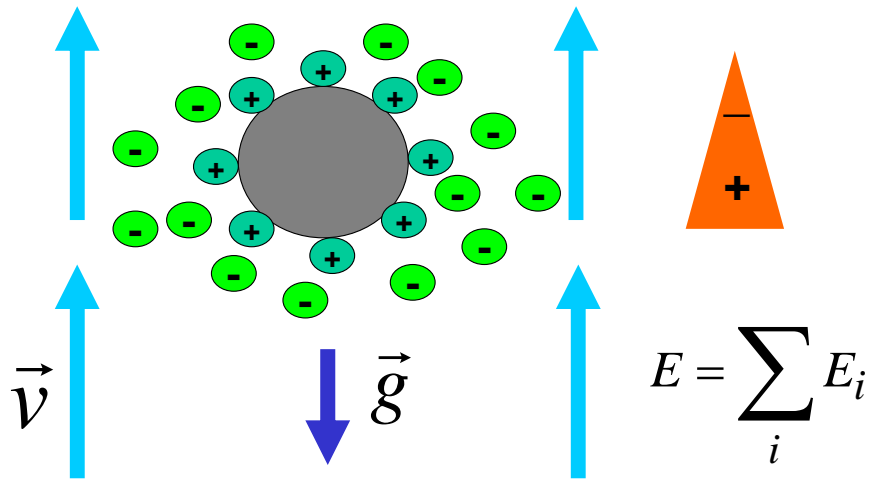


Fig. 5. Schematic presentation of sedimentation potential generation

After Dorn's discovery, several attempts were made to determine zeta potential of colloidal suspensions using sedimentation potential. In the early works (Quist and Washburn, 1940; Moza and Biswas, 1976), the slurries were prepared in a separate container and then allowed to fall through the settling tube and the consequent potential difference was measured using two electrodes set a distance apart in the tube. In more recent work, Ozaki et al. (1999) introduced a rotating column to eliminate drift and/or lack of symmetry of the measuring electrodes. The technique requires knowledge of the volume fraction of solids, which these methods either assumed or calculated assuming uniform particle flow during settling. Marlow and Rowell (1985), using turbidity, were the first to report in-situ volume fraction measurement. All the previous work also measured the conductivity of the medium and pH separately.

The sedimentation potential method has some advantages over other techniques of zeta potential measurement. It is applicable to more concentrated systems where %solid

can exceed 2%v/v compared to electrophoresis which cannot handle more than 0.1%v/v solid. The data can be related to visual records of dispersion or aggregation and the technique is applicable to mixed particle systems. These are the unique features that make the method suitable to apply in mineral processing.

The present work approaches an integrated technique to determine zeta potential by an in-process measurement of all the system variables using sedimentation potential method. The technique was verified on single minerals and then extended to characterize surface charge of mixed particle systems including ultramafic ore.

2.1.5. Electro-acoustic method

In a similar fashion to sedimentation potential, created by the distortion of electrical double layer (EDL) in an external force field (i.e. gravity), deformation of the ionic atmosphere under an acoustic field can generate a potential called colloid vibration potential (CVP) or a current known as colloid vibration current (CVI).

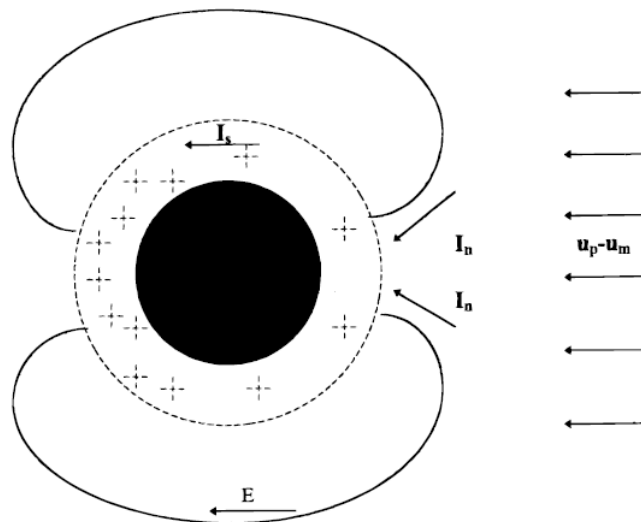


Fig. 6. Generation of dipole in an applied acoustic field (Dukhin et al., 2000)

It is assumed that the particle and the medium have a different density which is essential to induce relative motion by the acoustic field. Fig. 6 shows a negatively charged particle surrounded by positive counterions. Due to relative motion positive ions near the left particle pole increase in concentration compared to the right particle pole (in this example). The result is an induced dipole moment, positive on left pole and negative on the right. Booth and Enderby (1952) were the first to derive the expression that relates CVP to zeta potential under the assumptions of dilute suspension, non-conducting particles, low zeta potential and thin double layer. It is valid quantitatively for particles less than 300 nm:

$$CVP = \frac{2\phi\Delta P}{K_s} \frac{\rho - \rho_0}{\rho_0} \frac{\varepsilon_r - \varepsilon_0}{\eta} \zeta \quad (5)$$

Later, numerous works have extended the model to concentrated polydisperse colloid (Zharkikh and Shilov, 1981; Dukhin et al., 1999), conductive surfaces (Dukhin et al., 2000) and thick double layers (Shilov et al., 2004).

The commercial zeta potential and particle size analyzer based on electro-acoustic method, The AcoustoSizer IIs™ by Colloidal Dynamics Inc., claims to measure as high as 40%v/v solid with size range 0.02–10 μm. This method of measuring zeta potential has been established over a long period of time, as noted above. The sedimentation potential method has been far less explored.

2.2. Flotation

Flotation is commonly successful with massive/sulphide matrix ores but less so with the ultramafic ones. Low recovery of Ni and high MgO in the concentrates are commonly reported. Three possible factors were considered that can adversely affect flotation.

First, positively charged fine (less than 10 μm) MgO mineral particles (or more precisely positive sites on the MgO mineral particle surface) can be electrostatically attracted and adsorbed on negative Ni sulphide particles. This phenomenon is known as 'slime coating' which acts as a barrier for the collectors to be adsorbed on sulphides or attachment to bubbles or dilutes the concentrate when partially coated sulphides are recovered (Sun, 1943; Edwards et al., 1980).

One way to solve this problem is by using a dispersant, Carboxy Methyl Cellulose (CMC) which has preferential adsorption capability on MgO mineral both physically and chemically (Wellham et al., 1992; Hogendam et al., 1998). It alters the surface charge to become negative and suppresses the slime adsorption on the negatively charged Ni sulphides. Using CMC, Bremmel et al. (2005) improved Ni recovery in a system containing MgO minerals.

Physical removal of slime from the system can also improve flotation response. From extensive laboratory and plant flotation data, Trahar (1981) suggested separate treatment for sized fractions especially for ores hard to process. Using this concept, Senior and Thomas (2005) improved the recovery of Mt Keith's serpentine rich Ni ore by implementing a size-based flotation strategy. They used hydro-cyclones to classify the feed into three size fractions. This allowed them to vary feed rate and flotation conditions

depending on the physical and chemical nature of the particular size fraction. Using hydro-cyclones in a mini flotation circuit, Dai et al. (2009) showed an increase in Ni recovery and reduction of MgO in concentrates when processing Thompson area ultramafic ore. They concluded that the fine particles rejected to the cyclone overflow were responsible for slime coating. This ‘desliming’ process, though effective incurred considerable Ni loss (3.6% – 12.9%) to the overflow.

Flotation selectivity between pentlandite and pyrrhotite is another important issue processing Ni ores which is sensitive to pulp potential (Cheng et al., 1999). Flotation with xanthate collectors can involve dixanthogen formation by anodic oxidation of xanthate ion on the minerals and the cathodic reduction of oxygen (Majima and Takeda, 1968; Woods, 1976; Usul and Tolun, 1974):



Dixanthogen promotes pyrrhotite flotation (unwanted mineral in sulphide ore). Its formation is favoured at high pulp potential which is associated with sufficient dissolved oxygen in the pulp and/or pH below ca. 11 (Fuerstenau and Somasundaran, 2003). In oxygen deficient systems or at high pH the pyrrhotite rest potential is lower than the equilibrium potential for dixanthogen formation (Khan and Kelebek, 2004). Soda ash is commonly used to adjust the pH around 10 to assist selective flotation of pentlandite as the CO_3^{2-} ion provides additional benefit of sequestering Ca and Mg ions that can interfere with pentlandite flotation.

Operating at ca pH 10 also decreases the electropositivity of serpentine and reduces electrostatic attraction to sulphides. This pH may even act as a dispersant which improves separation efficiency (Eltham and Tilyard, 1973). Pietrobon et al. (1997) found a synergy between soda ash and CMC to give the best flotation recovery of pentlandite of Western Australian Ni ore containing MgO-bearing gangue minerals. Based on the above literature, a test procedure was adopted and referred to as ‘conventional sulphide flotation’. Results were subsequently compared with the procedure based on fibre disintegration developed in this study. The conventional laboratory test flowsheet is shown in Fig. 7.

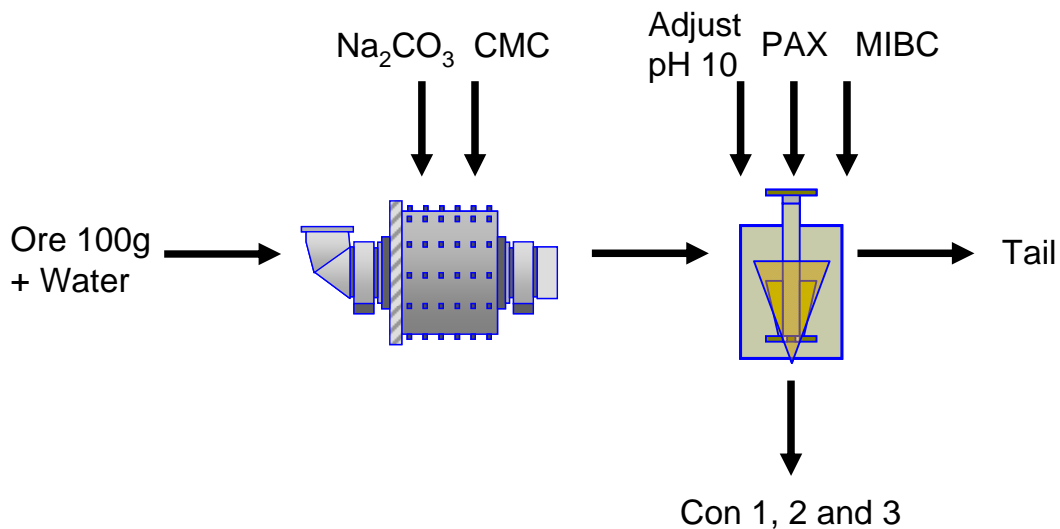


Fig. 7. ‘Conventional’ flotation procedure

In the basic pH range, adsorbed ionic species form thermodynamically stable positively charged metal hydroxides (Pugh and Tjus, 1987; Oliveira and Torem, 1996). In theory, negatively charged xanthate (collector) ions could electrostatically (or sometimes chemically) interact with these positive sites and cause flotation of otherwise hydrophilic

gangue minerals, a form of accidental activation. In recent work, Fornasiero and Ralston (2005) showed evidence of this mechanism in the case of lizardite (one of the polymorphs of serpentine) and chlorite by Cu and Ni ions in the pH region between 7 and 10. The presence of adsorbed ionic species was verified in this study using EDTA. Ethylenediaminetetraacetic acid (EDTA) is a strong chelating agent for a large number of metallic ions. It forms soluble complex compounds with metal atoms by stable coordinate bonding (Rao and Leja, 2003a).

The third possible cause of poor flotation response of ultramafic ores explored in this study is 'entanglement'. Physical entanglement of the fibrous serpentine with the sulphide particles reduces separation efficiency. High entanglement density also increases pulp viscosity which in turn inhibits bubble motion and bubble-particle mixing. In this study, 'entanglement' was countered using a fibre disintegration approach.

2.3. Fibre disintegration

The most prevalent polymorph of serpentine in the Thompson area ultramafic ore is chrysotile with idealized chemical composition $Mg_3Si_2O_5(OH)_4$. It comprises sheets of brucite (magnesium hydroxide) covalently bonded to sheets of tridymite (polymorph of quartz). The mismatch in spacing between Mg and Si atoms makes chrysotile curl into hollow tube-like fibres (Brindley and Brown, 1980; Wypych et al., 2005). The structure is shown schematically in Fig. 8.

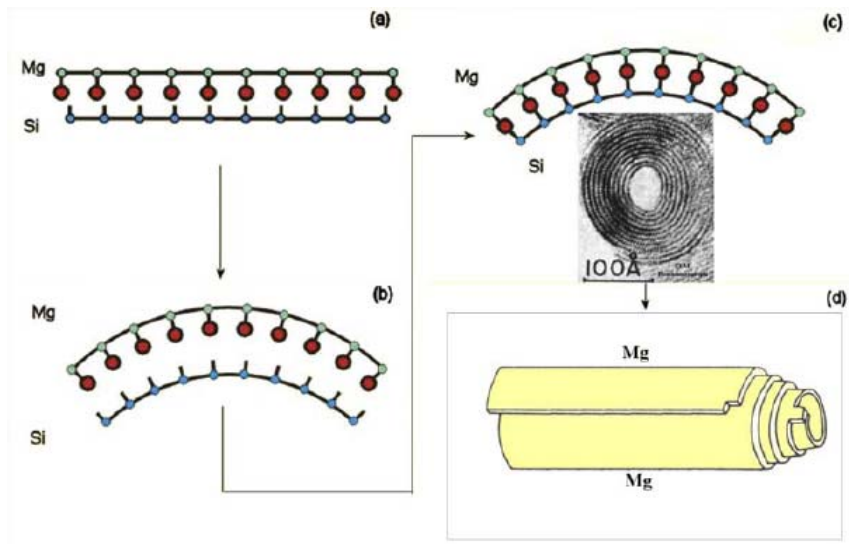
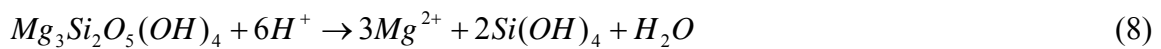


Fig. 8. Chrysotile fibre structure (Bernstein and Hoskins, 2006)

Recently, serpentine-rich ores have been investigated for CO₂ sequestration (Seifritz, 1990; Park and Fan, 2004; Fujii et al., 2010). By acid leaching, Mg can be removed from the brucite layer:



The conceptual process is shown in Fig. 9.

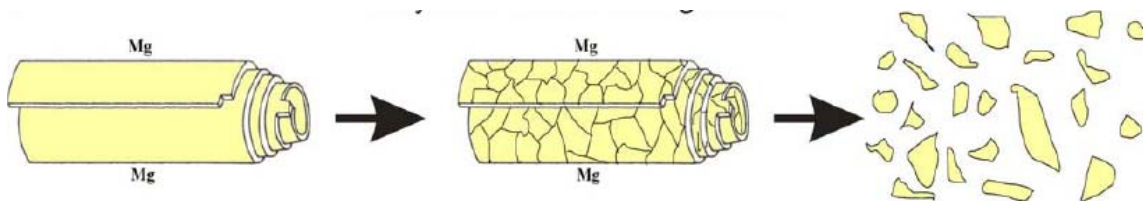
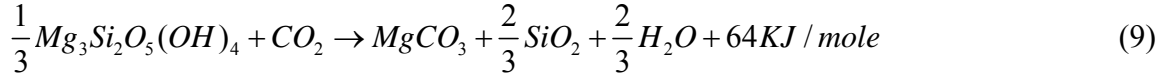


Fig. 9. Chrysotile fibre disintegration by acid attack (Bernstein and Hoskins, 2006)

The released Mg is then available to react with CO₂ to form environmentally benign and stable MgCO₃.



The remaining structure after leaching consists of hydrated amorphous silica without elasticity and dimensional stability that can be easily broken mechanically (Hargreavass and Taylor, 1946; Stumm, 1992). Park and Fan (2004) showed that the extraction of Mg is enhanced by combining acid attack with grinding which facilitates the exposure of the inner Mg layers to the acid. The combination leads to a possible treatment to effect fibre disintegration prior to flotation.

In the first flotation strategy, we used HCl (as used by Park and Fan (2004)) attack in a ceramic grinding mill. A factor that also impedes reaction is precipitation of the leached metal Mg ions. A strong chelating agent such as EDTA was considered to retard formation of precipitated layers and promote dissolution.

In the second flotation approach, we examined H₂SO₄ which is arguably the practical option, the acid being widely available as part of SO₂ abatement at smelters.

In the case of HCl, the slurry pH naturally rose with time allowing the addition of soda ash and the setting of other conditions typical of Ni sulphide ore flotation. This was not the case with H₂SO₄, the slurry remaining buffered at low pH (ca. 2). Although, xanthate collectors tend to decompose at low pH (Iwasaki and Cooke, 1958), it opened the possibility of collectorless flotation. Heiskanen et al. (1991) found that pentlandite (along with pyrrhotite) floated collectorlessly at pH 3-5. Sulphuric acid provides the oxidizing conditions to promote formation of polysulphide (metal deficient sulphide) and elemental sulphur which are the responsible hydrophobic species for collectorless flotation (Heyes and Trahar, 1977; Gardner and Woods, 1979; Rao and Leja, 2003b). The

oxidization (anodic) reactions are represented in (10) and (11) with oxygen acting as electron acceptor to provide the reduction (cathodic) reaction (12) and complete the redox couple. At the same time, the low pH prevents released metal ions from precipitating as hydroxides which can depress flotation (i.e. there is no need to consider EDTA).

Anodic reactions:



Cathodic reaction:



Another potentially useful outcome is that released Mg^{2+} ions may increase the ionic strength of the pulp liquor sufficient to inhibit bubble coalescence (Craig et al., 1993; Hofmeier et al., 1995; Laskowski et al., 2003) and reduce bubble size, normally the function of adding frother. It has been shown that an ionic strength > 0.4 gives similar bubble size and flotation response as ca. 10 ppm MIBC (methyl-iso-butyl-carbinol), a typical sulphide flotation plant frother and dosage (Quinn et al., 2007). The proposed treatment using sulphuric acid, therefore, may not only disintegrate fibres but produce a flotation environment requiring no collector or frother.

2.4. Surface charge characterization: bubble swarms

The first apparatus to measure charge on bubbles was a spinning tube device (McTaggart, 1922 and Alty, 1926) used to measure the electrophoretic mobility of gas

bubbles in aqueous solution. Bubbles generated at a capillary were injected into the axis of a rapidly rotating horizontal glass tube with both ends sealed by metal electrodes. The velocity of the bubbles along the axis was measured as a function of applied voltage. An objection is that an electric field applied along a charged wall generates a secondary flow due to electro-osmosis (Masliyah and Bhattacharjee, 2006) which corrupts bubble motion (Back and Gilman, 1938; Hsieh et al., 2006).

Improvements to the spinning tube technique were proposed by Graciaa and co-workers (Graciaa et al., 1995; Saulnier et al., 1996) from both experimental and theoretical perspectives. For example, charges at the glass-liquid interface were neutralized by depositing a polymeric material, diethylaminoethyl-dextran, and the model proposed by Sherwood (1986) for electrophoresis of gas bubbles in rotating fluid was used to calculate zeta potential.

The common approach to determining bubble charge is adapting the micro-electrophoresis technique used for particles. There are various approaches to introduce single or multiple bubbles (sub-100 μm) into a cell and visually track their motion in response to applied electric field. Small cells are used (ca. 500 mm^3) to reduce convection and measurements have to be taken precisely at the stationary plane (zero electro-osmotic velocity). Larger cells (10 x 10 x 25 cm) have been used, but they restrict measurement time to ca. 0.5 s due to convection effects (Sirois and Miller, 1973).

One of the earliest micro-electrophoretic apparatus for bubbles was developed by Collins et al. (1978). They generated bubbles by electrolysis from the tip of a thin platinum wire. Subsequent versions include: pressure-release to produce fine bubbles (Kubota et al., 1983); suspensions of bubbles (40-80 μm) flowed continuously through

the cell (Yoon and Jordan, 1986); and tracking bubbles at the stationary plane using a movable stage (Yang et al., 2001).

Techniques based on electrophoresis impose certain limitations: bubble size has to be fine ($< 50 \mu\text{m}$ preferred) to distinguish motion due to the electric field from buoyancy; single bubbles are tracked one at a time; measurements depend on operator's ability to keep the bubble in the field of view; and depth of field of view can be important especially when conditions are close to the iep where bubbles move slowly. Often zeta potential is quoted based on models developed for solid particles which do not strictly apply as bubbles are not rigid and are subject to distortion. This probably contributes to the variation in magnitude of reported bubble zeta potential (e.g. from 35 mV to 120 mV at pH 10 (Elmahdy, 2008; Takahashi, 2005)) and in iep (from pH 1.5 to 3.5 for inert gases (Li and Somasundaran, 1991; Yang et al., 2001)).

To relate the findings to flotation, however, the main objection is that flotation employs swarms of bubbles roughly 0.5 to 4 mm in diameter (Gorain et al., 1995). An argument can be advanced that it is prudent to measure bubble electrical charge under conditions that resemble flotation for the results to be applied with confidence.

Some work has been done under flotation-like conditions. Dibbs et al. (1974) measured the streaming current of bubble swarms in a water column in presence of inorganic electrolytes and dodecylamine hydrochloride (a cationic collector) using the results to interpret flotation of quartz. Usui and Sasaki (1978) measured swarm sedimentation potential to estimate bubble zeta potential in presence of ionic and nonionic surfactants. Neither approach was compared against other techniques to validate. One reason may be that converting sedimentation potential to zeta potential is

not straightforward (Dukhin, 1966; Hunter, 1981), which may also have contributed to the dependence of zeta potential on bubble size noted by Usui et al. (1981).

Sedimentation potential is a relatively simple yet powerful technique to characterize bubble surface charge. As no electric field is applied, there is no electro-osmosis. Sedimentation potential itself, without conversion to zeta potential, can provide valuable information regarding iep and interaction with solute species. The measurement system can be made to approach flotation in terms of bubble size distribution, gas holdup, and solution conductivity. This is a particular attraction for our purposes which include the eventual presence of particles. The disadvantage is that there is no commercial instrument available.

In this study we introduce a novel integrated apparatus that allows in-process measurement of all system variables related to bubble surface charge: sedimentation potential, solution conductivity, gas holdup, pH and bubble size distribution. To distinguish from our prior work using sedimentation potential for particles (Uddin et al., 2010) we will refer to bubble sedimentation (or swarm) potential as BSP. To validate, the iep in de-ionized water determined when BSP is zero was compared with literature values. The technique was then used to characterize bubble surface charge in the presence of non-ionic frothers, ionic collectors, and inorganic salts.

2.5. Surface charge characterization: bubbles in presence of particles

The possibility of an electrostatic origin of bubble-particle attachment in flotation systems has been entertained periodically. Dibbs et al. (1974) measured zeta potential of quartz and the streaming current of gas bubbles. Results were correlated with flotation

recovery of quartz with the cationic collector dodecylamine hydrochloride (DAC). Flotation recovery was found to increase as the streaming current was increased to more positive values by changing pH which was interpreted as due to increased attraction to the negatively-charged quartz particles. Cichos (1973) used the rotating tube method (McTaggart, 1922) to try to correlate flotation with the zeta potential of bubbles and particles. Collins and Jameson (1977) related flotation recovery of polystyrene particles in CTAB (cetyltrimethylammonium bromide) to electrophoretic mobility of the bubbles and particles. The flotation rate constant was found to decrease significantly as the positive charge on both bubbles and particles was increased, explained by double-layer repulsion. Similar findings were made by Fukui and Yuu (1980). Okada et al. (1990) measured the charge on bubbles and fine latex particles using a micro-electrophoresis apparatus under various experimental conditions and found that flotation efficiency was strongly influenced by the charge on bubbles and particles. Fan et al. (2003) studied the attachment of quartz particles with air bubbles in de-ionized water. The quartz particles attached to air bubbles and attachment increased with increasing pH even though both bubbles and particles were negatively charged. The proffered explanation was hydrogen bonding between OH^- on bubbles and either the oxygen atoms of the quartz or adsorbed OH on the quartz. Johnson et al. (2009) using AFM (atomic force microscopy) measurements, showed a long range repulsive force between silica glass bead and a micro-bubble in presence of anionic sodium dodecyl sulphate (SDS) and an attractive force in presence of cationic dodecyl trimethylammonium bromide (DTAB). Bubble charge reversal was observed with DTAB which correlated with the much higher bead recovery (99.5%) with DTAB than with SDS (6.4%).

There is no literature apparent describing measurement of bubble electrical charge in the presence of particles. In the current study, the bubble sedimentation (swarm) potential (BSP) apparatus (Uddin et al., 2011) is modified to measure BSP in the presence of particles.

2.6. Nomenclature

Symbols	Meaning	Units
E_s	Sedimentation potential	Volt/m
ζ	Zeta potential	Volt
η	Viscosity of suspension	Pa-sec.
η_0	Viscosity of medium	Pa-sec.
λ	Specific conductivity	S/m
ϵ_r	Relative permittivity of the medium	
ϵ_0	Permittivity of the free space, 8.85×10^{-12}	F/m
a	Particle radius	m
$1/\kappa$	Double layer thickness	m
v'	Sedimentation velocity	m/s
\bar{v}_e	Electrophoretic velocity	m/s
\bar{v}_{eo}	Electro-osmotic velocity	m/s
\bar{E}_{app}	Applied potential	Volt/m
μ_e	Electrophoretic mobility	(m/s)/(Volt/m)
E_{str}	Streaming potential	Volt/m
ΔP	Pressure differential	Pa
ρ	Particle density	Kg/m ³
ρ_0	Density of medium	Kg/m ³
K_s	Conductivity of suspension	Siemens
ϕ	Particle volume fraction	

2.7. References

- Alty, T., 1926. The origin of the electrical charge on small particles in water. Proceedings of the Royal Society of London, Series A, vol. 122 (760), pp. 235–251.
- Bach, N., Gilman, A., 1938. Electrokinetic potential at gas-liquid interfaces. Acta Physicochim URSS 9, 1.
- Bernstein, D. M., Hoskins, J. A., 2006. The health effects of chrysotile: current perspective based upon recent data. Regulatory Toxicology Pharmacology, 45, 252–264.
- Booth, F., Enderby, J. A., 1952. On electrical effects due to sound waves in colloidal suspensions, Proc. Phys. Soc. A 65, 321.
- Booth, F., 1954. Sedimentation potential and velocity of solid spherical particles. J. Chem. Phys, 22, 1956-1968.
- Bremmel, K. E., Fornasiero, D., Ralston, J., 2005. Pentlandite-lizardite interactions and implications for their separation by flotation. Colloid Surface A, 252, 207 – 212.
- Cheng, I., Iwasaki, I., Smith, K. A., 1999. Electrochemical study of multielectrode systems and their relevance to the differential flotation of complex sulfide ores. Mineral Metallurgical Process., 16(1), 69 – 71.
- Cichos, C., 1973. Effect of the electrokinetic potentials of air bubbles and mineral particles on flotation results. Freiburg Forschungs A 513, 7–23.
- Christoforou, C. C., Westermann-Clark, G. B., Anderson, J. L., 1985. The streaming potential and inadequacies of the Helmholtz equation. J. Colloid Interf. Sci., 106(1), 1-11.
- Collins, G. L., Jameson, G. J., 1977. Double-layer effects in the flotation of fine particles. Chem. Eng. Sci. 32, 239–246.
- Collins, G.L., Motarjemi, M., Jameson, G.J., 1978. A method for measuring the charge on small gas bubbles. J. Colloid Interf. Sci. 63, 69–75.
- Craig, V. S. J., Ninham, B. W., Pashley, R. M., 1993. The effect of electrolytes on bubble coalescence in water. J. Phys. Chem., 97, 10192 – 10197.
- Dai, Z., Bos, J-A. Quinn, P., Lee, A., Xu, M., 2009. Flowsheet development for thompson ultramafic low-grade nickel ores, in: Gomez, C. O.; Nasset, J. E.; Rao, S. R. (Eds.), Proc. Advances in Mineral Processing Science and Technology. Conference of Metallurgists, CIM, Sudbury, Ontario, pp. 217 – 228.

- Dibbs, H.P., Sirois, L.L., Bredin, R., 1974. Some electrical properties of bubbles and their role in the flotation of quartz. *Can. Metall. Quart.* 13, 395–404.
- Dorn, E., 1880, *Ann. Phys. (Leipzig)*, 10 (3), 46.
- Dukhin, S.S., 1966. In *Research in Surface Forces*, in: Derjaguin, B.V. (ed.), Translated from Russian by Consultants Bureau, New York, Vol. 2, pp. 54–74.
- Dukhin, S. S., Derjaguin, B. V., 1974. In Matijevic, E. (ed.), *Surface and Colloid Science*, Chapter 2, Vol. 7, Wiley, NY.
- Dukhin, A. S., Shilov, V. N., Borkovskaya, Y., 1999. Dynamic electrophoretic mobility in concentrated dispersed systems: Cell model. *Langmuir* 15, 3452-3457.
- Dukhin, A. S., Shilov, V. N., Ohshima, H., Goetz, P. J., 2000. Electroacoustic phenomena in concentrated dispersions: Effect of the surface conductivity. *Langmuir* 16, 2615-2620.
- Edwards, G.R., Kipkie, W. B., Agar, G. E., 1980. The effect of slime coating of the serpentine minerals, chrysotile and lizardite on pentlandite flotation. *Int. J. Miner. Process.*, 7, 33 – 42.
- Elmahdy, A.M., Mirnezami, M., Finch, J.A., 2008. Zeta potential of air bubbles in presence of frothers. *Int. J. Miner. Process.* 89, 40–43.
- Eltham, J. A., Tilyard, P. A., 1973. An approach to the flotation of Western Australian nickel ores. In: *Proceedings of the AusIMM Conference, WA*, pp. 417 – 429.
- Erickson, D., Li. D., 2001. Streaming potential and streaming current methods for characterizing heterogeneous solid surfaces. *J. Colloid Interf. Sci.*, 237(2), 283-289.
- Fan, X., Zhang, Z., Li, G., Rowson, N.A., 2004. Attachment of solid particles to air bubbles in surfactant-free aqueous solutions. *Chem. Eng. Sci.* 59, 2639–2645.
- Fornasiero, D., Ralston, J., 2005. Cu(II) and Ni(II) activation in the flotation of quartz, lizardite and chlorite. *Int. J. Miner. Process.*, 76, 75 – 81.
- Fuerstenau, M. C., Somasundaran, P., 2003. Flotation. In *Principles of Mineral Processing*, Fuerstenau, M. C., Han, K. N. (eds.), SME, Colorado, 2003.
- Fujii, T., Nakagawa, S., Sato, Y., Inomata, H., Hashida, T., 2010. Sorption characteristics of CO₂ on rocks and minerals in storing CO₂ processes”, *Nat. Resour. J.*, 1, 1 – 10.

- Fukui, Y., Yuu, S., 1980. Collection of submicron particles in electro-flotation. *Chem. Eng. Sci.* 35, 1097–1105.
- Gardner, J. R., Woods, R., 1979. An electrochemical investigation of the natural floatability of chalcopyrite. *Int. J. Miner. Process.*, 6, 1 – 16.
- Gorain, B. K., Franzidis, J. P., Manlapig, E. V., 1995. Studies on impeller type, impeller speed and air flow rate in an industrial scale flotation cell. Part 1: Effect on bubble size distribution. *Miner. Eng.* 8, 615–635.
- Graciaa, A., Morel, G., Saulner, P., Lachaise, J., Schechter, R. S., 1995. The ζ -Potential of gas bubbles. *J. Colloid Interf. Sci.* 172, 131–136.
- Hargreavass, A., Taylor, W. H., 1946. An X-Ray examination of decomposition products of chrysotile (asbestos) and serpentine. *Miner. Mag.*, 204 – 216.
- Heiskanen, K., Kirjavainen, V., Laapas, H., 1991. Possibilities of collectorless flotation in the treatment of pentlandite ores. *Int. J. Miner. Process.*, 263-274.
- Heyes, G. W.; Trahar, W. J., 1977. The natural floatability of chalcopyrite. *Int. J. Miner. Process.*, 4, 317 – 344.
- Hofmeier, U., Yaminsky, V. V., Christensen, H. K., 1995. Observations of solute effects on bubble formation. *J. Colloid Interf. Sci.*, 174, 199 – 210.
- Hogendam, C. W., de Keizer, A., Cohen, M. A., Bijsterbosch, B. H., 1998. Adsorption mechanisms of carboxymethyl cellulose on mineral surfaces. *Langmuir*, 14, 3825 – 3839.
- Homola, A., Robertson, A. A., 1975. A note on the applications of mass transport electrophoresis. *J. Colloid Interf. Sci.*, 51(1), 202-204.
- Hsieh, S. S., Lin, H-C., Lin, C. Y., 2006. Electroosmotic flow velocity measurement in a square microchannel. *Colloid Polymer Sci.*, 284, 1275-1286.
- Huckel, E., 1925. Zur Theorie konzentrierterer wasseriger Lo sungen starker Elektrolyte (Theory of concentrated aqueous solutions of strong electrolytes). *Physik. Z.*, 26(2), 93- 147.
- Hunter, R.J., 1981. The Zeta potential in Colloid Chemistry, Academic Press, London, pp. 117-118.
- Iwasaki, I., Cooke, S. R. B., 1958. The decomposition of xanthate in acid solution, *J. Am. Chem. Soc.* 80, 285 – 288.

- James A. M., 1979. Electrophoresis of Particles in Suspensions. In Good, R. J., Stromberg, R. S. (eds.), *Surface and Colloid Science*, Vol. 9, Plenum Press, NY.
- Johnson, D., Hilal, N., Waters, K., Kathryn, Hadler, K., Cilliers, J., 2009. Measurements of interactions between particles and charged microbubbles using a combined micro- and macroscopic strategy. *Langmuir* 25, 4880–4885.
- Khan, A., Kelebek, S., 2004. Electrochemical aspects of pyrrhotite and pentlandite in relation to their flotation with xanthate. Part – I: cyclic voltametry and rest potential measurements. *J. Applied Electrochemistry*, 34, 849 – 856.
- Kubota, K., Hayashi, S., and Inaoka, M., 1983. A convenient experimental method for measurement of zeta-potentials generating on the bubble suspended in aqueous surfactant solutions. *J. Colloid Interf. Sci.* 95, 362–369.
- Laskowski, J. S., Cho, Y. S.; Ding, K., 2003. Effect of frothers on bubble size and foam stability in potash ore flotation systems. *Can. J. Chem. Eng.*, 81, 63 – 69.
- Li, C., Somasundaran, P., 1991. Reversal of bubble charge in multivalent inorganic salt solutions – effect of magnesium. *J. Colloid Interf. Sci.* 146, 215–218.
- Majima, H., Takeda, M., 1968. Electrochemical studies of the xanthate-dixanthogen system on pyrite. *Trans. AIME*, 241, 431 – 436.
- Marlow, B. J., Rowell, R. L., 1985. Sedimentaon potential in acqueous electrolyte. *Langmuir*, 1, 83-90.
- Masliyah, J. H., Bhattacharjee, S., 2006. *Electrokinetic and Colloid Transport Phenomena*. Wiley-Interscience, NJ, pp. 230.
- McTaggart, M. A., 1922, *Philosophers' Magazine*, 44, 386.
- Moza, A. K., Biswas, A. K., 1976. Comparative sedimentation and electrophoresis studies for zeta-potential measurement. *Colloid Polymer Sci.*, 254, 522-529.
- Oka, K., Furusawa, K., 1998. Electrophoresis. In Ohshima, K., Furusawa, K. (eds.), *Electrical Phenomenon at Interfaces*, Marcel Dekker, NY, pp. 151.
- Okada, K., Akagi, Y., Kogure, M., Yoshioka, N., 1990. Effect of surface charges of bubbles and fine particles on air flotation process. *Can. J. Chem. Eng.* 68, 393–398.
- Oliveira, A. P., Torem, M. L., 1996. The influence of some metallic cations on deinking flotation. *Colloid Surface A*, 110, 75 – 85.

- Ozaki, M., Ando, T., Mizuno, K., 1999. A new method for the measurement of sedimentation potential: rotating column method. *Colloid Surface A*, 159, 477-480.
- Park, A-H. A., Fan, L-S., 2004. CO₂ mineral sequestration: physically activated dissolution of serpentine and pH swing process. *Chem. Eng. Sci.*, 59, 5241 – 5247.
- Pietrobon, M. C., Grano, S. R., Sobieraj, S., Ralston, J., 1997. Recovery mechanisms for pentlandite and MgO bearing gangue minerals in nickel ores from Western Australia. *Miner. Eng.*, 10, 775 – 786.
- Pugh, R. J., Tjus, K., 1987. Electrokinetic studies on Cu(II) hydroxide coated zinc sulfide particles. *J. Colloid Interf. Sci.*, 117, 231 – 241.
- Quinn, J. J., Kracht, W., Gomez, C. O., Gagnon, C., Finch, J. A., 2007. Comparing the effect of salts and frother (MIBC) on gas dispersion and froth properties. *Miner. Eng.*, 20, 1296 – 1302.
- Quist, J. D., Washburn, E. R., 1940. A study in electrokinetics. *J. Am. Chem. Soc.*, 62, 3169-3172.
- Rao, S. R., Leja, J., 2003a. *Surface Chemistry of Froth Flotation*, 2nd ed. Plenum Publishers, New York, Vol. 2, pp. 454.
- Rao, S. R., Leja, J., 2003b. *Surface Chemistry of Froth Flotation*, 2nd ed. Plenum Publishers, New York, Vol. 2, Chapter 8.
- Saville, D. A., 1982. The sedimentation potential in a dilute suspension. *Adv. Colloid Interface Sci.*, 16, 267-279.
- Saulnier, P., Lachaise, J., Morel, G., and Graciaa, A., 1996. Zeta potential of air bubbles in surfactant solutions. *J. Colloid Interf. Sci.* 182, 395 – 399.
- Seifritz, W., 1990. CO₂ Disposal by means of silicates. *Nature*, 345, 486.
- Senior, G. D., Thomas, S. A., 2005. Development and implementation of a new flowsheet for the flotation of a low grade nickel ore. *Int. J. Miner. Process.*, 78, 49 – 61.
- Sherwood, J. D., 1986. Electrophoresis of gas bubbles in a rotating fluid. *J. Fluid. Mech.* 162, 129–137.
- Shilov, V. N., Borkovskaja, Y. B., Dukhin, A. S., 2004. Electroacoustic theory for concentrated colloids with overlapped DLs at arbitrary kappa alpha. I. Application to nanocolloids and nonaqueous colloids. *J Colloid Interf. Sci.* 277, 347-358.

- Sirois, L. L., Millar, G., 1973. Method to study surface electrical characteristics on a single bubble. *Can. Metall. Quart.* 12, 281–284.
- Stumm, W., 1992. *Chemistry of the Solid-Water Interface*. Wiley-Interscience Publication, New York, pp. 523 – 598.
- Sun, S. C., 1943. The mechanism of slime coating. *Trans. AIME*, 153, 479 – 492.
- Takahashi, M., 2005. Zeta potential of microbubbles in aqueous solutions: Electrical properties of the gas-water interface. *J. Phys. Chem. B* 109, 21858–21864.
- Tison, R. P., 1977. Accurate electrophoretic analyses of concentrated suspensions (electrophoresis of concentrates). *J. Colloid Interf. Sci.*, 60(3), 519 – 528.
- Trahar, W. J., 1981. A rational interpretation of the role of particle size in flotation. *Int. J. Miner. Process.*, 8, 289 – 327.
- Uddin, S., Jin, L., Mirnezami, M., Finch, J. A., 2011. An Apparatus to Measure Electrical Charge of Bubble Swarms. In progress.
- Usui, S., Sasaki, H., 1978. Zeta potential measurements of bubbles in aqueous surfactant solutions. *J. Colloid Interf. Sci.* 65, 36–45.
- Usui, S., Sasaki, H., Matsukawa, H., 1981. The dependence of zeta potential on bubble size as determined by the dorn effect. *J. Colloid Interf. Sci.* 81, 80–84.
- Usul, A. H., Tolun, R., 1974. Electrochemical study of the pyrite-oxygen-xanthate system. *Int. J. Miner. Process.*, 1, 135 – 140.
- Wellham, E. J., Elber, L., Yan, D.S., 1992. The role of carboxy methyl cellulose in the flotation of a nickel sulphide transition ore. *Miner. Eng.*, 5, 381 – 395.
- Werner, C., Körber, H., Zimmermann, R., Dukhin, S., Jacobasch, H-J., 1998. Extended electrokinetic characterization of flat solid surfaces. *J. Colloid Interf. Sci.*, 208(1), 329-346.
- Woods, R., 1976. Electrochemistry of sulphide flotation. In *Flotation*, M.C. Fuerstenau (ed.), AIME, New York.
- Wypych, F., Adad, L. B., Mattoso, N., Marangon, A. A. S., Schreiner, W. H., 2005. Synthesis and characterization of disordered layered obtained by selective leaching of octahedral sheets from chrysotile and phlogopite structures. *J. Colloid Interf. Sci.*, 283, 107 – 112.

Yang, C., Dabros, T., Li, D., Czarnecki, J., Masliyah, J.H., 2001. Measurement of the zeta potential of gas bubbles in aqueous solutions by microelectrophoresis method. *J. Colloid Interf. Sci.* 243, 128–135.

Yoon, R.H., Yordan, J.L., 1986. Zeta-potential measurements on microbubbles generated using various surfactants. *J. Colloid Interf. Sci.* 113, 430–438.

3. A Surface Charge Characterization Device Using Sedimentation Potential for Single and Mixed Particle Systems

3.1. Abstract

An integrated device has been developed to measure sedimentation potential, conductivity and pH simultaneously of particulate systems. Maxwell's model was used to calculate volume fraction of solid from conductivity data. In this approach, all system variables are known and zeta potential can be calculated from the Smoluchowski equation. The technique is validated by comparing zeta potential vs. pH for alumina and silica suspensions with electrophoresis measurements. The technique was extended to mixed alumina/silica systems. Sufficient column height along with size difference between the two minerals allowed gravity fractionation during settling. Sedimentation potential measured over time identified the transition from one mineral to the next. X-ray diffraction analysis supported the correlation between surface charge and sample composition. This is a step towards characterizing surface charge of mixed systems of interest in mineral processing.

Keywords: Sedimentation potential, Zeta potential

Research highlights:

- Introduction of a new sedimentation potential apparatus.
- Validation of the technique by comparing to electrophoresis of pure oxide particles.
- Extension of the technique to multi-particle systems.
- Results from multi-particle tests evaluated and explained using phase analysis techniques.

3.2. Introduction

Surface charge is considered one of the most important properties of fine particulate systems (Hunter, 1981; Laskowski and Ralston, 1992; Kissa, 1999; Delgado, 2002). To identify dispersion and aggregation mechanisms, surface charge indicated by zeta potential is frequently measured in a wide range of industries, from pharmaceuticals to mineral processing. Among various approaches to measure surface charge, the sedimentation potential method has been less popular compared to others, partly because of the lack of time efficient and integrated measurement techniques that can be easily automated. The sedimentation potential method has some advantages: it is applicable to more concentrated systems compared to electrophoresis; and other data related to system dispersion or aggregation, including visual clues, can be collected simultaneously. These attributes are of interest in our studies on characterizing mineral processing systems.

The purpose of this paper is to introduce a surface charge characterization system based on sedimentation potential. We start with the theory of measurement to help place the apparatus design in context. Determinations on single minerals are verified by comparison with electrophoresis, and the method is then extended to binary systems.

3.3. Theory

3.3.1. Sedimentation and zeta potential

Sedimentation potential is the potential difference that arises when charged particles settle in a force field (usually gravity). Charge destabilization created by the fluid drag surrounding each falling particle induces numerous dipoles in the suspension. These individual dipoles sum to produce the macroscopic potential difference between two points in a column.

This phenomenon was first discovered by Dorn (1880) and is often called the “Dorn effect” (Booth, 1954; Saville, 1982).

For spherical, nonconducting, monodisperse suspensions with negligible particle-particle interaction and surface conduction, sedimentation potential can be related to zeta potential by the Smoluchowski equation (1921) (see nomenclature):

$$E_s = \frac{\varepsilon_r \varepsilon_0 \phi (\rho - \rho_0) g}{\eta \lambda} \zeta \quad (1)$$

This equation assumes the double layer thickness $1/\kappa$ is small relative to the particle radius a i.e., $\kappa a \gg 1$, and E_s can be expressed as follows:

$$E_s = ((E_B)_i - (E_O)_i) / H \quad (2)$$

where, E_B is a function of temperature, pH and electrode geometry.

Electrical and particle hydrodynamic interactions become a consideration at high concentrations ($\phi > 1.8\% v/v$ (Marlow and Rowell, 1985)) and the Smoluchowski equation needs to be modified.

Taking both electrical and hydrodynamic interactions into account, Levine et al. (1976) derived the following equation based on the Kuwabara cell model (1959):

$$E_{s(\text{mod})} = (9\varepsilon_r \varepsilon_0 v' \phi / (2\lambda a^2)) / \gamma(\kappa a, \phi) \quad (3)$$

where $\gamma(\kappa a, \phi)$ is a function of κa and ϕ .

For specific conditions, equation 3 can be solved analytically. For example, when $\kappa a = 10^3$ (10^{-4} M KCl) and $\phi < 0.1$ it simplifies to the following (Marlow and Rowell, 1985),

$$E_{s(\text{mod})} = E_s (20\phi + 1) (1 - (9\phi^{1/3} / 5) + \phi - (\phi^2 / 5)) \quad (4)$$

From equation 4 as $\phi \rightarrow 0$, $E_{s(\text{mod})} \rightarrow E_s$ which implies no correction to the Smoluchowski equation is necessary when the suspension is sufficiently dilute.

In addition to measuring E_s , equation 1 indicates that ϕ and η , the volume fraction of solid and suspension viscosity between the two points, respectively, are required.

3.3.2. Particle volume fraction: Maxwell's conductivity model

Maxwell's model (1904) relates the conductivity in heterogeneous media to the volume fraction of the constituent phases. This model was used in the present work to calculate the unsteady volume fraction of particles between the two electrodes during settling. The model can be expressed as follows:

$$\frac{K_s}{K_L} = \frac{1 + 2\beta\phi}{1 - \beta\phi} \quad (5)$$

$$\beta = \frac{K_p - K_L}{K_p + 2K_L} \quad (6)$$

One of the major assumptions is that the model neglects interaction with particles which means no disturbance in the surrounding electric field. Although the model is thus theoretically restricted to low concentration of dispersed phase, it has been used successfully in many concentrated systems (De La Rue and Tobias, 1959; Turner, 1976; Barchini and Saville, 1995), including mineral processing (Uribe-Salas et al., 1994; Banisi et al., 1994). For insulating particles where $K_p \ll K_L$, equation 5 can be written in the following form (Cruz et al., 2005):

$$\frac{K_s}{K_L} = \frac{1 - \phi}{1 + \phi/2} \quad (7)$$

from which, the following can be derived:

$$\phi = \frac{1 - \delta}{1 + \delta/2} \quad (8)$$

$$\delta = \frac{(R_B)_i}{(R_S)_i} \quad (9)$$

Resistance readings were converted to specific conductivity, λ , using the following relationship:

$$\lambda = \frac{H}{R_s A} \quad (10)$$

3.3.3. Viscosity of suspension

Einstein's equation for viscosity of dilute suspension of non-interfering spherical particles was used to calculate suspension viscosity in the present work. The analytical expression is (Abulnaga, 2002):

$$\eta = \eta_0(1 + 2.5\phi) \quad (11)$$

Equation 11 was experimentally verified by Eirich et al. (1936) and found to work well up to 4%v/v solid concentration.

3.4. Apparatus

3.4.1. Background

The general background was presented in chapter 2. The present chapter describes an integrated technique with in-process measurement of all the system variables. The method is tested on high purity alumina and silica samples.

3.4.2. Cell and accessories

The general setup is shown in Fig. 1. The glass tube was 2.5 cm inner diameter of modular design to give various lengths. Two pairs of Ag/AgCl electrodes (Warner Instruments Inc.) were mounted through stopcocks, each electrode in the pair set 20 cm apart. The Ag/AgCl

electrode pairs were connected to two separate channels of a Keithley 7700 20-Channel, Differential Multiplexer embedded in a Keithley 2700 Integra series multimeter. One pair of electrodes was used for potential difference measurement and the other for resistance measurement. Due to the high resistance of the suspension, the resistance measuring electrodes polarized and gave inaccurate readings. To eliminate the problem a flip switch was inserted between the source (multimeter) and the resistance measuring electrodes. The switch was used to alternate current flow direction after each measurement to reduce charge build-up on the electrodes. Slow polarization of potential measuring electrodes is also possible. The influence can be minimized by keeping updated information on background potential and subtracting from the suspension potential. The pH electrode (Cole-Parmer) inserted into the tube via a CG-350-03 glass joint was connected to another channel through an Oakton 510 benchtop pH meter. A vacuum pump was connected at the top of the tube to draw the electrolyte inside the column.

A program developed using Matlab R2008a carried out instrument control, data acquisition and data processing. This allows flexibility to design measurement sequences, and helps easy and quick post-processing of data. Interfacing was performed using VXIPnP driver with serial communication and SCPI (Standard Commands for Programmable Instrumentation) command format was used to control the multimeter.

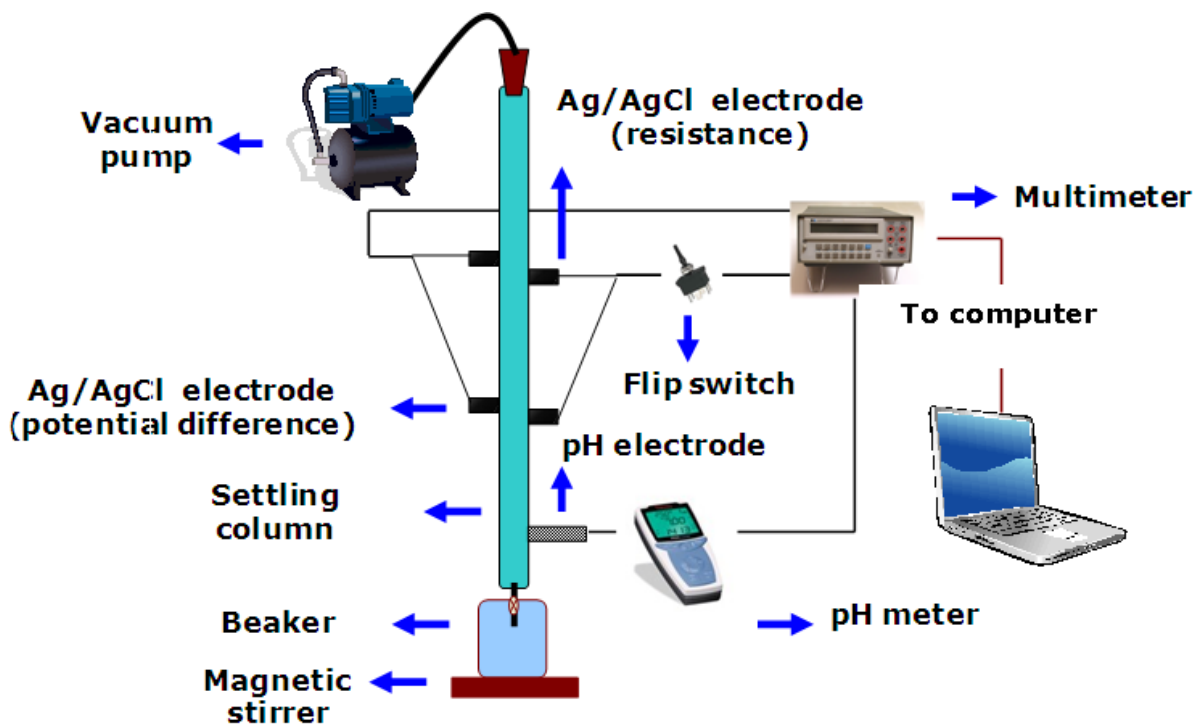


Fig. 1. Sedimentation apparatus and accessories

3.5. Experimental

3.5.1. Samples

The alumina sample was obtained from Sigma-Aldrich (CAS no. 1344-28-1) and was >99% pure. It was dry screened to isolate the target size of 25-38 μm and 53 – 75 μm . Silica was obtained from Opta Minerals (BARCO 32) and was >99.5% pure with reported average size of 0.34 mm. The sample was pulverized then dry screened to retrieve the target sizes of 25-38 μm and 53-75 μm . A size analysis was performed using Horiba LA 920 (laser scattering principle) and the results are given in Table 1. The sizes were selected by experimentation to give sufficient settling time for reliable potential measurements. Chemical and physical properties of the particles are given in Table 2.

Table 1

Size-related properties

Sample	Alumina	Silica
Median size (μm)	28	68
Mean size(μm)	27	69
Standard deviation (μm)	7	11
Coefficient of variation (%)	26	15

Table 2

Some chemical and physical properties

Sample	Alumina	Silica
Specific gravity	3.97	2.65
Melting point ($^{\circ}\text{C}$)	2040	1700
Chemical analysis (%)	$\text{Al}_2\text{O}_3 > 99.0$	$\text{SiO}_2 > 99.5$
	$\text{Na}_2\text{O} < 0.4$	$\text{TiO}_2 \sim 0.1$
	$\text{Fe}_2\text{O}_3 < 0.03$	$\text{K}_2\text{O} \sim 0.1$
	$\text{SiO}_2 < 0.03$	$\text{CaO} \sim 0.03$
		$\text{Fe}_2\text{O}_3 \sim 0.03$
		$\text{Al}_2\text{O}_3 \sim 0.01$

3.5.2. Procedure: single-mineral systems

The samples were washed thoroughly with deionised water (prepared by reverse osmosis) and suspensions prepared in a beaker by adding a known weight of sample to 500 mL deionised water. Background electrolyte was 10^{-4} M KCl (corresponding to equation 4). The suspension, 2% v/v in both cases, was conditioned over a magnetic stirrer for 30 minutes. For pH adjustment HCl and KOH were used.

After conditioning, the particles were allowed to settle in the beaker. The electrolyte supernatant was drawn into the column using the vacuum pump up to a pre-determined level and then the bottom valve on the tube was closed. The setup was left for 10 minutes to condition the electrodes before background potential was recorded. The potential difference and the resistance were measured and stored as the background values. The particles were transferred to the tube via a funnel through the top opening. The column was 77 cm long for these experiments.

After introducing the particles, the potential difference, resistance and pH readings were taken successively. Measurements were taken one after another to avoid possible interference. From resistance readings, volume fraction and specific conductivity were calculated. Potential difference sensed by the pH meter was converted to pH values using the linear relationship (1 pH \approx 59mV and 0 mV at pH 7). The suspensions were then drained to the beaker, the electrodes and column were cleaned with deionised water and the procedure repeated at a new pH.

3.5.3. Procedure: mixed-mineral systems

The objective was to correlate the components of a mixed $\text{SiO}_2/\text{Al}_2\text{O}_3$ system with surface charge. Sufficient particle size difference and length of the column were used for the

minerals to separate under gravity settling. The two test sets are given in Table 3. The pH was set above the iso-electric-point of both minerals to favour dispersion.

Table 3

Sample sets for mixed mineral tests

Sample	Silica (μm)	Alumina (μm)
Set 1	25 – 38	53 – 75
Set 2	53 – 75	25 – 38

Three 500 mL beakers were used. In two of the beakers, 500 mL suspension was prepared using 20 g alumina or 20 g silica with 10^{-3} M KCl as background electrolyte. The third beaker was filled with 500 mL background electrolyte. The pH of all three was adjusted to ca. 11. The beakers were conditioned over a magnetic stirrer for 30 minutes.

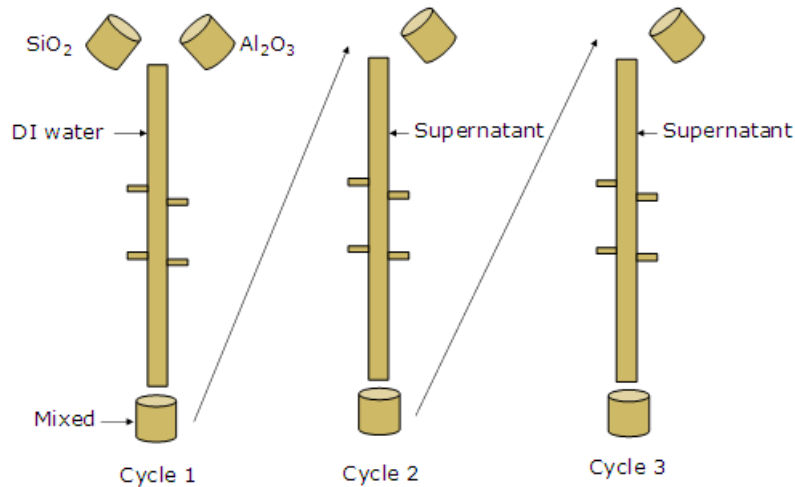


Fig. 2. Experimental cycles (first three are shown here)

To improve mineral separation the column length was increased by 30 cm (i.e., to 107 cm). After sample conditioning the column was filled with the electrolyte from the third beaker

and left for 10 minutes to condition the electrodes before background potential was recorded. The supernatant of the alumina and silica suspensions (i.e., from beakers 1 and 2) was decanted and the particles introduced from the top of the column. Potential difference was recorded as a function of time. This completed cycle 1 (Fig. 2). The column contents were then transferred to a beaker and conditioned for about 5 minutes. Particles were allowed to settle in the beaker and the column was re-filled with the supernatant. It was left in contact with the electrodes for 5 minutes while the suspension in the beaker was kept stirred. The background potential was measured and the suspension from the beaker was re-introduced to the column, initiating the start of cycle 2 (Fig. 2). The same procedure was repeated up to 6 times (or cycles; Fig. 2 illustrates the first three cycles). In this manner time was given to determine if particle surface properties changed due to inter-mineral contact.

In the last cycle settling particles were collected from the bottom of the column at three incremental times for X-ray diffraction (XRD) and scanning electron microscope (SEM) analysis. The first collected fraction was designated as first fraction and so on.

3.6. Results

3.6.1. Single-mineral systems

Figs. 3 and 4 show example potential difference for background and suspension as a function of time for the alumina sample at a pH below the iso-electric point (iep) (ca. pH 8) and above the iep (ca. pH 9), respectively. For positively charged particles (Fig. 3), concentration of negative ions (counterions) is higher in the diffuse part of the double layer and the dipoles created by fluid drag are negative in the upper part and positive in the lower part of the column. That is why the potential difference is more negative in the suspension than for the background.

The opposite is observed for negatively charged particles (Fig. 4). The E_s was calculated using equation 2 and subsequently corrected by equation 4.

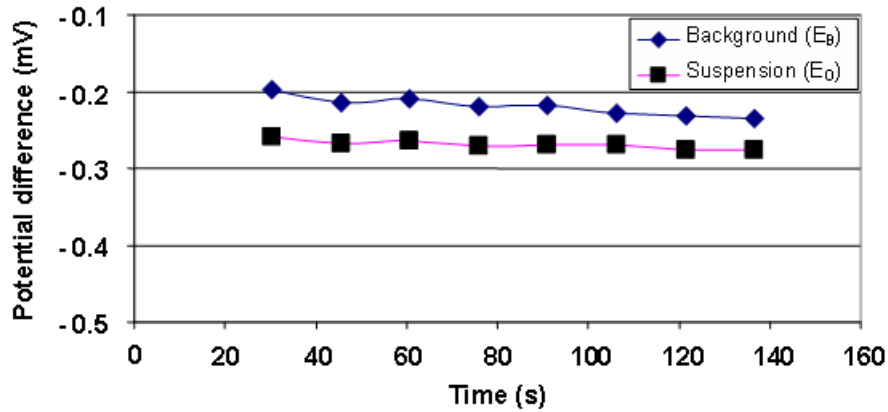


Fig. 3. Potential difference as a function of time for alumina (25- 38 μm) suspension at ca. pH 8

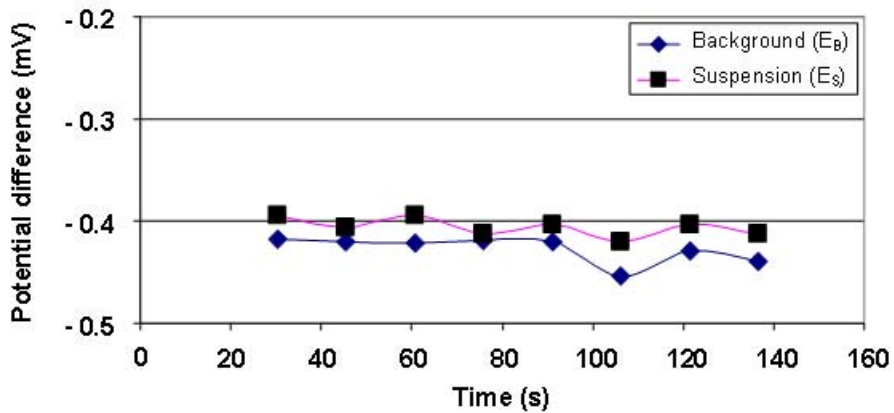


Fig. 4. Potential difference as a function of time for alumina (25- 38 μm) suspension at ca. pH 9

Fig. 5 shows an example of the variation of resistance for background and an alumina suspension. As alumina (and silica) particles are non-conducting, suspension resistance increases with increasing volume fraction of solid. The cycling pattern is due to the polarity reversal after

each measurement. Using equations 8 and 9, volume fraction of solid was calculated as a function of time from the resistance data (Fig. 6).

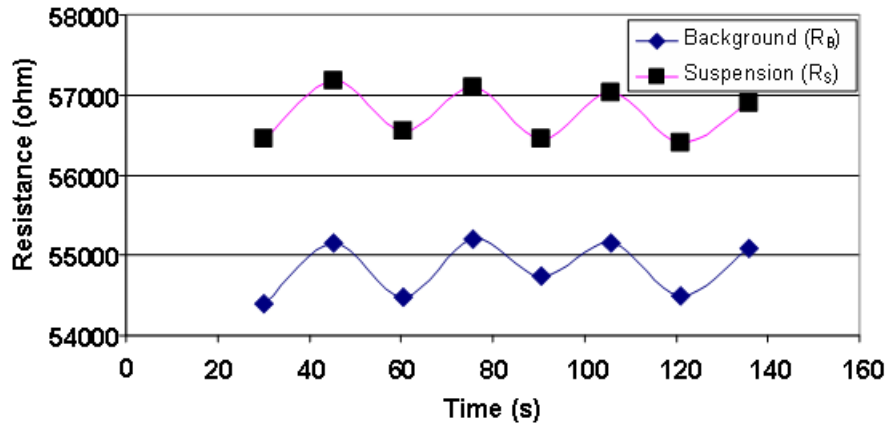


Fig. 5. Resistance as a function of time for alumina (25- 38 μm) suspension at $\text{pH} \approx 9$

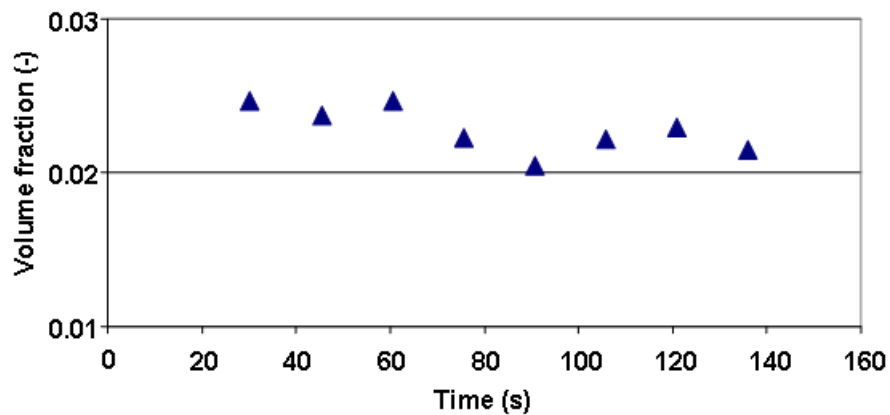


Fig. 6. Volume fraction as a function of time for alumina (25- 38 μm) suspension at $\text{pH} \approx 9$

Zeta potential as a function of pH was calculated using equation 1 (with the corrected value of E_s) from three separate experiments. Results are shown in Figs. 7 and 8 for alumina and silica, respectively, with the standard deviation indicated by the error bar. The zeta potentials compared well with those measured by electrophoresis (Brookhaven ZetaPlus) and corresponded to the known trend for these two materials (Rao and Leja, 2003; Somasundaran, 2008).

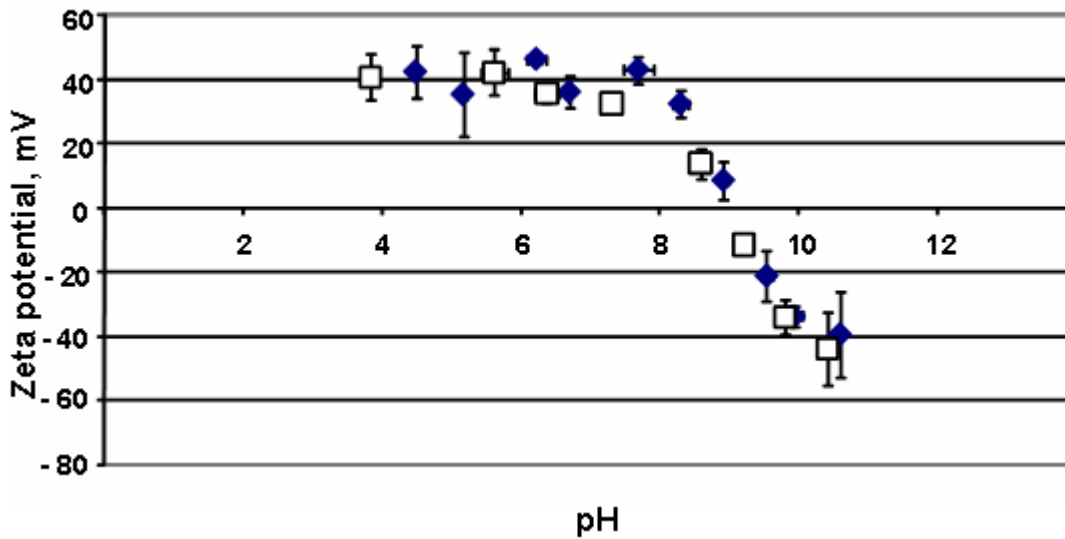


Fig. 7. Zeta potential as a function of pH for alumina (25- 38 μm) suspension: (◆) zeta potential measured by sedimentation method and (□) zeta potential measured by electrophoresis

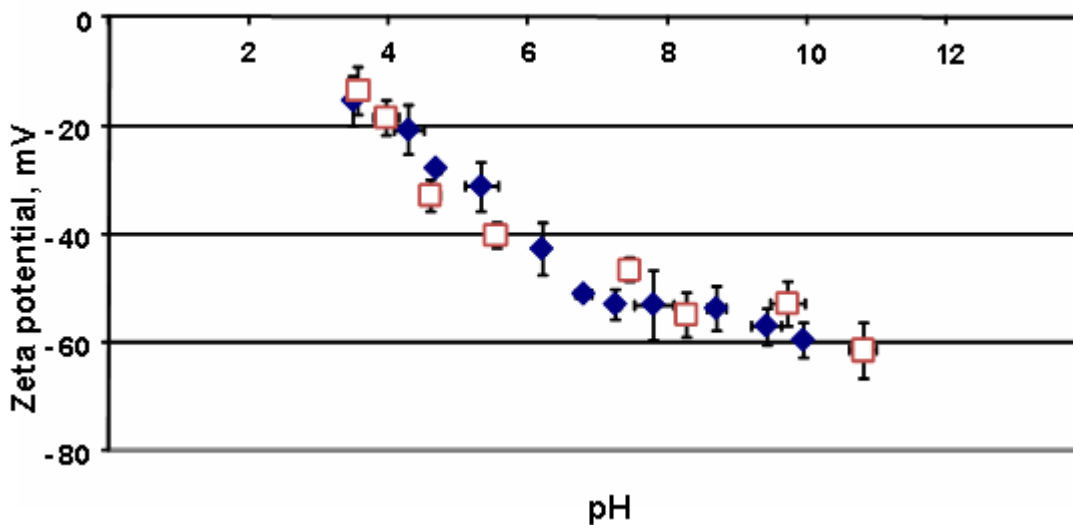


Fig. 8. Zeta potential as a function of pH for silica (53 – 75 μm) suspension: (◆) zeta potential measured by sedimentation method and (□) zeta potential measured by electrophoresis

3.6.2. Mixed-mineral systems

Thirty potential difference readings were taken on the suspension with 60s pause after every ten readings, which itself took about 60s. Background potentials were then subtracted to obtain the sedimentation potential. Fig. 9 shows the variation of sedimentation potential as a

function of time (number of readings) for the two sample sets. For set 1, Fig. 9a shows the sedimentation potential became more negative with time, corresponding to increasing concentration of the finer, slower settling silica; while Fig. 9b reveals the opposite trend as now (set 2) the slower settling mineral is alumina. From XRD analysis (Fig. 10) these trends were supported by the characteristic silica peak height ($2\theta \sim 26^\circ$) which increased with time for set 1 and decreased for set 2.

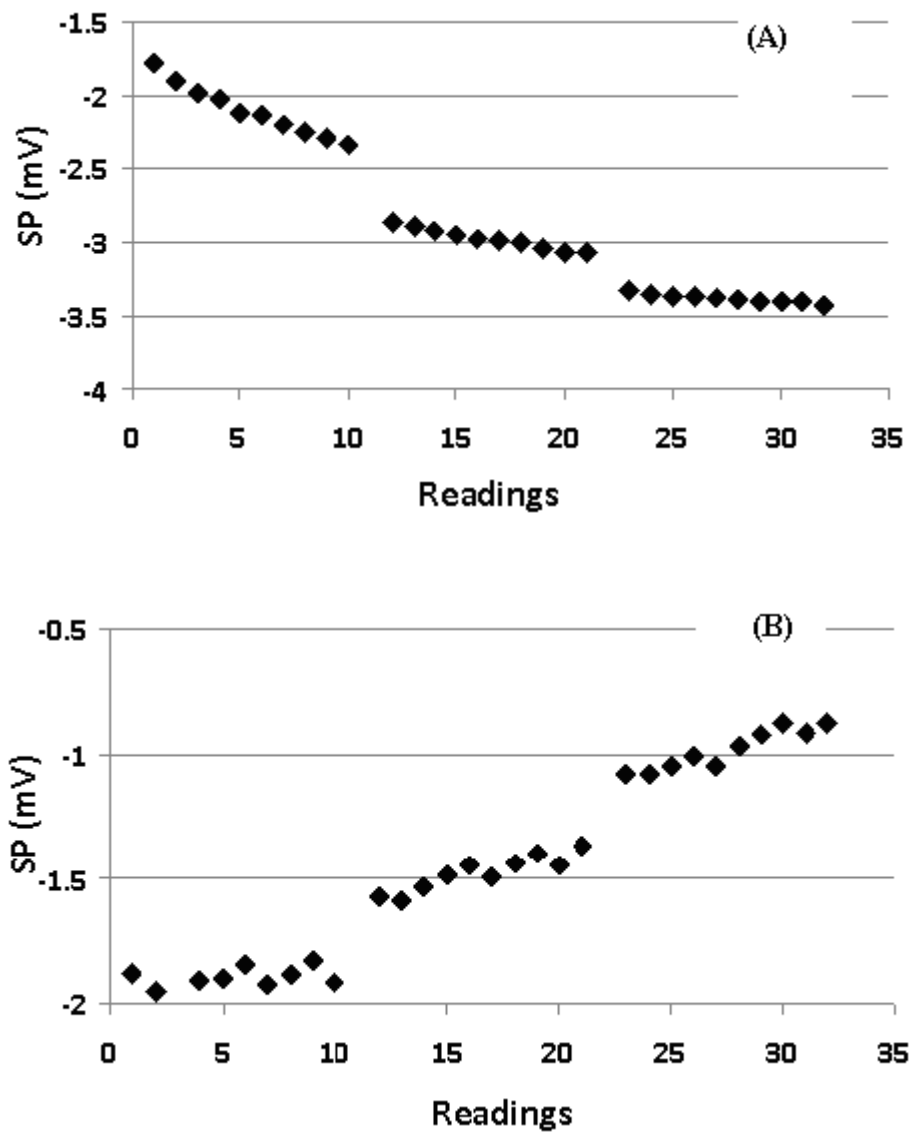


Fig. 9. Sedimentation potential (SP) as a function of time for set 1 (A) and set 2 (B) in cycle 2 Note: the three groups of 10 readings are the three fractions collected.

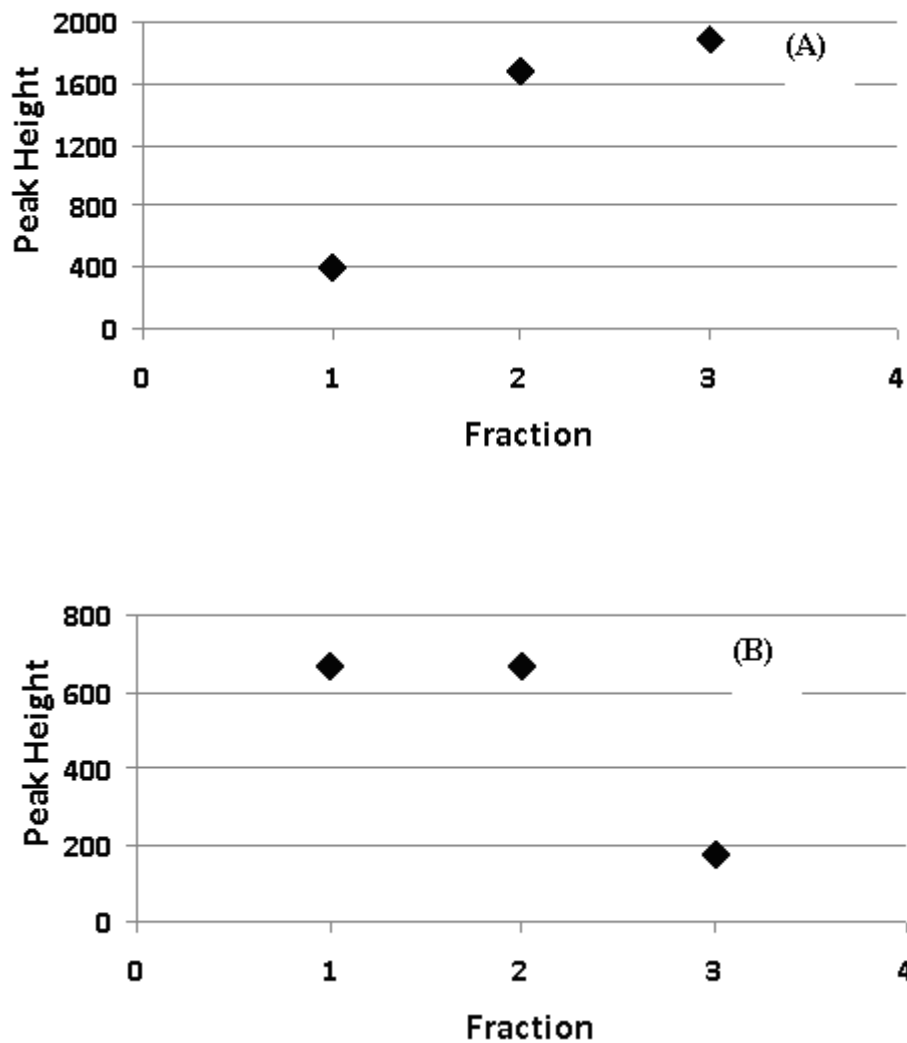


Fig. 10. Silica Peak Height @ 2 Theta ~ 26 deg. as a function of fraction for set 1 (A) and set 2 (B)

It was observed that the difference between the first and third fractions decreased with conditioning time (number of cycles). To track this behaviour the average of the ten readings of the third fraction, Avg(SP3), was subtracted from the average of the ten readings of first fraction, Avg(SP1). The decrease in absolute values is shown for set 1 in Fig. 11A for set 2 in Fig. 11B.

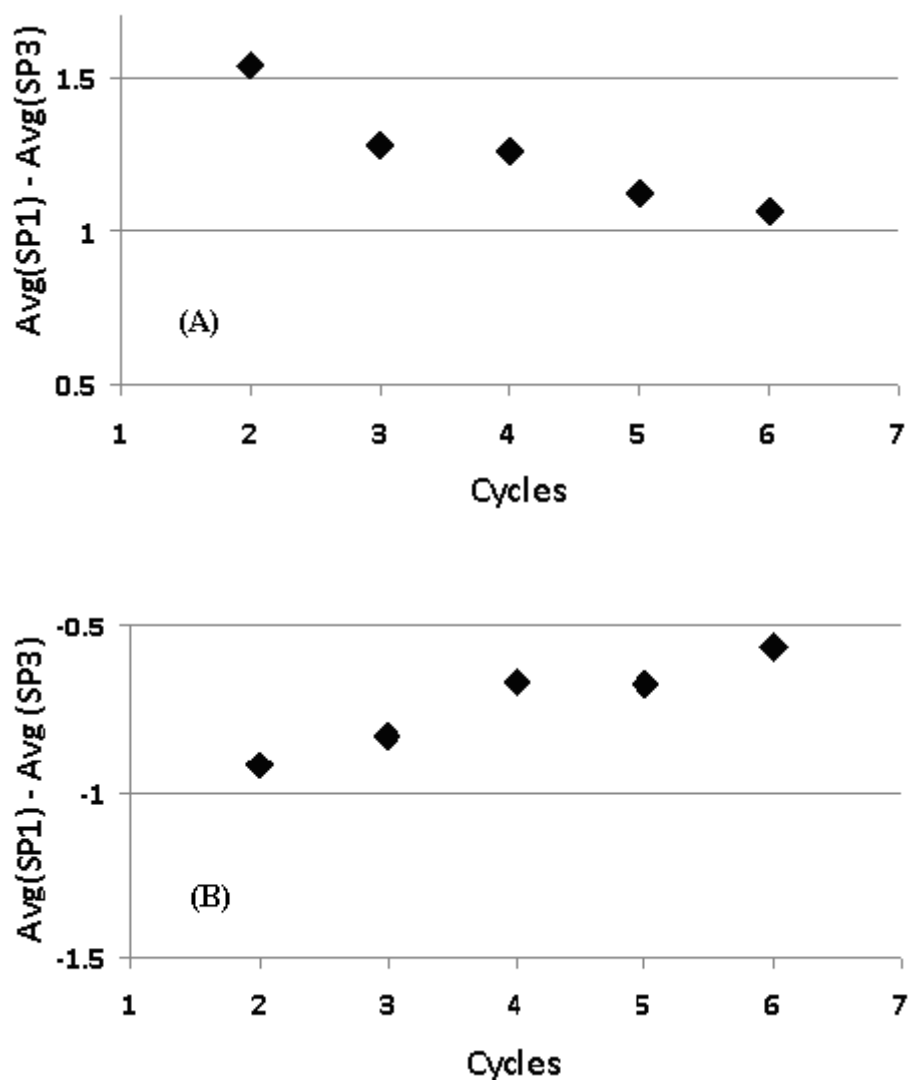


Fig. 11. Difference between Avg(SP1) and Avg(SP3) as a function of experimental cycles for set 1 (A) and set 2 (B)

Heterocoagulation was a suspected cause of the decreasing trend. The possibility was investigated using SEM-EDAX microanalysis. Little supporting evidence was found, for example Fig. 12 shows a non-aggregated sample with the two minerals clearly distinguished by the elemental analysis. We are left to consider the observation in Fig. 11 is due to cross-contamination of ions, released by the minerals.

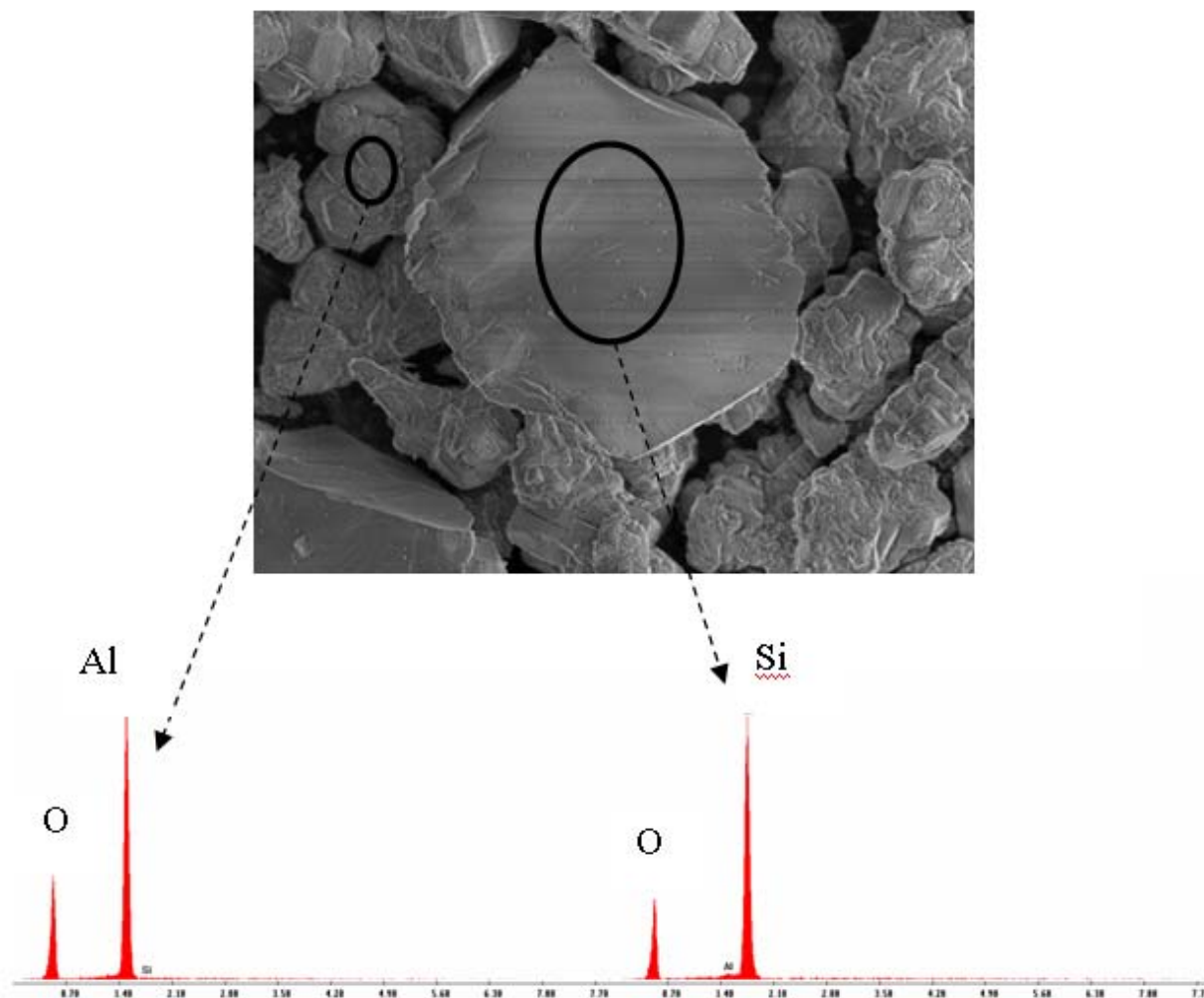


Fig. 12. SEM micrograph and EDAX Microanalysis on two selected particles for first fraction of set 2

3.7. Discussion

A method using sedimentation potential to indicate surface charge that measures all the required parameters on-line has been introduced. Background and suspension measurements were made close together in space and time in order that measurements refer to the suspension in the same state. The single-mineral tests, conducted under conditions to apply the Smoluchowski model, showed zeta potential results comparable to electrophoresis; and the mixed mineral tests showed trends in sedimentation potential reflective of the minerals present.

The technique initially involved drawing suspension into the tube but that was later changed in favour of drawing supernatant to provide the background potential and resistance readings. By drawing supernatant in from the bottom, turbulence and entrainment of bubbles associated with pouring from the top were minimized. This speeded up initiation of signal collection.

Subsequent introduction of solids is a source of disturbance. By experimentation, a sufficient distance was provided between the delivery point and the first electrode to minimize the impact.

It was understood that the potential difference was likely to vary only over a few millivolts, which requires meters with high precision. The Keithley 2700 has a maximum voltage resolution of 0.1 μV , which is sufficient for present purposes. For resistance measurements, the necessary alternating current to avoid electrode polarization was applied using a flip switch. This successfully yielded a reliable trend in resistance as a function of time to provide the % solids (by volume) data required to calculate zeta potential. The calculated % solid values were in accord with the amount of solid added.

To limit interference between the three readings (potential, resistance and pH), they were taken sequentially. On-line pH measurement proved helpful to check stability during a test.

The technique was explored to try to correlate sedimentation potential with the constituent minerals of a mixed system. In this, the sedimentation potential was used directly rather than converting to zeta potential as conditions no longer fitted the Smoluchowski model. For the intended purpose of characterizing samples of interest in mineral processing (e.g. ores) the sedimentation potential may be sufficient guide to surface charge. An analogy is using electrophoretic mobility rather than zeta potential in electrophoresis studies.

Figs. 7 and 8 confirm that at ca. pH 11 sedimentation potential of silica is more negative than the alumina. Sedimentation potential became more negative with time for set 1 (Fig. 9a), corresponding to the first fraction passing the electrodes being mostly alumina and later ones being progressively dominated by silica. Set 2 showed the opposite trend, as the fine fraction in this case is alumina.

Fractions collected from the bottom of the column were analyzed to correlate composition with the sedimentation potential data. The height of the XRD peak characteristic for silica was used for semi-quantitative analysis. Peak height as a function of fraction (Fig. 10) showed the dominance of silica in the third fraction of set 1 and first fraction of set 2.

A decreasing trend in sedimentation potential difference between fractions 1 and 3 with time (Fig. 11) suggested interaction between the minerals. SEM-EDAX microanalysis showed little sign of heterocoagulation (Fig. 12). Although it is appreciated that SEM analysis, by removing the sample from its environment, may introduce artefacts, the possibility of cross contamination by adsorption of dissolved ionic species is suggested, as reported by Healy et al. (1973) for an alumina/silica system. Surface analysis (e.g. by XPS and TOF-SIMS) may clarify the matter.

3.8. Conclusions

The present work has proposed a fully integrated sedimentation potential method for study of surface charge. In-process measurement of all system variables and continuous measurement capability give the setup advantages over prior sedimentation potential devices. The Matlab based system provided a powerful tool for control, data acquisition and post processing. The approach was validated by single-mineral tests which showed good agreement

with zeta potential measured by electrophoresis, and mixed-mineral tests which showed sedimentation potential variation reflective of the minerals present. Results from the $\text{SiO}_2/\text{Al}_2\text{O}_3$ mixed system show a possible use of this technique to characterize mineral processing systems.

3.9. Acknowledgements

The work was funded under the Chair in Mineral Processing sponsored by Vale, Teck Resources, Barrick Gold, Xstrata Process Support, Shell Canada, SGS Lakefield, COREM and Flottec, under the Natural Sciences and Engineering Research Council of Canada (NSERC) Collaborative Research and Development program.

3.10. Nomenclature

Symbols	Meaning	Units
i	Reading number	
E_s	Sedimentation potential	Volt/m
$E_{s(\text{mod})}$	Sedimentation potential modified	Volt/m
E_o	Suspension potential difference	Volt
E_B	Background potential difference	Volt
ϕ	Particle volume fraction	
ζ	Zeta potential	Volt
η	Viscosity of suspension	Pa-sec.
η_0	Viscosity of medium	
λ	Specific conductivity	S/m

ρ	Particle density	Kg/m ³
ρ_0	Density of medium	Kg/m ³
ε_r	Relative permittivity of the medium	
ε_0	Permittivity of the free space	F/m
a	Particle radius	m
$1/\kappa$	Double layer thickness	m
H	Distance between electrodes	m
v'	Sedimentation velocity	m/s
K_s	Conductivity of suspension	Siemens
K_L	Conductivity of medium	Siemens
K_p	Conductivity of particles	Siemens
R_B	Resistance of background	Ohm
R_s	Resistance of suspension	Ohm
A	Cross-sectional area	m ²

3.11. References

- Hunter, R. J., 1981. The Zeta Potential in Colloid Chemistry (Science), Academic Press, London.
- Laskowski, J. S., Ralston, J. (Editors), 1992. Colloid Chemistry in Mineral Processing, Elsevier, New York.
- Kissa, E., 1999. Dispersions: Characterization, Testing and Measurement, Marcel Dekker, New York.
- Delgado, A. V. (Editor), Interfacial Electrokinetics and Electrophoresis, CRC Press, Florida, 2002.

- Dorn, E., 1880, *Ann. Phys. (Leipzig)* 10, 46.
- Booth, F., 1954. Sedimentation potential and velocity of solid spherical particles. *J. Chem. Phys.* 22, 1956-1968.
- Saville, D. A., 1982. The sedimentation potential in a dilute suspension. *Adv. Colloid Interfac.* 16, 267-279.
- Smoluchowski, V., 1921. M. In *Graetz Handbuch der Electricitat und des Magnetismus*, VEB Georg Thieme: Barth, Leipzig, Vol II, 385.
- Marlow, B. J., Rowell, R. L., 1985. Sedimentation potential in aqueous electrolytes, *Langmuir*, 1, 83-90.
- Levine, S., Neale, G., Epstein, N., 1976. The prediction of electrokinetic phenomenon within multiparticle systems, *J. Colloid Interf. Sci.* 57, 424-437.
- Kuwabara, S. J., 1959. The forces experienced by randomly distributed parallel circular cylinders or spheres in a viscous flow of small Reynolds number. *J. Phys. Soc. Jpn.* 14. 522-527.
- Maxwell, J. C., 1904. *A Treatise on Electricity and Magnetism*, Clarendon, Oxford.
- De La Rue, R. E., Tobias, C. W., 1959. On the conductivity of dispersions. *J. Electrochem. Soc.* 106, 827-833.
- Turner, J. C. R., 1976. 2-Phase conductivity: The electrical conductance of liquid-fluidized beds of spheres. *Chem. Eng. Sci.* 31, 487-492.
- Barchini, R., Saville, D. A., 1995. Dielectric response measurements on concentrated colloidal dispersions. *J. Colloid Interf. Sci.* 173, 86-91.
- Uribe-Salas, A., Gomez, C. O., Finch, J. A., 1994. A conductivity technique for gas and solids hold-up determination in three-phase reactors. *Chem. Eng. Sci.* 49, 1-10.
- Banisi, S., Finch, J. A., Laplante, A. R., 1994. On-line gas and solids hold-up estimation in solid-liquid-gas systems. *Miner. Eng.* 7, 1099-1113.
- Cruz, C. D. R., Reinshagen, J., Oberacker, R., Segadaes, A. M., Hoffmann, M. J., Electrical conductivity and stability of concentrated aqueous alumina suspensions. *J. Colloid Interf. Sci.* 286, 579-588.
- Abulnaga, B. E., 2002. *Slurry Systems Handbook*, McGraw-Hill, United States, pp. 1.21.

Eirich, F., Margaretha, H., Bunzl, L., 1936. Untersuchungen über die viskosität von suspensionen und lösungen. 4. Über die viskosität von kugelsuspensionen. Kolloid-Z. 74 276.

Somasundaran, P., 2006. Encyclopedia of Surface and Colloid Science, CRC Press, New York.

Rao, R., Leja, J., 2003. Surface Chemistry of Froth Flotation, Springer, New York.

Healy, T. W., Wiese, G. R., Yates, D. E., Kavanagil, B. V., 1973. Heterocoagulation in mixed oxide colloidal dispersions. J. Colloid Interf. Sci. 42, 647-649.

4. An Apparatus to Measure Electrical Charge of Bubble Swarms

4.1 Abstract

The electrical charge on a bubble surface is frequently suspected of playing a role in bubble-bubble and bubble-particle interaction in flotation systems. An apparatus has been developed to characterize the charge by measuring the sedimentation potential of bubble swarms under conditions approaching flotation. The technique allows in-process measurement of all system variables associated with surface electrical charge: sedimentation potential, solution conductivity, gas holdup, pH and bubble size distribution. The method was validated by comparing with literature iso-electric point (iep) values. Sedimentation potential was measured as a function of concentration and pH for a series of non-ionic surfactants (frothers), ionic surfactant collectors and multivalent metal ions. Results showed good agreement with established theory and prior experimental findings.

Keywords:

Bubble electrical charge, sedimentation potential, flotation

Research highlights:

- Introduce an integrated device to measure bubble electrical charge and other relevant variables.
- Technique was validated comparing with available literature.

- Non-ionic surfactants (frother) showed insignificant effect on bubble charge compared to ionic surfactants.
- Ionic surfactants influences the charge based on their reactive group and concentration.
- Hydrolysable metal ions can, also, effect the charge apparently by electrostatically attracted and adsorbed on the bubble surface.

4.2. Introduction

Electrical charge at the gas-liquid interface may play a role in many engineering processes, including mineral flotation where it contributes to particle-bubble and bubble-bubble interactions. Gas bubbles in water (no additives) have reported iso-electric point (iep) in the range pH 1.5-4 (Li and Somasundaran, 1991; Yang et al., 2001; Takahashi, 2005). The commonly considered charging mechanisms are: preferential orientation of the water dipoles with hydrogen towards the water, which attracts anions to the interface (Alty, 1926); and adsorption of OH^- ions to satisfy hydration energy (Yoon and Yordan, 1986; Kim et al., 2000). The presence of many solute ions will influence bubble surface charge.

Our interest is flotation systems. Most bubble charge studies have used isolated bubbles of a size smaller from those in flotation practice; the purpose of this paper is to introduce an apparatus to measure bubble charge under conditions approaching flotation, notably swarms of bubbles of diameter ca. 0.5 – 4 mm.

4.3. Background to apparatus

Discussed in chapter 2.

In this paper we introduce a novel integrated apparatus that allows in-process measurement of all system variables related to bubble surface charge: sedimentation potential, solution conductivity, gas holdup, pH and bubble size distribution. To distinguish from our prior work using sedimentation potential for particles (Uddin et al., 2010) we will refer to bubble sedimentation (or swarm) potential as BSP. To validate, the iep in de-ionized water determined when BSP is zero was compared with literature values. The technique was then used to characterize bubble surface charge in the presence of non-ionic frothers, ionic collectors, and inorganic salts.

4.4. Theory

4.4.1. Sedimentation potential

Sedimentation potential is the potential difference that arises when charged particles (used generically to include droplets and bubbles as well as solids) move in a force field (usually gravity). Charge destabilization created by fluid drag around each particle induces corresponding dipoles. These individual dipoles sum to produce the macroscopic potential difference between two points in a column of the suspension. This phenomenon was discovered by Dorn and is often called the “Dorn effect” (Booth, 1954; Saville, 1982).

For spherical, non-conducting, mono-disperse suspensions with negligible particle-particle interaction and surface conduction, sedimentation potential can be related to zeta potential by the Smoluchowski equation assuming the double layer

thickness $1/\kappa$ is small relative to the particle radius a i.e., $\kappa a \gg 1$ (Smoluchowski, 1921)

(see nomenclature):

$$E_s = \frac{\varepsilon_r \varepsilon_0 \phi (\rho - \rho_0) g}{\eta \lambda} \zeta \quad (1)$$

with E_s expressed as:

$$E_s = ((E_o)_i - (E_B)_i) / H \quad (2)$$

where E_B is a function of temperature, pH and electrode geometry. Equation (1) indicates that E_s has the same sign as ζ and the iep (i.e., when $\zeta = 0$) is indicated by $E_s = 0$. These two features, the sign and iep, are the most important in interpreting flotation systems; consequently there is no need to convert E_s for it to have practical use (note, E_s calculation is different to that for particles as dipoles created in this case are opposite direction).

4.4.2. Gas holdup: Maxwell's conductivity model

Maxwell's model (Maxwell, 1904) relates conductivity of heterogeneous media to the volume fraction of the constituent phases. In the case of a non-conducting dispersed phase, i.e., bubbles in this work, the volume fraction of bubbles (i.e., gas holdup) can be expressed as follows:

$$\phi = \frac{1 - \delta}{1 + \delta / 2} \quad (3)$$

$$\delta = \frac{(R_o)_i}{(R_s)_i} \quad (4)$$

Although the model is theoretically restricted to low concentration of dispersed phase, it has been used successfully in many concentrated systems (Turner, 1976; Barchini and Saville, 1995), including mineral processing (Uribe-Salas et al., 1994).

4.5. Experimental

4.5.1. Cell and accessories

The setup is shown in Fig. 1. The glass column was 2.6 cm inner diameter and 1 m in length. Two pairs of Ag/AgCl electrodes (Warner Instruments Inc.) were mounted through stopcocks, each electrode in the pair set 50 cm apart. The Ag/AgCl electrode pairs were connected to two separate channels of an Agilent 34901A 20-Channel, Multiplexer embedded in an Agilent 34970A data acquisition/switch unit (multimeter). One pair of electrodes was used for potential difference measurement and the other for resistance (conductivity) measurement. For the latter, a flip switch was used to reverse the current flow direction after each measurement to reduce charge build-up on the electrodes. The pH electrode (Cole-Parmer) inserted into the column via a CG-350-03 glass joint was connected to another channel on the multimeter through an Oakton 510 benchtop pH meter. A porous plate sparger at the base of the column dispersed gas (air) into bubbles. Air flow was controlled via a calibrated flowmeter.

For determination of bubble size distribution, a version of the McGill Bubble Size Analyzer (Hernandez-Aguilar and Finch, 2005; Gomez and Finch, 2007) was used. It comprised a 15° inclined removable 12 x 6 x 20 cm rectangular Plexiglas viewing chamber attached to the top of the column with a glass window for bubble imaging (Cannon EOS 500D, EF 100mm f/2.8 USM Macro Lens) (Fig. 2). The angled viewing window spreads bubbles into a near monolayer and provides an unambiguous definition

of the focal plane In-house image analysis software generates the size distribution and metrics such as arithmetic mean diameter d_{10} and Sauter mean diameter, d_{32} (Gomez and Finch, 2007).

A program developed using Matlab R2008a performed instrument control, data acquisition and data processing. This allowed flexibility to design measurement sequences and provide rapid post-processing of data. Interfacing was performed using VXIPnP driver with serial communication and SCPI (Standard Commands for Programmable Instrumentation) command format was used to control the multimeter.

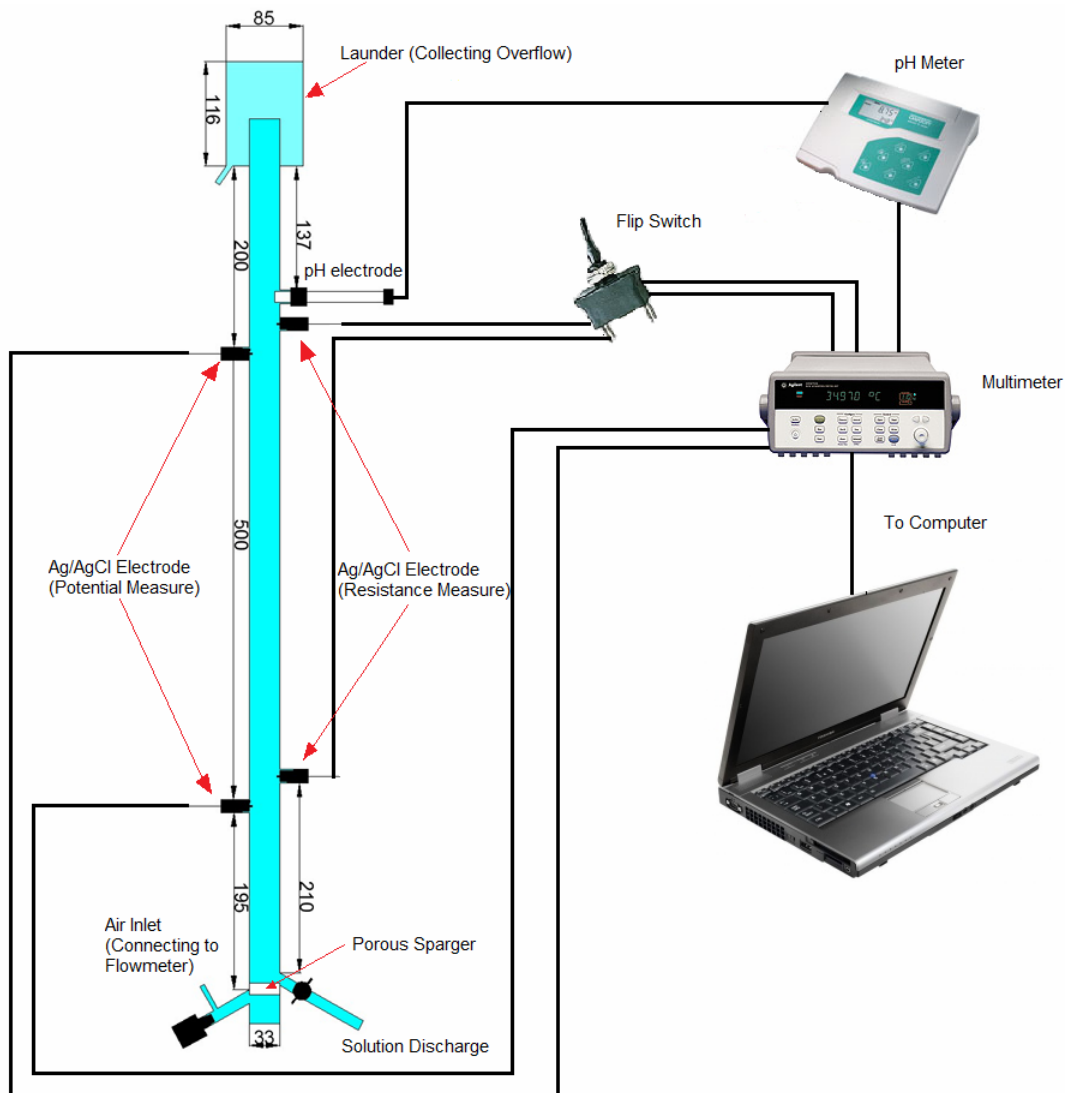


Fig. 1. Bubble column and accessories (dimensions in mm)

4.5.2. Procedure

Test solutions were prepared using de-ionized water with 10^{-2} M KCl as background electrolyte. The solution was conditioned over a magnetic stirrer for 30 minutes and transferred to the column, which is thoroughly cleaned with de-ionized water before each run. Bubbles were introduced by flowing air through the sparger at 10 mL/min. Ten minutes were allowed to let the system reach steady-state indicated by resistance measurements becoming steady. Each set of resistance measurements consisted of initially taking 5 readings at 10 s interval and when two consecutive sets reported similar resistance values, potential measurements were initiated, taken every 5 min. When the standard deviation of the mean of two successive measurements became less than 0.1 mV, the potential was recorded as E_O . Air flow was then stopped, 5 minutes allowed to expel the bubbles, and potentials were measured and recorded as E_B . For pH adjustment HCl and KOH were used. The same procedure was followed with the various solutes tested (Table 1). Selected conditions were repeated to estimate the standard deviation.

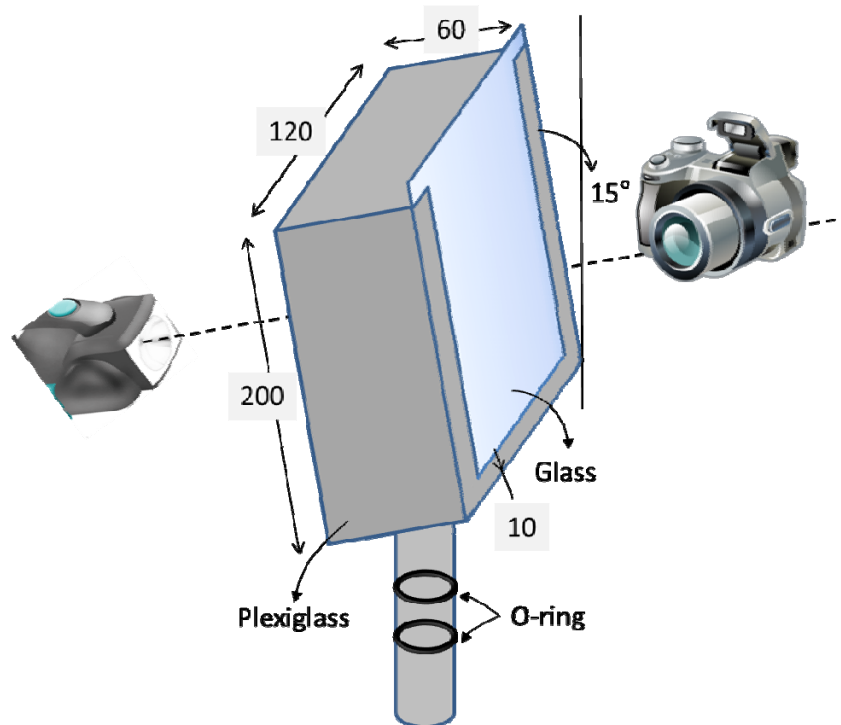


Fig. 2. Bubble size analyzer (dimensions in mm)

Table 1

Description of reagents used (RG – Reagent grade)

Reagents	Chemical formula	F.W.	Status	Purity	Source
Nonionic surfactants					
MIBC	$(\text{CH}_3)_2\text{CHCH}_2\text{CHOHCH}_3$	264.37	Liquid	RG	Sigma-Aldrich
DF250	$\text{CH}_3(\text{C}_3\text{H}_5\text{O})_4\text{OH}$	102.18	Liquid	RG	Dow Chemical
Ionic surfactants					
SHS	$\text{C}_{16}\text{H}_{33}\text{SO}_4\text{Na}$	344.49	Solid	RG	Alfa Aesar
HTAB	$\text{C}_{16}\text{H}_{33}(\text{CH}_3)_3\text{NBr}$	364.44	Solid	RG	Fisher Scientific
Chloride salts					
Potassium	KCl	74.55	Solid	RG	MP Biomedicals
Magnesium	MgCl_2	95.21	Solid	98%	Sigma-Aldrich

4.6. Results

4.6.1. Examples of basic readings

Fig. 3 shows potential difference for background and bubble swarm as a function of readings at ca. pH 3 and 8 (i.e., respectively below and above the expected iep based on the literature). For positively charged bubbles (pH 3, Fig. 3A), the concentration of negative ions (counterions) is higher in the diffuse part of the double layer and the dipoles created by fluid drag are more positive in the upper part than in the lower part of the column. That is why the potential difference is more positive with bubbles than without (i.e., more positive than the background). The opposite is observed for negatively charged bubbles (pH 8, Fig. 3B).

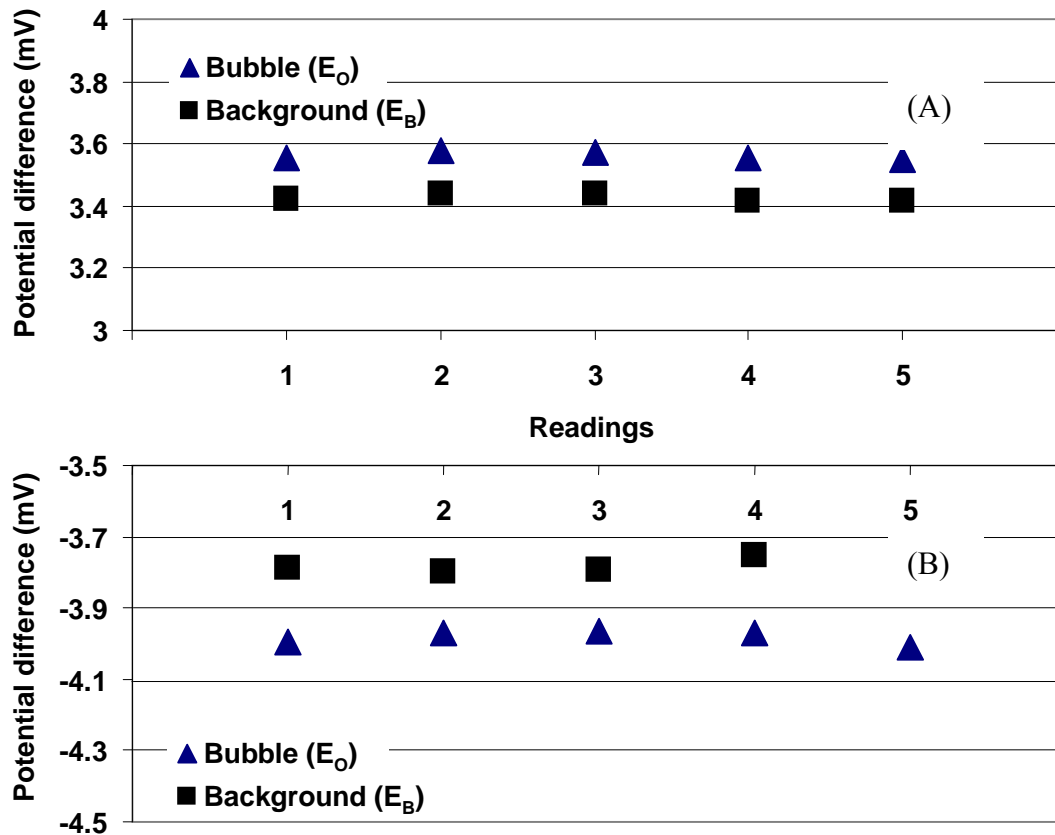


Fig. 3. Potential difference for background (E_B) and in presence of bubbles (E_O) as a function of readings (A) pH ca. 3 and (B) pH ca. 8

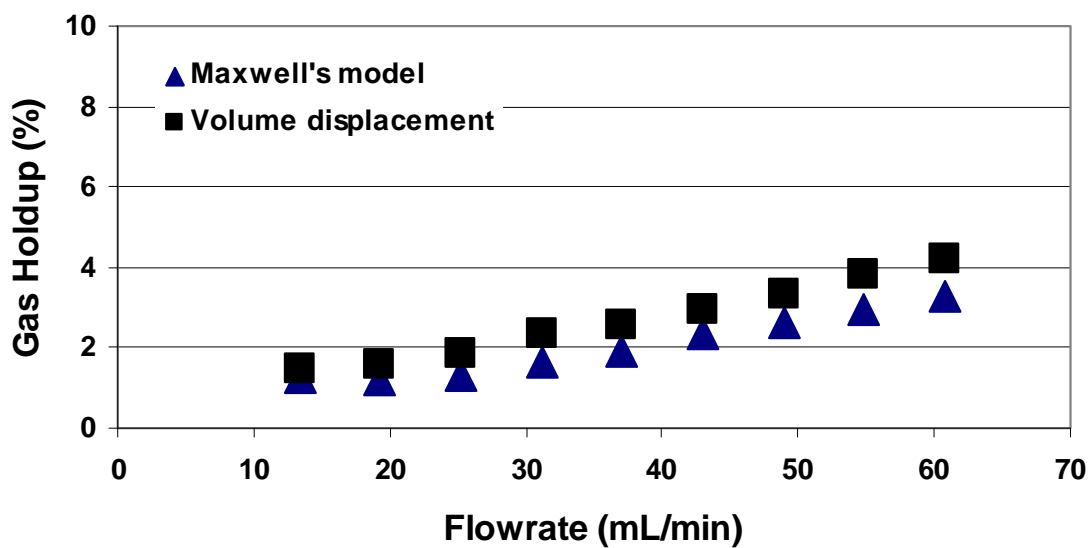


Fig. 4. Gas holdup vs. flowrate in presence of (DF250, pH ca. 6.0)

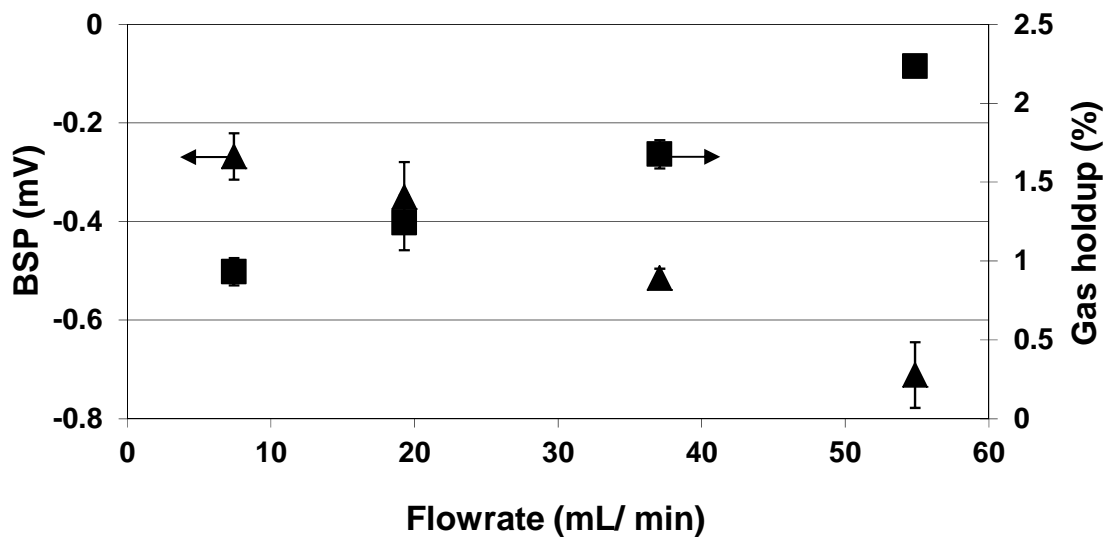


Fig. 5. Bubble sedimentation potential (BSP) and gas holdup as a function of flowrate in presence of 5×10^{-5} M SHS (pH ca. 6.0)

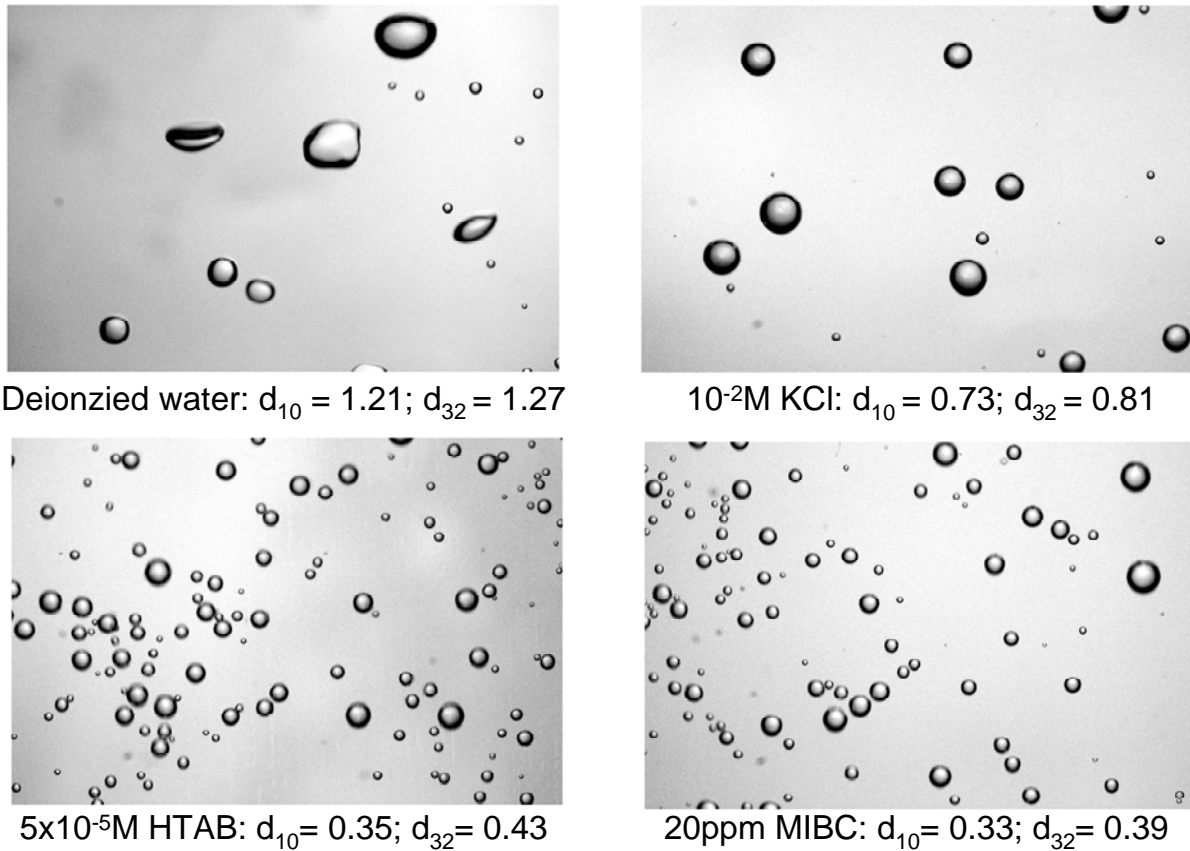


Fig. 6. Bubble size in presence of, from top left to bottom right: de-ionized water (only), 10^{-2} M KCl, HTAB and MIBC (dimensions in mm)

Fig. 4 compares gas holdup estimated from Maxwell's model (equations 3 and 4) with direct measurement by the bed expansion method (there was no froth present which otherwise complicates the expansion method).

Fig. 5 shows the effect of increasing air flowrate which increases the BSP and the gas holdup. The link is the increase in number of bubbles that increase gas holdup and create more dipoles which constitute the macroscopic potential difference.

Fig. 6 gives examples of the impact on bubble size distribution of the three of reagents; the reagents decrease size, especially the two surfactants, and increase bubble

sphericity, in line with expectation. The bubble sizes with surfactant are at the low end of the range in flotation systems.

The basic readings support that the setup faithfully measures the parameters required to interpret BSP.

4.6.2. Validation: Determination of iep for de-ionized water

The BSP as a function of pH in water alone is shown in Fig. 7. (Standard deviation of 3 repeats is indicated by the error bar.) The potential decreased from +0.2 to -0.4 mV as pH was increased from 3 to 9. The indicated iep ($E_s = 0$) is ca. pH 4.0. The zeta potential (ZP) vs. pH reported by Takahashi (2005) for air bubbles is included in Fig. 7 and follows a similar trend to the present study.

From the literature, the reported iep for water alone and method used are compared with the result from BSP in Table 2. The range in iep is pH 1.5 – 4.0 with our BSP at the high end. In a recent atomic force microscopy (AFM) study, Tabor et al. (2011) found that the iep of two inert gases (Ar and N₂) and air were close to pH 3.0 and 4.0, respectively. The higher iep in air was attributed to the presence of CO₂. The iep found here is in agreement with this higher iep.

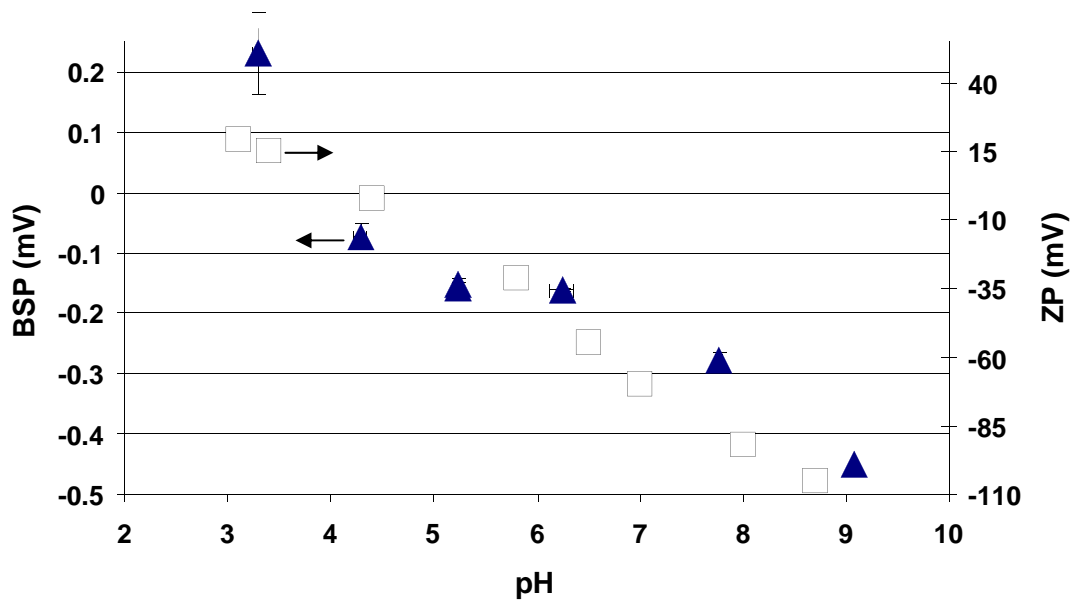


Fig. 7. Bubble sedimentation potential (BSP) of bubbles as a function of pH in de-ionized water (\blacktriangle , 10^{-2} M KCl background, error bar represents standard deviation of 3 repeats) compared with zeta potential (ZP) data of Takahashi (2005) (\square)

Table 2

Method of measurement and iso-electric-point of bubbles in purified water from literature

iep	Bubble formation, background electrolyte and method	Avg. size	Gas	Reference
2.5	Dissolved air vessel (electrophoresis)	33 μm	Air	Okada et al., 1990
1.5	Injecting gas through a glass frit, 10^{-2} M NaCl (electrophoresis)	< 5 μm	N ₂	Li and Somasundaran (1991)
3-3.5	Electrochemical, 10^{-2} M NaCl (electrophoresis)	30 μm	H ₂	Yang et al. (2001)
3-3.5	Ultrasonic cavitation, 10^{-3} M KCl (electrophoresis)	750 nm	Vacuum	Cho et al. (2005)
~ 4.0	Centrifugal force (electrophoresis)	~ 40 μm	Air	Takahashi (2005)
3.2	Ultrasonic cavitation, 10^{-3} M KCl (electrophoresis)	~ 10 μm	Vacuum	Elmahdy et al. (2008)
~ 3.0	Capillary (electrophoresis)	1.3 mm	N ₂	Creux et al., 2009
~ 3.0	Cantilever (AFM)	125 μm	Ar, N ₂	Tabor et al., 2011
~ 4.0			Air	
~ 4.0	Injecting gas through porous sparger, 10^{-2} M KCl (sedimentation)	~ 1 mm	Air	This study

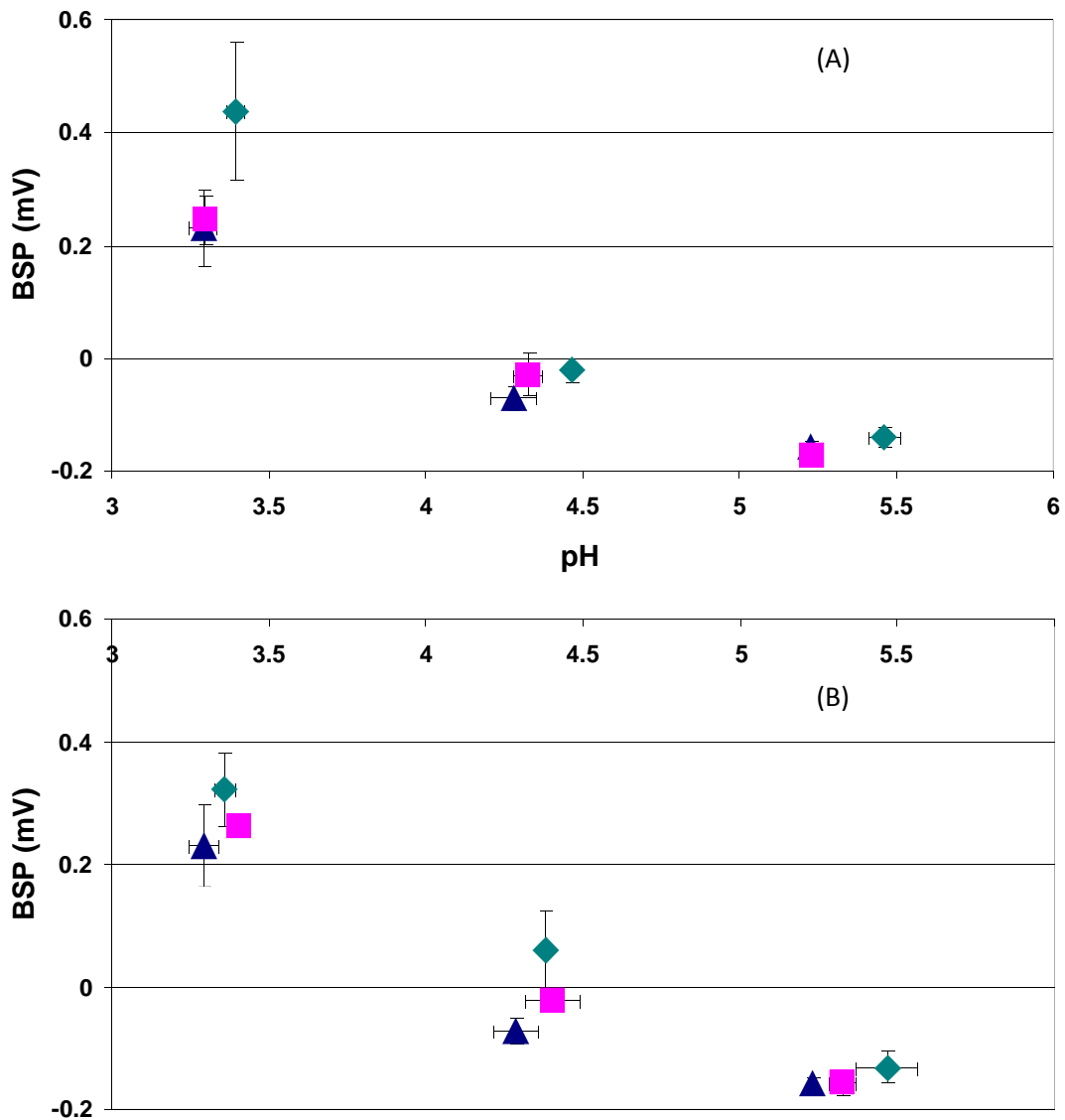


Fig. 8. Bubble sedimentation Potential (BSP) as function of pH in (A) MIBC and (B) DF250 at concentrations of (▲) 0, (■) 10, and (◆) 100 ppm and natural pH (ca. 6)

4.6.3. Effect of non-ionic surfactant (frother)

Fig. 8 shows the effect of MIBC and DF250 frothers on bubble sedimentation potential. There is no significant effect up to 100 ppm which is about 10 times the concentration used in flotation practice (Gelinas and Finch, 2005). We can conclude that

in flotation these frothers do not have an impact on bubble surface charge, as anticipated, from similar findings for non-ionic surfactants (Yoon and Yordan, 1986; Elmahdy et al., 2008).

4.6.4. Ionic surfactants

Fig. 9 shows results obtained with the anionic surfactant sodium hexadecyl sulphate (SHS) and cationic surfactant hexadecyltrimethylammonium bromide (HTAB) at natural pH. In the presence of the anionic surfactant the BSP became more negative and in presence of the cationic surfactant the BSP switched to positive values. This corresponds to the expected orientation with the hydrocarbon chain on the air side of the bubble surface and the charged head group on the water side (which determines the bubble charge), as shown by others (Usui and Sasaki, 1978; Yoon and Yordan, 1986). The increase in absolute BSP with increasing surfactant concentration tracks the increased adsorption, which seems to level off for HTAB above ca. 5×10^{-5} M. There was considerable froth formed with HTAB at $> 5 \times 10^{-5}$ M, which may indicate that surfactant was partitioned to the froth, i.e., the concentration in the BSP measurement section was lower than the quoted which may contribute to the ‘levelling off’ of the BSP.

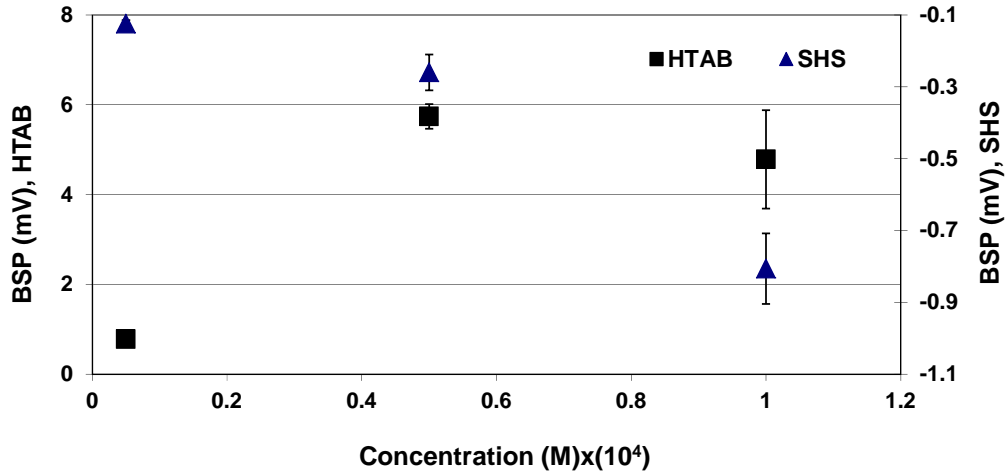


Fig. 9. Effect of ionic surfactant concentration on bubble sedimentation potential (BSP) in presence of SHS (anionic) and HTAB (cationic) (pH ca. 6)

4.6.5. Effect of Mg ions

Fig. 10 shows the effect of 10^{-2} M Mg (added as MgCl_2 with 10^{-3} M KCl as background) on BSP as a function of pH. From pH 5 up to pH 9 the BSP increased, became slightly positive then decreased as pH was further increased. This response and the two charge reversals have been reported previously for bubbles (Li and Somasundaran, 1991; Han et al., 2004) and are well known in the case of particles (James and Healy, 1972; Fuerstenau and Palmer, 1976).

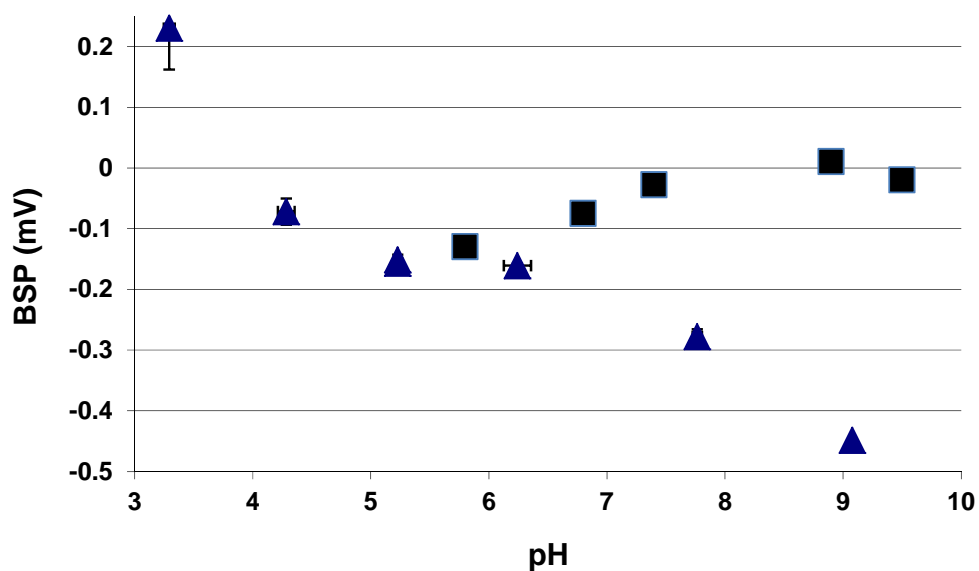


Fig. 10. Bubble sedimentation potential (BSP) vs. pH in presence of 10^{-2} M $MgCl_2$ (■) compared BSP in water alone (▲)

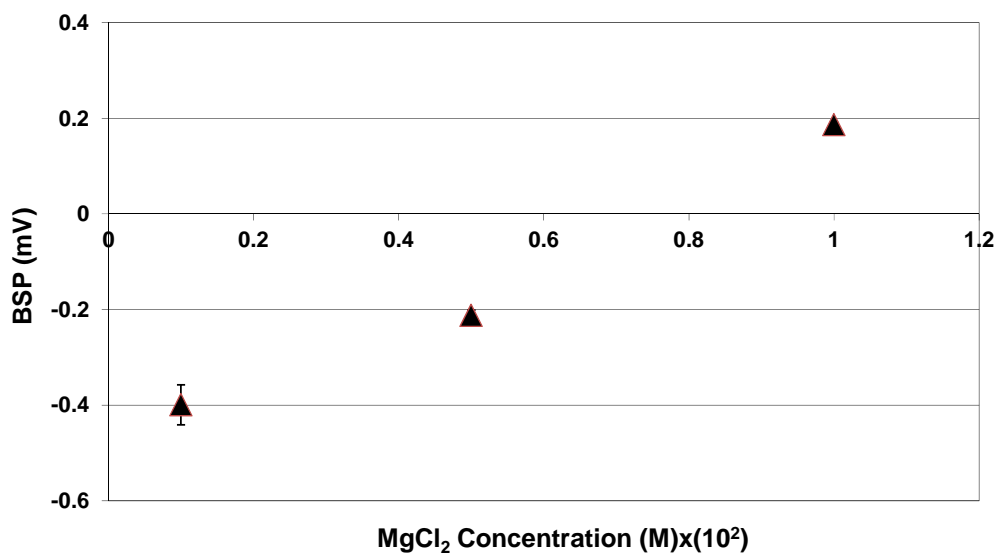


Fig. 11. Bubble sedimentation potential (BSP) as a function of Mg concentration (as $MgCl_2$) added to fixed concentration of SHS (5×10^{-5} M)

Fig. 11 shows effect of the addition of Mg^{2+} (as $MgCl_2$) to 5×10^{-5} M SHS at natural pH (ca. 6.0). A shift of sedimentation potential to more positive value is observed

with increasing Mg^{2+} concentration with charge reversal at ca. $8 \times 10^{-3} M$ Mg. In this case, the anionic SHS is either electrostatically attracting Mg^{2+} as a counter ion, or is adsorbing an Mg-SHS complex.

4.7. Discussion

A method using sedimentation potential to reveal surface charge characteristics of bubbles in a swarm under flotation-like conditions has been introduced. The bubble sedimentation potential (BSP) reveals the two important flotation-related features, sign of bubble charge and iso-electric point (iep), without need to convert to zeta potential. The system was validated by showing good agreement between the iso-electric point (iep) for bubbles reported in the literature and that measured here when $BSP = 0$ for water alone. Our BSP result was on the high end of the range (iep ca pH 4) which is close to the recent result of Tabor et al. (2011). They attributed the high-end value to CO_2 and formation of species which displace OH^- from the bubble surface and raise the iep compared to inert (CO_2 -free) gases. The agreement with results on single and often quite small bubbles (Table 2) also suggests that neither bubble size nor the presence of multiple bubbles affects the iep.

The acidic iep of bubbles indicates OH^- uptake at the gas-liquid interface is favoured over H^+ . One explanation is that the hydration energy of H^+ (-1127 KJ/mol) is higher than for OH^- (-489KJ/mol) (Yoon and Yordan, 1986; Kim et al., 2000). A counter-argument is that increasing $MgCl_2$ concentration decreases the negative potential (as seen here) although the hydration energy of Mg^{2+} (-1904 KJ/mol) is higher than the anion Cl^- (-363 KJ/mol). Takahashi (2005) suggested bubble electrical charge is related

to the hydrogen bonding network at the gas-liquid interface. Since H^+ and OH^- are elements of this network, they are more attracted to the interface than to staying in the bulk phase. To explain the negative charge, the OH^- may more involved in the network formation. In another explanation, Gray-Weale and Beattie (2009) suggest that OH^- suppresses collective dipole moment fluctuations in the surrounding water molecules which exerts a force that attracts OH^- to the region of lower relative permittivity, i.e., the gas-liquid interface.

To generate the small bubbles (ca. 1 mm) in flotation machines usually requires the presence of surfactants called frothers (Exceptions are cases where surfactants are produced naturally as in oil sands processing (Zhou et al., 2000) or systems with high salt concentration (Quinn et al., 2007)). Frothers are non-ionic surfactants and, as supported here, are not expected to affect bubble charge. At 100 ppm frother concentration, there is arguably an increase in iep, with DF250 (Fig. 8B) showing a larger increase than MIBC. This may linked to the oxygen to carbon ratio which is higher in the case of DF250 (0.42) than MIBC (0.17) making the DF250 molecule more basic which could shift the iep to more alkaline pH (Yoon and Yordan, 1986). Given that practical flotation systems do not have such high frother concentrations further speculation is not warranted.

In contrast to frothers, the impact of ionic surfactants was significant (Fig. 9). The type and concentration of the head group on the bubble surface strongly influenced the BSP, the anionic SHS driving the charge more negative and the cationic HTAB reversing charge. The main purpose of collectors is to render selected particles hydrophobic but it is evident that these collectors markedly influence bubble properties as well. While particle hydrophobicity is the dominant factor in attachment to bubbles it is possible that

bubble charge plays a role in some cases (Johnson et al., 2009). The set-up is being adapted to include particles to try to test this possibility.

Along with ionic surfactants, Fig. 10 also shows the strong effect of an inorganic cation, Mg^{2+} . This effect on bubble charge is common to a range of inorganic salts, the cation apparently invariably being the active partner compared to the anion. The choice of Mg here is its common presence in flotation process water and the fact it can influence flotation at low concentration (a few ppm), often lower than an equally common cation Ca (Mirnezami et al., 2004). The impact of Mg^{2+} on bubble charge is similar to that observed on particles, giving two charge reversals, ca. pH 9-10 and pH 12. From knowledge of the species present as a function of pH the electrokinetic behaviour of particles has been explained (Fuerstenau and Palmer, 1976). At $pH < 6$ Mg^{2+} dominates and appears to be largely surface inactive; from pH 6 – 9 the monohydroxide $Mg(OH)^+$ forms which is more active and can react with surface OH to give surface $-O-Mg^+$ sites, the reaction product explaining how the surface can reverse in charge. At $pH > 10$ $Mg(OH)_{2(s)}$ dominates and these precipitates form on the surface either in situ (the particle acts as nucleation site) or by hetero-coagulation. In either case the particle charge now takes on the characteristics of $Mg(OH)_{2(s)}$ which, having an iep ca. pH 12, explains the second charge reversal. The similarity of the BSP-pH trend to the particle zeta potential-pH trend suggests a similar mechanism. Thus we envisage as pH is increased into the alkaline region first $-O-Mg^+$ surface sites on the bubble then coatings of $Mg(OH)_{2(s)}$. What effect such altered bubble surfaces have on interaction with particles is largely unexplored.

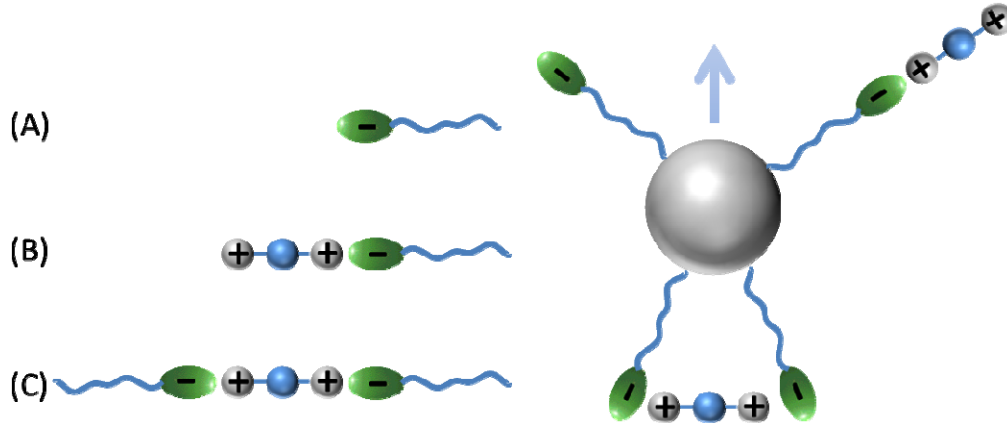


Fig. 12. Three possible arrangements in the SHS - Mg^{2+} system as a function of increasing relative concentration of Mg (A, B, C)

The tests showing Mg could counter the charge due to SHS (Fig 11) indicates Mg may also influence the action of collector. When Mg^{2+} is added to SHS, it can be arranged in three ways (Fig. 12) depending on the concentration of both species. At Mg^{2+} concentrations much less than SHS the bubble charge is dictated by the surfactant alone (arrangement A). As the relative concentration of Mg^{2+} increases, more B occurs and now the negative charge due to surfactant is countered by exposed Mg^+ sites. Further increase in relative concentration may see the SHS neutralized as $Mg(SHS)_2$ species with remaining Mg^{2+} imposing positive charges depending on pH as discussed above. Whether these effects on bubble charge hamper (or enhance) particle attachment in flotation is not known that the novel measurement system introduced here may help elucidate.

While particle flotation is our main interest it is appreciated that metal ion-surfactant interaction is at the heart of ion and precipitate flotation schemes of water treatment (Sebba, 1959; Nicol et al., 1992; Tessele et al., 1998), including removal of

Mg^{2+} by a similar reagent to that employed here, sodium dodecylsulfate (SDS) (Walkowiak, 1991; Doyle, 2003). Again, by directly incorporating knowledge of the bubble charging properties we may gain insight into these processes.

4.8. Conclusions

The present work has introduced an integrated apparatus that allows in-process measurement of system variables correspond to electrokinetics of bubble swarms viz: bubble sedimentation potential (BSP), conductivity, gas holdup, pH and bubble size distribution. The approach was validated by showing good agreement with literature iso-electric point values for purified water. In presence of non-ionic surfactant (frother) bubble charge is largely unaffected. The presence of cationic surfactant HTAB changed bubble charge to positive while anionic surfactant SHS enhanced bubble negative charge. The action of Mg^{2+} appears to be similar to that on particles giving two charge reversals as pH is raised reflecting the Mg species present. Adding Mg reversed the sign with SHS and is explained in terms of possible species formed.

4.9. Acknowledgements

The work was funded under the Chair in Mineral Processing sponsored by Vale, Teck Resources, Barrick Gold, Xstrata Process Support, Shell Canada, SGS Lakefield, COREM and Flottec, under the Natural Sciences and Engineering Research Council of Canada (NSERC) Collaborative Research and Development program.

4.10. Nomenclature

Symbols	Meaning	Units
i	Reading number	
E_s	Sedimentation potential	Volt/m
E_o	Bubble potential difference	Volt
E_B	Background potential difference	Volt
ϕ	Particle/bubble volume fraction	
ζ	Zeta potential	Volt
η	Viscosity of suspension	Pa-sec.
λ	Specific conductivity	S/m
ρ	Particle density	Kg/m ³
ρ_0	Density of medium	Kg/m ³
ϵ_r	Relative permittivity of the medium	
ϵ_0	Permittivity of the free space	F/m
a	Particle radius	m
$1/\kappa$	Double layer thickness	m
H	Distance between electrodes	m
R_B	Resistance of background	Ohm
R_s	Resistance with bubbles	Ohm

4.11. References

- Alty, T., 1926. The origin of the electrical charge on small particles in water. Proceedings of the Royal Society of London, Series A, vol. 122 (760), pp. 235–251.
- Barchini, R., Saville, D. A., 1995. Dielectric response measurements on concentrated colloidal dispersions. *J. Colloid Interf. Sci.* 173, 86–91.
- Booth, F., 1954. Sedimentation potential and velocity of solid spherical particles. *J. Chem. Phys.* 22, 1956–1968.
- Cho, S.H., Kimb, J.Y., Chuna, J.H., Kima, J.D., 2005. Ultrasonic formation of nanobubbles and their zeta-potentials in aqueous electrolyte and surfactant solutions. *Colloid Surface A* 269, 28–34.
- Collins, G.L., Motarjemi, M., Jameson, G.J., 1978. A method for measuring the charge on small gas bubbles. *J. Colloid Interf. Sci.* 63, 69–75.
- Creux, P., Lachaise, J., Graciaa, A., Beattie, J. K., Djerdjev, A. M., 2009. Strong specific hydroxide ion binding at the pristine oil/water and air/water interfaces. *J. Phys. Chem. B* 113, 14146–14150.
- Doyle, F. M., 2003. Ion flotation—its potential for hydrometallurgical operations. *Int. J. Miner. Process.* 72, 387–399.
- Elmahdy, A.M., Mirnezami, M., Finch, J.A., 2008. Zeta potential of air bubbles in presence of frothers. *Int. J. Miner. Process.* 89, 40–43.
- Fan, X., Zhang, Z., Li, G., Rowson, N.A., 2004. Attachment of solid particles to air bubbles in surfactant-free aqueous solutions. *Chem. Eng. Sci.* 59, 2639–2645.
- Fuerstenau, M. C., Palmer, B. R., 1976. Anionic flotation of oxides and silicates, In: M.C. Fuerstenau, M. C. (Ed), *Flotation-A.M. Gaudin Memorial Volume*, Vol. 1, AIME, New York, pp. 148–196.
- Gélinas, S., Finch, J. A., 2007. Frother analysis: some plant experiences. *Miner. Eng.* 20 1303–1308.
- Gomez, C. O., Finch, J. A., 2007. Gas dispersion measurements in flotation cells. *Int. J. Miner. Process.* 84, 51–58.
- Gorain, B. K., Franzidis, J. P., Manlapig, E. V., 1995. Studies on impeller type, impeller speed and air flow rate in an industrial scale flotation cell. Part 1: Effect on bubble size distribution. *Miner. Eng.* 8, 615–635.
- Gray-Weale, A., Beattie, J. K., 2009. An explanation for the charge on water's surface. *Phys. Chem. Chem. Phys.* 11, 10994–11005.

- Han, M.Y., Ahn, H.J., Shin, M.S., Kim, S.R., 2004. The effect of divalent metal ions on the zeta potential of bubbles. *Water Sci. Technol.* 50, 49–56.
- Hernandez-Aguilar, J., Finch, J. A., 2005. Validation of bubble sizes obtained with incoherent imaging on a sloped window. *Chem. Eng. Sci.*, 60, 3323–3336.
- Kim, J.Y., Song, M.G., Kim, J.D., 2000. Zeta potential of nanobubbles generated by ultrasonication in aqueous alkyl polyglycoside solutions. *J. Colloid Interf. Sci.* 223, 285–291.
- James, R. O., Healy, T. W., 1972. Adsorption of hydrolysable metal ions at the oxide-water interface, Part I, II and III: *J. Colloid Interf. Sci.* 40, 42-52, 53-64, 65-81.
- Johnson, D., Hilal, N., Waters, K., Kathryn, Hadler, K., Cilliers, J., 2009. Measurements of interactions between particles and charged microbubbles using a combined micro- and macroscopic strategy. *Langmuir* 25, 4880–4885.
- Kubota, K., Hayashi, S., and Inaoka, M., 1983. A convenient experimental method for measurement of zeta-potentials generating on the bubble suspended in aqueous surfactant solutions. *J. Colloid Interf. Sci.* 95, 362–369.
- Li, C., Somasundaran, P., 1991. Reversal of bubble charge in multivalent inorganic salt solutions – effect of magnesium. *J. Colloid Interf. Sci.* 146, 215–218.
- Maxwell, J.C., 1904. *A Treatise on Electricity and Magnetism*, Clarendon, Oxford, 1904.
- Mirnezami, M., Hashemi, M. S., Finch, J. A., 2004. Aggregation: Case of Ca ions and Mg(OH)₂ coated silica, In : 5th UBC-McGill Symposium on Fundamentals in Mineral Processing (Ed. J. Laskowski), CIM, Hamilton, pp. 149-158.
- Nicol, S.K., Galvin, K.P., Engel, M.D., 1992. Ion flotation—potential applications to mineral processing. *Miner. Eng.* 5 (10–12), 1259– 1275.
- Okada, K., Akagi, Y., Kogure, M, Yoshioka, N., 1990. Effect of surface charges of bubbles and fine particles on air flotation process. *Can. J. Chem. Eng.*, 68, 393 – 398.
- Quinn, J. J., Kracht, W., Gomez, C. O., Gagnon, C., Finch, J. A., 2007. Comparing the effect of salts and frother (MIBC) on gas dispersion and froth properties. *Miner. Eng.*, 20, 1296 – 1302.
- Saville, D. A., 1982. The sedimentation potential in a dilute suspension, *Adv. Colloid Interface Sci.* 16, 267-279.

- Sebba, F., 1959. Concentration by ion flotation. *Nature* 184, 1062–1063.
- Sherwood, J. D., 1986. Electrophoresis of gas bubbles in a rotating fluid. *J. Fluid. Mech.* 162, 129–137.
- Tabor, R. F., Chan, D. Y. C., Grieser, F., Dagastine, R. R., 2011. Anomalous stability of carbon dioxide in pH-controlled bubble coalescence. *Angew. Chem. Int. Ed.* 50, 3454–3456.
- Takahashi, M., 2005. Zeta potential of microbubbles in aqueous solutions: Electrical properties of the gas-water interface. *J. Phys. Chem. B* 109, 21858–21864.
- Tessele, F., Misra, M., Rubio, J., 1998. Removal of Hg, As and Se from gold cyanide leach solutions by dissolved air flotation. *Miner. Eng.* 11 (6), 535– 543.
- Turner, J. C. R., 1976. 2-Phase conductivity: The electrical conductance of liquid-fluidized beds of spheres. *Chem. Eng. Sci.* 31, 487–492.
- Uribe-Salas, A., Gomez, C. O., Finch, J. A., 1994. A conductivity technique for gas and solids hold-up determination in three-phase reactors. *Chem. Eng. Sci.* 49, 1–10.
- Usui, S., Sasaki, H., 1978. Zeta potential measurements of bubbles in aqueous surfactant solutions. *J. Colloid Interf. Sci.* 65, 36–45.
- Usui, S., Sasaki, H., Matsukawa, H., 1981. The dependence of zeta potential on bubble size as determined by the dorn effect. *J. Colloid Interf. Sci.* 81, 80–84.
- Walkowiak, W., 1991. Mechanism of selective ion flotation: 1. Selective flotation of transitional metal cations. *Separ. Sci. Technol.* 26 (4), 559– 568.
- Yang, C., Dabros, T., Li, D., Czarnecki, J., Masliyah, J.H., 2001. Measurement of the zeta potential of gas bubbles in aqueous solutions by microelectrophoresis method. *J. Colloid Interf. Sci.* 243, 128–135.
- Yoon, R.H., Yordan, J.L., 1986. Zeta-potential measurements on microbubbles generated using various surfactants. *J. Colloid Interf. Sci.* 113, 430–438.
- Zhou, Z., Xu, Z., Masliyah, J., 2000. Effect of natural surfactants released from athabasca oil sands on air holdup in a water column. *Can. J. Chem. Eng.* 78, 617 – 624.

5. Effect of Particles on the Electrical Charge of Gas Bubbles in Flotation

5.1. Abstract

In this paper, a bubble sedimentation potential (BSP) setup is extended to include particles. Provided particle suspension concentration was not too high, BSP could be measured and interaction with particles followed. With increasing particle concentration, when alumina was made hydrophobic with an anionic surfactant (collector) the bubble became less negative and with silica made hydrophobic by a cationic collector the bubble became less positive. In presence of frother (non-ionic surfactant), a small increase in BSP was noted with alumina but not with silica. To aid interpretation, bubble-particle attachment was visualized at a pendant bubble exposed to agitated suspensions. Attachment between oppositely charged non-hydrophobic particles and bubbles was observed. By adding surfactant to give the bubble the same charge as the particles the extent of non-hydrophobic particle pick-up was diminished. Under these conditions BSP could not be measured attributed to bubbles and particles being well dispersed and giving competing bubble and particle sedimentation potential data. The experiments were extended to clinochrysotile, the dominant fraction of Thompson ultramafic Ni-ore, and a possibility of manipulating bubble charge to depress clinochrysotile is discussed.

Keywords:

Bubble-particle attachment, sedimentation potential, surfactant

Research highlights:

- Modify bubble sedimentation potential (BSP) apparatus to include particles.
- Determine impact using alumina, silica and clinochrysotile derived from ore.
- BSP change significant with particles made hydrophobic by ionic collectors.
- BSP showed some indication of interaction with non-hydrophobic particles.
- Direct attachment of non-hydrophobic particles observed.

5.2. Introduction

Flotation separates hydrophobic particles from hydrophilic particles by attachment to bubbles. First developed in the mining industry it is now used in a variety of industries, e.g. water treatment, petrochemical, paper manufacturing, food processing (Rousseau, 1987). Attachment of hydrophobic particles is the dominant recovery process but other processes lead to some recovery of non-hydrophobic (hydrophilic) particles. Entrainment is the major mechanism but electrostatic interactions, dependent on the relative electric charge on bubbles and particles, is sometimes suspected (Mayers, 1991). Given the usually large amount of hydrophilic gangue to be rejected any level of attachment due to electrostatic interactions could lead to significant downgrading of concentrate. The possibility of electrostatic interaction in recovery of clinochrysotile was raised by research into processing ultramafic Ni-ore from the Thompson nickel belt in northern Manitoba (Xu et al., 2011) which stimulated the present enquiry.

The recovery of hydrophilic particles is most often attributed to entrainment (Trahar, 1981). The mechanism can be identified, for example, by correlating with water recovery. Any attempt to isolate an electrostatic bubble-particle interaction contribution

to hydrophilic particle recovery by flotation experiments would be overwhelmed by the mass recovered by entrainment. A more direct investigation of bubble-particle interaction is required.

In a previous study an apparatus was developed to follow charge on particles by measuring the particle sedimentation potential (PSP) (Uddin et al., 2010). This was subsequently modified to measure bubble sedimentation potential (BSP) (Uddin et al., 2011). This paper describes further adaptation to measure BSP in presence of particles. This offers one way to investigate charge dependent bubble-particle interactions under flotation-like conditions. To help interpret the data a second approach was also taken, namely visual inspection of a pendant bubble exposed to agitated suspensions.

5.3. Background

5.3.1. Particle charging

The surface of particles and bubbles in electrolyte solutions acquires charge by various mechanisms (Hunter, 1991). For many minerals, the main mechanism results from a hydrated surface. Generally, hydration products react with H^+ to form positive sites and OH^- to form negative sites.

For bubbles in water alone the iso-electric point is ca. pH 1.5-4 (Li and Somasundaran, 1991; Yang et al., 2001; Takahashi, 2005) hence over most of the pH range the charge is negative. This has led to two commonly considered surface charging mechanisms: preferential orientation of the water dipoles with hydrogen towards the water, which attracts OH^- to the interface (Alty, 1926); and adsorption of OH^- ions to satisfy hydration energy (Yoon and Yordan, 1986; Kim et al., 2000). In flotation-related

studies, measurement of bubble charge reveals interaction with collectors and inorganic ions (Usui and Sasaki, 1978; Li and Somasundaran, 1991; Uddin et al., 2011). The purpose of this study is to track bubble charge in the presence of particles to reveal interaction mechanisms.

5.3.2. Bubble-particle electrostatic interaction studies

Discussed in chapter 2.

There is no literature apparent describing measurement of bubble electrical charge in the presence of particles. In the current study, a previously developed bubble sedimentation (swarm) potential (BSP) apparatus (Uddin et al., 2011) is modified to measure BSP in the presence of particles.

5.3.3. Sedimentation potential

Sedimentation potential (SP) is the potential difference that arises when charged particles (a generic term that includes bubbles and droplets) move in a force field (usually gravity). Charge destabilization created by the fluid drag surrounding each particle induces corresponding dipoles in the suspension. These individual dipoles sum to produce the macroscopic potential difference between two points in a column. This phenomenon was discovered by Dorn and is often called the “Dorn effect” (Booth, 1954; Saville, 1982).

5.4. Experimental

5.4.1. Reagents and minerals

The reagents and particles used are summarized in Table 1 and 2, respectively. The reagents included two commercial frothers (non-ionic surfactants), two ionic surfactant collectors, KCl to provide background electrolyte. Alumina and silica were selected as model solids providing, respectively, positive and negative charge at natural pH. The clinochrysotile was derived from a sample of Thompson ultramafic Ni-ore (provided by Vale) by a dry separation technique. X-ray diffraction identified the product as mostly clinochrysotile (Fig. 1), the dominant gangue mineral in that ore (Dai et al., 2009).

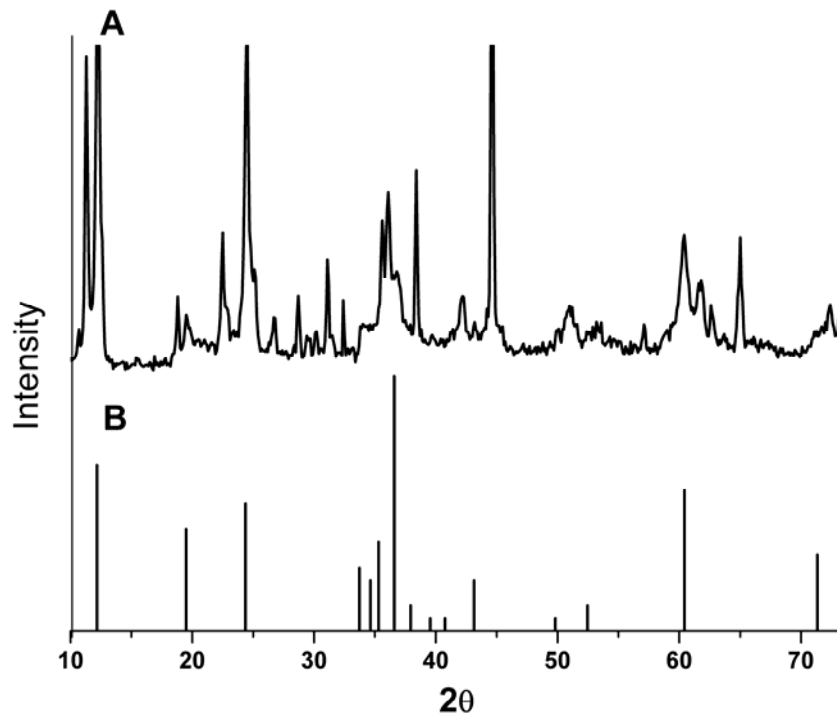


Fig. 1. XRD of (A) sample derived from ore and (B) match for clinochrysotile

Table 1

Description of reagents used (RG – Reagent grade)

Reagents	Chemical formula	F.W.	Status	Purity	Source
Nonionic surfactants					
MIBC	$(\text{CH}_3)_2\text{CHCH}_2\text{CHOHCH}_3$	264.37	Liquid	RG	Sigma-Aldrich
DF250	$\text{CH}_3(\text{C}_3\text{H}_6\text{O})_4\text{OH}$	102.18	Liquid	RG	Dow Chemical
Ionic surfactants					
SHS	$\text{C}_{16}\text{H}_{33}\text{NaO}_4\text{S}$	344.49	Solid	RG	Alfa Aesar
HTAB	$\text{C}_{16}\text{H}_{33}(\text{CH}_3)_3\text{NBr}$	364.44	Solid	RG	Fisher Scientific
Salts					
Potassium chloride	KCl	74.55	Solid	RG	MP Biomedicals

Table 2

Description of particles used

Particle	Source	IEP	IEP Reference
Alumina	Sigma-Aldrich (CAS no. 1344-28-1)	~ 9.0	Uddin et al. (2010)
Silica	Opta Minerals (BARCO 32)	~ 2.0	Uddin et al. (2010)
Clinochrysotile	Vale's Thompson ultramafic ore	~ 10.0	Alvarez-silva et al. (2010)

5.4.2. Apparatus

5.4.2.1. Bubble sedimentation potential

The apparatus is shown in Fig. 2. The glass column was 2.6 cm inner diameter and 1 m in length. Two pairs of Ag/AgCl electrodes (Warner Instruments Inc.) were mounted through stopcocks with each electrode in the pair set 50 cm apart. The Ag/AgCl electrode pairs were connected to two separate channels of an Agilent 34901A 20-Channel, Multiplexer embedded in an Agilent 34970A data acquisition/switch unit (multimeter). One pair of electrodes was used for potential difference measurement and the other for resistance (conductivity) measurement. For the latter, a flip switch was included to reverse polarity to avoid charge build-up on the electrodes. The pH electrode (Cole-Parmer) inserted into the column via a CG-350-03 glass joint was connected to another channel on the multimeter through an Oakton 510 benchtop pH meter. A porous plate sparger at the base of the column dispersed air into bubbles. Air flow was controlled via a calibrated flowmeter. A Masterflex pump was used to circulate the overflow to the cell.

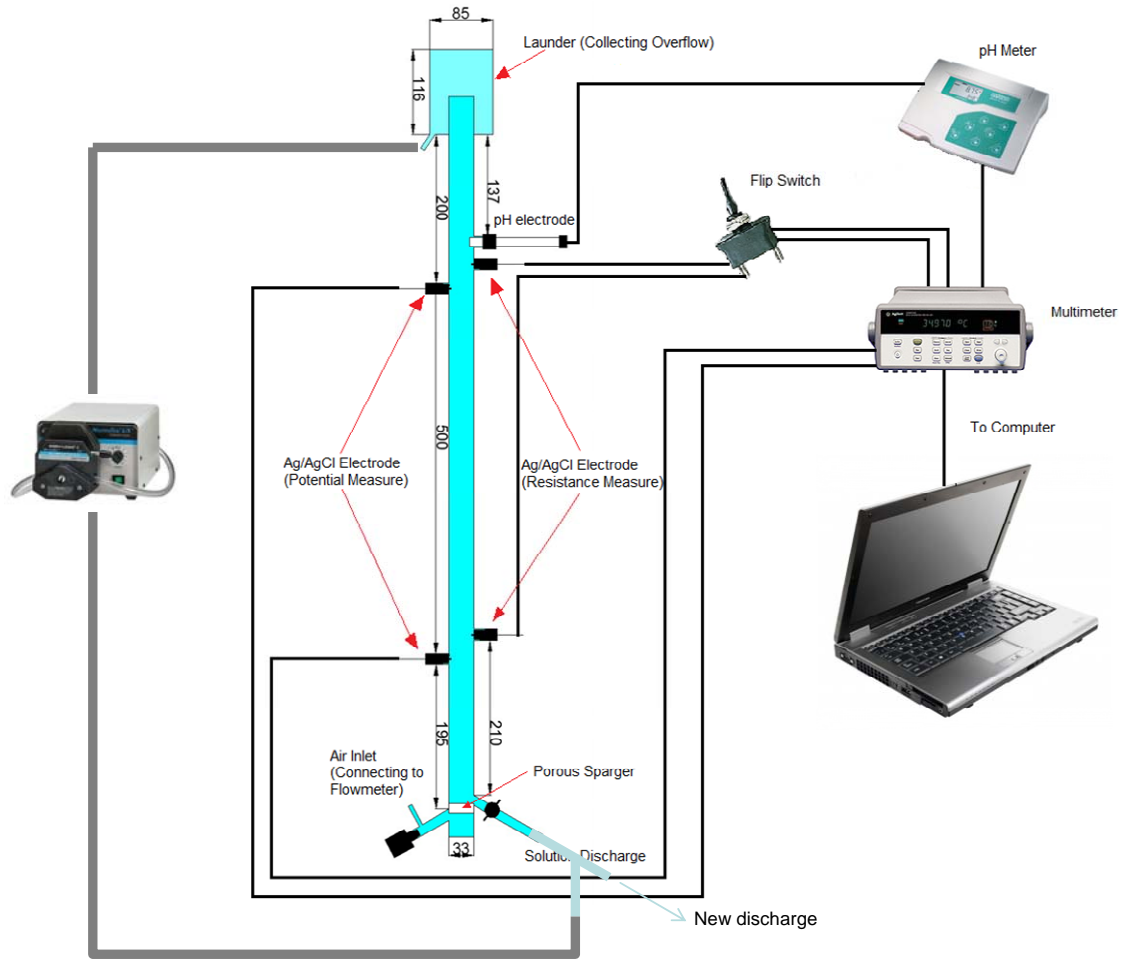


Fig. 2. Apparatus to measure bubble sedimentation potential in presence of particles (dimensions in millimetre)

The technique for measuring BSP (in absence of particles) was validated by showing the iso-electric point (iep) given when BSP is zero compared well with range (pH 3.2 – 4) determined by other techniques (Table 3). The iep with air is generally higher than for inert gases which Tabor et al. (2011) attributed to CO₂ producing some surface species.

Table 3

Iso-electric-point of bubbles from the literature compared to sedimentation method (last row); taken from Uddin et al. (2011)

I _{ep}	Bubble formation, background electrolyte and method	Avg. size	Gas	Reference
3-3.5	Ultrasonic cavitation, 10 ⁻³ M KCl (electrophoresis)	750 nm	Vacuum	Cho et al. (2005)
~ 4.0	Centrifugal force (electrophoresis)	~ 40 μm	Air	Takahashi (2005)
3.2	Ultrasonic cavitation, 10 ⁻³ M KCl (electrophoresis)	~ 10 μm	Vacuum	Elmahdy et al. (2008)
~ 3.0	Capillary (electrophoresis)	1.3 mm	N ₂	Creux et al.(2009)
~ 3.0	Cantilever (AFM)	125 μm	Ar, N ₂	Tabor et al. (2011)
~ 4.0			Air	
~ 4.0	Injecting gas through porous sparger, 10 ⁻² M KCl (BSP)	~ 1 mm	Air	Uddin et al. (2011)

5.4.2.2. Visualization

The setup consists of a 300 mL beaker placed in a rectangular water-filled Plexiglas tank perched on a magnetic stirrer (Fig. 3). A graduated syringe introduced equal volume (0.015 mL, 2 mm) air bubbles into an agitated suspension of particles. Imaging was by digital camera (Canon EOS 500D, EF 100mm f/2.8 USM Macro Lens).

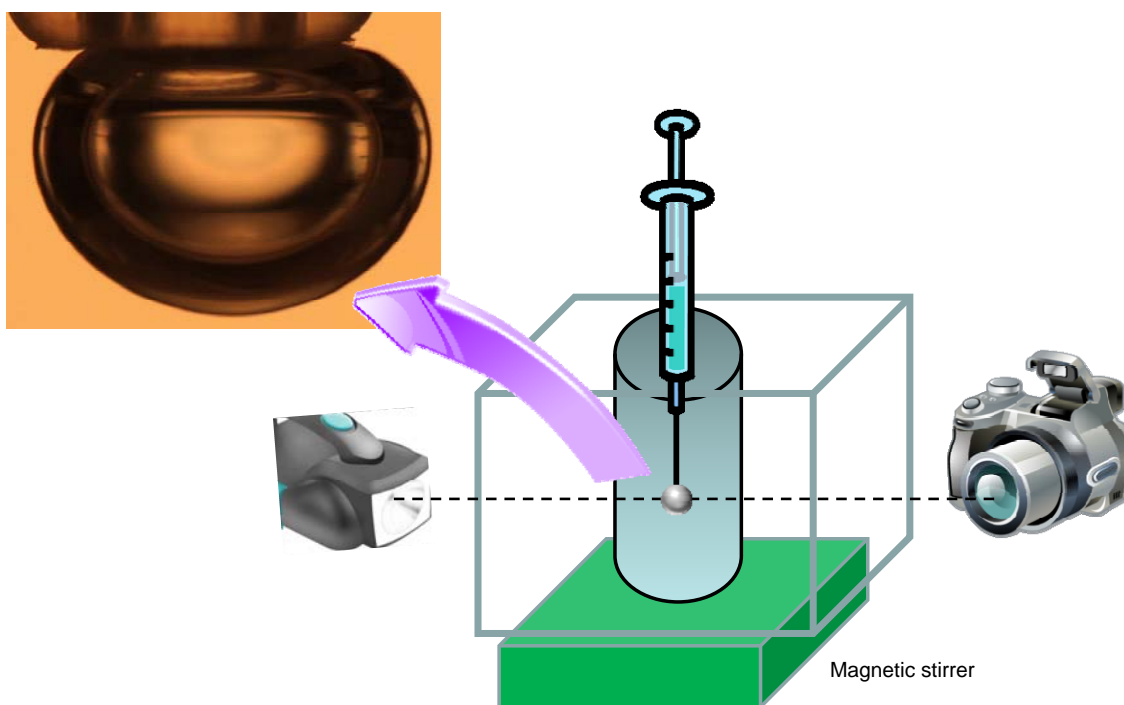


Fig. 3. Set-up for visual investigation of bubble-particle attachment

5.4.3. Procedure

5.4.3.1 Bubble sedimentation potential

Suspensions of $-25\ \mu\text{m}$ particles were prepared using de-ionized water with 10^{-2}M to 10^{-3}M KCl as background electrolyte. All tests were performed at natural pH which remained between 6 and 7. The suspension was agitated over a magnetic stirrer for 30 minutes and transferred to the column. Bubbles were introduced by flowing air through the sparger at 50 mL/min. Ten minutes was sufficient for the system to reach steady-state (signals became steady). Potential measurements were initiated, comprised of 10 readings at 10 s intervals taken every 2 min. When the standard deviation of the mean of two successive measurements was less than 0.1 mV, the potential was recorded as E_o . Air

flow was stopped, 5 minutes allowed to expel the bubbles, then potentials were measured and recorded as E_B . Sedimentation potential E_s was calculated using the following:

$$E_s = ((E_O)_i - (E_B)_i) / H \quad (1)$$

where H is the distance between two electrodes. Selected conditions were repeated 3 times to estimate the standard deviation indicated by the ‘error’ bar on the Figures.

5.4.3.2 Visualization

For these tests, suspensions of sized particles were prepared in a similar fashion as above. Bubbles were generated in the suspension using the syringe. Stirring was continued for 1 min then the stirrer was switched off to allow the particles to settle to image the bubble.

5.4.3.3 Micro-electrophoresis

Interpreting electrostatic interaction requires particle charge as well as bubble charge. Ideally the former should be obtained by resorting to the PSP set-up (Uddin et al., 2010) but at the particle concentrations used here the potential signals were too low to be reliable. To provide the particle information electrophoresis (Brookhaven ZetaPlus) was employed. Samples prepared in the same manner as the sedimentation potential tests.

5.5. Results

5.5.1. Bubble sedimentation potential

5.5.1.1 Alumina and silica

Fig. 4 shows the effect of adding alumina and silica to water that contains frother (DF250, 20 ppm). The bubble sedimentation potential (BSP) became less negative with increasing alumina content but the presence of silica gave no apparent effect. Zero particle concentration gave a BSP ca. -3.5 mV, i.e., close to the 0.05 g particle case.

Fig. 5 shows the effect on BSP of alumina and silica particles in 10^{-5} M SHS and 10^{-5} M HTAB solutions, respectively. The impact is marked compared to frother: the BSP becomes less negative with increasing alumina and becomes less positive with increasing silica. The observation reflects bubble-particle hydrophobic interaction with the anionic collector-treated alumina and cationic collector-treated silica.

Experiments conducted in alumina-HTAB and silica-SHS systems, i.e., where particles are not made hydrophobic, gave BSP signals too noisy to interpret.

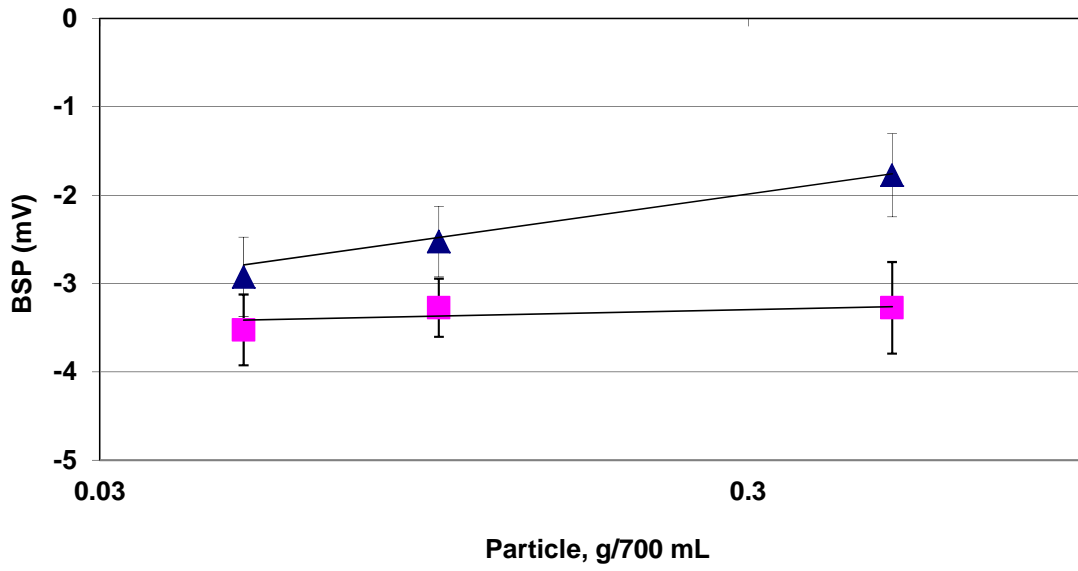


Fig. 4. Bubble sedimentation potential (BSP) as a function of particle concentration, (▲) alumina and (■) silica in presence of 20 ppm DF250

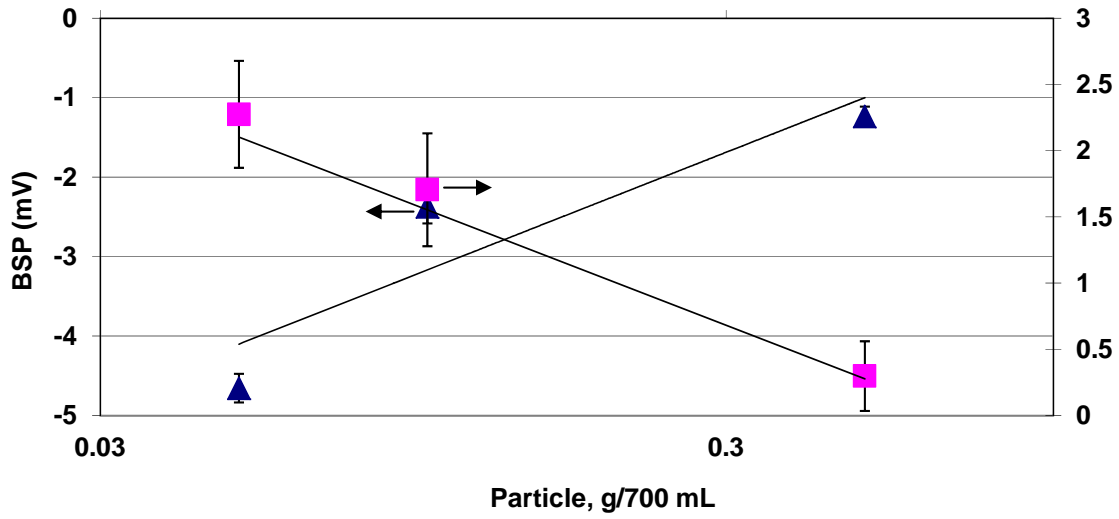


Fig. 5. Bubble sedimentation potential (BSP) as a function of particle concentration, (▲) alumina + SHS and (■) silica + HTAB (Note: BSP in absence of particles is close to the value at 0.05 g/700 mL)

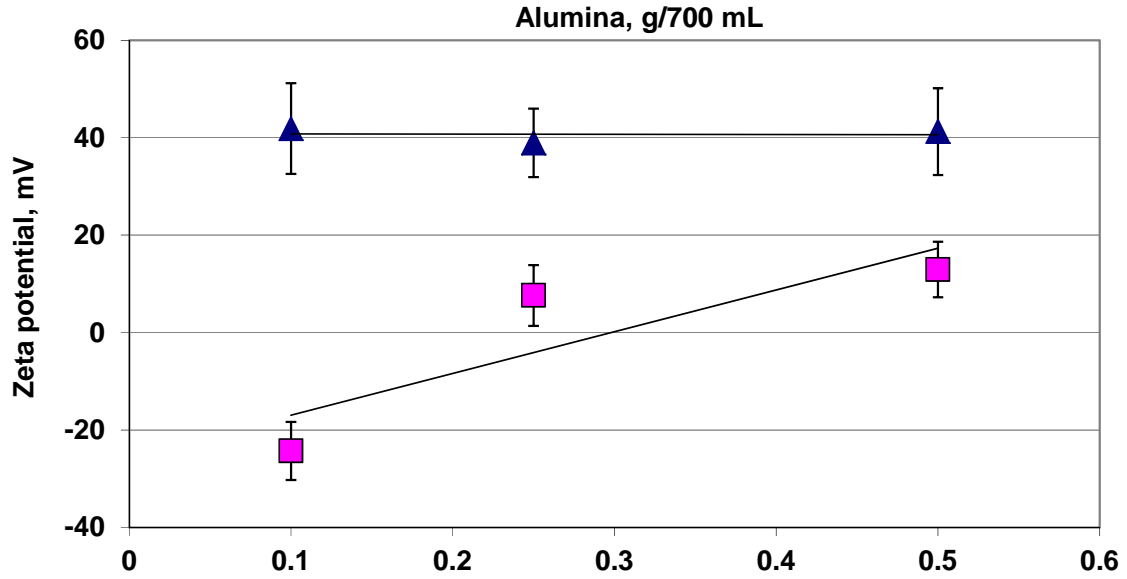


Fig. 6. Zeta potential (ZP) as a function of alumina particle concentration, (▲) alumina only and (■) alumina + SHS

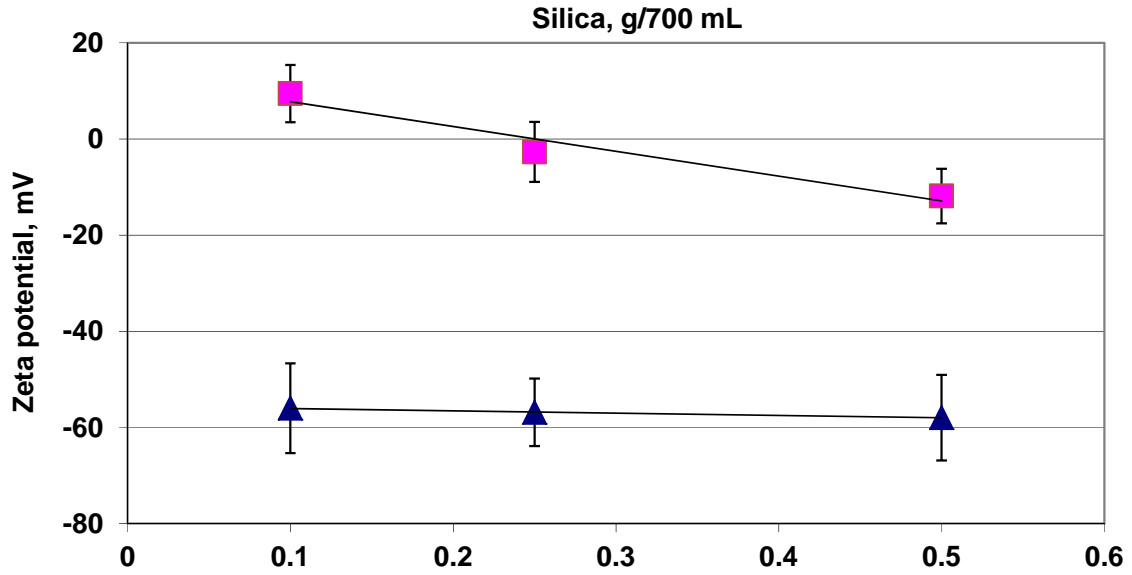


Fig. 7. Zeta potential (ZP) as a function of silica particle concentration, (▲) silica only and (■) silica + HTAB

Figs. 6 and 7 show zeta potential as function of particle concentration measured by electrophoresis. Increasing silica and alumina concentration in the absence of reagents did not change the zeta potential, silica remaining steady at -55 mV and alumina at $+40$ mV. With increasing particle concentration in the presence of HTAB the zeta potential of silica decreased from $+9$ mV to -12 mV and in the case of alumina in the presence of SHS the zeta potential rose from -24 mV to $+13$ mV. This change with particle concentration indicates less reagent per unit surface area of particle.

5.5.1.2. Clinochrysotile

Fig. 8 shows the presence of clinochrysotile had little effect in systems with just background electrolyte and frother, the consistent increase in BSP at the highest concentration not being statistically significant. (The higher KCl concentration without frother was to try to preserve the same bubble size by increasing ionic strength; the higher magnitude of BSP with frother indicates bubbles were smaller, i.e., larger in number and carried more total charge.)

Fig. 9 shows the BSP increased in the clinochrysotile-SHS system as particle concentration was increased. The result is similar to the alumina-SHS system implying attachment of hydrophobic anionic collector-treated clinochrysotile. Also similar to the tests with alumina was the failure to measure BSP in the clinochrysotile-HTAB case.

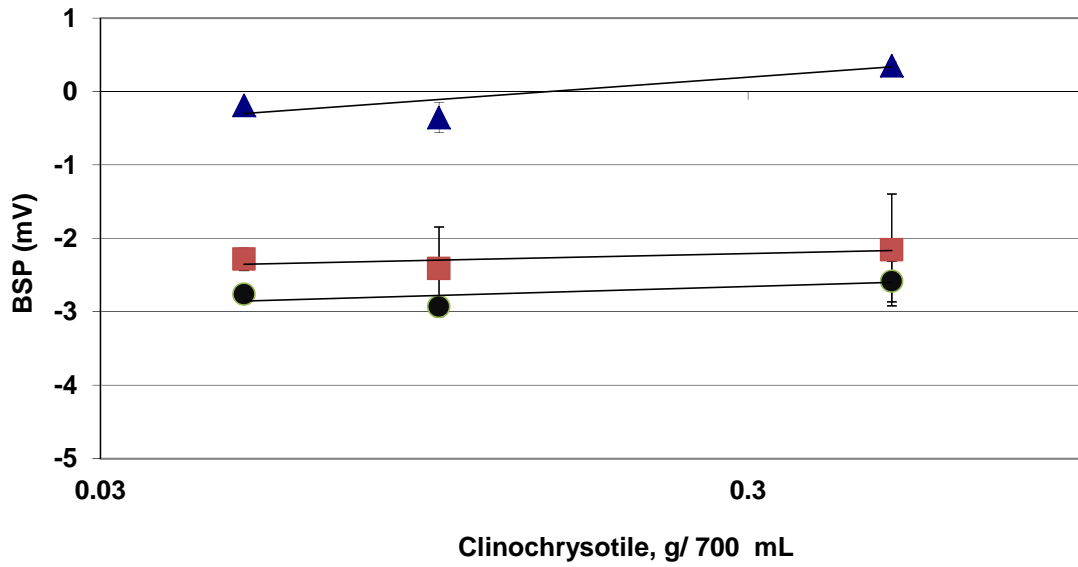


Fig. 8. Bubble sedimentation potential (BSP) as a function of clinochrysoile particle concentration in (▲) 10^{-2} M KCl, (■) 10^{-3} M KCl + MIBC (20 ppm) and (●) 10^{-3} M KCl + DF250 (20 ppm)

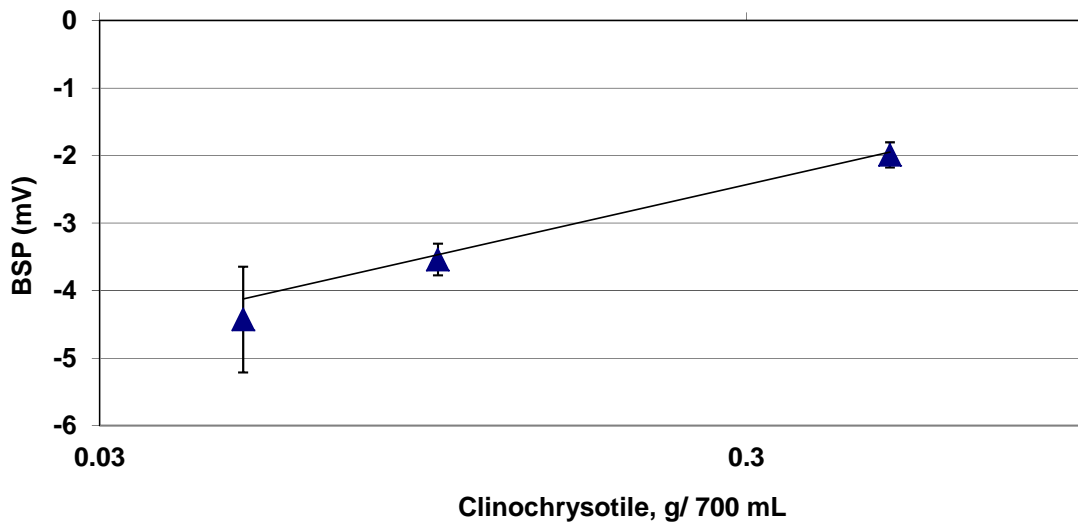


Fig. 9. Bubble sedimentation potential (BSP) as a function of clinochrysoile concentration in SHS

5.5.2. Visualization tests

Fig. 10 shows increasing coverage as concentration of particles is increased in the alumina-SHS system. Attachment is due to particle hydrophobicity and corresponds to the impact on BSP in this system (Fig. 5). Fig. 11 examines the situation where the alumina is not hydrophobic. It shows attachment increases with decreasing particle size with just frother (DF250) present. This implies attachment by non-hydrophobic interactions, which could be electrostatic in the case of alumina. This possibility is emphasized by the observation in the presence of HTAB, where almost complete elimination of the 25-38 μm size class occurs, the bubble now having a positive charge (ca. +2.5 mV, Fig. 5).

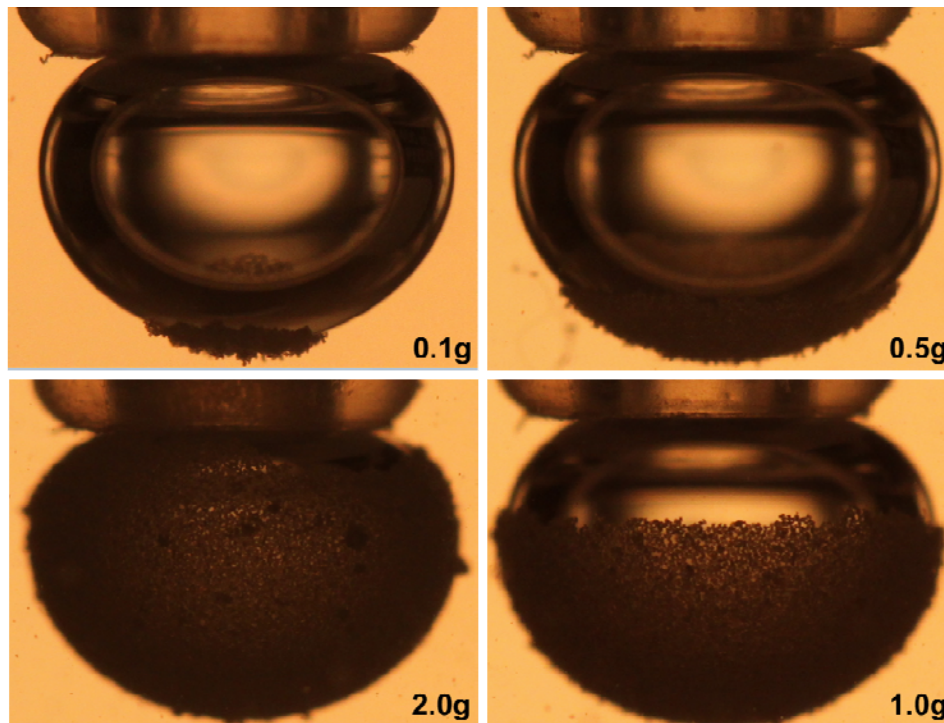


Fig . 10. Results of visualization tests: alumina (38-44 μm)-SHS system with increasing particle concentration (in 300mL)

Fig. 12 shows silica attachment in three systems: with cationic collector HTAB, non-ionic frother DF250 and anionic collector SHS. High coverage was observed with HTAB; some attachment with DF250, despite both bubble and silica being negatively charged at natural pH; and negligible attachment with SHS. The observations mirror those in the alumina systems: extensive attachment of hydrophobic silica; some attachment by non-hydrophobic interactions; and elimination of the latter by (in this case) increasing the negative charge on the bubble.

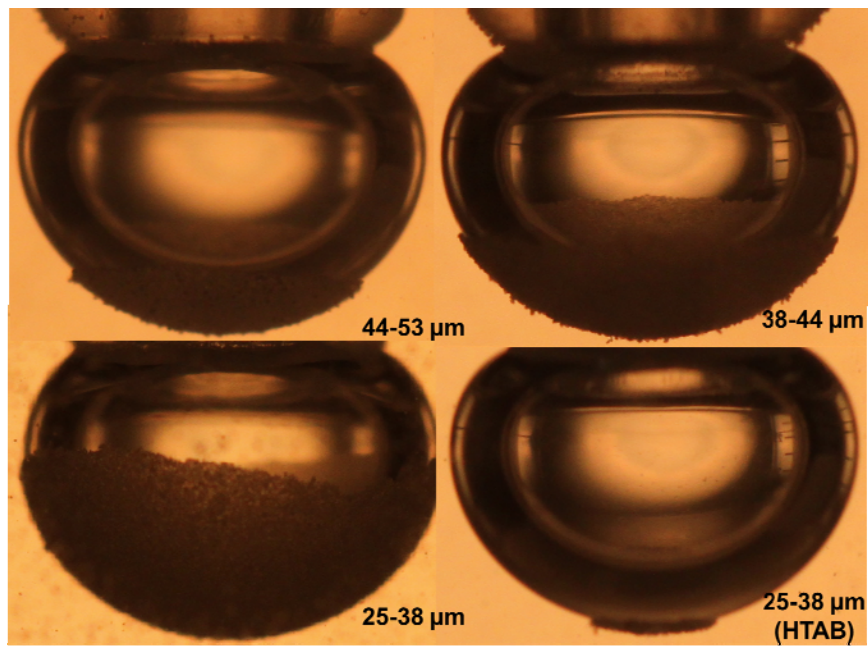


Fig. 11. Results of visualization tests: alumina-DF250 at three particle sizes; and alumina-HTAB with 25-38 μm particles (all concentrations, 2g/300mL)

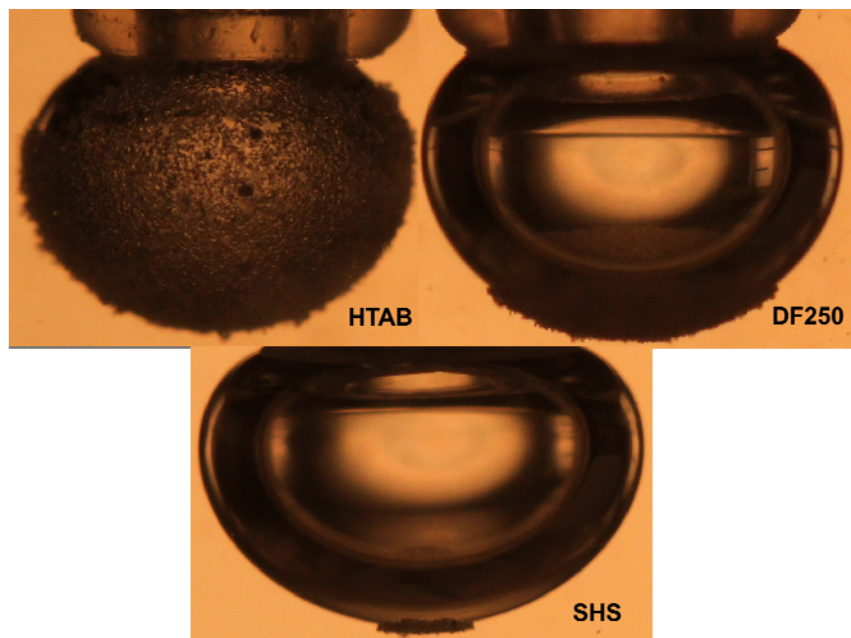


Fig. 12. Results of visualization tests: silica (2g/300mL, 38-44 μm) in presence HTAB, DF250 and SHS

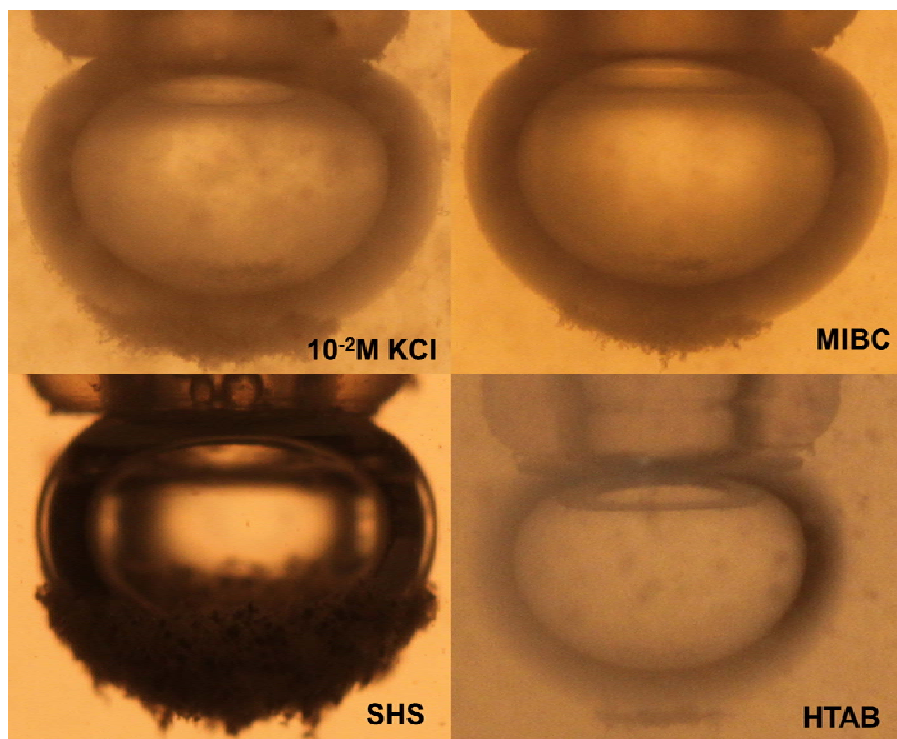


Fig. 13. Results of visualization tests: clinochrysoile (2g/300mL, -25 μm) with background electrolyte, SHS, MIBC, and HTAB

Extending the test to clinochrysotile proved difficult because the fibres remained suspended and reduced image quality. Fig. 13 nevertheless shows attachment of hydrophobized (by SHS) particles (picture quality here was good because so many particles were attached and removed from suspension) and some pick-up by non-hydrophobic interactions (KCl, MIBC cases) with virtual elimination of attachment by applying a positive charge to the bubble with HTAB evidenced by both the fewer particles apparent on the bubble and the increased ‘cloudiness’ of the suspension.

5.6. Discussion

By adapting prior equipment and procedures a technique has been introduced to determine the interaction of particles with bubbles by monitoring the bubble sedimentation potential, BSP. Adaptations included using higher air rates than before (Uddin et al., 2011) to increase the sensitivity to changes in BSP and using lower particle concentrations (Uddin et al., 2010) to reduce signal noise that proved excessive at concentrations above ca. 0.5-1.0 g/700 mL. The increase in noise is interpreted as resulting when a large number of dispersed particles are present giving competing particle sedimentation potential (PSP) data. A difficulty in separating BSP and PSP was anticipated, but it seems that so long as sufficient particles are removed by the bubbles a clean BSP signal is generated.

A significant change in BSP was observed when particles were made hydrophobic (Figs. 5 and 9). In the alumina-SHS system, the bubble became progressively less negative as the amount of alumina was increased, which corresponds to the charge on the attaching particles tending to increase as noted in (Fig 6). In the silica-HTAB system, the

bubble had switched from negative to positive charge and as the amount of silica was increased the BSP became less positive indicating attachment of progressively less positively charged particles, again as noted in Fig 7. In both systems the bubble charge was affected by the ionic surfactants at least as much as the particles.

Compared to being hydrophobic, the fact that the particles are charged is not significant in attachment. But there appears to be some non-hydrophobic attachment when combining the BSP data in the presence of nonionic frother (Fig. 4) with the visualization data (Figs. 10 and 11). With increasing addition of alumina, the BSP became slightly less negative, implying uptake of some positively charged particles. With silica there was no change in BSP. Alone, this is clearly inconclusive. The images, however, speak to attachment of both alumina and silica in presence of just background electrolyte and frother. This is reinforced when ionic surfactant is added that does not adsorb at the particle but does at the bubble, giving the bubble either the same positive charge as the particles in the HTAB-alumina case or increasing the same negative charge in the SHS-silica case: in those latter two cases the bubbles were almost devoid of particle pick-up. This helps interpret why the BSP could not be measured in those cases, the signals becoming too noisy; it appears to be associated with particles well dispersed from bubbles giving too high a suspension concentration, which was known from the outset to prevent measurement of BSP.

Non-hydrophobic attachment of alumina could be ascribed to electrostatic interaction, but for silica, while heterocoagulation of like-charged particles is known (e.g. DiFeo et al., 2001), other mechanisms, e.g. H-bonding (Fan et al., 2003), may have to be

entertained. The key point, however, is that manipulating bubble charge reduced both alumina and silica particle attachment.

Development of the test setup was prompted by trying to address whether bubble-particle electrostatic interaction could contribute to recovery of clinochrysotile in processing an ultramafic Ni-ore. The BSP data were not supportive, not registering any significant change as particle concentration was increased (Fig. 8). The visualization tests, however, did reveal a possible non-hydrophobic interaction (Fig. 12): there is evidence of pick-up of clinochrysotile particles in background electrolyte and frother solutions which was reduced when the bubble was rendered positive by HTAB. In this regard clinochrysotile acted similarly to alumina attributable to their common positive charge at natural pH. Whether addition of HTAB (or other cationic surfactants, not necessarily collectors) offers a processing opportunity to depress clinochrysotile by targeting bubble charge will be explored. The results (Figs. 9 and 13) also introduce another processing possibility, reverse flotation employing SHS (or other anionic collectors).

5.7. Conclusions

An apparatus to measure bubble sedimentation potential (BSP) in presence of particles is described. Provided the particle suspension was dilute the BSP could be measured and bubble-particle interactions followed. Attachment of hydrophobic particles is clearly evident in the BSP in the case of alumina, silica and clinochrysotile. The BSP gave ambiguous evidence of attachment of non-hydrophobic particles. Images of a bubble exposed to agitated suspensions, however, did indicate attachment of non-

hydrophobic particles. Pick-up was significantly reduced by addition of ionic surfactant that gave the bubble the same charge as the particle, cationic in case of alumina and clinochrysotile and anionic in case of silica. Under these conditions BSP could not be measured which is attributed to the particles being well dispersed from the bubbles leading to too high a particle suspension concentration which gives interfering particle sedimentation potentials. The findings open the possibility of manipulating bubble charge to depress unwanted minerals.

5.8. Acknowledgements

The work was funded under the Chair in Mineral Processing sponsored by Vale, Teck Resources, Barrick Gold, Xstrata Process Support, Shell Canada, SGS Lakefield, COREM and Flottec, under the Natural Sciences and Engineering Research Council of Canada (NSERC) Collaborative Research and Development program.

5.9. References

- Alty, T., 1926. The origin of the electrical charge on small particles in water. Proceedings of the Royal Society of London, Series A, vol. 122 (760), pp. 235–251.
- Alvarez-Silva, M., Uribe-Salas, A., Mirnezami, M., Finch, J. A., 2010. The point of zero charge of phyllosilicate minerals using the Mular–Roberts titration technique. *Miner. Eng.*, 23, 383 – 389.
- Booth, F., 1954. Sedimentation potential and velocity of solid spherical particles. *J. Chem. Phys.*, 22, 1956-1968.
- Cho, S.H., Kimb, J.Y., Chuna, J.H., Kima, J.D., 2005. Ultrasonic formation of nanobubbles and their zeta-potentials in aqueous electrolyte and surfactant solutions. *Colloid Surface A* 269, 28–34.

- Creux, P., Lachaise, J., Graciaa, A., Beattie, J. K., Djerdjev, A. M., 2009. Strong specific hydroxide ion binding at the pristine oil/water and air/water interfaces. *J. Phys. Chem. B* 113, 14146–14150.
- Dai, Z., Bos, J-A. Quinn, P., Lee, A., Xu, M., 2009. Flowsheet development for thompson ultramafic low-grade nickel ores, in: Gomez, C. O.; Nessel, J. E.; Rao, S. R. (Eds.), *Proc. Advances in Mineral Processing Science and Technology. Conference of Metallurgists, CIM, Sudbury, Ontario*, pp. 217 – 228.
- Derjaguin, B. V., Shukakindes, N. D., 1961. Dependence of the floatability of antimonite on the value of zeta potential. *Trans. Inst. Min. Met.* 70, 569–574.
- Dibbs, H.P., Sirois, L.L., Bredin, R., 1974. Some electrical properties of bubbles and their role in the flotation of quartz. *Can. Metall. Quart.* 13, 395–404.
- DiFeo, A., Xu, Z., Finch, J.A., 2001. Sphalerite / silica interactions effect of pH and calcium ions. *Int. J. Miner. Process.* 61, 57–71.
- Elmahdy, A.M., Mirnezami, M., Finch, J.A., 2008. Zeta potential of air bubbles in presence of frothers. *Int. J. Miner. Process.* 89, 40–43.
- Fan, X., Zhang, Z., Li, G., Rowson, N.A., 2004. Attachment of solid particles to air bubbles in surfactant-free aqueous solutions. *Chem. Eng. Sci.* 59, 2639–2645.
- Hunter, R. J., 1991. *Foundations of Colloid Science, Vol. 1*, Claredon Press, Oxford, pp. 374.
- Johnson, D., Hilal, N., Waters, K., Kathryn, Hadler, K., Cilliers, J., 2009. Measurements of interactions between particles and charged microbubbles using a combined micro- and macroscopic strategy. *Langmuir* 25, 4880–4885.
- Kim, J.Y., Song, M.G., Kim, J.D., 2000. Zeta potential of nanobubbles generated by ultrasonication in aqueous alkyl polyglycoside solutions. *J. Colloid Interf. Sci.* 223, 285–291.
- Li, C., Somasundaran, P., 1991. Reversal of bubble charge in multivalent inorganic salt solutions – effect of magnesium. *J. Colloid Interf. Sci.* 146, 215–218.
- McTaggart, M. A., 1922, *Philosophers’ Magazine*, 44, 386.
- Myers, D., 1991. *Surfaces, Interfaces, and Colloids: Principles and Applications*. VCH Publishers, Inc., New York, pp. 69–84.
- Okada, K., Akagi, Y., Kogure, M., Yoshioka, N., 1990. Effect of surface charges of bubbles and fine particles on air flotation process. *Can. J. Chem. Eng.* 68, 393–398.

- Saville, D. A., 1982. The sedimentation potential in a dilute suspension. *Adv. Colloid Interface Sci.*, 16, 267-279.
- Rousseau, R. W., 1987. *Handbook of Separation Process Technology*. Wiley-Interscience, USA, pp. 822.
- Tabor, R. F., Chan, D. Y. C., Grieser, F., Dagastine, R. R., 2011. Anomalous stability of carbon dioxide in pH-controlled bubble coalescence. *Angew. Chem. Int. Ed.* 50, 3454–3456.
- Takahashi, M., 2005. Zeta potential of microbubbles in aqueous solutions: Electrical properties of the gas-water interface. *J. Phys. Chem. B* 109, 21858–21864.
- Trahar, W. J., 1981. A rational interpretation of the role of particle size in flotation. *Int. J. Miner. Process.*, 8, 289 – 327.
- Uddin, S., Mirnezami, M., Finch, J. A., 2010. A surface charge characterization device using sedimentation potential for single and mixed particle systems. *Colloid Surface A*, 371, 64–70.
- Uddin, S., Jin, L., Mirnezami, M., Finch, J. A., 2011. An Apparatus to Measure Electrical Charge of Bubble Swarms. In progress.
- Usui, S., Sasaki, H., 1978. Zeta potential measurements of bubbles in aqueous surfactant solutions. *J. Colloid Interf. Sci.* 65, 36–45.
- Xu, M., Scholey, K., Marcuson, S., 2011. Vale-Cytec-University Research Consortium on Processing Low Grade Ultramafic Nickel Ore. Conference of Metallurgists, CIM, Montreal, Canada.
- Yang, C., Dabros, T., Li, D., Czarnecki, J., Masliyah, J.H., 2001. Measurement of the zeta potential of gas bubbles in aqueous solutions by microelectrophoresis method. *J. Colloid Interf. Sci.* 243, 128–135.
- Yoon, R.H., Yordan, J.L., 1986. Zeta-potential measurements on microbubbles generated using various surfactants. *J. Colloid Interf. Sci.* 113, 430–438.

6. Fibre Disintegration and Flotation of an Ultramafic Ore

6.1. Abstract

Ultramafic deposits are potential resources of nickel. Recovery by flotation is challenged by the fibrous nature of these ores owing to the presence of serpentine minerals. The fibres create physical entanglement that reduces selectivity and hinders bubble motion. As an approach, technology developed to improve CO₂ sequestration of serpentines is considered as an ore treatment step. This involves strong acid attack to dissolve magnesium from the serpentine lattice and weaken the fibre structure coupled with mechanical attrition this leads to fibre disintegration. An ultramafic ore was subjected to up to 15wt% HCl attack in a ceramic ball mill. Subsequent flotation using amyl xanthate, soda ash and MIBC gave significantly improved results over untreated ore.

Keywords: Ultramafic deposits, chemical/mechanical treatment, fibre disintegration

Research highlights:

- Surface charge characterization of ultramafic Ni-ore.
- Visual observation of the settling behaviour.
- Investigation of possible causes of poor flotation response.
- A fibre disintegration technique was devised.
- Significant improvement in flotation response after fibre disintegration was observed.

6.2. Introduction

In this chapter surface charge characterization of a Thompson ultramafic ore sample was conducted using the in-house designed sedimentation potential apparatus. Flotation tests were used along with the sedimentation potential measurements to determine possible reasons behind poor separation seen with this type of ore. Significant selectivity between Ni-sulphides and MgO-bearing gangue minerals was achieved using an ore treatment approach based on fibre disintegration.

6.3. Background

The background was discussed in chapter 2.

6.4. Experimental

6.4.1. Ore mineralogy

Vale provided the sample. It comprised mostly serpentine (63%) and olivine (12%) with minor dolomite and Mg chlorite as the major sources of Mg. From X-ray diffraction the dominant serpentine mineral was identified as clinochrysotile (Fig. 1). Naturally hydrophobic talc was low (<1%). The main iron minerals were pyrrhotite (5%) and magnetite (6%).

The principal Ni sulphide mineral was pentlandite with minor violarite, mackinawite and millerite (grade ca. 0.6% Ni). Trace amount of Cu, Co and Cr were also present.

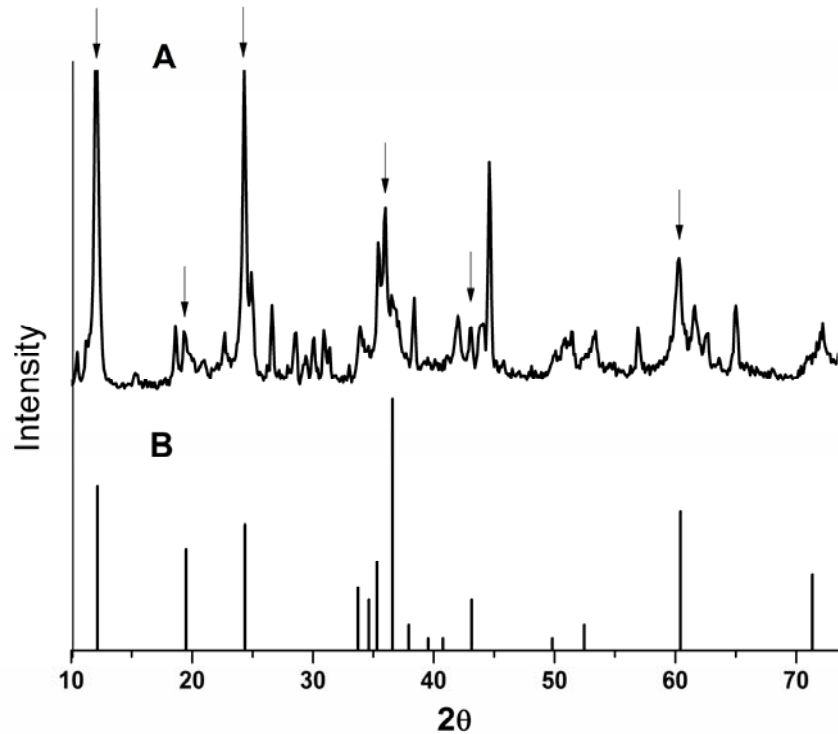


Fig. 1. The X-ray powder diffraction pattern of the ore together with the match for clinochrysotile from a search of the Powder Diffraction File # 00-052-1562 (PDF), (vertical lines, major peaks are indicated with arrows)

6.4.2. Sedimentation potential

For sedimentation tests 2 g ore samples were washed with de-ionised water and 500 mL suspensions were prepared with the same water and 10^{-3} M KCl was used as background electrolyte. For pH adjustment HCl and KOH were used. Details on the apparatus and experimental procedure are shown in a previous publication (Uddin et al., 2010) and chapter 3.

6.4.3. Grinding

Grinding was performed in a 15x15 cm ceramic ball mill with 3 cm and 1.8 cm diameter zirconium oxide balls. A 100 g sample was slurried with 800 mL de-ionized water. Acid (HCl 10N) added to 5 wt%, 10 wt% and 15 wt% in water along with 1wt% EDTA. Grinding time was

set to 4 hrs. To the ground sample CMC was added (0.05 g) and the product was aged in the mill for 12 hrs during which the pH rose to near neutral. This allowed the addition of soda ash and the setting of other conditions typical of Ni-sulphide ore flotation. A sample of supernatant was taken for assaying (ICP-OES). The slurry was then transferred to the flotation cell.

6.4.4. Flotation

A Denver flotation cell was employed. The total slurry volume was adjusted to 1 L (i.e., slurry density is 10 wt% solids). The pH was adjusted and stabilized at pH ca. 10 using soda ash. As collector, 0.004 g potassium amyl xanthate (PAX), purified by acetone dissolution and precipitation into petroleum ether, was used with a conditioning time of 5 minutes. Frother MIBC (0.002 g) was then added and the system conditioned for a further for 5 minutes prior to introducing air. Three concentrates were taken at 1, 2 and 4 minutes. They, along with the tails, were filtered, oven dried weighed and assayed (ICP-OES). A schematic of the procedure is shown in Fig. 2. Except acid addition and aging, the rest of the procedure is adopted from conventional Ni-sulphide flotation practice.

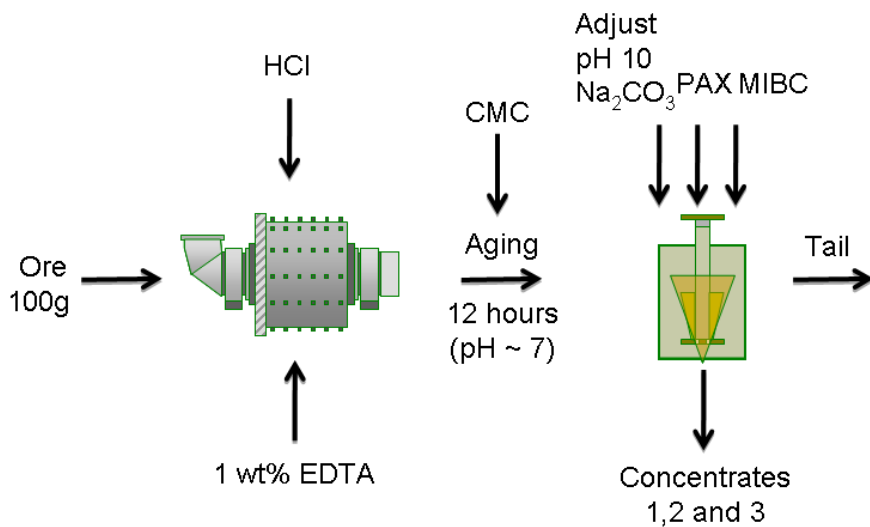


Fig. 2. Flow sheet for fibre disintegration / flotation tests

6.4.5. *Illustration of fibre disintegration*

To demonstrate the changes due to the combined chemical and mechanical treatment, the following test work was performed. Five g of the ground ore (without any reagent) and 80 mL deionized water at 90 wt% HCl was placed in an 8x8 cm ceramic mill with 1 cm zirconium oxide balls and ground for 4 hrs. A higher concentration of acid than in the flotation tests was needed to achieve detectable physical changes in the fibres. After grinding, the samples were filtered and dried. To image physical changes, electron beam analysis was used (Philips XL30 FEG-SEM with Genesis EDS/X-ray microanalysis system). Powdered samples were mounted on carbon tape and were wafer-coated with gold/palladium (Anatech Hummer VI sputtering system).

For XPS measurements (Thermo Scientific K-Alpha) an Al K α X-ray source at 1486.6 eV was used operated at 200 W. The vacuum in the analyzer chamber was at $\sim 10^{-10}$ Torr. High resolution spectra were taken at a take-off angle of 90°, with a pass energy of 20 eV and steps of 0.05 eV. The binding energy scale of the instrument was calibrated using the Au(4f)_{7/2} (BE = 84.0 eV) lines of metallic gold. Samples were in the form of dry powder mounted on conductive carbon tape. No effects due to charging or X-ray damage were observed.

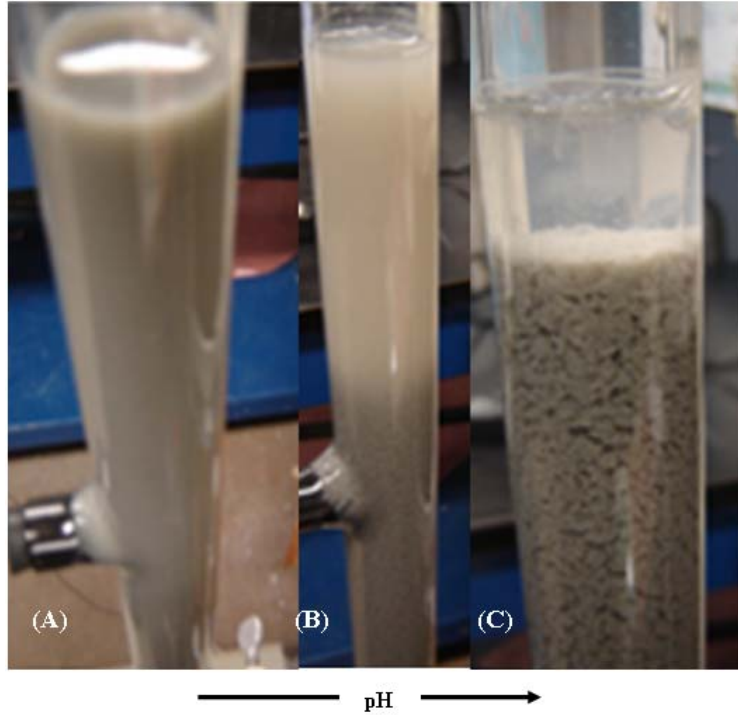


Fig. 3. Settling slurry in different pH conditions; (A) Dispersed, (B) Partially agglomerated and (C) Agglomerated

6.5. Results

6.5.1. Sedimentation tests

Fig. 3 shows the variation of dispersion/agglomeration characteristics of the ore with pH. At low pH the ore becomes dispersed and at higher pH it appears to be agglomerated.

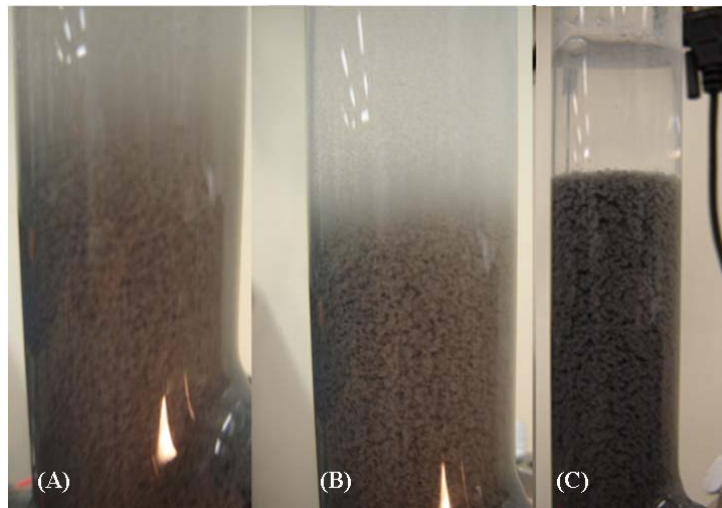


Fig. 4. Settling slurry at (A) pH 9, (B) pH 11 and (C) pH 11 with EDTA

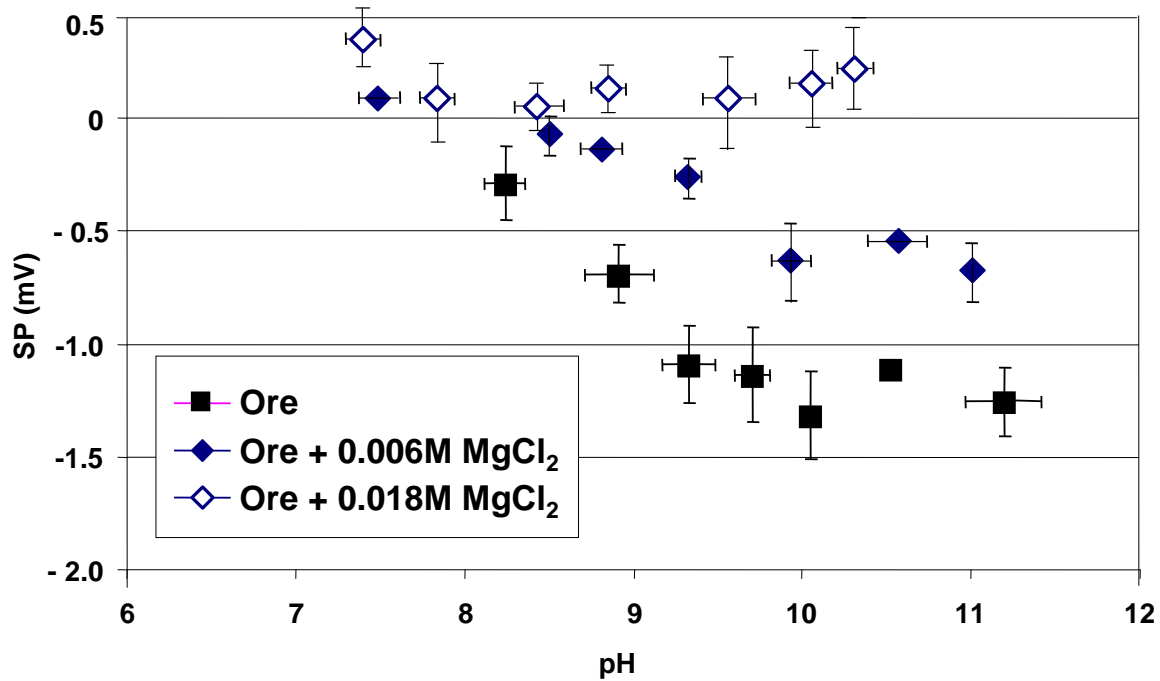


Fig. 5. Particle sedimentation potential (SP) as a function of pH at different Mg concentration

Fig. 4 shows visual observations on the supernatant. It appeared white at ca. pH 9 and at higher pH (ca. 11) it became clear with dispersed white particles. Ore conditioned with EDTA showed a clean supernatant over ca. pH 9-12.

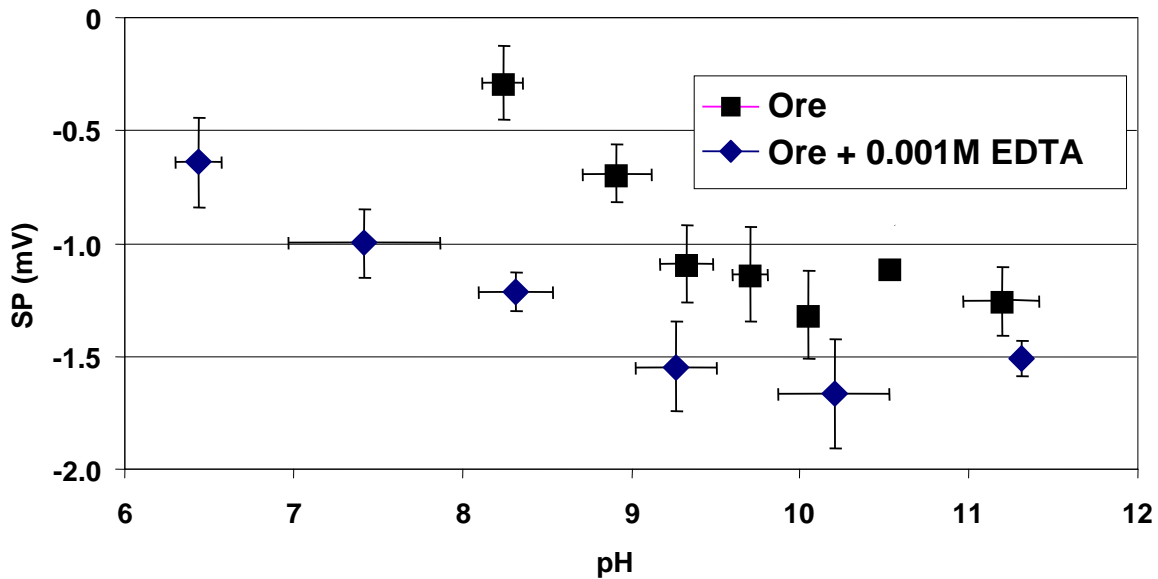


Fig. 6. Sedimentation potential as a function of pH: effect of EDTA

Ore showed a decreasing potential trend with pH and the iep (the pH value at which the net E_s signal from the ore components is zero) can be inferred at ca. pH 8. Adding Mg^{2+} ions to the system makes the surface more electro-positive (Fig. 5) but shift in iep is negligible. The change in potential is probably due to precipitation of hydrolysis products of Mg. Fig. 6 shows the effect of EDTA which decreases the potential and the iep of the system. This was probably achieved by removing positive metal ions that would otherwise be precipitated to make the surface more electro-positive and possibly changing interface Mg/Si ratio at the same time.

6.5.2. Effect of acid treatment

As a guide to fibre disintegration, Fig. 7 shows the concentration of Mg in solution after grinding as a function of acid addition. Higher dissolution of Mg corresponds to higher dimensional instability and disintegration of fibres. There is a notable increase in dissolution of Mg from 0 wt% to 5 wt% HCl with further increases on acid addition up to 15wt% at which point approximately 12wt% Mg had been extracted into solution. At the same time, approximately 4 wt% Ni and 2 wt% Fe were lost to solution as shown in Table 1. EDTA, as a weak acid and chelating agent can also increase the dissolution of Mg to some extent (Fig. 7).

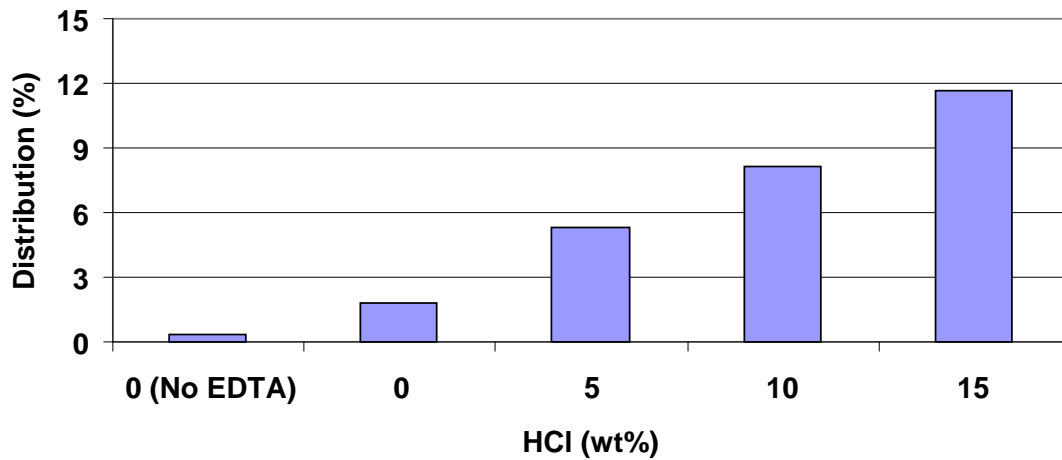


Fig. 7. Distribution of wt% Mg in the solution as function of HCl concentration in presence of 1wt% EDTA ('No EDTA' refers to untreated ore, from 0% acid and so on contain 1wt% EDTA)

6.5.3. Flotation

Fig. 8 shows the froth appearance as a function of HCl addition. At zero to 5wt% HCl the froth appeared barren but at 10wt% it took on the shiny metallic lustre typical of froth with sulphide minerals.

Table 1

Metallurgical balance (average of the two tests): leach/grind with 15wt% HCl and flotation

	Mass (g)	Assay (%)			Distribution (%)		
		Ni	Mg	Fe	Ni	Mg	Fe
Leaching							
Sol (L, g/L)	1	0.02	2.67	0.24	-	-	-
Mass Loss	7.46				4.08	11.6	2.1
Flotation							
Con 1	3.53	7.74	4.107	43.55	49.34	0.6	14.9
Con 2	3.71	2.31	13.71	28.45	15.48	2.4	10.2
Con 3	6.62	1.05	18.6	16.97	12.56	5.9	10.8
Tail	78.65	0.13	20.95	8.13	18.52	79.2	61.9
Head	100	0.55	20.46	10.33	100	100	100

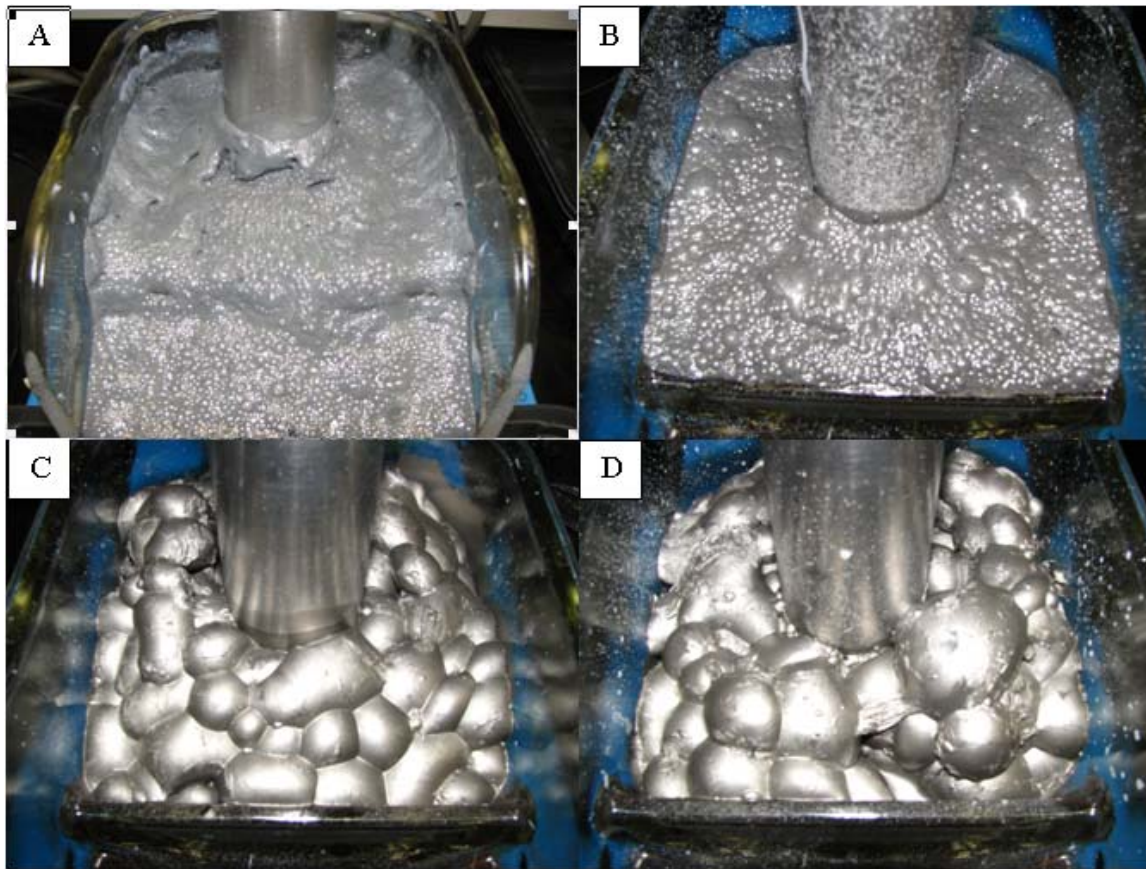


Fig. 8. Froth appearance at (A) 0 wt% HCl, (B) 5 wt% HCl, (C) 10 wt% HCl and (D) 15 wt% HCl

The corresponding Ni grade vs. recovery is shown in Fig. 9. About 80% Ni recovery at 3% Ni grade was achieved with 15wt% HCl (i.e., enrichment ratio ca. 5), which is a significant improvement compared to the untreated ore which only achieved 55% Ni recovery by concentrate 3. The improvement was due to increased selectivity against the MgO minerals: Fig. 10 indicates that at 90% MgO rejection (i.e., recovery to tails) the treated ore yielded ca. 80% Ni recovery with 15wt% HCl while the untreated ore gave only ca. 45% Ni recovery. This limited separation for untreated ore is seen by others (Dai et al., 2009). The addition of EDTA alone did not enhance metallurgy, as evident from Figs. 9 and 10.

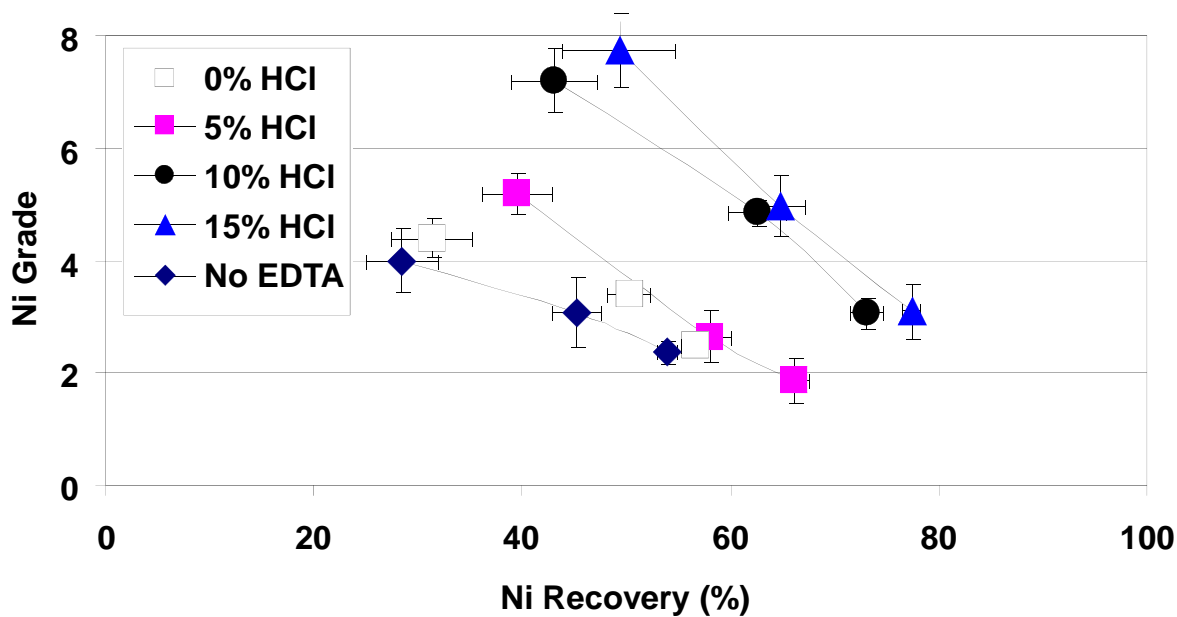


Fig. 9. Ni grade vs. recovery as a function of HCl concentration in ore treatment step

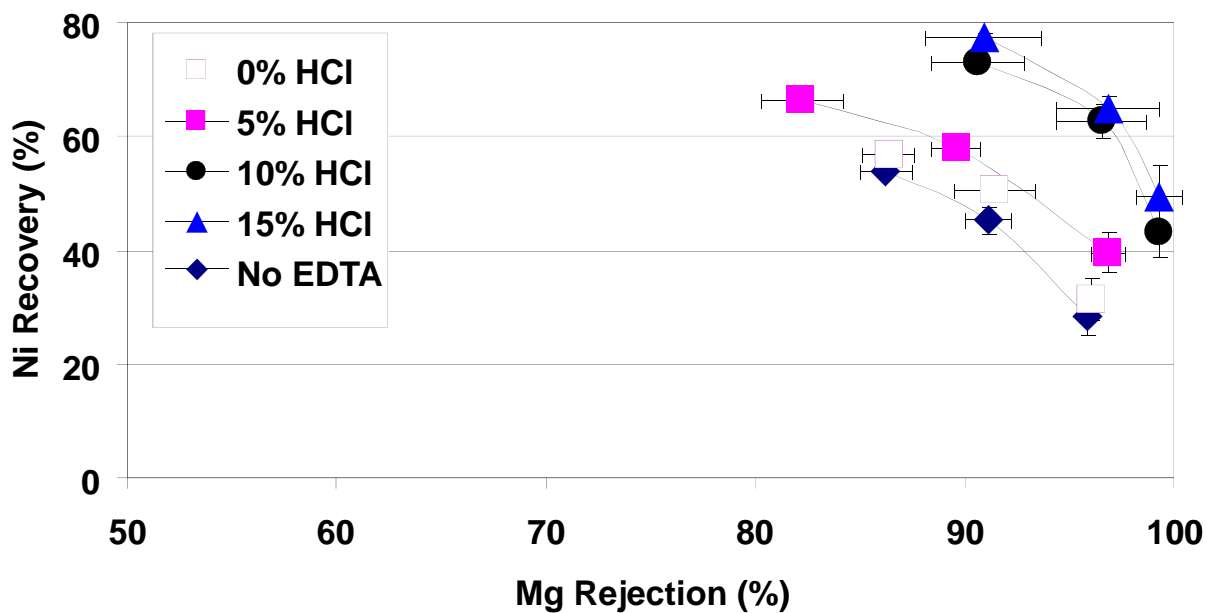


Fig. 10. Ni recovery vs. MgO rejection as a function of HCl concentration

As another indication of enhanced selectivity Fig. 11 shows insol (i.e. insoluble component after acid digestion for assaying) content in concentrate 1 and in the tail is similar at zero HCl but by 15wt% HCl there is a significant difference, concentrate 1 showing < 10% insol while the tail approaches 40%.

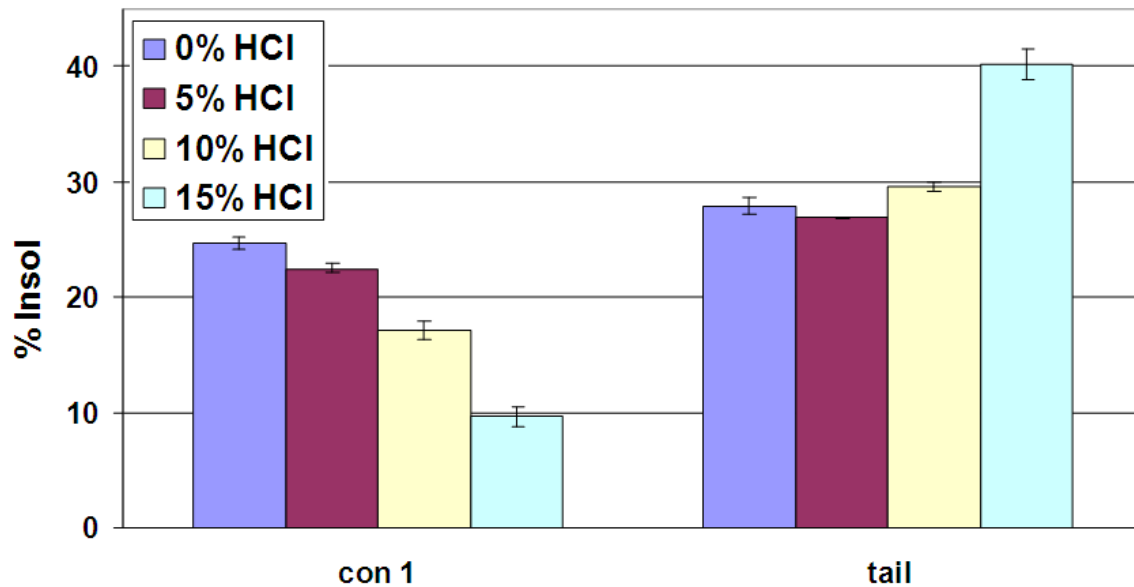


Fig. 11. Insol content in concentrate 1 and tail as a function of acid concentration

6.5.4. Illustrating fibre disintegration

The SEM image (Fig. 12A) reveals the long fibres in the ground untreated sample while acid-treated samples show few of these long interconnected fibres the sample instead being dominated by short, apparently broken ones (Figs. 12B and 12C). Higher magnification is used to visualize one of the short fibre bundles (Fig 12C). Corresponding microanalysis (Fig. 12D) shows Mg, Si and O, i.e., the elements of serpentine, and the shape suggests the chrysotile polymorph.

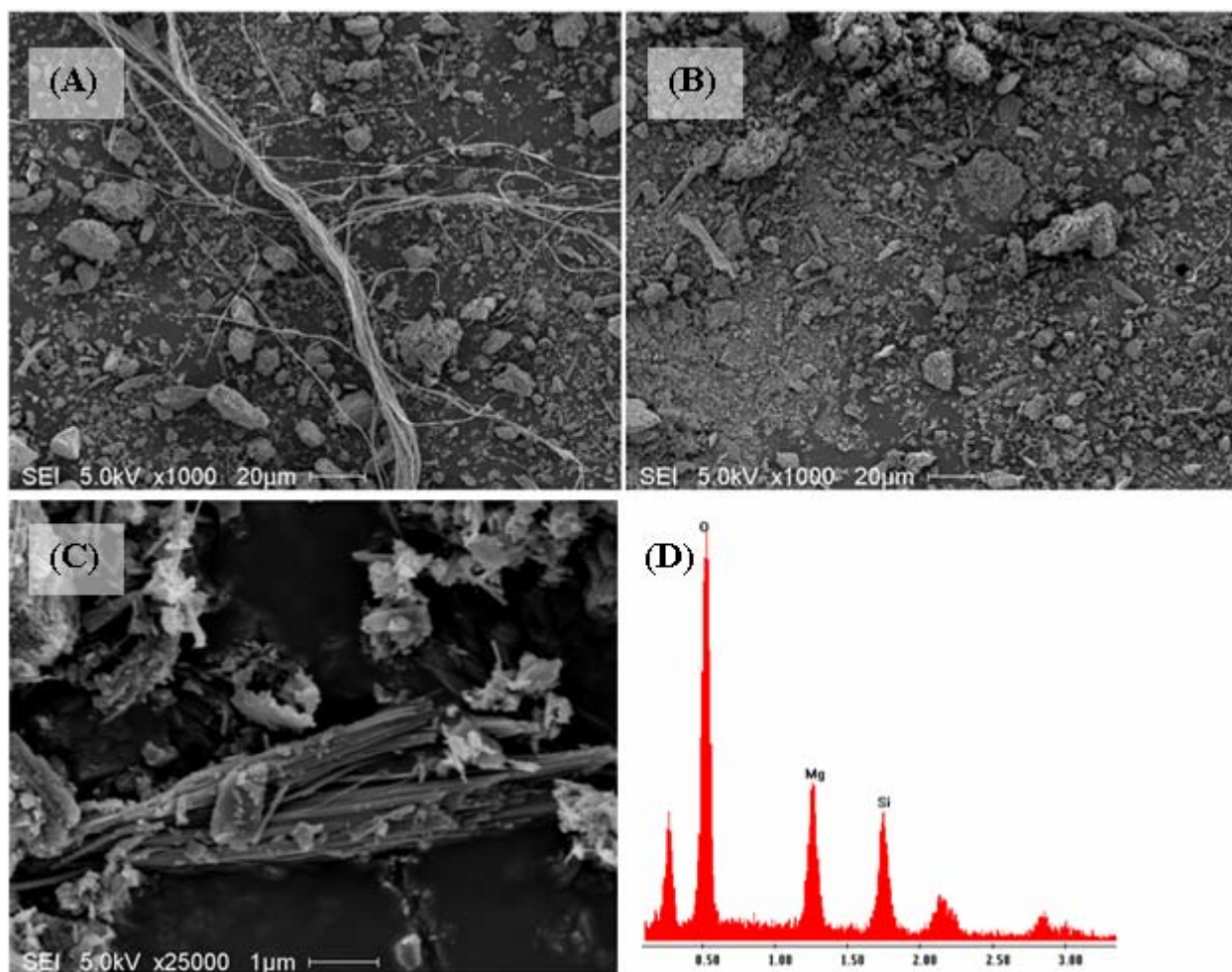


Fig. 12. Ore sample (A) untreated; (B) ground with HCl, (C) short fibres in it and (D) corresponding microanalysis

High-resolution XPS results for the Si2p and Mg1s peaks of untreated and HCl treated ore samples are shown in Fig. 13. The binding energy of Si2p peak, ca. 103 eV, reflects Si in a silicate matrix (Moulder et al., 1992). Spectra suggest considerable enrichment of Si relative to Mg after the acid treatment. Fig. 14 shows XPS O1s peak. The acid treated sample shows a higher O1s binding energy (532.0 eV) than the untreated one (531.5 eV). This may be linked to the addition of hydroxyl groups to the silicon-rich layer of the treated ore (reaction 2). For the Si2p, Mg1s and O1s cases, the broader peak of the treated sample is indicative of the presence of different chemical states.

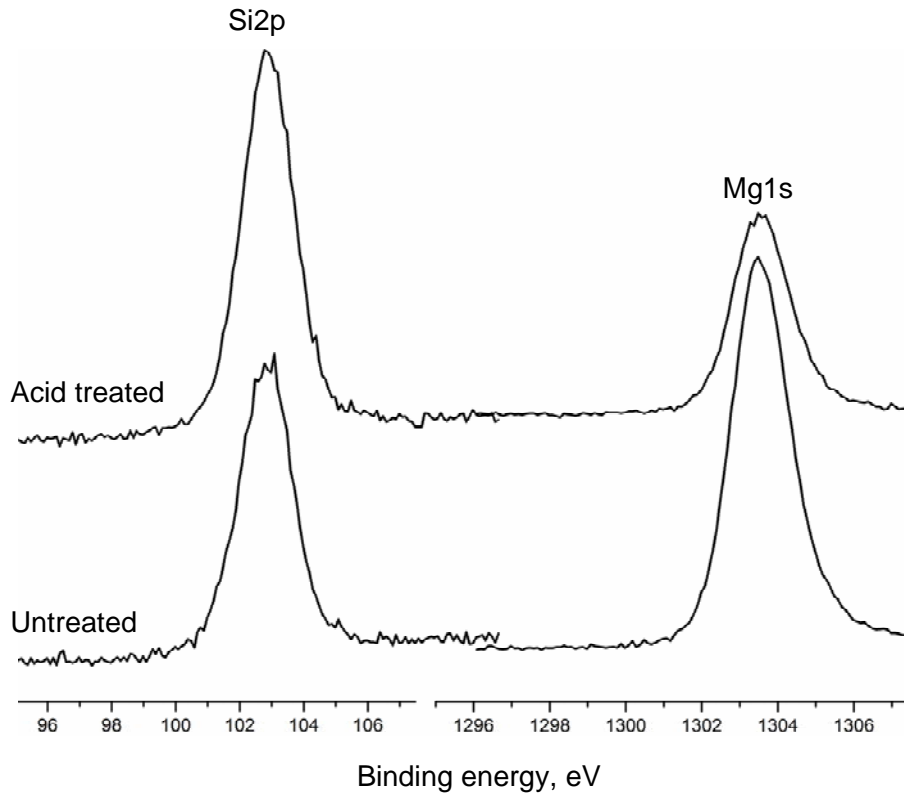


Fig. 13. XPS analysis for untreated and acid treated ore. Si2p and Mg1s peaks are indicated.

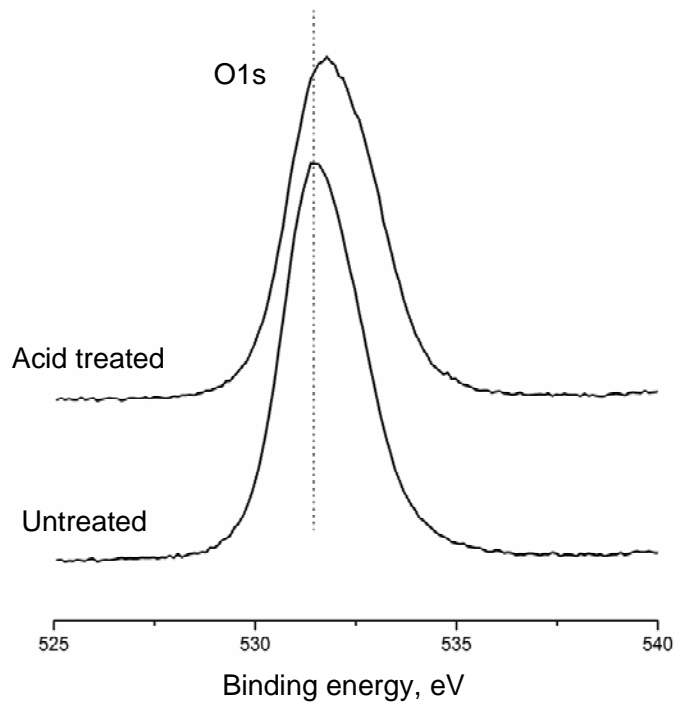


Fig. 14. XPS high-resolution spectra of O1s peak for untreated and acid treated ore

6.6. Discussion

Particle sedimentation potential (PSP) studies on a sample of ultramafic ore show a continuous decrease in PSP as pH increases from 8-10 to remain stable at negative potential from pH 10-11.5. The ore iep is ca. pH 8. It seems that the iep is not completely dominated by the major serpentine (chrysotile) component minerals (iep ~ pH 10) but is influenced by the other minerals, i.e., olivine (iep ~ pH 4.5), pyrrhotite (~ 5.8) and magnetite (~ 5-6.5).

Experiments conducted to determine the effect of Mg showed at 0.006M a small variation in the PSP and shift in iep from 8 to 8.5. Apparently, adsorption of Mg cations to the negative sites of the ore particles shifts the overall potential to more positive values. An increase in concentration to 0.018M had a pronounced effect on PSP which was positive over the studied pH range. This effect of Mg is well known in the case of particles (Palmer and Fuerstenau, 1976), and as chapter 4 indicates is also the observation for bubbles.

Addition of 0.001M EDTA shifted the potential to more negative values along with considerable decrease in iep (~ 5). The effect of EDTA can be twofold. First, as a chelating agent, it can remove adsorbed positively charged metal ions from the surface to expose more negative sites; and second, as a weak acid, EDTA can reduce Mg/Si ratio at the interface by extracting Mg. Since electrokinetics of serpentine in aqueous electrolyte strongly depends on Mg/Si atomic ratio at the solid/liquid interface (Tartaj et al., 2000) both effects can decrease the PSP and the iep of the system.

The action of EDTA may affect flotation either by lowering the possibility of non-sulphide gangue activation by metal ions or by countering the tendency of hetero-coagulation or slime coating. The negligible impact on Ni-metallurgy and MgO-rejection using EDTA (Figs 9

and 10) suggest that metal ion activation or slime coating are not key factors influencing flotation in this system.

To study the other possible flotation determining factor – ‘entanglement’ – a fibre disintegration technique was devised combining both chemical (HCl and EDTA) and physical (grinding) treatment. The release of extracted Mg noted here (ca. 12% with 15 wt% HCl) infers fibre disruption. The effect was achieved at the ‘cost’ of 4% Ni loss, although it is possible that some of the dissolved Ni may come from the fibrous minerals from which Ni is unrecoverable anyway by flotation.

Chrysotile is one of the strongest asbestos-type minerals (Kogel et al., 2006). Higher acid strength was used to prepare samples to achieve easily identified changes in the fibres. Broken short fibres (Fig. 12), dominant in the treated sample, suggest a possible mechanism where acid attack initiates numerous cracks on fibres followed by breakage through impact of the grinding media.

In flotation, the visual evidence in the froth phase is striking (Fig. 8), the froth at 0 and 5wt% HCl appearing barren, and at 10 and 15wt% HCl treatment showing evidence of high loading with sulphide minerals. Flotation results (Figs. 9 and 10) showed a notable improvement in Ni and MgO mineral selectivity using a conventional Ni-sulphide flotation reagent suite after applying the fibre disintegration treatment. The results suggest 80% Ni recovery at 90% MgO rejection is possible in the rougher stage with the 15wt% HCl treatment.

Selectivity against MgO minerals may be further promoted by the chemical attack lowering the Mg/Si ratio on the mineral surface, which reduces the fibre (chrysotile) iep and thus tends to reduce slime coating on Ni-minerals by reducing the pH range over which the two

mineral have opposite charge. A significant increase in Si2p peak intensity relative to Mg1s in the treated sample in the XPS studies is indicative of decreasing Mg/Si ratio (Figs. 13 and 14).

This ore treatment, based on technology for enhancing carbon dioxide sequestration of serpentine minerals, appears technically attractive. Economics is something else. The choice of HCl was made based upon the CO₂ sequestration literature; sulphuric acid is likely the more practical (economic) choice, especially if a local supply from a Ni smelter practising SO₂ abatement is available. Chapter 7 explores the use of sulphuric acid. If there is nearby CO₂ emission source the tails may represent a sequestration opportunity. In the case of the Thompson area this 'local' source could be from the oil sands processing industry which is eager to find a CO₂ control solution. As the demand to 'fix' CO₂ grows the definition of 'nearby' might be quite flexible. Future investigations should include the CO₂ sequestration capacity of the tails.

6.7. Conclusions

Surface charge characteristics of an ultramafic ore, measured by the particle sedimentation potential method, inferred of a mix serpentine and other minerals to explain the low iep, pH 8 compared to the iep of serpentine, ca. pH 10. Particle sedimentation potential (PSP) and flotation tests with EDTA implied that MgO-bearing gangue activation by metal ions or 'slime coating' are not major causes of poor flotation response of this type of ore. Using a fibre disintegration ore treatment process based on emerging technology for enhancing carbon dioxide sequestration, flotation selectivity was significantly improved. This corresponded to a marked change in the appearance of the fibres which became short and un-entangled after treatment.

6.8. Acknowledgements

The funding from and permission to publish by Vale is greatly appreciated. We also acknowledge Vale for organizing the progress review meetings on Ultramafic Ore Research which provided an exceptional opportunity to share knowledge between researchers from McGill University, McMaster University, Columbia University, Cytec Industries Inc. and Vale Base Metals Technology Development.

6.9. References

- Bremmel, K. E., Fornasiero, D., Ralston, J., 2005. Pentlandite-lizardite interactions and implications for their separation by flotation. *Colloid Surface A*, 252, 207 – 212.
- Brindley, G. W., Brown, G., 1980. *Crystal Structures of Clay Minerals and Their X-Ray Identification*. Mineralogical Society, London.
- Dalvi, A. D., Bacon W.G., Osborne, R. C., 2004. The past and the future of nickel laterites. In: *Proceedings of PDAC International Convention, Toronto, 2004*.
- Dai, Z., Bos, J-A. Quinn, P., Lee, A., Xu, M., 2009. Flowsheet development for thompson ultramafic low-grade nickel ores, in: Gomez, C. O.; Nasset, J. E.; Rao, S. R. (Eds.), *Proc. Advances in Mineral Processing Science and Technology. Conference of Metallurgists, CIM, Sudbury, Ontario*, pp. 217 – 228.
- Edwards, G.R., Kipkie, W. B., Agar, G. E., 1980. The effect of slime coating of the serpentine minerals, chrysotile and lizardite on pentlandite flotation. *Int. J. Miner. Process.*, 7, 33 – 42.
- Fuerstenau, M. C., Somasundaran, P., 2003. Flotation, in: Fuerstenau, M. C., Han, K. N., (Eds.), *Principles of Mineral Processing*. SME, Colorado, pp. 245.
- Fornasiero, D., Ralston, J., 2005. Cu(II) and Ni(II) activation in the flotation of quartz, lizardite and chlorite. *Int. J. Miner. Process.*, 76, 75 – 81.
- Hogendam, C. W., de Keizer, A., Cohen, M. A., Bijsterbosch, B. H., 1998. Adsorption mechanisms of carboxymethyl cellulose on mineral surfaces. *Langmuir*, 14, 3825 – 3839.
- Kogel, J. E., Trivedi, N. C., Barker, J. M., Krukowski, S. T., (Eds.), 2006. *Industrial Minerals and Rocks: Commodities, Markets and Uses*. SME, Colorado, pp. 199.

- Mani, H, Xu, M., Quinn, P., Stratton-Crawley, R., 1997. The effect of ultramafic mineralogy on pentlandite flotation, in: Finch, J. A., Rao, S. R., Holubec, I. (Eds.), Proc. Processing of Complex Ores, Conference of Metallurgists, CIM, Sudbury, Ontario, 1997, pp. 63 – 76.
- Moulder, J.F., Stickle, W.F., Sobol, P.E., Bomben, K.D., 1992. Handbook of X-ray Photoelectron Spectroscopy. Perkin-Elmer Corp., Eden Prairie, MN, USA.
- Oliveira, A. P., Torem, M. L., 1996. The influence of some metallic cations on deinking flotation. *Colloid Surface A*, 110, 75 – 85.
- Park, A-H. A., Fan, L-S., 2004. CO₂ mineral sequestration: physically activated dissolution of serpentine and pH swing process. *Chem. Eng. Sci.*, 59, 5241 – 5247.
- Powder Diffraction File, International Centre for Diffraction Data, Newtown Square, PA, USA
- Pugh, R. J., Tjus, K., 1987. Electrokinetic studies on Cu(II) hydroxide coated zinc sulfide particles. *J. Colloid Interf. Sci.*, 117, 231 – 241.
- Sun, S. C., 1943. The mechanism of slime coating. *Trans. AIME*, 153, 479 – 492.
- Senior, G. D., Thomas, S. A., 2005. Development and implementation of a new flowsheet for the flotation of a low grade nickel ore. *Int. J. Miner. Process.*, 78, 49 – 61.
- Tartaj, P.; Cerpa, A.; Garcia-Gonzalez, M. T.; Serna, C. J., 2000. Surface instability of serpentine in aqueous suspensions. *J. Colloid Interf. Sci.*, 231, 176 – 181.
- Trahar, W. J., 1981. A rational interpretation of the role of particle size in flotation. *Int. J. Miner. Process.*, 8, 289 – 327.
- Uddin, S., Mirnezami, M., Finch, J. A., 2010. A surface charge characterization device using sedimentation potential for single and mixed particle systems. *Colloid Surface A*, 371, 64–70.
- Xu, Z., Rao, S. R., Finch, J. A., Kelebek, S., Wells, P., 1997. “Role of Diethylenetriamine (DETA) in Pentlandite-pyrrhotite Separation: I. Complexation of Metals with DETA”, *Trans. IMM: Sect. C*, 106, C15–C20, 1997.
- Wypych, F., Adad, L. B., Mattoso, N., Marangon, A. A. S., Schreiner, W. H., 2005. Synthesis and characterization of disordered layered obtained by selective leaching of octahedral sheets from chrysotile and phlogopite structures. *J. Colloid Interf. Sci.*, 283, 107 – 112.

7. Processing an Ultramafic Ore Using Fibre Disintegration by Acid

Attack

7.1. Abstract

Ultramafic ores are a potential major resource of nickel. For the Thompson area deposits of northern Manitoba, Canada, a processing challenge is the serpentine polymorph chrysotile, the dominant gangue mineral. Due to its fibrous nature chrysotile causes physical entanglement and increased pulp viscosity which reduces selectivity in flotation. The proposed approach involves disintegration of the fibres by a combination of chemical (H_2SO_4) and mechanical (grinding) treatment adapting technology explored for CO_2 sequestration. The use of H_2SO_4 also led to collectorless flotation traced to elemental sulphur formation, and release of magnesium increased solution ionic strength sufficient to eliminate the need for frother. Significant improvement in Ni grade-recovery with higher rejection of MgO-bearing gangue was achieved compared to untreated ore. Structural changes in the fibres were followed using spectroscopic techniques. A mechanism of fibre disintegration is suggested.

Keywords: Ultramafic deposits, chemical/mechanical treatment, fibre disintegration, flotation, collectorless flotation

Research highlights:

- A processing route has been designed for serpentine rich ultramafic Ni-ore.
- Process based on fibre disintegration by combined chemical/mechanical treatment.

- Low pH slurry after the treatment effects collectorless flotation.
- Significant improvement in Ni-metallurgy and MgO rejection was achieved.
- A mechanism of fibre disintegration is proposed.

7.2. Introduction

The purpose of this paper is to propose an alternative route to fibre removal based on disintegrating the fibres by chemical-mechanical attack.

7.3. Background

The background was discussed in chapter 2.

7.4. Experimental

7.4.1. Ore mineralogy

The sample was supplied by Vale and is the same as discussed in chapter 6.

7.4.2. Flotation without acid treatment

Grinding used a 15 x 15 cm ceramic ball mill with 40%v/v charge of 3, 1.8 and 1 cm diameter zirconium oxide balls. A 100 g sample was slurried with 800 mL water; and 1 wt% soda ash and 0.05 g CMC were added prior to grinding for 1 hr. A sample of supernatant was taken for assaying (ICP-OES) after grinding to determine dissolved species. The slurry was then transferred to a Denver flotation cell.

For flotation, the slurry volume was adjusted to 1 L (i.e., slurry density is 10 wt% solids). Soda ash was added to bring pH to 10. As collector, 0.004 g of purified potassium-amyl-xanthate (PAX) was used with a conditioning time of 5 minutes (based

on scaling down the aeration time used by Heiskanen et al. (1991)). Impeller speed was 1500 rpm. Frother MIBC (0.002 g) was added and conditioned for a further 5 minutes prior to introducing air (flow rate 5 L/min). Three concentrates were taken at 1, 2 and 4 minutes. They along with the tails, were filtered, oven dried, weighed and assayed (ICP-OES). This procedure is based on Ni sulphide flotation practice.

7.4.3. Flotation with acid treatment

The same grinding mill was used but this time the 100 g sample was slurried with 800 mL of 15 wt% sulphuric acid (H_2SO_4). The acid concentration was selected based on the previous work (Uddin et al., 2010). There were two approaches taken to encourage oxidation and collectorless flotation: 2-hr aging in the ball mill followed by addition of DF250 (polypropylene methyl ether) frother (0.002 g) (MIBC did not produce adequate froth in this case); or, 5-min aeration (5 L/min) in the Denver cell with flotation of the first two concentrates without frother and with 0.002 g DF250 addition prior to collecting the third concentrate. The common conditions were: grinding time 1 hr, slurry volume adjusted to 1 L for flotation, and three concentrates (5, 10 and 15 minutes) collected. For both approaches, the experiments were conducted three times. The flowsheet is shown in Fig. 1.

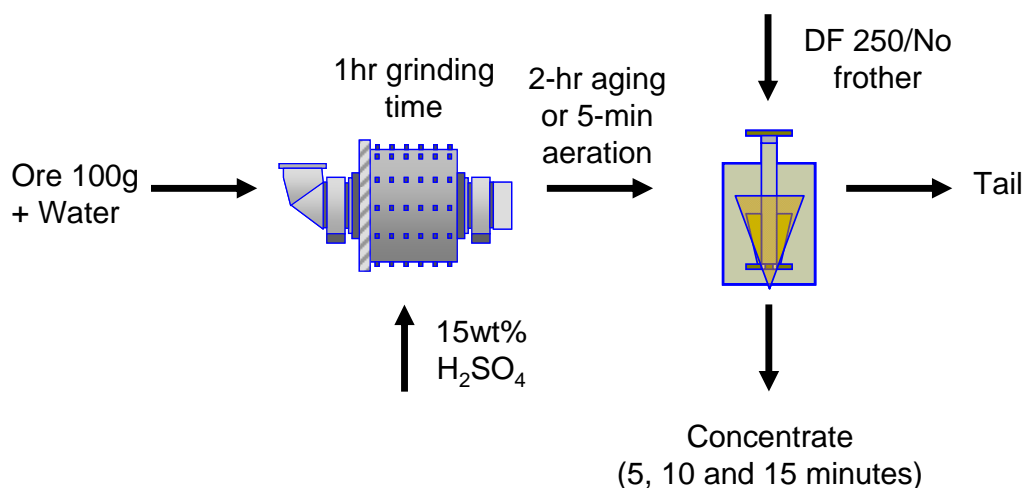


Fig. 1. Flowsheet with acid treatment

7.4.4. Illustration of fibre disintegration

In these tests 1 g of ore ground (1 hr) without acid was transferred to an 8 x 8 cm ceramic mill with 1-cm zirconium oxide grinding media (40% v/v charge). The sample was ground for a further hour in the presence of 5 mL HCl or H₂SO₄, equivalent to ca. 500 wt% acid. A higher concentration of acid than in the flotation tests was needed to achieve detectable physical changes in the fibres. After grinding, the samples were filtered, dried and analyzed.

7.4.5. Analytical methods

X-ray diffraction (American Instruments Inc., Cu target at 20 mA, 40 kV) was used to determine mineral phases. Fourier transformation infrared spectroscopy (FT-IR; Model 1600, Perkin Elmer) was used to identify changes in molecular structure. Disks were prepared by mixing 200 mg KBr and 3-4 mg of sample. Electron beam analysis (Philips XL30 FEG-SEM with Genesis EDS/X-ray microanalysis system) was used to

image physical changes. Powdered samples were mounted on carbon tape and wafer-coated with gold/palladium (Anatech Hummer VI sputtering system).

A test was performed to extract hydrophobic species from concentrate produced in approach 2 using toluene at 70-80°C (Becze et al., 2009). Extracted material was precipitated by evaporation and analyzed with SEM-EDS and Raman spectroscopy. For the latter, spectra of the extract and a standard elemental sulphur sample (Sigma-Aldrich) were collected using an inVia Raman microscope (Renishaw). Laser excitation was provided by a polarized He-Ne laser operating at 632 nm.

7.4.6. Bubble size distribution

Acid treatment produced a pulp liquor of ionic strength ca. 0.85 (considering SO₄, Mg, Fe and Ni ions in solution). To simulate and determine the effect on bubble size, a solution containing 4 g/L Mg (as MgSO₄, ionic strength ca. 0.7) was prepared and placed in a 110 x 10 cm bubble column with a rigid, vertical cylindrical porous sparger. Bubble size distribution (BSD) was determined using the McGill Bubble Size Analyzer (MBSA) (Hernandez-Aguilar and Finch, 2005) at a gas superficial velocity of 0.5 cm/s. Images were collected and processed using a 10-bit digital camera driven by commercial software (Northern Eclipse, Empix Imaging Inc.). Typically, 500 bubble images were processed for each test. The BSD data are presented as number mean (d_{10}) and Sauter mean diameter (d_{32}).

7.5. Results

7.5.1. Effect of acid treatment

An indication of fibre disintegration is the extraction of Mg. Table 1 shows the 15 wt% H₂SO₄ extracts ca. 25% of the Mg yielding a solution concentration ca. 6-7 g/L Mg. At the same time, ca. 4% Ni and 12% Fe were lost to solution (standard deviation included on the Table). It was noted that slurry flowability increased after acid treatment.

Table 1

Metallurgical balance (average of the three tests): leach and flotation, approach 1 (A) and approach 2 (B). (Note: composition of ‘mass loss’ is inferred from grams mass loss and solution assay; standard deviation on element mass loss based on three tests is included)
A) Approach 1: 2-hr aging and frother (DF250) addition.

	Mass (g)	Assay (%)			Distribution (%)		
		Ni	Mg	Fe	Ni	Mg	Fe
Leaching							
Sol (L, g/L)	1	0.03	6.89	1.60	-	-	-
Mass Loss	14.13				4.2 (± 0.2)	26.6 (± 3.0)	12.2 (± 1.5)
Flotation							
Con 1	6.80	5.24	9.75	28.34	52.9	3.4	13.2
Con 2	5.93	2.38	14.28	23.83	18.6	4.6	9.3
Con 3	4.69	1.25	13.56	18.55	7.6	5.1	6.4
Tail	68.43	0.17	21.68	10.21	16.5	60.2	58.7
Head	100	0.67	23.46	12.30	100	100	100

B) Approach 2: 5-min aeration, no frother for cons 1 and 2.

	Mass (%)	Assay (%)			Distribution (%)		
		Ni	Mg	Fe	Ni	Mg	Fe
Leaching							
Sol (L, g/L)	1	0.02	6.35	1.36	-	-	-
Mass Loss	10.87	-	-	-	3.8 (± 0.3)	25.3 (± 3.8)	11.1 (± 1.2)
Flotation							
Con 1	9.27	4.79	8.56	31.64	70.1	3.1	26.2
Con 2	7.30	0.76	14.74	13.20	8.6	3.6	8.6
Con 3	6.52	0.35	18.16	8.31	3.6	2.6	4.8
Tail	66.01	0.13	21.41	8.26	13.6	65.1	49.1
Head	100	0.63	23.80	11.12	100	100	100

7.5.2. Flotation

The slurry pH was stable after grinding with H₂SO₄ (ca. pH 2). Fig. 2 compares the froth appearance of the treated and untreated sample after the first minute of flotation (approach 1). For treated sample the froth had the metallic sheen typical of a sulphide float compared to the dull appearance for the untreated sample.

Fig. 3 shows the Ni grade vs. recovery (cumulative) for both approaches. The three points correspond to the three concentrates 1, 2 and 3, and the error bars are the range for the three tests. The results are similar: about 80% Ni recovery at 2.5-3.5% Ni grade was achieved with the treated sample (enrichment ratio ca. 4.5); a significant improvement compared to the untreated case which achieved only 50% Ni recovery by concentrate 3. This corresponds to increased selectivity against the MgO minerals: Fig. 4 indicates that at 90% MgO rejection (i.e., recovery to tails) the treated sample yielded ca.

80% Ni recovery while the untreated sample gave only ca. 45% Ni recovery. This limited separation for untreated ore is seen by others (Dai et al., 2009).

The main gangue contaminant in the concentrate was pyrrhotite (Po) as indicated in the XRD pattern (Fig. 6). From the Fe assay and assuming no other Fe-bearing mineral in the concentrate besides pentlandite, the pyrrhotite content at 80% Ni recovery was ca. 30%. The collectorless flotation at ca. pH 2 was evidently selective against MgO but not Po, as the work of Heiskanen et al. (1991) would support.

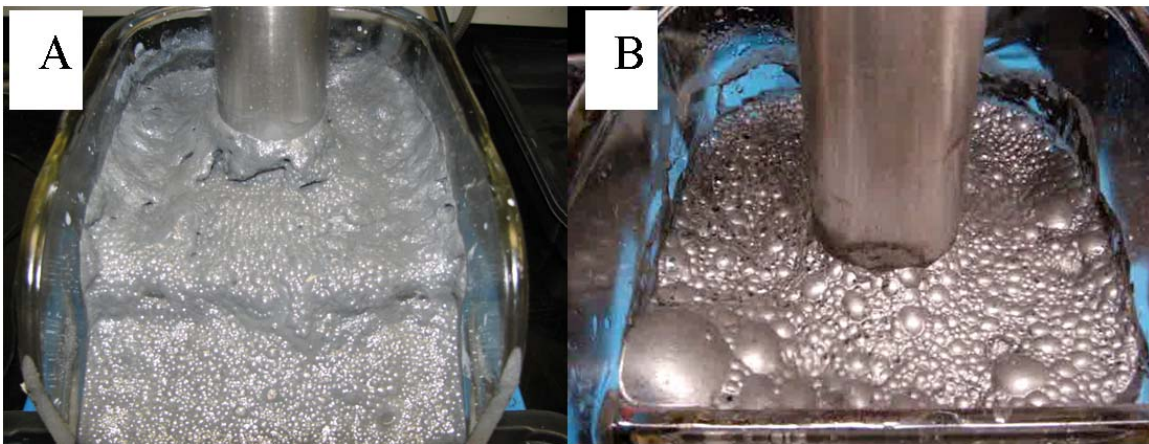


Fig. 2. Froth appearance after 1 min (A) untreated ore, (B) treated with 15 wt% H₂SO₄ (approach 1)

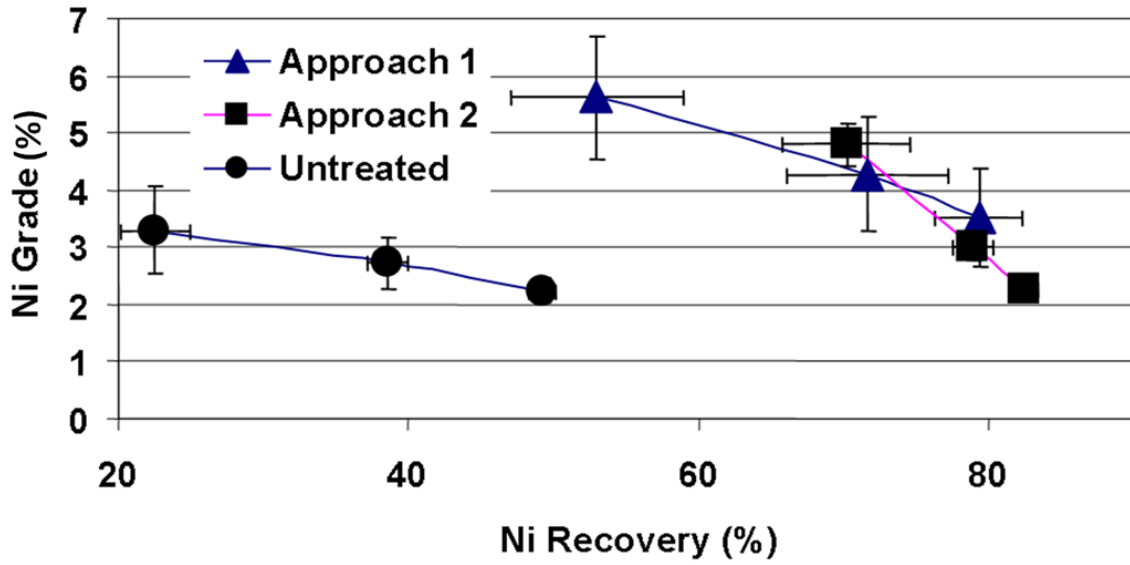


Fig. 3. Nickel grade vs. recovery: treated (approaches 1 and 2) vs. untreated ore (note error bars are the range for the three repeats)

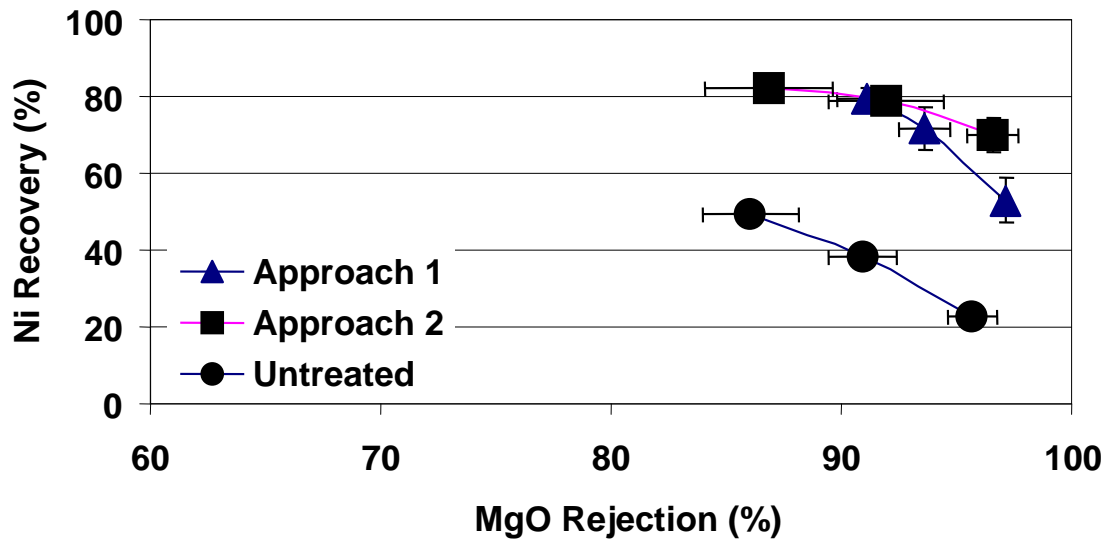


Fig. 4. Nickel recovery vs. MgO rejection: treated (approaches 1 and 2) vs. untreated ore

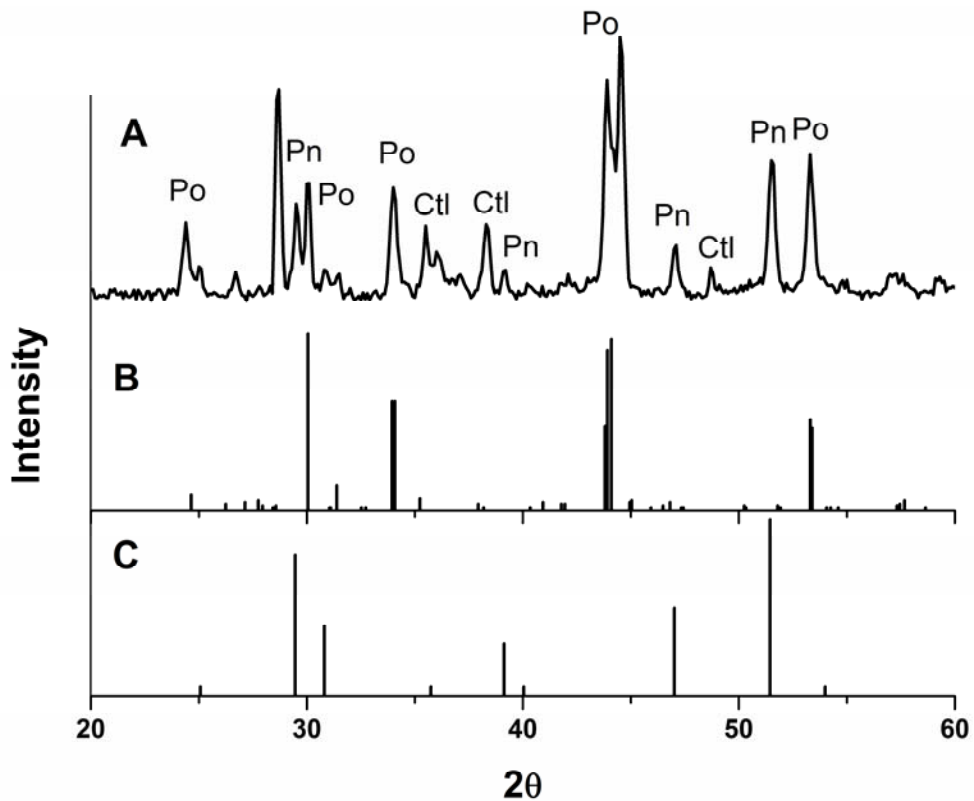


Fig. 5. XRD of (A) concentrate 1 from approach 1 and match for (B) pyrrhotite (Po) and (C) pentlandite (Pn) (clinochrysotile (Ctl) – cf Fig. 1, chapter 6)

7.5.3. Illustrating fibre disintegration

The tests described in this section were done at the higher acid concentration than that used in flotation. Fig. 6 shows FT-IR spectra over two frequency ranges, 500 to 2000 cm^{-1} (left-hand figure) and 3000 to 4000 cm^{-1} (right-hand figure). The major absorption bands are identified based on the literature (Nyquist and Kagel, 1971; Sugama et al., 1998). The band at 3680 cm^{-1} with the shoulder at 3640 cm^{-1} represents the stretching vibration of hydroxyl in $\text{Mg}(\text{OH})_2$. The 3410 and 1640 cm^{-1} bands relate to stretching and bending modes of H_2O and the bands at 1080 and 970 cm^{-1} corresponds to Si-O-Si and Si-O⁻ stretching, respectively. The important features of the samples ground with acid include reduction of band intensity at 3680 and 3640 cm^{-1} , growth of bands at 3410 and

1640 cm^{-1} , gradual conversion of bands at 1080 and 970 cm^{-1} into shoulders and emergence of bands at 1220 and 810 cm^{-1} .

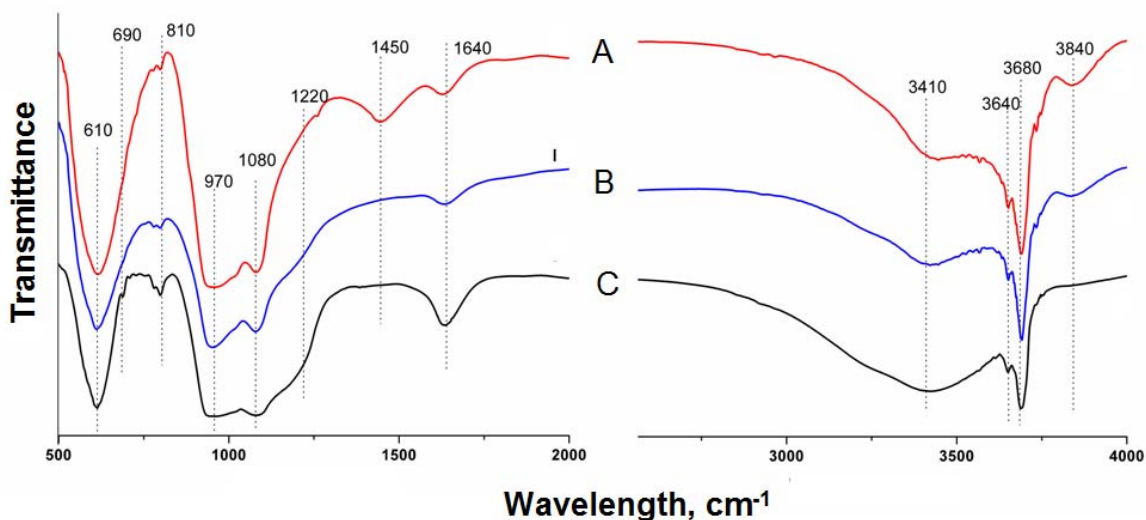


Fig. 6. FT-IR spectra 500 to 2000 cm^{-1} (left) and 3000 to 4000 cm^{-1} (right) of (A) ground, untreated ore; (B) ground ore, HCl; and (C) ground ore, H_2SO_4

X-ray diffraction patterns are shown in Fig. 7. There is apparent attenuation of the chrysotile-related peaks (marked by arrows) in the samples ground with acid. The SEM image (Fig. 8A) reveals the long fibres in the ground untreated sample while acid-treated samples – even at the higher magnification – show few of these long interconnected fibres being instead dominated by short, apparently broken fibres (Figs. 8B and 8C). Higher magnification is used to visualize one of the short fibre bundles (Fig 8D).

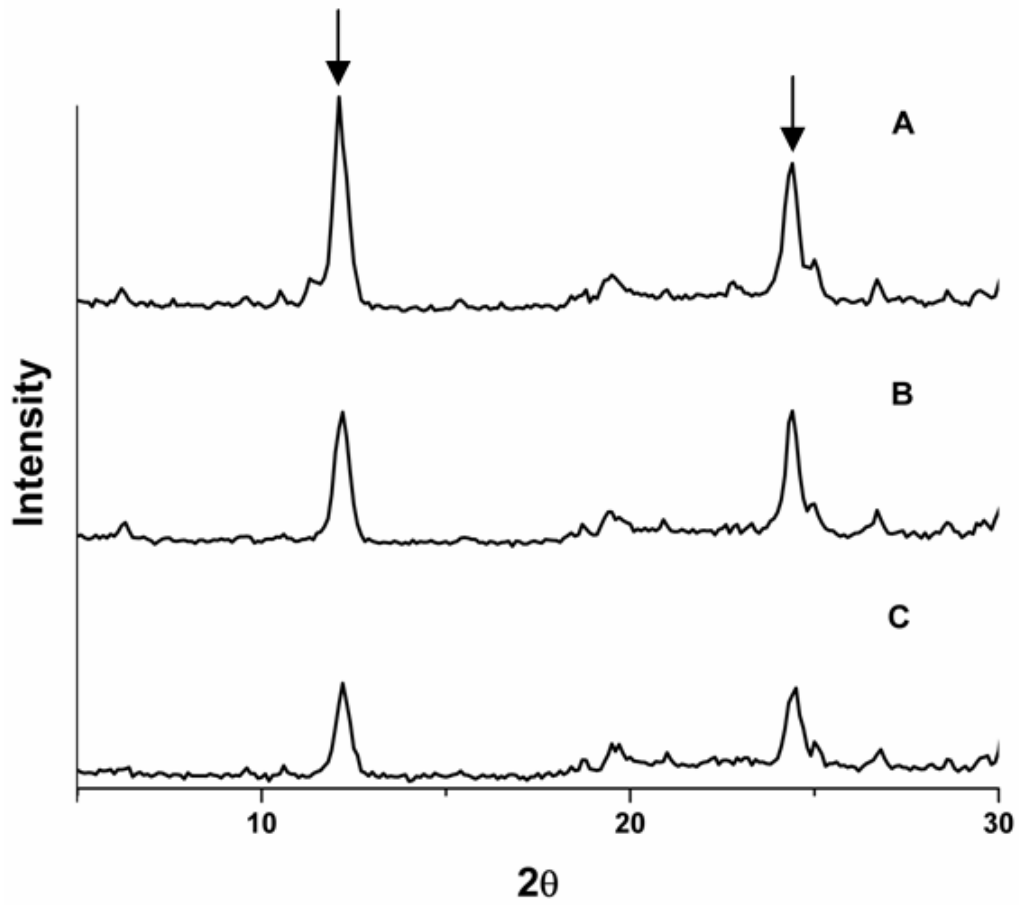


Fig. 7. XRD of (A) ground ore, ground with (B) HCl and (C) H_2SO_4

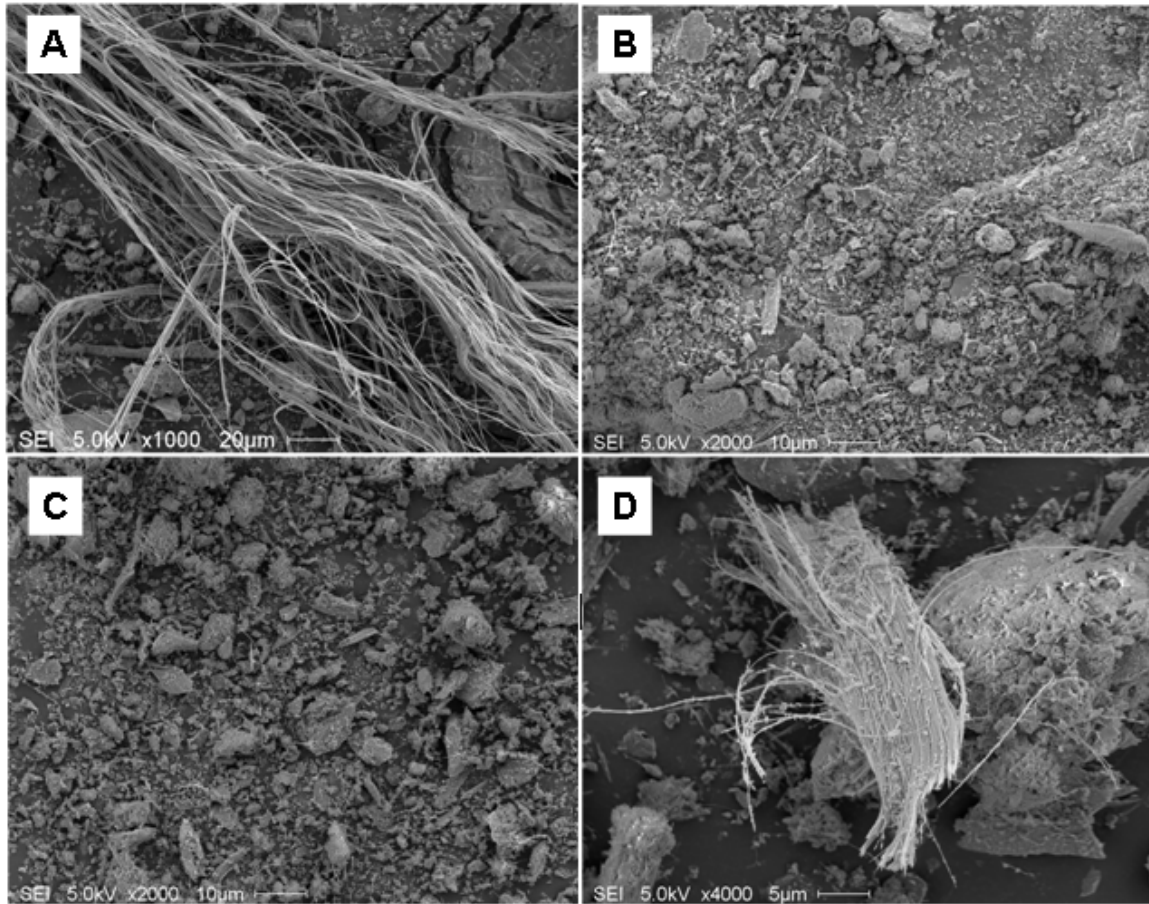


Fig. 8. Ore sample (A) untreated; ground with (B) HCl, and (C), (D) H₂SO₄

7.5.4. Bubble size

Fig. 9 shows bubble size in tap water and in 4 g/L Mg solution with H₂SO₄ added to pH 2.8. A considerable decrease in bubble size (Sauter mean reducing from ca. 4 mm to ca. 0.6 mm) was observed in the salt solution compared to tap water.

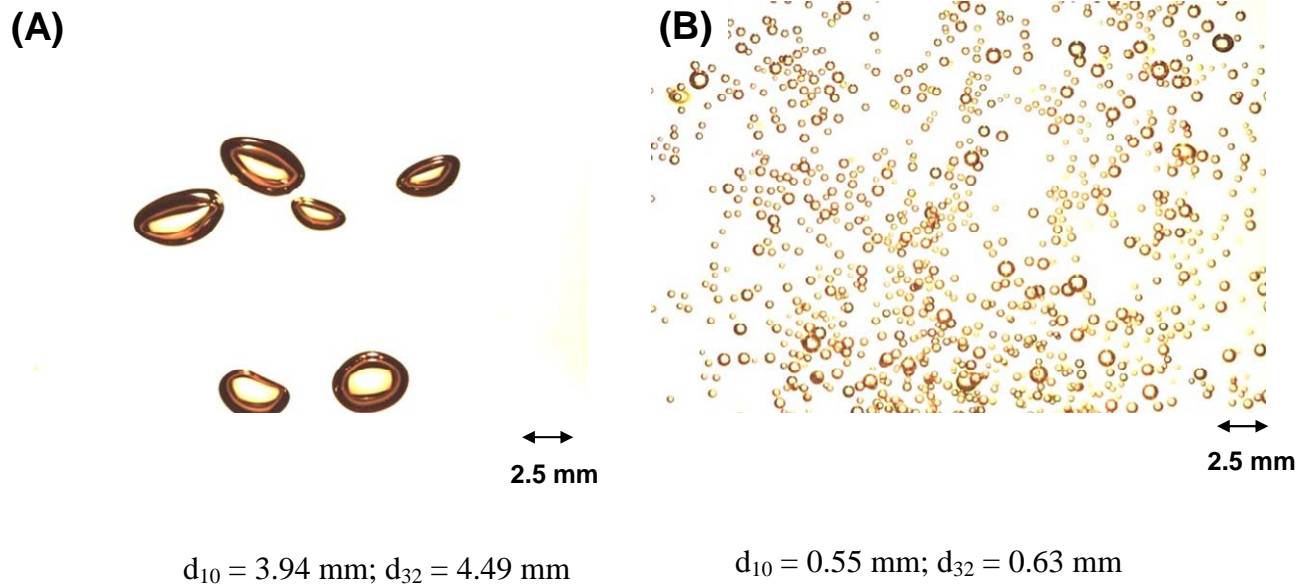


Fig. 9. Bubble size distribution in (A) tap water and (B) MgSO_4 (pH 2.8) solution

7.5.5. Evidence of elemental sulphur

SEM-EDS analysis of the substance extracted from the concentrate (approach 2, concentrate 1) is shown in Fig. 10. The crystalline-looking material is evidently sulphur. The Raman spectrum confirms sulphur by comparison with a standard sample (Fig. 11). X-ray photoelectron spectroscopy (XPS) studies (not shown) were performed to try to identify the polysulphide species. But, probably due to low concentration, decoupling polysulphide peaks from elemental sulphur in the spectra was not possible.

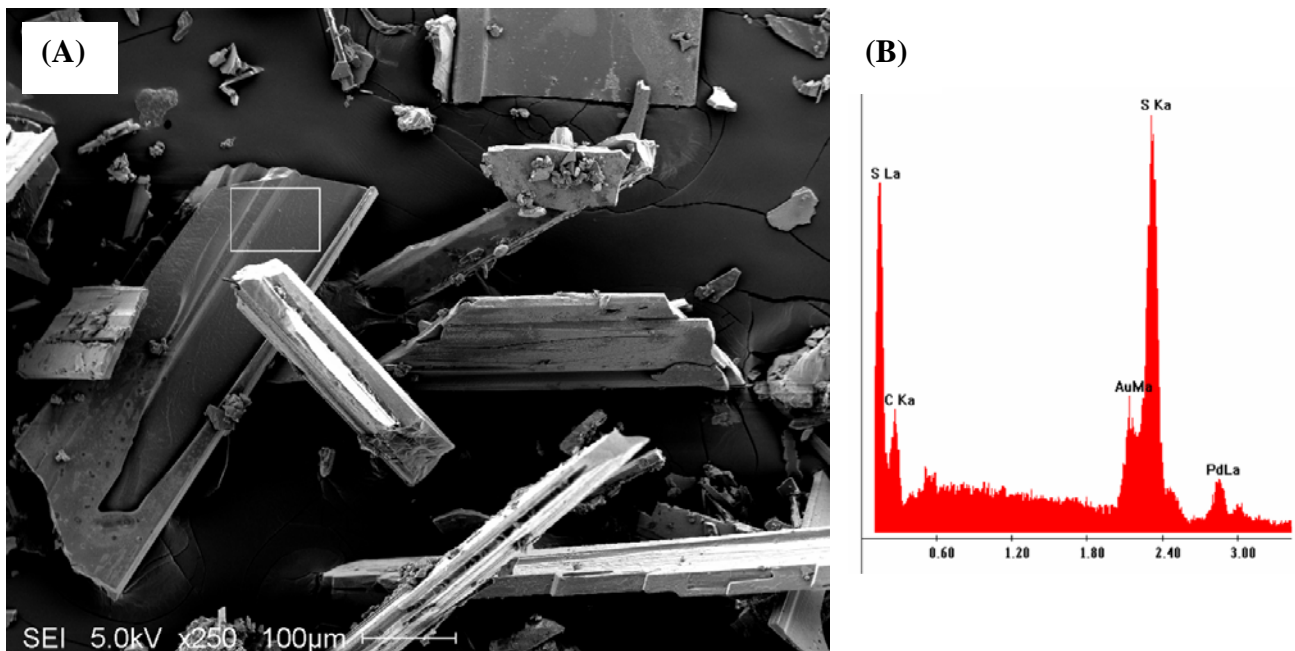


Fig. 10. (A) Extracted crystalline substance from concentrate and (B) microanalysis on one of the crystals

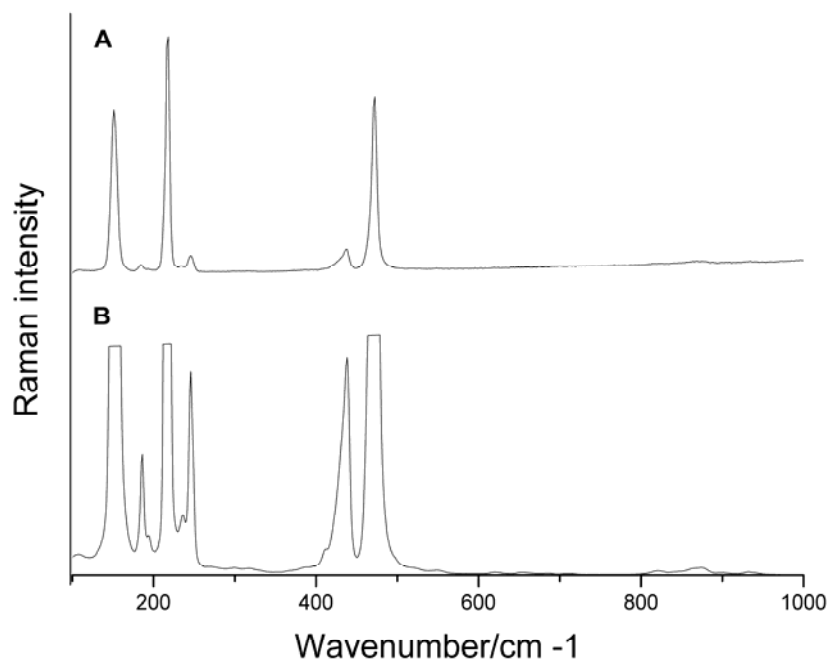


Fig. 11. Raman spectra of the (A) extracted material and (B) standard sample of elemental sulphur

7.6. Discussion

The positive impact on mineral separation of the acid/grind treatment is evident in the improved Ni grade-recovery and rejection of MgO minerals compared to the untreated case. The treatment was adapted from work to enhance CO₂ sequestration which employs acid attack on serpentine minerals to release Mg (to react with CO₂).

The ca. 25% release of Mg here infers fibre disruption and the sensed increase in slurry flowability (reduced viscosity) implies the targeted improvement in rheological character was achieved. The cost was ca. 4% Ni loss, although it is possible some of the dissolved Ni came from minerals other than Ni sulphides which are otherwise unrecoverable by flotation.

Chrysotile is one of the strongest asbestos-type minerals (Kogel et al., 2006). It is not easily broken by grinding but with sufficient acid breakage is demonstrated (Fig. 8). In the FT-IR spectra (Fig. 6) the reduction of the Mg-OH band at 3680 cm⁻¹ and transition to a shoulder of the Si-O band at 970 cm⁻¹ on acid treatment can be interpreted as breakage of the external Mg(OH)₂ layers on the serpentine; and the growth of the bands at 3410, 1640 and 1220 cm⁻¹ can be interpreted as hydration of the exposed inner siliceous structure. Apparent attenuation of the chrysotile-related line intensities in the XRD pattern after acid treatment (Fig. 7) is also evident in the literature (Sugama et al., 1998).

Fig. 12 suggests the possible breakage mechanism resulting from acid attack: cracks are initiated by extraction of Mg from the surface followed by rapid crack growth in this 'corroding' environment. That fibre breakage was not evident at the 15 wt% acid flotation condition is attributed to limited breakage which is difficult to locate in a small

amount of sample. The higher acid strength tests clearly show breakage and the mechanism in Fig. 12 seems plausible.

Leaching of Mg will also alter surface charge on serpentine. Poor separation of pentlandite from serpentine has been attributed to hetero-coagulation of the minerals which carry opposite charge, serpentine positive and pentlandite negative, at alkaline flotation pH (Edwards et al., 1980). Loss of Mg will tend to reduce the charge on serpentine (Tartaj et al., 2000) making electrostatic interaction with pentlandite less likely. At the high ionic strength of the leach solution measuring particle surface charge is difficult so this possibility has not been verified.

The acid treatment induced flotation without collector or frother. The collectorless response was traced to formation of elemental sulphur that is known to be promoted at low pH (Heiskanen et al., 1991). Just 5-minute aeration created the collectorless response. The 'frotherless' flotation was related to the ionic strength of the leach liquor exceeding ca. 0.4 where it is known that bubble size reduction at least equivalent to conventional frothers is realized with Mg salts. Bubble size reduction is a necessary condition to increase flotation kinetics and hence capacity of the flotation machine. High ionic strength may have other effects related to particle and bubble charging but these are considered secondary to the impact on bubble size. The product of flotation while encouragingly low in MgO minerals is high in pyrrhotite. Pentlandite/pyrrhotite separation is a common problem processing Ni-sulphide ores and various technologies exist.

A conceptual circuit based on the findings and assuming a supply of H₂SO₄ is presented in Fig. 13. Apart from the potential to resolve problems associated with fibrous minerals the proposed route turns two liabilities, SO₂ (captured as H₂SO₄) and MgO-rich tails (possible candidate for CO₂ capture), into potential assets.

An economic assessment is beyond the scope of the paper. Milling and ancillary equipment suited to concentrated acid is required and while there is some offset in operating cost through reduced collector and frother demand this is likely to be minor compared to the cost of acid which would likely have to be available locally. Nevertheless the proposed process for ultramafic ore does offer an opportunity that may fit conditions somewhere sometime in the future as Ni supplies tighten.

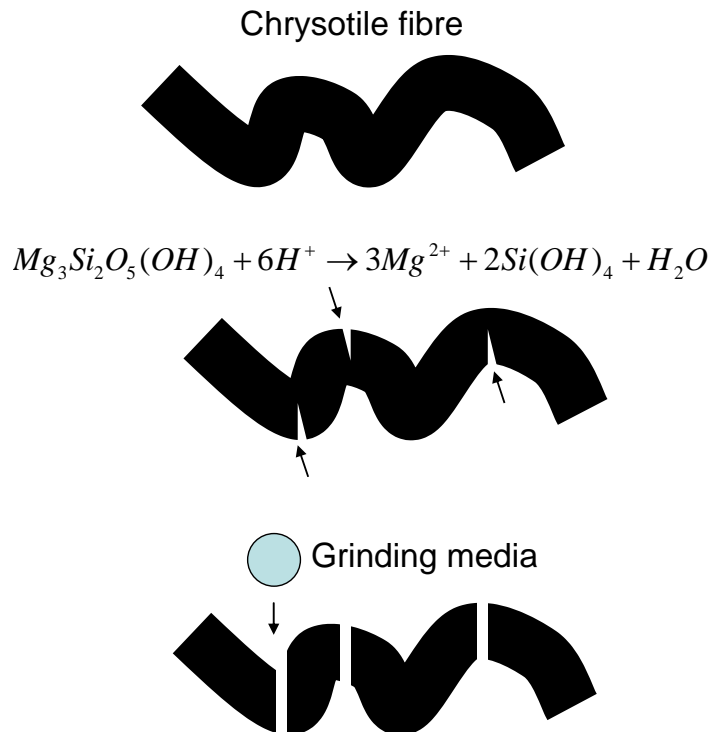


Fig. 12. A possible mechanism of fibre disintegration

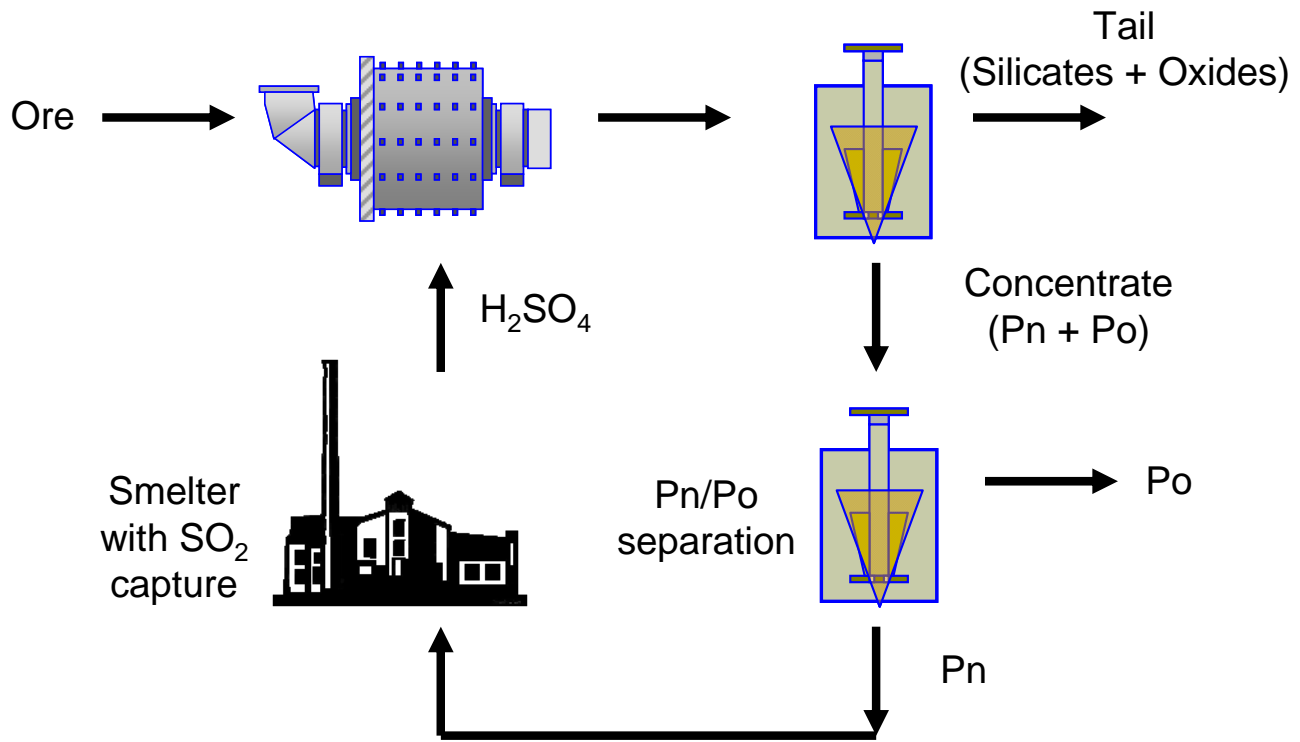


Fig. 13. A conceptual circuit to process ultramafic ore (Pn – Pentlandite; Po – Pyrrhotite)

7.7. Conclusions

Sulphuric acid/grinding treatment gave marked improvement in pentlandite-MgO mineral separation in flotation of an ultramafic ore. The improvement is attributed to disintegration of sufficient serpentine (clinochrysotile) fibres to reduce entanglement and pulp viscosity that otherwise hinder selective flotation. Fibre disintegration was indicated by significant (ca. 25%) Mg loss to solution and supported by electron beam and spectroscopic analyses. About 4% Ni is lost to solution. The treatment induced flotation without collector, shown to be due to elemental sulphur formation; and without frother, shown to be due to high ionic strength of the leach solution.

7.8. Acknowledgements

The funding from and permission to publish by Vale is greatly appreciated. We also acknowledge Vale for organizing the progress review meetings on Ultramafic Ore Research which provided an exceptional opportunity to share knowledge between researchers from McGill University, McMaster University, Columbia University, Cytac Industries Inc. and Vale Base Metals Technology Development. In the work at McGill we thank Mr. Wei Zhang for assistance in bubble sizing; and Dr. Mario Gomez for assistance with Raman spectroscopy.

7.9. References

- Becze, L.; Gomez, M. A.; Le Berre, J. F.; Pierre, B.; Demopoulos, G. P., 2009. Formation of massive gunningite-jarosite scale in an industrial zinc pressure leach autoclave – A characterization study. *Can. Metall. Quart.*, 48, 99 – 108.
- Brindley, G. W., Brown, G., 1980. *Crystal Structures of Clay Minerals and Their X-Ray Identification*. Mineralogical Society, London.
- Craig, V. S. J., Ninham, B. W., Pashley, R. M., 1993. The effect of electrolytes on bubble coalescence in water. *J. Phys. Chem.*, 97, 10192 – 10197.
- Dai, Z., Bos, J-A. Quinn, P., Lee, A., Xu, M., 2009. Flowsheet development for thompson ultramafic low-grade nickel ores, in: Gomez, C. O.; Nessel, J. E.; Rao, S. R. (Eds.), *Proc. Advances in Mineral Processing Science and Technology. Conference of Metallurgists, CIM, Sudbury, Ontario*, pp. 217 – 228.
- Dalvi, A. D., Bacon W.G., Osborne, R. C., 2004. The past and the future of nickel laterites. In: *Proceedings of PDAC International Convention, Toronto, 2004*.
- Edwards, G.R., Kipkie, W. B., Agar, G. E., 1980. The effect of slime coating of the serpentine minerals, chrysotile and lizardite on pentlandite flotation. *Int. J. Miner. Process.*, 7, 33 – 42.
- Fuerstenau, M. C., Somasundaran, P., 2003. Flotation, in: Fuerstenau, M. C., Han, K. N., (Eds.), *Principles of Mineral Processing*. SME, Colorado, pp. 245.

- Fujii, T., Nakagawa, S., Sato, Y., Inomata, H., Hashida, T., 2010. Sorption characteristics of CO₂ on rocks and minerals in storing CO₂ processes”, *Nat. Resour. J.*, 1, 1 – 10.
- Gardner, J. R., Woods, R., 1979. An electrochemical investigation of the natural floatability of chalcopyrite. *Int. J. Miner. Process.*, 6, 1 – 16.
- Hargreavass, A., Taylor, W. H., 1946. An X-Ray examination of decomposition products of chrysotile (asbestos) and serpentine. *Miner. Mag.*, 204 – 216.
- Hernandez-Aguilar, J., Finch, J. A., 2005. Validation of bubble sizes obtained with incoherent imaging on a sloped window. *Chem. Eng. Sci.*, 60, 3323–3336.
- Heiskanen, K., Kirjavainen, V., Laapas, H., 1991. Possibilities of collectorless flotation in the treatment of pentlandite ores. *Int. J. Miner. Process.*, 263-274.
- Heyes, G. W.; Trahar, W. J., 1977. The natural floatability of chalcopyrite. *Int. J. Miner. Process.*, 4, 317 – 344.
- Hofmeier, U.; Yaminsky, V. V.; Christensen, H. K., 1995. Observations of solute effects on bubble formation. *J. Colloid Interf. Sci.*, 174, 199 – 210.
- Hurlbut, C. S., Sharp W. E., 1998. *Dana's Minerals and How to Study Them*. John Wiley & Sons, New York, Chapter 7.
- Kogel, J. E., Trivedi, N. C., Barker, J. M., Krukowski, S. T., (Eds.), 2006. *Industrial Minerals and Rocks: Commodities, Markets and Uses*. SME, Colorado, pp. 199.
- Laskowski, J. S.; Cho, Y. S.; Ding, K., 2003. Effect of frothers on bubble size and foam stability in potash ore flotation systems. *Can. J. Chem. Eng.*, 81, 63 – 69.
- Mani, H, Xu, M., Quinn, P., Stratton-Crawley, R., 1997. The effect of ultramafic mineralogy on pentlandite flotation, in: Finch, J. A., Rao, S. R., Holubec, I. (Eds.), *Proc. Processing of Complex Ores, Conference of Metallurgists, CIM, Sudbury, Ontario, 1997*, pp. 63 – 76.
- Nyquist, R. A., Kagel, R. O., 1971. *Infrared Spectra of Inorganic Compounds*. Academic Press, New York.
- Park, A-H. A., Fan, L-S., 2004. CO₂ mineral sequestration: physically activated dissolution of serpentine and pH swing process. *Chem. Eng. Sci.*, 59, 5241 – 5247.
- Pietrobon, M. C., Grano, S. R., Sobieraj, S., Ralston, J., 1997. Recovery mechanisms for pentlandite and MgO bearing gangue minerals in nickel ores from Western Australia. *Miner. Eng.*, 10, 775 – 786.

- Quinn, J. J., Kracht, W., Gomez, C. O., Gagnon, C., Finch, J. A., 2007. Comparing the effect of salts and frother (MIBC) on gas dispersion and froth properties. *Miner. Eng.*, 20, 1296 – 1302.
- Rao, S. R., Leja, J., 2003. *Surface Chemistry of Froth Flotation*, 2nd ed. Plenum Publishers, New York, Vol. 2, Chapter 8.
- Seifritz, W., 1990. CO₂ Disposal by means of silicates. *Nature*, 345, 486.
- Senior, G. D., Thomas, S. A., 2005. Development and implementation of a new flowsheet for the flotation of a low grade nickel ore”, *Int. J. Miner. Process.*, 78, 49 – 61.
- Stumm, W., 1992. *Chemistry of the Solid-Water Interface*. Wiley-Interscience Publication, New York, pp. 523 – 598.
- Sugama, T., Sabatini, R., Petrakis, L., 1998. Decomposition of chrysotile asbestos by fluorosulfonic acid. *Ind. Eng. Chem. Res.*, 37, 79-88.
- Tartaj, P.; Cerpa, A.; Garcia-Gonzalez, M. T.; Serna, C. J., 2000. Surface instability of serpentine in aqueous suspensions. *J. Colloid Interf. Sci.*, 231, 176 – 181.
- Uddin, S., Mirnezami, M., Rao, S. R., Finch, J. A., 2010. Effect of fibre disintegration on flotation of an ultramafic Ni-Ore, in: Pawlik, M. (Ed.), *Proc. Rheology in Minerals Processing, Conference of Metallurgists, CIM, Vancouver, BC*, pp. 307 – 317.
- Wellham, E. J., Elber, L., Yan, D.S., 1992. The role of carboxy methyl cellulose in the flotation of a nickel sulphide transition ore. *Miner. Eng.*, 5, 381 – 395.
- Wypych, F., Adad, L. B., Mattoso, N., Marangon, A. A. S., Schreiner, W. H., 2005. Synthesis and characterization of disordered layered obtained by selective leaching of octahedral sheets from chrysotile and phlogopite structures. *J. Colloid Interf. Sci.*, 283, 107 – 112.
- Xu, Z., Rao, S. R., Finch, J. A., Kelebek, S., Wells, P., 1997. “Role of Diethylenetriamine (DETA) in Pentlandite-pyrrhotite Separation: I. Complexation of Metals with DETA”, *Trans. IMM: Sect. C*, 106, C15–C20, 1997.

8. Conclusions and Perspectives

8.1. Conclusions and contributions to original knowledge

8.1.1. Overview

The first part of the research (chapters 3 - 6) focused on developing surface charge characterization devices based on the sedimentation potential principle. Chapter 3 described a particle sedimentation potential (PSP) apparatus and procedure capable of working with single and mixed particle systems (i.e. ore). Unique advantages of sedimentation method include visual recording of agglomeration/dispersion characteristics, gravity separation inside the column followed by measuring the potentials of different density fractions and lower cost of the apparatus (at least one tenth of available commercial zeta potential analyzers). Chapter 4 adapted the apparatus and method for bubbles, the bubble sedimentation (swarm) potential (BSP); and chapter 5 combined bubble and particles to measure BSP in the presence of particles. Chapter 6 discusses observations using the PSP setup for a sample of ultramafic ore. Finally, in chapters 6 and 7, the fibre disintegration technique is discussed using flotation and structural characterizations.

8.1.2. Surface charge study: particles

Though promising, sedimentation potential method has been far less explored compared to the other methods of surface charge characterization. Consequently, the first objective of the research was to demonstrate the technique and build an integrated, user-friendly apparatus using this method. The research demonstrated a fully integrated

sedimentation potential apparatus with the ability to measure all system variables on-line. The Matlab based system provided a fast and powerful tool for control, data acquisition and post processing. The technique was validated by single mineral tests which showed good agreement with zeta potential measured by electrophoresis in the case of PSP and by showing good agreement with iso-electric point in the case of BSP.

For the PSP case, tests were designed to determine if the technique can handle mixed systems. Experiments were performed with synthetic mixtures of coarse and fine SiO₂ and Al₂O₃ particles in such a way that facilitated gravity separation inside the column. This allowed collection of fractions with time for analysis to compare against the potential-time signals. Results showed sedimentation potential variation reflective of the minerals present. Longer aging time showed smaller difference between fractions, a behavior reported before in the literature and attributed to cross-contamination by cations (Healy et al., 1973).

In another part of the sedimentation potential research (chapter 6), application to surface charge characterization of an ultramafic ore sample was investigated. Visually the sedimentation column showed the following: the ore forms an agglomerated mass at natural pH (ca. 9); at acidic pH, the slurry seemed dispersed; addition of EDTA cleared the supernatant by solubilizing metal ions, e.g. Mg²⁺, which stops formation of Mg(OH)_{2(s)} precipitates that remain dispersed.

From sedimentation potential measurements, the iep of the ore was found to ca. pH 8, lower than for chrysotile (~ pH 10), the major fraction of the ore. The difference in iep may result from the other minor mineral fractions e.g. olivine, pyrrhotite and magnetite all of which have iep's lower than pH 8.

Measurements with Mg cations showed a shift in the PSP to more positive values at alkaline pH, including charge reversal at high enough Mg concentrations, while the iep remained relatively unaffected. This is the common response to the presence of Mg and was, for example, reported for serpentine by Tartaj et al. (2000).

The addition of EDTA made the PSP more negative as well as decreasing the iep from ca. pH 8 to ca. pH 5. This effect can be attributed to the fact that EDTA is a chelating agent and may expose more negative sites by removing cations from the surface. It may also selectively extract Mg from the surface lattice and lower the Mg/Si ratio which lowers the iep of serpentine particles (Tartaj et al., 2000).

There may be a benefit to lowering the iep as this reduces the tendency of hetero-coagulation or ‘slime coating’ which should improve flotation if this was a prime cause behind poor selectivity in processing ultramafic ore. Another purpose of using a chelating agent is to suppress non-sulphide gangue from being activated by metal ions. Flotation tests showed that both Ni-metallurgy and MgO rejection, however, were unaffected by EDTA addition. This led to suggest that the cause of poor metallurgy is ‘entanglement’ which results from the large mass of chrysotile fibre in the ore.

8.1.3. Surface charge study: bubbles

The PSP apparatus was adapted first to measure bubble sedimentation (swarm) potential (BSP) (chapter 4) then further adapted to measure BSP in the presence of particles (chapter 5). The latter objective was to examine attachment bubble/particle interaction mechanisms under flotation-like conditions. Although attachment of hydrophobic particles is the dominant recovery process in flotation, electrostatic

interaction, which depends on the electrical charge on both bubbles and particles, is sometimes considered. The possibility raised of electrostatic interaction between positively charged clinochrysotile in processing an ultramafic Ni-ore and negatively charged gas bubbles (at natural pH) (Xu et al., 2011) instigated the research to test the possibility.

Like the PSP technique the BSP apparatus allowed in-process measurement of all system variables associated with surface electrical charge: swarm potential, solution conductivity, gas holdup, pH and bubble size distribution. The method was validated by comparing with literature iso-electric point (iep) values.

The iep of gas bubbles in purified water reported in literature is between pH 1.5-4.0. In the most recent study Tabor et al. (2011) testing an ultra-pure water system using atomic force microscopy (AFM) showed the iep close to pH 3.0 for inert gas bubbles (N_2 , H_2 and close to pH 4.0 for air bubbles, the higher value in the latter case being attributed to presence of CO_2 . The iep found in the present work was also pH 4.0 for air bubbles. The similarity of iep regardless of bubble size and presence of multiple bubbles noted by comparing all data sources indicates the iep is independent of these factors.

The commercial non-ionic surfactants (frothers) MIBC and DF250 are used to reduce bubble size in flotation cells; in the present work they showed little impact on BSP up to typical flotation dosages of ca. 20 ppm. These findings are similar to previous observations (Yoon and Yordan, 1986; Elmahdy et al., 2008). It suggests that there is no influence of surface electrical charge in bubble size reduction or coalescence prevention achieved with frothers. In contrast, ionic surfactants had significant influence on bubble charge (as well as bubble size reduction) dictated by the nature of the polar group: the

anionic surfactant SHS made the charge more negative and cationic HTAB reversed charge to positive and with both surfactants an increase in concentration increased the magnitude of the charge.

The presence of metal ions also influences the charge depending on concentration and pH. Tests were performed to reveal the interaction between the bubble and Mg ions (added as MgCl_2). The Mg ions increased the charge on the bubble eventually reversing the charge. There are two factors that influence the result: the nature of the adsorbed hydrolyzed species, and the extent of surface coverage. The initial shift of the negative potential to more positive ones was by adsorption of Mg^{2+} on the interface. As pH is increased above pH 6, the Mg is increasingly present $\text{Mg}(\text{OH})_{2(\text{s})}$ and the bubble charge progressively approaches that of the positively charged $\text{Mg}(\text{OH})_{2(\text{s})}$ precipitates (iep ca. pH 12) with the net potential depending on the amount of $\text{Mg}(\text{OH})_{2(\text{s})}$ at the surface. Similar behavior was found by other researchers in the presence of metal ions (Li and Somasundaran, 1991; Yang et al., 2001; Han et al., 2004).

In the presence of the anionic surfactant SHS the addition of Mg ions also shifted the negatively charged bubbles to positive values. A mechanism based on possible Mg-SHS reaction products was discussed.

Modifications to measure BSP in presence of particles included a Masterflex pump to circulate the overflow to the cell and the use of higher air rates to increase the magnitude and hence sensitivity of the BSP. Particle concentration was kept sufficiently low to avoid corrupting the BSP signal. To aid interpretation, bubble-particle attachment was visualized at a pendant bubble exposed to agitated suspensions and the zeta potential as a function of particle concentration was measured using electrophoresis.

The BSP and the visualization tests showed unambiguous evidence of attachment of hydrophobic particles in the case of alumina, silica and clinochrysotile. Some evidence of attachment of non-hydrophobic particles was shown in the BSP tests but the visual tests strongly indicated attachment of non-hydrophobic particles, especially of the finer size fractions. Pick-up was significantly reduced by addition of surfactant that gave the bubble the same sign charge as the particle, cationic in case of alumina and clinochrysotile and anionic in case of silica. This study (chapter 5) thus introduced a possibility of manipulating bubble charge to depress unwanted minerals.

8.1.4. Fibre disintegration

The study of PSP on ore led the second part of the research, to study the effect of fibre disintegration (chapters 7 and 8). The approach involved attacking the fibres by a combination of chemical (acid) and mechanical (grinding) treatment adapting technology explored for CO₂ sequestration. Strong acid was necessary to dissolve magnesium from the serpentine lattice and weaken the structure which coupled with the mechanical attrition in grinding led to fibre disintegration.

The first trials used HCl (up to 15 wt%) in a ceramic ball mill. The resulting slurry was allowed to stand (aged) in the mill during which the pH rose to near neutral to allow the addition of soda ash and the setting of other conditions typical of Ni-sulphide ore flotation. Flotation results with 10-15 wt% HCl showed significant improvement in Ni recovery and MgO rejection over untreated ore. This implies that ‘entanglement’ played a role in limiting separation of ultramafic ore. By possibly lowering the Mg/Si

ratio on the mineral surface, the chemical attack may also reduce slime coating, i.e., yielding a secondary beneficial effect on flotation.

The second trials (chapter 7) substituted H_2SO_4 for HCl . After treatment, low and stable pH (~ 2.0) slurry was produced, which permitted collectorless flotation. Before flotation either aging or aeration increased the hydrophobicity of the sulphides by inducing polysulphide and elemental sulphur formation which are the hydrophobic species. The high ionic strength of the supernatant due to Mg extraction also eliminated need for frother to reduce bubble size. Flotation gave about 80% Ni recovery with 90% MgO rejection at 2.5-3.5% Ni grade (an upgrading ratio of about 5) is possible at the rougher flotation stage. This concentrate can be further upgraded in cleaner stages.

Structural changes in the fibres were followed using SEM-EDS and spectroscopic techniques, namely XRD, Micro-Raman, FT-IR and XPS. SEM showed the treated sample is no longer dominated by long, interconnected fibres but rather comprises short, isolated fibres. FT-IR spectra showed a reduction of the Mg-OH band at 3680 cm^{-1} and transition to a shoulder of the Si-O band at 970 cm^{-1} upon acid treatment and the growth of the bands at 3410 , 1640 and 1220 cm^{-1} which correspond to the disruption of the external $\text{Mg}(\text{OH})_2$ layers of serpentine and hydration of the exposed inner siliceous structure. The XRD pattern offered some evidence of structural change, the general lowering in peak intensity may indicate decreased crystallinity associated with fibre disintegration.

Based on the above analysis a fibre disintegration mechanism was proposed. It involves crack initiation on the fibre surface due to Mg extraction in the acidic environment which leads to crack growth and breakage upon subsequent impact by

grinding media. Breakage exposes the inside of the fibres to acid and the process proceeds. The outcome is the short fibres that reduce entanglement density or conversely increase free volume. This is believed to be the key to the improved metallurgy compared to untreated ore.

The use of H_2SO_4 holds some practical merit especially if there is a local Ni smelter producing the acid as part of SO_2 abatement. The fact that flotation can be conducted at the natural pH of the treated slurry ($< \text{pH } 2$) without collector and frother suggests that reagent costs are minimal. This does not, of course, avoid the need for a local cheap supply of acid, or avoid costs associated with grinding mills and flotation cells constructed to withstand the harsh conditions.

Another potential practical aspect of the treatment is the possibility to use the tailings for CO_2 sequestration. Among other CO_2 removal methods, mineral carbonation is relatively new but has potential to sequester CO_2 in a safe and permanent manner since the binding reactions are exothermic in nature (Lackner et al., 1995). Typically, serpentine rich materials (because of their high concentration of Mg are considered. The first step is to leach as much Mg as possible. It was found that the combination of chemical and mechanical treatment gave the best leaching performance, which is why this was adopted in the present study. In the next step, leached Mg is reacted with CO_2 to form carbonates. It was also shown that serpentine can be made reactive by grinding long enough to destroy the crystal structure which allows access to Mg in the structure and substantial carbonation can be achieved even at room temperature. Thus both leached Mg and the Mg in structurally disrupted serpentine rich tailing can be utilized for CO_2 sequestration.

8.2. Future directions

8.2.1. Modification of the PSP apparatus

The literature (Marlow and Rowell, 1985) indicates that the Smoluchowski equation begins to deviate appreciably at particle concentration greater than $\sim 1.8\%v/v$. Solids concentration used in this research (chapter 3) was $2\%v/v$ and employed a correction factor given by Marlow and Rowell (1985) which is an approximation of the equations derived by Levine et al. (1976). Exact solution of the set of non-linear equations derived by Levine et al. (1976) is required to calculate zeta potential for systems more concentrated than $2\%v/v$. Thus, going to more than $2\%v/v$ would require a new software suite to be written. This could form a part of future work.

The limit was set at $2\%v/v$ in order to calculate zeta potential to compare with those derived from electrophoresis as a test of validity. Sedimentation potential itself can be measured for higher %solids. In a design improvement, a continuous particle flow (e.g. using a Masterflex pump) is a possibility. It would facilitate the procedure by establishing a steady flow of particles over longer period of time.

8.2.2. Ore flotation: test with higher feed concentration

Regarding the flotation of ultramafic Ni-ore, a couple of ideas can be tested. One of the major impacts of the combined treatment on the slurry is the significant reduction of viscosity observed during slurry handling. Some rheological measurements by varying acid or feed concentration (% solids) could prove insightful. In the current research $10\%w/w$ was used. Flotation tests should be performed followed by the combined treatment at increased % solids to determine the optimum point where the flotation

response starts to deteriorate. Higher feed concentration corresponds to higher productivity, thus it would be fruitful to identify maximum feed concentration that can be used without hampering overall performance. Nevertheless, it can be inferred that maximum usable feed concentration using the combined treatment would be much higher than the untreated ore.

8.2.3. Micro-flotation using ionic collectors

Chapter 5 showed the possibility of manipulating bubble charge to depress unwanted minerals. Some flotation tests are suggested in this regard. Tests can be done on silica-SHS, alumina-HTAB and clinochrysotile-HTAB system and compared the results with silica-HTAB, alumina-SHS and clinochrysotile-SHS system for further establishment of the idea.

8.3. References

- Alty, T., 1926. The origin of the electrical charge on small particles in water. Proceedings of the Royal Society of London, Series A, vol. 122 (760), pp. 235–251.
- Conway, B. E., 1978. The evaluation and use of properties of individual ions in solution. *J. Solution Chem.*, 7, 721–770.
- Elmahdy, A.M., Mirnezami, M., Finch, J.A., 2008. Zeta potential of air bubbles in presence of frothers. *Int. J. Miner. Process.* 89, 40–43.
- Healy, T. W., Wiese, G. R., Yates, D. E., Kavanagil, B. V., 1973. Heterocoagulation in mixed oxide colloidal dispersions. *J. Colloid Interface Sci.*, 42, 647-649.
- Han, M. Y., Ahn, H. J., Shin, M. S., Kim, S. R., 2004. The effect of divalent metal ions on the zeta potential of bubbles. *Water Sci. Technol.*, 50, 49– 56.
- Lackner, K., Wendt, C. H., Butt, D. P., Joyce, E. L. JR., Sharp, D. H., 1995. Carbon dioxide disposal in carbonate minerals. *Energy*, 20, 1153–1170.

- Levine, S., Neale, G., Epstein, N., 1976. The prediction of electrokinetic phenomenon within multiparticle systems, *J. Colloid Interf. Sci.* 57, 424-437.
- Li, C., Somasundaran, P., 1991. Reversal of bubble charge in multivalent inorganic salt solutions – effect of magnesium. *J. Colloid Interf. Sci.* 146, 215–218.
- Marlow, B. J., Rowell, R. L., 1985. Sedimentation potential in aqueous electrolytes, *Langmuir*, 1, 83-90.
- Tabor, R. F., Chan, D. Y. C., Grieser, F., Dagastine, R. R., 2011. Anomalous stability of carbon dioxide in pH-controlled bubble coalescence. *Angew. Chem. Int. Ed.* 50, 3454–3456.
- Takahashi, M., 2005. Zeta potential of microbubbles in aqueous solutions: Electrical properties of the gas-water interface. *J. Phys. Chem. B* 109, 21858–21864.
- Tartaj, P., Cerpa, A., Garcia-Gonzalez, M. T., Serna, C. J., 2000. Surface instability of serpentine in aqueous suspensions. *J. Colloid Interf. Sci.*, 231, 176 – 181.
- Xu, M., Scholey, K., Marcuson, S., 2011. Vale-Cytec-University Research Consortium on Processing Low Grade Ultramafic Nickel Ore. Conference of Metallurgists (COM), 2011, Montreal, Canada.
- Yang, C., Dabros, T., Li, D., Czarnecki, J., Masliyah, J.H., 2001. Measurement of the zeta potential of gas bubbles in aqueous solutions by microelectrophoresis method. *J. Colloid Interf. Sci.* 243, 128–135.

Appendices

Appendix I – Sedimentation potential setup: particles

Fig. 1 shows the actual view of sedimentation potential apparatus and accessories for particles.

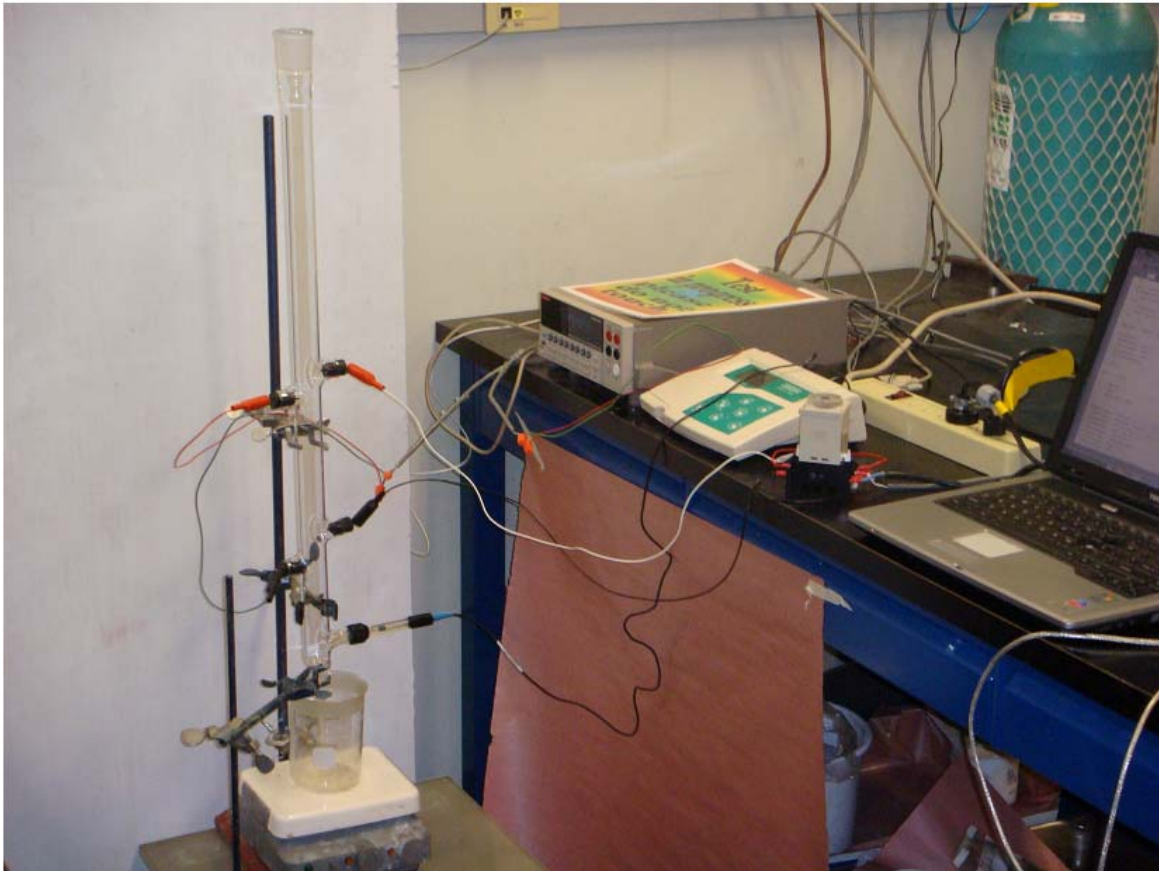


Fig. 1. Particle sedimentation apparatus with accessories

Appendix II – Additional characterizations from chapter 7

Slurry pH was found to be stable after the combined treatment using H_2SO_4 . pH in different aging times is shown in Fig. 2.

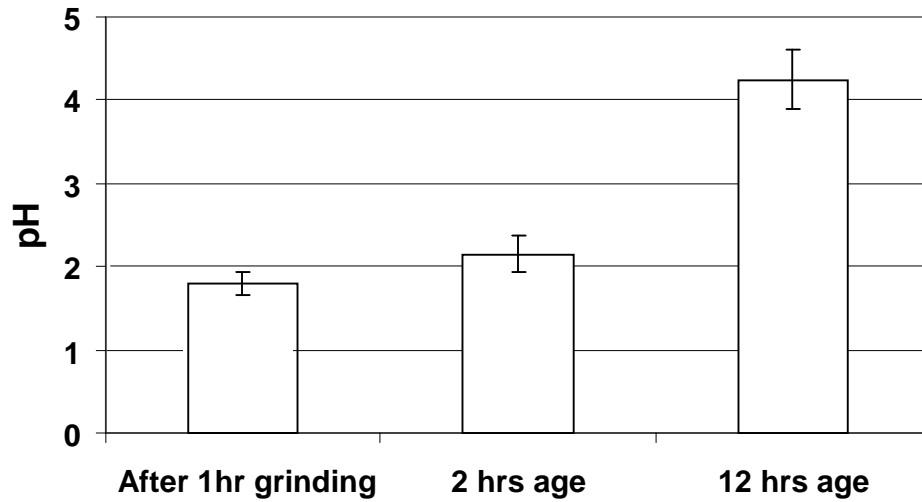


Fig. 2. Slurry pH in different aging times

Fig. 3 shows the froth appearance of the treated slurry with aeration time (no frother). As aeration time increases, the froth appearance darkens which corresponds to froth becoming loaded with sulphide particles. Aeration facilitates oxidation reactions (10-12 in chapter 2) which promote the formation of elemental sulphur (imparts hydrophobicity to sulphide particles). Another important observation (Fig. 3) was stable froth after aeration.

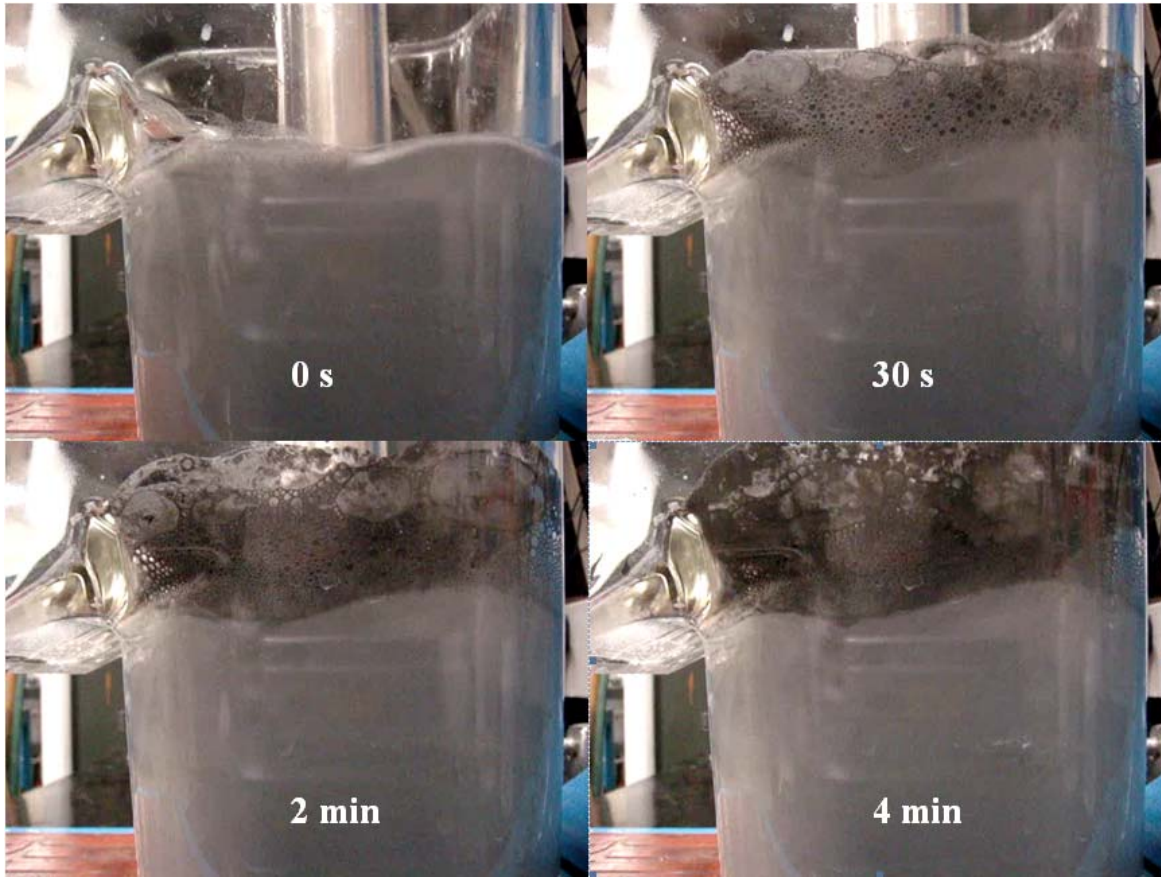


Fig. 3. Froth phase with aeration time

XRD of the concentrate with frother and no-frother is shown in Fig. 4. Less intensity of the clinochrysotile peaks in no-frother condition suggests cleaner separation. Frother addition may deteriorate the separation by floating less hydrophobic middling particles composed of both sulphides and MgO-minerals.

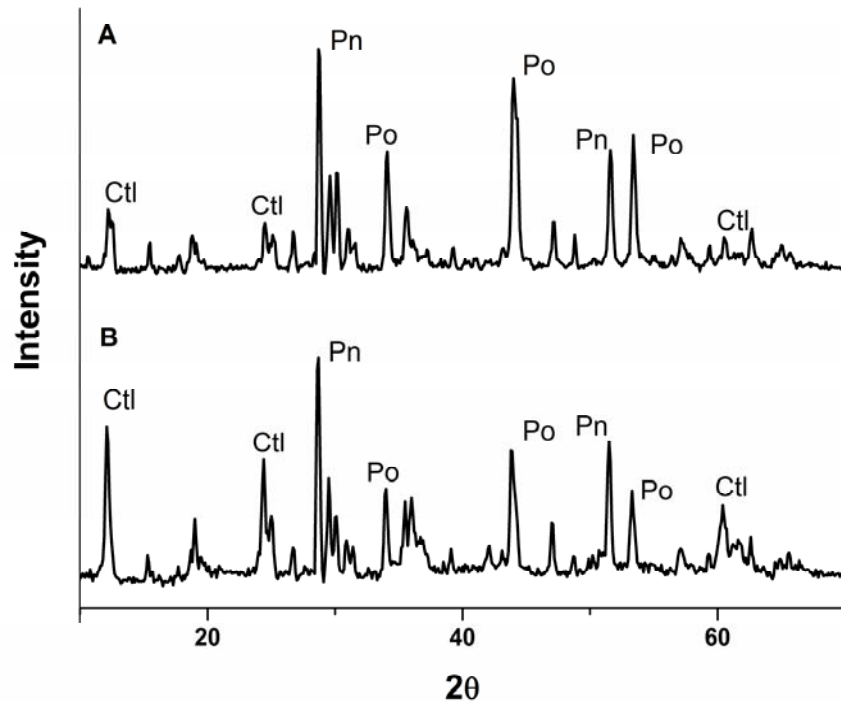


Fig. 4. XRD of the concentrate in (A) no-frother and (B) with frother

Metal deficient sulphides or polysulphides and elemental sulphur are known to be the responsible species to impart hydrophobicity to sulphide particles in collectorless flotation. Stability of polysulphides is pH dependent. It was shown that concentration of polysulphides is negligible compared to elemental sulphur at pH 6 while at pH 8 polysulphides are dominant (Chen and Morris, 1972). Due to the polar nature of S^- ions, hydrophobicity developed by polysulphides is less than elemental sulphur (Luttrell and Yoon, 1984). This is probably another reason for higher floatability at low pH in case of collectorless flotation. In chapter 7, the existence of elemental sulphur in concentrate was proved using SEM-EDS and Micro-Raman. XPS was performed to identify polysulphide species and is shown in Fig. 5. A strong SO_4^{2-} peak was visible but clear identification of polysulphide in the spectra was not possible.

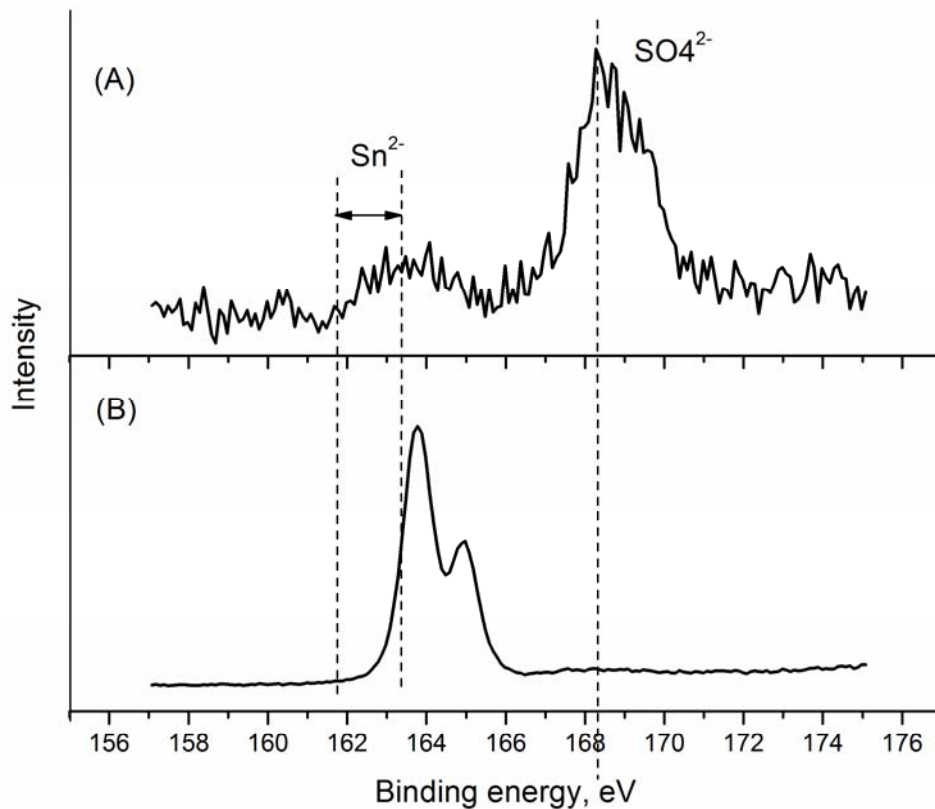


Fig. 5. XPS spectra of the (A) concentrate and (B) standard sample of elemental sulphur

Appendix III – Gravity separation

No gravity separation was observed during free settling of ultramafic ore. An standard technique, Mozley Table (Fig. 6), was trialed. The Mozley Table introduces shear flow on a thin layer of slurry which may detach the entangled particles from fibres and effect physical separation. Visual observations, XRD, SEM were used to analyze the effectiveness of this technique for this type of ore.



Fig. 6. Mozley Table

Experimental

After grinding (for an hour) the slurry was transferred to a container and allowed to settle for an hour. Supernatant was then decanted by siphoning. The sample was divided into three fractions named heavy, middle and light using the Mozley Table. After separation the samples were dried in an oven at 150°C, weighed and the heavy, middle and light fractions were found ca. 10%, 15% and 75% respectively.

Results

The three separated ore fractions are shown in Fig. 7. Color difference between the heavy and light fractions can easily be seen. Denser fractions were found to be the darker ones. Microanalysis of the fractions was performed using SEM-EDAX. Different areas of the same sample were analyzed. For brevity, only the Microanalysis from the representative areas is illustrated in Figs. 8 and 9.



Fig. 7. Three gravity separated fractions: heavy, middle and light

Microanalysis of the heavy fraction (Fig. 8) showed dominance of Fe and S in the sample. Presence of certain amount of Mg, Si and O is also evident. The light fraction (Fig. 9) was dominated by Mg, Si and O. SEM analysis was supported by XRD data shown in Figs. 10 and 11. XRD of the heavy fraction showed a good match with pyrrhotite and magnetite (Fig10) while the light fraction matched with clinochrysotile

(Fig. 11). Light fraction also accord well with the ore itself except the absence of peaks which may correspond to Fe-bearing minerals, i.e. pyrrhotite and magnetite (Fig. 12).

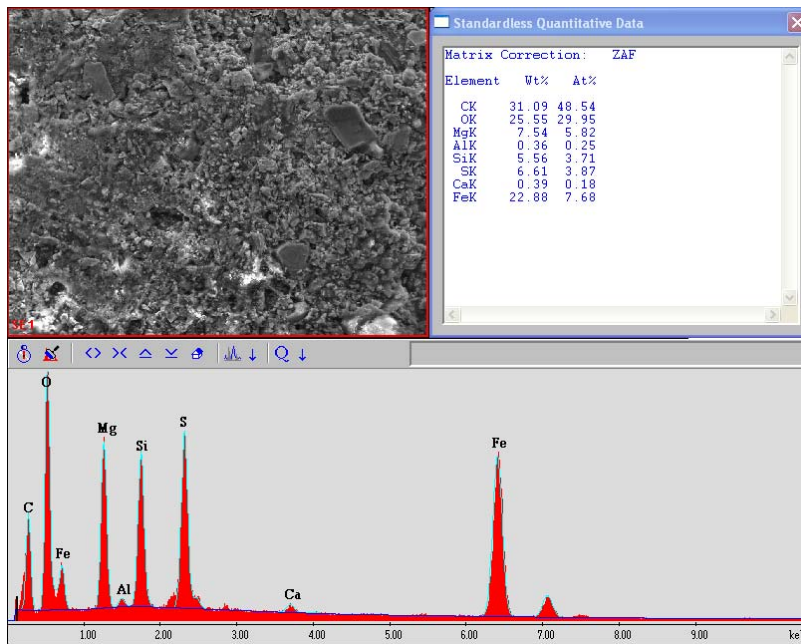


Fig. 8. Microanalysis of heavy fraction

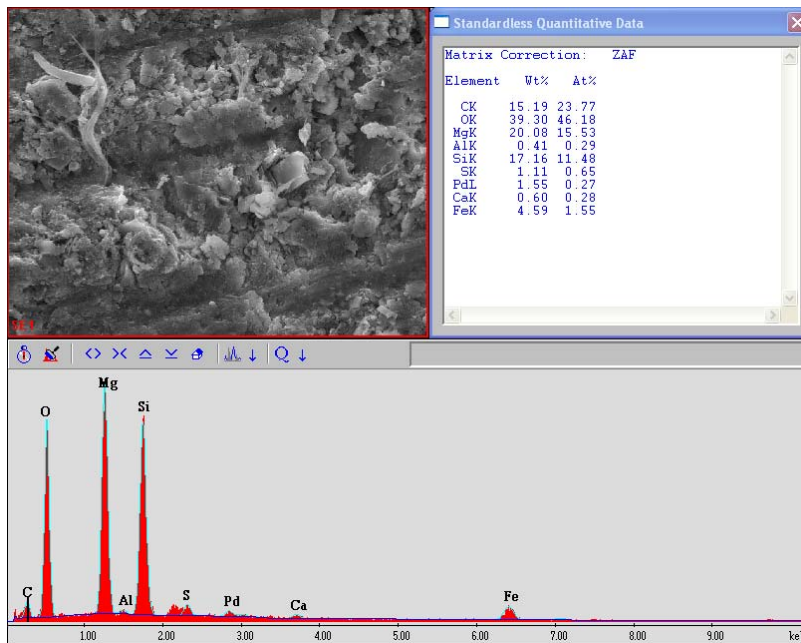


Fig. 9. Microanalysis of light fraction

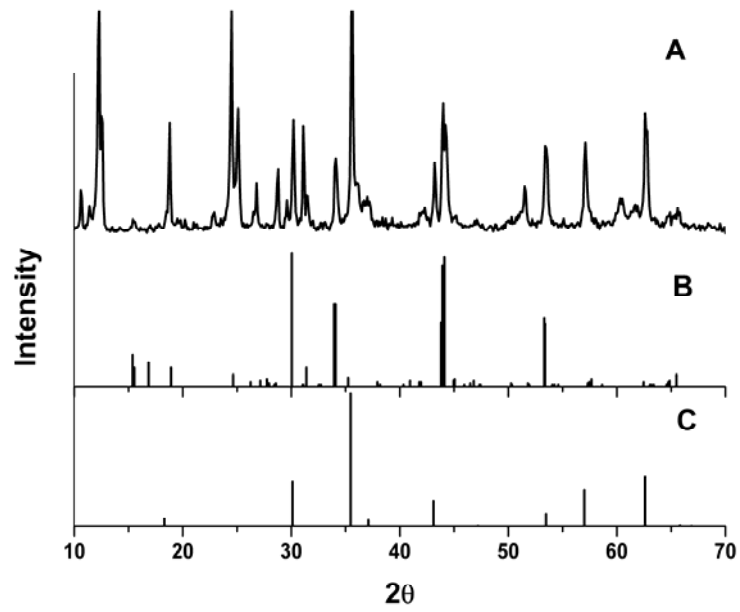


Fig. 10. XRD of (A) heavy fraction and match for (B) pyrrhotite and (C) magnetite

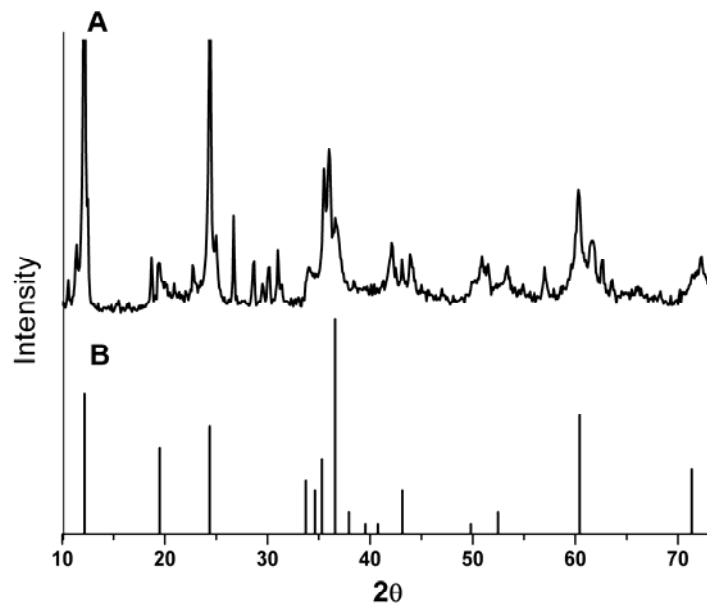


Fig. 11. XRD of (A) light fraction and match for (B) clinochrysoile

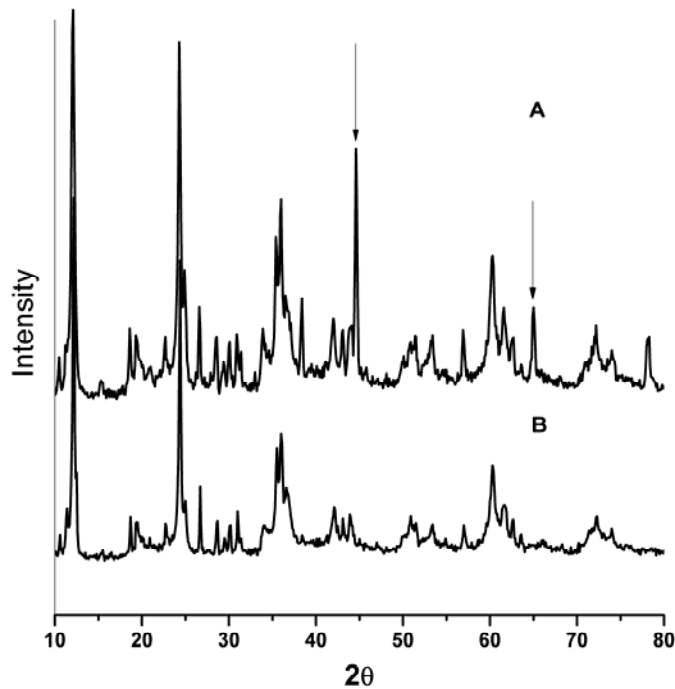


Fig. 12. XRD of (A) ore and (B) light fraction (note: peaks in A at ca. $2\theta=44^\circ$ and 65° may come from pyrrhotite and magnetite – cf Fig. 10)

Discussion

As fibrous chrysotile entangles the other minerals, conventional gravity separation by free fall of particles is not successful in separating various density fractions in the ore. In the current work, Mozley Table was used to separate the ore fractions. The motion of the table induces shear in the thin layer of slurry. This helps to detach the entrapped sulphides from the fibres and then separates them based on gravity. This is evident in visual observation, microanalysis and in XRD.

Appendix IV – Sedimentation potential setup: bubble swarms

Fig. 13 shows the sedimentation potential apparatus and accessories for bubble swarms.



Fig. 13. Sedimentation potential apparatus for bubble swarms

Appendix V – Sample MatLab program to calculate zeta potential

```
%%%%%%%%%%%%%%%%%%%%%%%%%%%%%%%%%%%%%%%%%%%%%%%%%%%%%%%%%%%%%%%%%%%%%%%%%
%%% DCV: DC voltage measurement %%%%%%%%%%%%%%%%%%%%%%%%%%%%%%%%%%%%%%%%%%%%%%%%%%%%%%%%%%%%%%%%%%%%%%%%%%

obj1 = instrfind('Type', 'serial', 'Port', 'COM1', 'Tag',
'');
if isempty(obj1)
    obj1 = serial('COM1');
else
    fclose(obj1);
    obj1 = obj1(1);
end

set(obj1, 'Timeout', 2)

fopen(obj1);
fprintf(obj1, ':ABORT');
fprintf(obj1, '*RST');
fprintf(obj1, '*IDN?');
idn = fscanf(obj1)

fprintf(obj1, 'CONF:VOLT 0.1, 6.5, (@107)');
fprintf(obj1, 'SENS:FUNC "VOLT", (@107)');
fprintf(obj1, 'VOLT:RANG 1, (@107)');
fprintf(obj1, 'ROUT:CLOS (@107)');
fprintf(obj1, 'TRIG:TIM 1');
fprintf(obj1, 'FORM:ELEM READ');
fprintf(obj1, 'TRAC:CLE');
fprintf(obj1, 'INIT');
fprintf(obj1, 'TRACE:FEED:CONT NEXT');
fprintf(obj1, 'TRAC:DATA?');
fprintf(obj1, 'READ?');

OP = scanstr(obj1)
A = OP(2);
B = cell2mat(A);
C = B(1:16)
D = strread(C)
fclose(obj1)

%%%%%%%%%%%%%%%%%%%%%%%%%%%%%%%%%%%%%%%%%%%%%%%%%%%%%%%%%%%%%%%%%%%%%%%%%
%%% R2: Resistance measurement %%%%%%%%%%%%%%%%%%%%%%%%%%%%%%%%%%%%%%%%%%%%%%%%%%%%%%%%%%%%%%%%%%%%%%%%%%
```

```

obj1 = instrfind('Type', 'serial', 'Port', 'COM1', 'Tag',
'');
if isempty(obj1)
    obj1 = serial('COM1');
else
    fclose(obj1);
    obj1 = obj1(1);
end

set(obj1, 'Timeout', 2)

fopen(obj1);
fprintf(obj1, ':ABORT')
fprintf(obj1, '*RST');
fprintf(obj1, '*IDN?');
idn = fscanf(obj1)

fprintf(obj1, 'CONF:RES 1e6, 6.5, (@101)');
fprintf(obj1, 'SENS:FUNC "RES", (@101)');
fprintf(obj1, 'RES:RANG:AUTO ON, (@101)');
fprintf(obj1, 'ROUT:CLOS (@101)');
fprintf(obj1, 'TRIG:TIM 1');
fprintf(obj1, 'FORM:ELEM READ');
fprintf(obj1, 'TRAC:CLE');
fprintf(obj1, 'INIT');
fprintf(obj1, 'TRACE:FEED:CONT NEXT');
fprintf(obj1, 'TRAC:DATA?');
fprintf(obj1, 'READ?');

OP = scanstr(obj1)
A = OP(2)
B = cell2mat(A)
C = B(1:16)
D = strread(C)
fclose(obj1)

%%%%%%%%%%

%%% pH: pH measurement %%%%%%%%%%%

obj1 = instrfind('Type', 'serial', 'Port', 'COM1', 'Tag',
'');
if isempty(obj1)
    obj1 = serial('COM1');
else
    fclose(obj1);

```

```

    obj1 = obj1(1);
end

set(obj1, 'Timeout', 2)

fopen(obj1);
fprintf(obj1, ':ABORT');
fprintf(obj1, '*RST');
fprintf(obj1, '*IDN?');
idn = fscanf(obj1)

fprintf(obj1, 'CONF:VOLT 10, 6.5, (@108)');
fprintf(obj1, 'SENS:FUNC "VOLT", (@108)');
fprintf(obj1, 'VOLT:RANG:AUTO ON, (@108)');
fprintf(obj1, 'ROUT:CLOS (@108)');
fprintf(obj1, 'TRIG:TIM 1');
fprintf(obj1, 'FORM:ELEM READ');
fprintf(obj1, 'TRAC:CLE');
fprintf(obj1, 'INIT');
fprintf(obj1, 'TRACE:FEED:CONT NEXT');
fprintf(obj1, 'TRAC:DATA?');
fprintf(obj1, 'READ?');

OP = scanstr(obj1)
A = OP(2);
B = cell2mat(A);
C = B(1:16)
D = strread(C)
fclose(obj1)

%%%%%%%%%%%%%%%%%%%%%%%%%%%%%%%%%%%%%%%%%%%%%%%%%%%%%%%%%%%%%%%%%%%%%%%%%%
%%% Calculate zeta potential %%%%%%%%%%%%%%%%%%%%%%%%%%%%%%%%%%%%%%%%%%%%%%%%%%%%%%%%%%%%%%%%%%%%%%%%%%%

% Background Calculation

% Main Loop

for i = 1:10

Test = i

DCV
data1(Test,1) = D

R2

```

```

data1(Test,2) = D

pH
data1(Test,3) = D

save data1

% clear all force

end

% Average potential difference for background

SumDCV1 = data1(1,1) + data1(3,1) + data1(5,1)+ data1(7,1) +
data1(9,1)
AvgDCV1 = SumDCV1/5.0

SumDCV2 = data1(2,1) + data1(4,1) + data1(6,1)+ data1(8,1) +
data1(10,1)
AvgDCV2 = SumDCV1/5.0

% Average resistance for background

SumR21 = data1(1,2) + data1(3,2) + data1(5,2)+ data1(7,2) +
data1(9,2)
AvgR21 = SumR21/5.0

SumR22 = data1(2,2) + data1(4,2) + data1(6,2)+ data1(8,2) +
data1(10,2)
AvgR22 = SumR22/5.0

%%%%%%%%%%%%%%%%%%%%%%%%%%%%%%%%%%%%%%%%%%%%%%%%%%%%%%%%%%%%%%%%%%%%%%%%

% Suspension calculation

% Constants

DieC = 80.0           % Dielectric constant
Visc = 0.0093        % Viscosity
VacPr = 8.854e-14    % Vacuum permittivity
GrAcc = 980.00       % Gravitational acceleration
RhoP = 2.65          % Particle density (silica)
RhoM = 1.00          % Density of the medium (water)

% Main Loop

for i = 1:10

```

```

Test = i

% Average potential difference for suspension

DCV
data2(Test,1) = D

if(rem(i,2)~=0)
VPCM = (data2(Test,1)-AvgDCV1)/20
data2(Test,4) = VPCM
end

if(rem(i,2)==0)
VPCM = (data2(Test,1)-AvgDCV2)/20
data2(Test,4) = VPCM
end

% Average resistance for suspension, volume fraction of
% solid (FaiP) and specific resistance (R2SP)
R2
data2(Test,2) = D

if(rem(i,2)~=0)
Const = AvgR21/data2(Test,2)
FaiP = (1.0-Const)/((Const/2.0)+1.0)
data2(Test,5) = FaiP
R2SP = 0.097*data2(Test,2)
data2(Test,6) = R2SP
end

if(rem(i,2)==0)
Const = AvgR22/data2(Test,2)
FaiP = (1.0-Const)/((Const/2.0)+1.0)
data2(Test,5) = FaiP
R2SP = 0.097*data2(Test,2)
data2(Test,6) = R2SP
end

% Calculation of pH

pH
data2(Test,3) = D

pHV = (0.3842 - data2(Test,3))/0.0585
data2(Test,7) = pHV

```

```
% Calculate and save zeta potential

ZetPt = (Visc*(1.0/R2SP)*VPCM)/(DieC*VacPr*FaiP*(RhoP -
RhoM)*GrAcc)
data2(Test,8) = ZetPt

save data2

%clear all force

end

%%%%%%%%%%%%%%%%%%%%%%%%%%%%%%%%%%%%%%%%%%%%%%%%%%%%%%%%%%%%%%%%%%%%%%%%%
```

References

Chen, K. Y., Morris, J. C., 1972. Kinetics of oxidation of aqueous sulfide by O₂. Environ. Sci. Technol. 6, 529–537.

Luttrell, G. H., Yoon, R.-H., 1984. Surface studies of the collectorless flotation of chalcopyrite”, Colloid Surface A, 12, 239 – 254.